Auxin and strigolactone non-canonical signaling regulating development in *Arabidopsis thaliana*

by

Michelle Gallei

June, 2022

A thesis submitted to the
Graduate School
of the
Institute of Science and Technology Austria
in partial fulfillment of the requirements
for the degree of
Doctor of Philosophy

Committee in charge:
Martin Loose, Chair
Jiří Friml
Eva Benková
Eilon Shani

The thesis of Michelle Gallei, titled *Auxin and strigolactone non-canonical signaling regulating development in Arabidopsis thaliana*, is approved by:

Supervisor: Jiří Friml, IST Austria, Klosterneuburg, Austria

Signature: _____

Committee Member: Eva Benková, IST Austria, Klosterneuburg, Austria

Signature: _____

Committee Member: Eilon Shani, Tel Aviv University, Tel Aviv, Isareal

Signature: _____

Exam Chair: Martin Loose, IST Austria, Klosterneuburg, Austria

Signature: _____

Signed page is on file

IST Austria Thesis, ISSN: 2663-337X
ISBN: 978-3-99078-019-0

I hereby declare that this dissertation is my own work and that it does not contain other people's work without this being so stated; this thesis does not contain my previous work without this being stated, and the bibliography contains all the literature that I used in writing the dissertation.

I declare that this is a true copy of my thesis, including any final revisions, as approved by my thesis committee, and that this thesis has not been submitted for a higher degree to any other university or institution.

I certify that any republication of materials presented in this thesis has been approved by the relevant publishers and co-authors.

Signature: _____

Michelle Gallei

June, 2022

Signed page is on the file.

Abstract

Plant growth and development is well known to be both, flexible and dynamic. The high capacity for post-embryonic organ formation and tissue regeneration requires tightly regulated intercellular communication and coordinated tissue polarization. One of the most important drivers for patterning and polarity in plant development is the phytohormone auxin. Auxin has the unique characteristic to establish polarized channels for its own active directional cell to cell transport. This fascinating phenomenon is called auxin canalization. Those auxin transport channels are characterized by the expression and polar, subcellular localization of PIN auxin efflux carriers. PIN proteins have the ability to dynamically change their localization and auxin itself can affect this by interfering with trafficking. Most of the underlying molecular mechanisms of canalization still remain enigmatic. What is known so far is that canonical auxin signaling is indispensable but also other non-canonical signaling components are thought to play a role. In order to shed light into the mysteries auf auxin canalization this study revisits the branches of auxin signaling in detail. Further a new auxin analogue, PISA, is developed which triggers auxin-like responses but does not directly activate canonical transcriptional auxin signaling. We revisit the direct auxin effect on PIN trafficking where we found that, contradictory to previous observations, auxin is very specifically promoting endocytosis of PIN2 but has no overall effect on endocytosis. Further, we evaluate which cellular processes related to PIN subcellular dynamics are involved in the establishment of auxin conducting channels and the formation of vascular tissue. We are re-evaluating the function of AUXIN BINDING PROTEIN 1 (ABP1) and provide a comprehensive picture about its developmental phneotypes and involvement in auxin signaling and canalization. Lastly, we are focusing on the crosstalk between the hormone strigolactone (SL) and auxin and found that SL is interfering with essentially all processes involved in auxin canalization in a non-transcriptional manner. Lastly we identify a new way of SL perception and signaling which is emanating from mitochondria, is independent of canonical SL signaling and is modulating primary root growth.

Acknowledgements

First, I want to thank my supervisor Jiří Friml for giving me the opportunity to pursue my PhD in his wonderful lab. Jiří, thank you for always believing in me, encouraging me, being approachable and for all the glasses of wine we had together. The combination of having a great boss and a group full of fantastic people made my PhD experience unique and unforgettable. My gratitude goes to all previuos and current colleagues – each of you had their very own way to make my journey special. Inge, thank you for all the help you provided throughout the last 4 years. I really enjoyed and am still enjoying our outdoor adventures, hikes and trips! Christina, thank you for always reading my mind and understanding everything! Karolina, thank you for all the parties, shots and amazing talks! Dorota, Aline and David, I hope you will keep our beloved chocolate club alive to make the days sweeter! And thank you for being the best non-noisy desk neighbours I can imagine! David Z., thank you for listening to me for hours over hours and hours and for all the great laughs we shared. Han, thank you for being the sweetest person I ever met! Syamala, I am eternally grateful for everything you ever did for me and all adventures we shared, you are simply the best! Angela, I am so happy you started working at IST. Thank you for all Wednesday Schnitzel-Kartoffel lunches, Earl breaks and baby duck watching.

Further, I have to thank my friends from my previous lab Gesa, Lisa, André, Sam and Bente for all their support, (online-) game nights and Fräulein Rosé evenings. I can't wait to be reunited with all of you in Vienna again!

My special thanks and gratitude goes to my beloved "Vienna-friends". I am thankful for my ladybugs Christine, Selma, Vicky and Valerie. They always believed in me and cheered for me when I needed it the most. Daniel, thank you for being the most understanding and amazing person! Thank you for all the fun and too funny evenings and parties and all the great talks! Kerstin, thank you for being the best WGoderdochmehr roommate ever! Rafaela and Matthias, thank you for always being there and understanding and all our lock-down zoom nights.

André, thank you for being the most patient and genuine person I have ever met. Thank you for always making me food and laugh – the two most important things!

Last but not least I'm utterly grateful for my family who always believed in me and supported me in any decision I took. Without their support I would not be the person I am now.

About the Author

Michelle Gallei finished her Bachelor's degree at the University of Vienna in the field of genetics and molecular biology. During her Bachelor studies she worked for over two years as an intern at the Gregor Mendel Institute (GMI) in Vienna, where she focused on the biotrophic interaction between the crop plant maize and the fungus *Ustilago maydis*. Afterwards Michelle joined the Master's program at the University of Vienna focusing on genetics and developmental biology. During her Master studies Michelle worked as an intern at the Medical University of Vienna with focus on establishing tumor organoids as model systems. For her Master thesis work she joined the Friml group at IST Austria where she worked on deciphering non-canonical auxin signaling. Michelle stayed for her PhD studies at the Friml group to study auxin signaling, auxin canalization and non-canonical strigolactone signaling in more detail.

List of Publications Appearing in the Thesis

1. **Gallei M**, Luschnig C, Friml J. Auxin signalling in growth: Schrödinger's cat out of the bag. *Curr Opin Plant Biol*. 2020;53:43-49. doi:10.1016/j.pbi.2019.10.003

2. Narasimhan M, **Gallei M**, Tan S, et al. Systematic analysis of specific and nonspecific auxin effects on endocytosis and trafficking. *Plant Physiol*. 2021;186(2):1122-1142. doi:10.1093/PLPHYS/KIAB134

3. Mazur E, **Gallei M**, Adamowski M, Han H, Robert HS, Friml J. Clathrin-mediated trafficking and PIN trafficking are required for auxin canalization and vascular tissue formation in Arabidopsis. *Plant Sci*. 2020;293. doi:10.1016/j.plantsci.2020.110414

4. Friml J, **Gallei M**, Gelová Z, et al. ABP1-TMK auxin perception mediates rapid phosphorylation for regeneration and auxin canalization. *Nature*. 2021 - under revision

5. Zhang J, Mazur E, Balla J, **Gallei M**, et al. Strigolactones inhibit auxin feedback on PIN-dependent auxin transport canalization. *Nat Commun*. 2020;11(1). doi:10.1038/s41467-020-17252-y

6. **Gallei M**, Lee A, Baster P, Pěnčík A, Pottie R, Molnar G, et al. SLs inhibit root growth by promoting mitochondrial retrograde signaling independently of MAX2. 2022. -in preperation

7. Li L, **Gallei M**, Friml J. Bending to auxin: fast acid growth for tropisms. *Trends Plant Sci*. 2021:1-10. doi:10.1016/j.tplants.2021.11.006

8. Oochi A, Hajny J, Fukui K, Nakao Y, **Gallei M**, et al. Pinstatic acid promotes auxin transport by inhibiting pin internalization. *Plant Physiol*. 2019;180(2):1152-1165. doi:10.1104/pp.19.00201

9. Gelová Z, **Gallei M**, Pernisová M, et al. Developmental roles of Auxin Binding Protein 1 in Arabidopsis thaliana. *Plant Sci*. 2021;303. doi:10.1016/j.plantsci.2020.110750

Table of Contents

List of Figures

List of Abbreviations

2,4-D	2,4-dichlorophenoxyacetic acid
5-F-IAA	5-fluoroindole-3-acetic acid
2-NAA	2-naphthalene acetic acid
5DS	(+)-5-deoxystrigol
AA	Antimycin-A
ABA	abscisic acid
ABP1	AUXIN BINDING PROTEIN 1
AOX	alternative oxidase
ARF GEF	adenosine-ribosylation-factor type small GTPases
BA	benzoic acid
BFA	Brefeldin A
BSA	bovine serum albumin
CCP	clathrin-coated pit
ccvTIR1	concave TIR1
CD	Circular Dichroism
CHX	cycloheximide
CME	clathrin-mediated endocytosis
cvxIAA	Convex IAA
D14	DWARF14
DAA	days after application
DARTS	Drug Affinity Responsive Target Stability
DAW	days after wounding
DEG	differentially expressed gene
DEX	dexamethasone
ECD	extracellular domain
EE	early endosome
EM	Electron Microscopy
ER	endoplasmic reticulum
GCI	Grating-Coupled Interferometry
GO	gene ontology
IAA	indole-3-acetic acid
IAR4	IAA-ALANINE RESISTANT4
InDel	insertion/deletion
KR	karrikin
LatB	Latrunculin B
LC-MS	liquid chromatography-mass spectrometry
LE	late endosomal

LR	lateral root
MAB1	MACCI-BOU
MAX2	MORE AXILLARY GROWTH2
MDM	Mitochondrial Dysfunction Motif
MDS	Mitochondrial Dysfunction Stimulon
MPK	Mitogen-activated protein kinase
MS	Murashige and Skoog
MS-MRM	Mass Spectrometry-Multiple Reaction Monitoring
MST	Microscale Thermophoresis
NAA	1-naphthalene acetic acid
PAT	Polar auxin transport
PDC	Pyruvate Dehydrogenase Complex
PEO-IAA	α-(phenyl ethyl-2-one)-indole-3-acetic acid
PEPR1	PEP Receptor1
PIG1	Plant Insensitive to GR24
PIN	PIN-FORMED
PISA	Pinstatic acid
PM	plasma membrane
RCR	Respiratory Control Ratio
ROS	reactive oxygen species
RT	Room temperature
SA	salicylic acid
SAUR	SMALL AUXIN UP-REGULATED
SCF	SKP1-Cullin-F-box complex
SEC	size exclusion
SL	strigolactone
SMXL	SUPPRESSOR OF MAX2 LIKE
SRM	selective reaction monitoring
SSLP	simple sequence length polymorphisms
TBO	toluidine blue
TCA	tricarboxylic acid
TF	transcription factor
TGN	Trans golgi network
TIBA	triiodobenzoic acid
TIR1	TRANSPORT INHIBITOR RESPONSE 1
TMK1	TRANSMEMBRANE KINASE 1
TPL	TOPLESS
WRKY	WRKY DNA-BINDING PROTEIN

1. Introduction

Plant growth and development is a very flexible and dynamic process which adapts to many environmental cues using endogenous signals to coordinate these responses. Fundamental to these processes are small signaling molecules, the plant hormones. Typically they are acting at extremely low concentrations either locally or in a distant part of the plant (Gray, 2004). One of the most studied hormones is auxin, which was described by Darwin in 1880 as an endogenous chemical signal which influences the effect of light on grass (Darwin and Darwin 1880). Many years later this signal was characterized to be indole-3-acetic acid (IAA), the most abundant form of endogenous auxin (Kögl et al. 1934). Since then auxin was studied extensively and was found to play a major role in almost all growth and developmental processes in plants like embryogenesis (Liu, 1993), organogenesis (reviewed in Bohn-Courseau, 2010), root and shoot development (Overvoorde et al., 2010; Vernoux et al., 2010) as well as tropic responses (Firn & Digby, 1980).

1.1 Auxin canalization

In comparison to animals, plant development is unique. This is mainly because essentially all plant organs like new leaves, flowers and roots high have a very high capability of post embryonic organ formation, but also because of the high capability of tissue regeneration after wounding (Steeves 1989). *De novo* tissue patterning important for organ formation, vascular formation, maintainance of apical dominance, shoot branching and re-patterning of tissues after wounding depends on the polarization in a coordinated manner of individual cells which are then leading to whole tissues polrization. One of the most important drivers for this is the hormone auxin. Auxin alone is able to establish its own polarized transport channels (Grones and Friml 2015). The production of auxin happens to a large extend in the immature shoot-organs. The vascular strands are then transporting the produced auxin to the roots (reviewed in Hajný et al 2022). The canalization hypothesis, which was first formed by Tsvi Sachs (Sachs, 1975), describes this unique transport properties of auxin. Auxin is transported actively, from cell to cell and in a directional manner. This works by self-regulating the polarity of its own flow by working itself as a polarizing cue (Sachs 1975; Sachs 1991; Sauer et al. 2006). The direction and throughput of the auxin flow is mediated by plasma membrane (PM) localized

auxin export proteins, the PIN-FORMED (PIN) efflux carriers (Wiśniewska et al., 2006). The auxin flow strongly depends on the polar localization of those PIN proteins. PINs are gradually polarized from the auxin source into narrow channels (Wisniewska et al. 2006; Adamowski et al. 2015). Localized and polarized PIN1 expression and thus directional auxin transport routes demarcate the position of future vascular strands (Balla et al. 2011; Benkova et al. 2003; Mazur et al. 2020; Verna et al. 2019). To ensure correct tissue patterning and vascular development, PIN subcellular localization must be tightly regulated. PIN proteins have the ability to change their subcellular localization dynamically by clathrin-mediated endocytosis (CME) and auxin can interferre with this trafficking process (Geldner et al. 2001; Dhonukshe et al. 2007; Kleine-Vehn 2008a, 2008b).

Even though auxin canalization was shown to be crucial in a magnitude of processes most of the underlying molecular mechanisms still remain enigmatic (Reviewed in Hajny et al 2021). What is known so far is that the canonical TIR1/AFB auxin transcriptional pathway is indispensable for auxin feedback on PIN polarity (Prát et al. 2018; Hajný et al. 2022). But also other non-canonical regulators like TRANSMEMBRANE KINASE 1 (TMK1), AUXIN BINDING PROTEIN 1 (ABP1) and WRKY DNA-BINDING PROTEIN 23 (WRKY23) were either shown or proposed to have a role in auxin canalization (Hajný et al. 2022).

1.2 Auxin signaling

Auxin acts as a general coordinator in a multitude of processes connected to plant growth and development. The specificity however is not given by the signal itself but rather by the way how the cells perceive and integrate this signal. A very well characterized mechanism is through changes in transcriptional levels of auxin inducible genes. This mechanism, the canonical signaling, is responsible for a wide variety of the auxin signaling output, however there is pressing evidence that this relatively slow transcriptional pathway is not sufficient to explain all of the observed auxin responses. Some auxin actions are happening too fast and within seconds which is a timeframe too fast to be dependent on transcription (reviewed in Gallei et al. 2020). After all, it was shown that transcriptional auxin signaling requires at least 10-15 minutes to be carried out (Badescu and Napier 2006).

The following review (Gallei et al. 2020) will give a more comprehensive picture about canonical and non-canonical auxin signaling with their involved transcriptional and non-transcriptional responses.

1.2.1 Auxin signaling in growth: Schrödinger's cat out of the bag

Adapted and modified from:

Gallei M, Luschnig C, Friml J. *Auxin signalling in growth: Schrödinger's cat out of the bag*. Curr Opin Plant Biol. 2020;53:43-49. doi:10.1016/j.pbi.2019.10.003

The phytohormone auxin acts as an amazingly versatile coordinator of plant growth and development. With its morphogen-like properties, auxin controls sites and timing of differentiation and/or growth responses both in quantitative and qualitative terms. Specificity in the auxin response depends largely on distinct modes of signal transmission, by which individual cells perceive and convert auxin signal into a remarkable diversity of responses. The best understood, or so-called canonical mechanism of auxin perception ultimately results in variable adjustments of the cellular transcriptome, via a short, nuclear signal transduction pathway. Additional findings that accumulated over decades implied that an additional, presumably, cell surface-based auxin perception mechanism mediates very rapid cellular responses and decisively contributes to the overall cell's hormonal response. Recent investigations into both, nuclear and cell surface auxin signalling challenged this assumed partition of roles for different auxin signalling pathways and revealed an unexpected complexity in transcriptional and non-transcriptional cellular responses mediated by auxin.

1.2.1.1 Setting the stage

1.2.1.1.1 Transcriptional signalling: the TIR1 nuclear gang

A long-standing enigma in auxin signalling has been how it is possible that such a simple chemical compound like the most common naturally occurring form of auxin, indole-3-acetic acid (IAA) can regulate such a broad variety of seemingly unrelated developmental responses ranging from e.g. the apical-basal patterning in embryogenesis to tropic growth responses. This has been explained on the one hand by additional levels of regulation at the tissue level directed by localized auxin biosynthesis[1] and directional, intercellular auxin transport[2]. These processes mediate differential auxin distribution, which in specific cells activates nuclear auxin signalling

leading to transcriptional reprogramming. The seemingly simple transcriptional pathway depends on nuclear TIR1/AFB auxin receptors and is capable to remodel the transcriptome in different contexts very differently[3]. TIR1/AFB bind auxin and at the same time act as F-box ubiquitin ligases mediating ubiquitination and protein degradation of Aux/IAAs transcriptional repressors that interact and modulate activity of AUXIN RESPONSE FACTOR (ARF) transcription factors (Figure 1). The complexity of transcriptional auxin responses is believed to originate from several hundred possible combinations of downstream Aux/IAA repressors and ARF transcriptional regulators, the latter recognizing auxin response elements (AREs) in the promoter region of auxin-controlled genes with variable specificity and affinity[4].

1.2.1.1.2 Transcriptional signalling: the ETTIN shortcut

Another mode of action by which auxin can control ARF-mediated transcription is linked to ARF3 also called ETTIN (ETT), a proposed auxin sensor that acts in gynoecium development[5]. This ARF is somewhat unusual, as it lacks the PB1 domain, required for the binding between ARFs and Aux/IAA proteins, therefore, ETT is unable to interact with proteins of the canonical auxin signalling machinery[6]. Consistently, auxin responses mediated by ETT/ARF3 have been suggested to occur independently of the TIR1/AFB pathway[5]. Instead, ETT harbours a long and intrinsically disordered C-terminal domain (ES-domain), which contains a nuclear localization signal and a Serine patch, likely to serve as a target site for multiple protein kinases[7]. The ETT ES-domain is essential for interaction with a range of transcriptional regulators controlling plant morphogenesis, such as INDEHISCENT (IND), REPLUMLESS (RPL), and BREVIPEDICELLUS (BP). Increasing auxin levels cause dissociation of these complexes, resulting in transcriptional reprogramming. Such auxin sensing occurs via ETT, highlighting an ability of auxin to directly affect the activity of transcription factors[5,7]. However, it is still unknown, how exactly auxin leads to the dissociation of these protein complexes and further structural analysis is required to characterize this novel auxin binding domain, mediating alternative auxin signalling in plant development.

1.2.1.1.3 Non-transcriptional signalling: the cell periphery underdogs

Although many developmental roles of auxin can be attributed to this variety of transcriptional responses, there are auxin-regulated processes that occur too rapidly to involve modulation of transcription. The examples of fast auxin responses include: *(i)* Ca^{2+}influx across the plasma membrane and alkalization of the apoplast occurring already within 10 seconds[8,9]; *(ii)* rapid cell expansion concomitant with microtubule cytoskeleton re-arrangement[10,11,12]; and *(iii)*

inhibition of PIN endocytic recycling and clathrin-mediated endocytosis, which occurs independently of transcription or the TIR1/AFB-Aux/IAA pathway[13,14] (Figure 1).

The molecular basis of such rapid auxin signalling has not been clarified, but the AUXIN BINDING PROTEIN 1 (ABP1) was implicated in some of these processes[15], simply due to the lack of better candidates. ABP1 has been known for almost forty years and was repeatedly and independently identified in multiple plant species, based on its ability to bind auxin[16,17,18], but remained an outsider in the auxin field for decades. A breakthrough came with identification of an ABP1 interactor, the receptor-like kinase TRANSMEMBRANE KINASE 1 (TMK1). The auxin-mediated TMK1 - ABP1 association at the plasma membrane was proposed to constitute auxin an receptor complex, activating downstream cellular processes such as those regulated by Rho of Plants (ROP) cellular switches[19,20]. However, recent clarifications that embryo lethal phenotypes are not due to *abp1* loss-of-function[21,22,23] as originally assumed, rose serious doubts about the physiological relevance of this signalling mechanism and leave the question on the function of ABP1 unclarified. Thus, apart from this frustrating lack of knowledge, we are still rather clueless about pathways that may be responsible for the fast, non-transcriptional auxin responses.

1.2.1.2 Recent additions to the auxin signalling toolbox

Most of our knowledge about auxin signalling pathways has been obtained by biochemistry and classical genetic approaches in *Arabidopsis thaliana*. Recently, sophisticated chemical tools have been developed. Synthetic auxin analogues turned out to be useful to obtain insights into the complex auxin-triggered signalling pathways. For example, 5-fluoroindole-3-acetic acid (5-F-IAA) was used to discriminate between transcriptional and non-transcriptional auxin signalling pathways, as it activates transcription but is not able to inhibit endocytosis as natural or other synthetic auxins do[24]. Additionally, PEO-IAA and auxinol are potent auxin antagonists of the TIR1/AFB pathway[25]. Another recently identified auxin analogue, Pinstatic acid (PISA), is not perceived by TIR1/AFB receptors but still triggers distinct auxin responses, such as inhibition of PIN internalization from the plasma membrane[13,14], hypocotyl elongation[26] and adventitious root formation[27]. Thus, although molecular components involved in PISA-triggered responses are still unknown, PISA may become a powerful tool for deciphering TIR1/AFB-independent auxin signalling[28].

The most sophisticated tool for discrimination between different auxin signalling pathways employs a combination of a structurally modified ligand and a genetically engineered binding

site in the corresponding receptor[29]. Convex IAA (cvxIAA), a synthetic IAA-derivative does not bind to TIR1/AFB receptors and thus does not trigger cellular auxin responses, unless applied on a transgenic line expressing the structurally engineered receptor, concave TIR1 (ccvTIR1) (Figure 2). Importantly, neither cvxIAA nor ccvTIR appear to cross-react with endogenous signalling elements due to the lack of naturally occurring binding partners, nonetheless, until the molecular basis of the other auxin receptor(s) will be clarified, we do not know whether cvxIAA might interact with any of these enigmatic binding sites. Regardless, the cvxIAA/ccvTIR1 system allows rigorous *in planta* analysis of the involvement of the TIR1/AFB pathway in distinct auxin responses. Proof of principle has been provided by employing the cvxIAA/ccvTIR1 for dissecting distinct functions of TIR1/AFB signalling in auxin-dependent regulation of organ growth[29,30].

1.2.1.3 Enigma of opposite auxin effects on growth

1.2.1.3.1 Growth promotion in shoots

Auxin regulation of plant growth fascinates biologists for almost a century, mainly because of the mystery that in aerial organs such as the hypocotyl, auxin promotes growth, whereas the identical auxin stimulus leads to a growth inhibition in roots[31,32]. Growth promotion in the shoots is believed to result from a loosening of the cell wall, resulting from auxin-induced extrusion of protons into the apoplast by the action of the plasma membrane H^+-ATPases[33,34]. This mechanism, also referred to as 'acid growth hypothesis', had been debated for a long time, as it was unclear how nuclear TIR1/AFB pathway-mediated adjustments in gene transcription could account for a growth response that occurs relatively rapidly and is mediated ultimately by processes at the cell surface[32]. Furthermore, *tir1/afb* mutant hypocotyls still elongate following auxin application[34,35]. Therefore, also ABP1 involvement was considered, supported by the fact that auxin-mediated plasma membrane hyperpolarization and swelling of protoplasts is antagonized by antibody-mediated ABP1 inhibition[11] and protoplasts from the abp1 mutant plants do not swell in response to auxin [36]. Several recent studies, including those using cvxIAA/ccvTIR1, unequivocally placed auxin-mediated apoplast acidification and concomitant growth promotion downstream of the TIR1/AFB-Aux/IAA transcriptional pathway[37,29]. In fact, non-canonical auxin signalling is dispensable for apoplast acidification and growth promotion[37]. The mechanism responsible for shoot growth promotion has been linked to transcriptional control of *SMALL AUXIN UP-REGULATED* (*SAUR*) gene family members by TIR1/AFB pathway[38]. SAURs impact on phosphatase PP2C-mediated control of H^+-ATPase phosphorylation leading to their activationand finally to the extrusion of protons

into the apoplast[39]. However, it cannot be categorically excluded that transcription-independent regulatory switches, such as control of protein stability also modulate SAUR activity in response to auxin[38].

1.2.1.3.2 Growth inhibition in roots

In contrast to effects on shoot growth, auxin inhibits root elongation growth. This classical auxin response has been used in numerous forward genetic screens to identify key components of nuclear, transcriptional auxin signalling, including the TIR1 receptor for this pathway[40]. Auxin is effective already at nanomolar concentrations and responses become apparent very fast[31]. This remained puzzling, given that the intact TIR1/AFB nuclear pathway is required for this growth response, yet the short latency period between stimulation and response argued against the involvement of transcriptional reprograming in root growth inhibition. Advancement in technology, specifically, vertical stage confocal microscopy[41] combined with root microfluidics allowed to study root growth responses to auxin with extremely high spatiotemporal resolution. Combining this setup with genetic tools, including *tir1/afb* mutants, PEO-IAA and cvxIAA confirmed (*i*) the dependence on TIR1/AFB nuclear signalling; (*ii*) response faster than 30 seconds and (*iii*) no requirement for *de novo* protein synthesis[30]. Importantly, the inhibitory auxin effect can be reverted rapidly, reflected in recovery of root growth already 2 minutes after auxin withdrawal. Furthermore testing of auxin uptake mutants together with modelling approaches, indicated that the auxin signal required for this response is perceived intracellularly[30] Thus we are dealing with a paradox, in which auxin-mediated control of root growth does not depend on transcriptional regulation, but depends on nuclear TIR1/AFB signalling so far only associated with transcriptional control of auxin responses.

Other auxin-elicited processes with an extremely short latency period include plasma membrane depolarization[42] and regulation of cytosolic Ca^{2+} levels that depends on the activity of the Ca^{2+} channel CNGC14[9] (Figure 1). These responses are too fast to involve transcriptional reprograming and thus the underlying mechanism has been matter of some debate, with both ABP1 and TIR1/AFB being considered. A recent study in *Arabidopsis thaliana* root hairs linked these rapid, auxin-mediated Ca^{2+} waves with cellular auxin influx and, significantly, with the TIR1/AFB signalling pathway[43].

Thus, whilst the TIR1/AFB nuclear pathway has so far been exclusively linked to the regulation of transcription via Aux/IAA and ARF transcriptional modules, recent results establish an unknown, non-transcriptional branch of this pathway mediating rapid inhibition of the root

growth[30] (Figure 1). Despite the certainty, regarding the involvement of TIR1/AFB receptors, the immediate downstream signalling and the actual cellular mechanisms leading to the reversible inhibition of growth, remain to be elucidated. Considering the speed of the response, it is likely that a drop of cellular turgor associated with an increase of the apoplastic pH, as shown for long-term auxin effect[44], are involved. Similarly, despite cellular Ca^{2+} homeostasis has been repeatedly proposed to play an important role[8,9], its causal involvement in auxin-mediated root growth control still needs to be demonstrated.

1.2.1.3.3 Differential growth

Some developmental processes require coordinated growth promotion and inhibition simultaneously. An excellent example is the apical hook, a structure developing in the dark to protect the delicate apical meristem structures, while it penetrates the soil. It forms by differential elongation growth, involving auxin accumulating at the inner side of the hook, where growth is inhibited[45,46,47]. Thus unlike other processes described for apical plant parts, in which auxin promotes growth, this correlation between locally elevated auxin concentrations and growth inhibition is unusual and has been mechanistically unclear.

A recent breakthrough study highlighted an involvement of TMK1 in this process. TMK1 has been originally implicated as cell surface transmitter of extracellular auxin signal perceived presumably by the ABP1[19]. Whilst a participation of the notorious ABP1 has been put into doubt, the phenotypic defects in *tmk1* and related loss-of-function mutants, which include defects in apical hook formation, clearly links this family of receptor-like kinases to developmental regulations, possibly linked to auxin action[19]. In the past, TMK1 was proposed to be involved in fast, non-transcriptional auxin signalling[48] and recently linked to activation of MPK (Mitogen-activated protein kinase) signaling during lateral root organogenesis[49].

Nonetheless, unexpectedly, it is transcriptional auxin signalling, by which TMK1 regulates apical hook development[49]. This novel mechanism involves auxin-dependent cleavage and nuclear translocation of the TMK1 intracellular kinase domain. Once in the nucleus, TMK1 kinase domain binds to and phosphorylates a set of atypical Aux/IAA, namely IAA32 and IAA34, transcriptional repressors, which lack a conserved DII domain. Therefore, unlike conventional Aux/IAAs, they cannot interact with TIR1/AFB auxin receptors, but still interact with certain ARF transcription factors, thereby modulating the transcription of auxin responsive genes, uncoupled from TIR1/AFB activity[50] (Figure 1).

It is important to stress that, whilst both TMK1- and TIR1/AFB-dependent auxin signalling converge on gene transcription regulation, modes of action differ substantially. In conventional TIR1/AFB signalling, Aux/IAA proteins get ubiquitinated and degraded in response to auxin, while the TMK1-mediated pathway results in Aux/IAA phosphorylation and stabilization. Furthermore, TIR1/AFB activity is confined mainly to the nucleus, whereas TMK1 is supposed to perceive auxin outside the cell, nonetheless, by an unclear mechanism. Apart from our current lack of knowledge, concerning mechanisms, by which TMK1 might sense extracellular auxin, it remains to be determined how these two distinct signalling pathways might be coordinated in the spatiotemporal regulation of hormonal growth responses. Regardless, by the addition of the TMK1-based mechanism to the known TIR1/AFB regulations, the auxin-mediated regulation of growth can be switched from promotion to inhibition thus allowing differential growth for the apical hook formation.

1.2.1.4 Conclusions

Five years ago, the roadmap of cellular auxin signalling appeared clarified in its major outlines. The so-called canonical, nuclear, TIR1/AFB-based auxin signalling pathway had been associated exclusively with regulation of gene transcription. This was complemented by the TMK1/ABP1 signalling module, which was much less characterized, but believed to act at the cell surface and to mediate mainly rapid, non-transcriptional responses. Recent findings shattered this comfortable picture about division of labour in auxin signalling: (*i*) ABP1 *in planta* roles are questioned due to faulty genetic material used; (*ii*) TIR1/AFB pathway has been shown to mediate also rapid, non-transcriptional auxin responses by an entirely unknown mechanism; (*iii*) On the other hand, TMK1 pathway also mediate auxin effects on transcription, converging with the TIR1/AFB pathway on the overlapping set of ARF transcriptional regulators; and (*iv*) not least, auxin has been shown to directly affect the activity of the atypical ARF transcription factor ETTIN.

Thus, it is an exciting time; the distinction between what we started to call canonical and non-canonical pathways became unclear, many questions await further investigation and we can soon expect many new insights about how the most versatile signal in plants, auxin, executes a multitude of its developmental and physiological roles.

1.2.1.5 Acknowledgements

Research in J.F. laboratory is funded by the European Union's Horizon2020 program (ERC grant agreement n° 742985); C.L. is supported by the Austrian Science Fund (FWF grant P 31493).

1.2.1.6 Figures

Figure 1 - Graphical abstract of auxin-mediated signalling processes

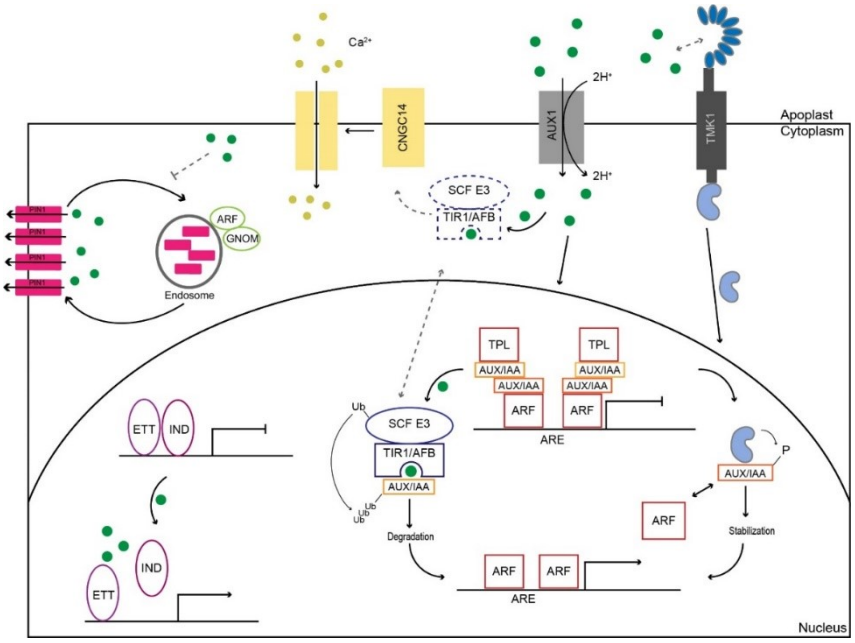

Figure 1 Section 1.2 - Graphical abstract of auxin-mediated signalling processes

Auxin (green filled circles) is transported into the cell via AUX1, presumably acting as H+ symporter. In the nucleus, auxin binds to the TIR1/AFB-Aux/IAA receptor complex and activates transcription via ubiquitination and degradation of Aux/IAA transcriptional repressors, which releases repressive ARF-Aux/IAA-TPL (TOPLESS) complexes. Furthermore, auxin in the nucleus also releases the repressive complex between ETT/ARF3 and other transcription factors such as IND, causing transcriptional reprogramming required for various developmental processes. A fraction of the TIR1/AFB-Aux/IAA receptor complex is likely to reside also in the cytoplasm, where it regulates Ca2+ influx (yellow filled circles) with involvement of the CNGC14 channel (yellow) and concomitantly inhibits root growth by an unknown mechanism. Another mechanistically unclear auxin-mediated process occurring outside of the nucleus causes modulation of the constitutive endocytic recycling of PIN auxin transporters (magenta), which requires GNOM ARF-GEF activity. An apoplastic auxin stimulus can trigger the cleavage of the C-terminal kinase domain of TMK1. The C-terminal part (blue) translocates to the nucleus, where it activates transcription by binding to the non-canonical AUX/IAAs. Dashed lines indicate elements of signalling pathways that remain to be clarified.

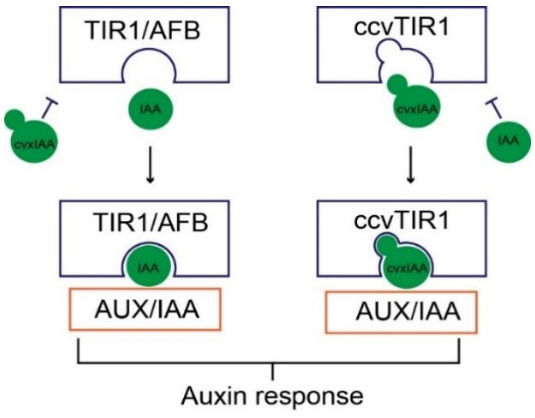

Figure 2 Section 1.2 - The engineered convexIAA-concaveTIR1 pair

Figure 2 - The engineered convexIAA-concaveTIR1 pair

The engineered cvxIAA is unable to bind the endogenous TIR1/AFB receptors but recognizes the engineered ccvTIR1 version, which, in turn, does not bind the endogenous auxin, IAA. The downstream auxin response is triggered only, when both endogenous components or the two engineered components come together.

1.2.1.7 References

1. Stepanova AN, Alonso JM (2019). From Ethylene-Auxin Interactions to Auxin Biosynthesis and Signal Integration. Plant Cell. 31(7):1393-1394. doi:10.1105/tpc.19.00339
2. Adamowski M, Friml J. (2015) PIN-Dependent Auxin Transport: Action, Regulation, and Evolution. Plant Cell Online. doi:10.1105/tpc.114.134874
3. Leyser O. (2018). Auxin Signaling. Plant Physiol. 465-479. doi:10.1104/pp.17.00765
4. Weijers D, Wagner D. (2016). Transcriptional Responses to the Auxin Hormone. Annu Rev Plant Biol. doi:10.1146/annurev-arplant-043015-112122
5. Simonini S, Deb J, Moubayidin L, et al. (2016). A noncanonical auxin-sensing mechanism is required for organ morphogenesis in Arabidopsis. doi:10.1101/gad.285361.116.
6. Guilfoyle TJ. (2015). The PB1 Domain in Auxin Response Factor and Aux / IAA Proteins : A Versatile Protein Interaction Module in the Auxin Response. doi:10.1105/tpc.114.132753
7. Simonini S, Mas PJ, Mas CMVS, Østergaard L, Hart DJ (2018). Auxin sensing is a property of an unstructured domain in the Auxin Response Factor ETTIN of Arabidopsis thaliana. doi:10.1038/s41598-018-31634-9
8. Monshausen GB, Miller ND, Murphy AS, Gilroy S. (2011). Dynamics of auxin-dependent Ca2+and pH signaling in root growth revealed by integrating high-resolution imaging with automated computer vision-based analysis. Plant J. doi:10.1111/j.1365-313X.2010.04423.x
9. Shih H, Depew CL, Miller ND, et al. (2015). The Cyclic Nucleotide-Gated Channel CNGC14 Regulates Root Gravitropism in Arabidopsis thaliana Report The Cyclic Nucleotide-Gated Channel CNGC14 Regulates Root Gravitropism in Arabidopsis thaliana. CURBIO. doi:10.1016/j.cub.2015.10.025
10. Chen X, Grandont L, Li H, et al. (2014). Inhibition of cell expansion by rapid ABP1-mediated auxin effect on microtubules. Nature. doi:10.1038/nature13889
11. Steffens B, Feckler C, Palme K, Christian M, Böttger M, Lüthen H. (2001). The auxin signal for protoplast swelling is perceived by extracellular ABP1. Plant J. doi:10.1046/j.1365-313X.2001.01103.x
12. Adamowski M, Li L, Friml J. Reorientation of Cortical Microtubule Arrays in the Hypocotyl of Arabidopsis thaliana Is Induced by the Cell Growth Process and Independent of Auxin Signaling. Int J Mol Sci. 2019;20(13):3337. doi:10.3390/ijms20133337
13. Paciorek T, Zažímalová E, Ruthardt N, et al. (2005). Auxin inhibits endocytosis and promotes its own efflux from cells. Nature. doi:10.1038/nature03633
14. Robert S, Kleine-Vehn J, Barbez E, et al. (2010). ABP1 mediates auxin inhibition of clathrin-dependent endocytosis in Arabidopsis. Cell. doi:10.1016/j.cell.2010.09.027
15. Grones P, Friml J. (2015) Auxin transporters and binding proteins at a glance. J Cell Sci. doi:10.1242/jcs.159418
16. Lobler M, Klambt D. (1985). Auxin-binding Protein from Coleoptile Membranes of Corn (Zea mays L.)
17. Zea L, Lobler M, Klambt D. (1985). Auxin-binding Protein from Coleoptile Membranes of Corn from.
18. Annegret Rück, Klaus Palme Michael A. Venis, Richard M. Napier (1993). Patch-clamp analysis establishes a role for an auxin binding protein in the auxin stimulation of plasma membrane current in Zea mays protoplasts. Pant J.
19. Dai N, Wang W, Patterson SE, Bleecker AB. (2013). The TMK Subfamily of Receptor-Like Kinases in Arabidopsis Display an Essential Role in Growth and a Reduced Sensitivity to Auxin. doi:10.1371/journal.pone.0060990
20. Xu, T., Dai, N., Chen, J., Nagawa, S., Cao, M., Li, H., Zhou, Z., Chen, X., De Rycke, R., Rakusova, H., et al. (2014). Cell surface ABP1-TMK auxin-sensing complex activates ROP GTPase signaling. Science 343, 1025–1028
21. Gao Y, Zhang Y, Zhang D, Dai X, Estelle M, Zhao Y. (2015). Auxin binding protein 1 (ABP1) is not required for either auxin signaling or Arabidopsis development. doi:10.1073/pnas.1500365112
22. Grones P, Chen X, Simon S, et al. (2015). Auxin-binding pocket of ABP1 is crucial for its gain-of-function cellular and developmental roles. J Exp Bot. doi:10.1093/jxb/erv177
23. Michalko J, Dravecká M, Bollenbach T, Friml J. (2015). Embryo-lethal phenotypes in early abp1 mutants are due to disruption of the neighboring BSM gene. F1000Research. doi:10.12688/f1000research.7143.1
24. Simon S, Kubeš M, Baster P, et al. (2013). Defining the selectivity of processes along the auxin response chain: A study using auxin analogues. New Phytol. doi:10.1111/nph.12437
25. Hayashi KI, Neve J, Hirose M, et al. (2012). Rational design of an auxin antagonist of the SCF TIR1 auxin receptor complex. ACS Chem Biol. doi:10.1021/cb200404c

26. Gray WM, Östin A, Sandberg G, Romano CP, Estelle M. (1998). High temperature promotes auxin-mediated hypocotyl elongation in Arabidopsis. Proc Natl Acad Sci U S A. doi:10.1073/pnas.95.12.7197
27. De Klerk GJ, Van Der Krieken W, De Jong JC. (1999). The formation of adventitious roots: New concepts, new possibilities. Vitr Cell Dev Biol - Plant. doi:10.1007/s11627-999-0076-z
28. Hayashi K, Oochi A, Hajny J, et al. (2019) Pinstatic Acid Promotes Auxin Transport by Inhibiting PIN Internalization. Plant Physiol. 2019. doi:10.1104/pp.19.00201
29. Uchida N, Takahashi K, Iwasaki R, et al. (2018) Chemical hijacking of auxin signaling with an engineered auxin – TIR1 pair. Nat Publ Gr. doi:10.1038/nchembio.2555
30. Fendrych M, Akhmanova M, Merrin J, et al. (2018) Rapid and reversible root growth inhibition by TIR1 auxin signalling. Nat Plants. doi:10.1038/s41477-018-0190-1
31. Evans ML, Ishikawa H. (1994). Responses of Arabidopsis roots to auxin studied with high temporal resolution : Comparison of wild type and auxin-response mutants.
32. Pflanzenphysiologie FB, Kassel U. Tansley (1994). The current status of the acid-growth hypothesis.
33. Mcqueen-mason S, Durachko DM, Cosgrove DJ. (1992). Two Endogenous Pmteins That lnduce Cell Wall Extension in Plants.
34. Takahashi K1, Hayashi K, Kinoshita T. (2012). Auxin Activates the Plasma Membrane H + -ATPase by Phosphorylation during Hypocotyl Elongation. doi:10.1104/pp.112.196428
35. Schenck D, Christian M, Jones A, Lüthen H. (2010). Rapid auxin-induced cell expansion and gene expression: a four-decade-old question revisited. Plant Physiol. doi:10.1104/pp.109.149591
36. Dahlke RI, Fraas S, Ullrich KK, et al. (2017) Protoplast swelling and hypocotyl growth depend on different auxin signaling pathways. Plant Physiol. 175(2):982-994. doi:10.1104/pp.17.00733
37. Fendrych M, Leung J, Friml J. (2016). TIR1/AFB-Aux/IAA auxin perception mediates rapid cell wall acidification and growth of Arabidopsis hypocotyls. eLife. doi: 10.7554/eLife.19048.
38. Spartz AK, Lee SH, Wenger JP, et al. (2012). The SAUR19 subfamily of SMALL AUXIN UP RNA genes promote cell expansion. Plant J. doi:10.1111/j.1365-313X.2012.04946.x
39. Spartz AK, Ren H, Park MY, et al. (2014). SAUR inhibition of PP2C-D phosphatases activates plasma membrane H+-ATPases to promote cell expansion in Arabidopsis. Plant Cell. 2014;26(5):2129-2142. doi:10.1105/tpc.114.126037
40. Ruegger M, Dewey E, Gray WM, Hobbie L, Turner J, Estelle M. (1998). The TIR1 protein of Arabidopsis functions in auxin response and is related to human SKP2 and yeast Grr1p. Genes Dev. doi:10.1101/gad.12.2.198
41. von Wangenheim D, Hauschild R, Fendrych M, Barone V, Benková E, Friml J. (2017). Live tracking of moving samples in confocal microscopy for vertically grown roots. Elife. doi:10.7554/eLife.26792
42. Bates, G. W. & Goldsmith, M. H. M. (1983). Rapid response of the plasma-membrane potential in oat coleoptiles to auxin and other weak acids. Planta
43. Dindas, J. et al. (2018) AUX1-mediated root hair auxin influx governs SCF(TIR1/AFB)-type Ca(2+) signaling. Nature communications. doi:10.1038/s41467-018-03582-5
44. Barbez E, Dünser K, Gaidora A, Lendl T, Busch W. (2017). Auxin steers root cell expansion via apoplastic pH regulation in Arabidopsis thaliana. Proc Natl Acad Sci U S A. doi:10.1073/pnas.1613499114
45. Žádníkova P, Petrášek J, Marhavý P, et al. (2010). Role of PIN-mediated auxin efflux in apical hook development of Arabidopsis thaliana. Development. doi:10.1242/dev.041277
46. Žádníková P, Wabnik K, Abuzeineh A, et al. (2016). A model of differential growth-guided apical hook formation in plants. Plant Cell. doi:10.1105/tpc.15.00569
47. Vandenbussche F, Petrášek J, Žádníková P, et al. (2010). The auxin influx carriers AUX1 and LAX3 are involved in auxin-ethylene interactions during apical hook development in Arabidopsis thaliana seedlings. Development. doi:10.1242/dev.040790
48. Grones P, Friml J. (2015). ABP1: Finally docking. Mol Plant. doi:10.1016/j.molp.2014.12.013
49. Cao M, Chen R, Li P, et al. (2019). TMK1-mediated auxin signalling regulates differential growth of the apical hook. Nature. doi:10.1038/s41586-019-1069-7
50. Huang R, Zheng R, He J, et al. (2019). Noncanonical auxin signaling regulates cell division pattern during lateral root development. PNAS. doi:10.1073/pnas.1910916116

2. Results and discussion

The result section includes all relevant research articles covering auxin signaling, auxin canalization and hormonal crosstalk between auxin and strigolactone. The chapters span over the involvement and regulation of endocytosis by auxin in canalization, the role of ABP1 in non-canonical auxin signaling and finally to the cross-talk of strigolactone in auxin canalization and non-canonical SL signaling and perception. Each research articles is included with a short introduction to the main topic of the study and the most relevant findings are summarized. Contributions of Michelle Gallei to each research article are outlined in the respective section.

2.1 Systematic analysis of specific and nonspecific auxin effects on endocytosis and trafficking

Adapted and modified from:

Narasimhan M, **Gallei M**, Tan S, et al. *Systematic analysis of specific and nonspecific auxin effects on endocytosis and trafficking*. Plant Physiol. 2021;186(2):1122-1142. doi:10.1093/PLPHYS/KIAB134

Auxins were thought to stabilize PINs at the PM by interfering with their own internalization and interfering with overall endocytosis in general (Paciorek 2005). This study is based on the use of the fungal toxin Brefeldin A (BFA) which is inhibiting transport and hence leads to the accumulation of plasma membrane proteins which are constitutively internalized, amongst others, of PINs, in intracellular BFA bodies (Geldner et al 2001). Recent studies were contradicting this finding which brought the auxin effect on endocytosis in general, but especially on PIN internalization, into question (Paponov et al., 2019; Jasik et al. 2016).

Our study aims to clarify those opposing findings and interpretations and further presents new insights into auxin regulation of endocytosis and constitutive endocytic trafficking. To differentiate between specific and nonspecific auxin effects for good we used IAA and NAA, concentrations from 10 nM to 100 mM and treatment durations ranging from 5 min to 2 h. We found that NAA as well as IAA are interfering with BFA body formation, making the use of BFA problematic for assessing auxin effects on endocytosis. Further we found that auxins do not have a general effect on the overall endocytic rate of the cell. However we found that IAA

and NAA promote specifically the endocytosis of PIN2, but not of PIN1 or other cargoes. Thus, the effects of auxin on endocytosis are according to this study opposite to those originally proposed and seem to be much more specific than initially thought.

Contributions Michelle Gallei:

- Assisting with writing the manuscript
- Correcting the manuscript
- Construction of the figures
- BFA experiments with CHX and data analysis (Figure 1)
- ST-YFP/ARF immunolocalizations (Figure S2E)
- Revising the manuscript according to reviewer comments

2.1.1 Introduction

A multitude of developmental processes throughout the lifecycle of a plant, such as organ formation, embryonic axis establishment and tropic responses are regulated by the local accumulation and asymmetric distribution of the growth regulating hormone, auxin (Bargmann et al. 2013; Lavy et al. 2016; Gallei et al. 2020). The formation and maintenance of directional polar auxin transport (PAT) between cells is regulated by polarly localized plasma membrane (PM)-based auxin efflux carries from the PIN protein family (Adamowski et al. 2015; Grones et al. 2015).

Auxin itself has the ability to dynamically change the subcellular localization of PINs at the PM by forming a feedback loop between auxin signaling and transport (Ravichandran et al. 2020). This was proposed to facilitate the rise of new polarized routes of auxin transport (Mazur et al. 2016; Prát et al. 2018; Mazur et al. 2020a). This canalization mechanism plays a role in the developmental processes involving flexible formation of new vasculature, such as leaf venation (Scarpella et al. 2006), vasculature regeneration after wounding (Sauer et al. 2006; Mazur et al. 2016; Mazur et al. 2020b) and connecting organs at the shoot apical meristem (Benkova et al. 2003) or lateral buds to pre-existing vasculature (Balla et al. 2011; Shinohara et al. 2013; Zhang et al. 2020). Furthermore, auxin-mediated changes in PIN polarity were also observed during apical-basal axis formation during embryogenesis (Robert et al. 2018, 2013; Wabnik et al. 2013) or during termination of shoot bending responses (Rakusová et al. 2016, 2019).

Dynamic changes in PIN polarity including those mediated by auxin itself have been linked to constitutive PIN cycling from and to the PM (Geldner et al. 2001; Dhonukshe et al. 2007; Kleine-Vehn 2008a, 2008b). Constitutive internalization and recycling of PINs is also important for the regulation of steady-state PIN polarity (Kleine-Vehn et al. 2011; Glanc et al. 2018), and interference with this process, for example, by disturbing phosphorylation and dephosphorylation switches, leads to severe growth defects (Barbosa et al. 2018; Grones et al. 2018).

The constitutive internalization of PINs was shown to be through clathrin-mediated endocytosis (CME) (Dhonukshe et al. 2007; Kitakura et al. 2011; Adamowski et al. 2018). By nonspecifically interfering with CME, auxin could increase its own efflux by stabilizing PINs at the PM and consequently organize PAT within tissues (Paciorek et al. 2005; Robert et al., 2010). This is unlike most other hormones, which regulate the endocytosis of their own receptors and related proteins but not overall endocytosis of the cell (Irani et al. 2012; Di Rubbo et al. 2013; Belda-Palazon et al. 2016). However this is complicated by the fact that auxin imparts two opposite effects on PINs. Studies have shown that over long-term (>2 h) auxin causes the loss of PIN2 and its subsequent degradation (Abas et al. 2006). Notably canalization-related PIN polarity changes at the PM occur at a similar time-frame (Vieten et al. 2005; Sauer et al. 2006; Baster et al. 2013). In contrast, short-term auxin treatments (< 1 h) stabilize PINs at the PM by inhibiting CME (Paciorek et al. 2005; Robert et al. 2010; Oochi et al. 2019).

Various auxin effects on PIN trafficking have been observed using different auxin isoforms; however, the synthetic auxin 1-naphthalene acetic acid (NAA) was used preferentially in most studies (Paciorek et al. 2005; Abas et al. 2006; Robert et al. 2010) due to its reported higher stability in comparison to the natural auxin, indole-3-acetic acid (IAA), (Paciorek et al. 2005). However, there have been a number of recent reports that show that the natural auxin, IAA, mediates its effect rapidly (faster than a minute) and remains active and effective for an extended period of time, such as 48 h (Eliasson et al. 1989; Fendrych et al. 2018). The half-life of active IAA was estimated by UPLC-MS to be 35 h (Paponov et al. 2019). The property of auxin to interfere with endocytosis and related processes was mainly inferred indirectly by the use of Brefeldin-A (BFA). BFA is a fungal toxin, which inhibits trafficking from endosomes to the PM, by targeting the guanosine nucleotide exchange factor of adenosine-ribosylation-factor type small GTPases (ARF GEF) known as GNOM (Geldner et al. 2003; Naramoto et al. 2014). Consequently BFA treatment causes reversible aggregation of endosomes into 'BFA bodies' in Arabidopsis roots (Paciorek et al. 2005; Kania et al. 2018; Zhang et al. 2020). As

BFA has no direct effect on the endocytic rate of cargoes from the PM to the endosomes (Naramoto et al. 2010), observation of endocytosed cargoes in the BFA bodies has been extensively used as an indirect measure of the internalization rate (Geldner at al. 2001). When co-treating with BFA and auxin, intracellular accumulation of PIN1, PIN2 and other cargo proteins in BFA bodies is inhibited suggesting a decrease in the endocytosis of these cargoes (Paciorek et al. 2005). The auxin effect on endocytosis, more specifically on CME, has been further supported by auxin-mediated inhibition of internalization of the endocytic tracer FM4-64 (Jelínková et al. 2010) and reduced clathrin incidence at the PM (Paciorek et al. 2005; Robert et al. 2010). This auxin effect on endocytosis is non-transcriptional and does not require the canonical TIR1/AFB auxin pathway but has been linked to the Auxin Binding Protein 1 (ABP1), based on the gain-of-function and generic, conditional loss-of-function studies (Robert et al. 2010; Grones et al. 2015). However, due to the lack of obvious phenotypic defects in the verified *abp1* knock-out alleles (Gao et al. 2015; Grones et al. 2015; Michalko et al. 2016; Gelová et al. 2020), the cellular function of ABP1 remain to be understood.

In addition to the short-term auxin inhibitory effect on overall endocytic processes, prolonged auxin treatments lead to a decrease in the PM or microsomal fraction incidence of some cargoes, in particular, PIN2. This would imply an increase in endocytosis and degradation (Abas et al. 2006; Baster et al. 2013). Use of the photo-convertible fluorescent variants of PIN2 confirmed this auxin-mediated PIN2 degradation and also revealed a significant contribution of *de novo* synthesized PIN2 to the PIN2 protein pool accumulating in BFA bodies (Jasik et al 2016; Salanenka et al. 2018). Moreover, PIN1 accumulation in the BFA bodies can be inhibited not only by active auxins, such as NAA, but also its inactive analogue, 2-NAA (Paponov et al.2019); however, previously it was shown that 2-NAA was less effective in mediating the process (Paciorek et al. 2005).

All these partly contradictory observations and interpretations are hard to reconcile into a coherent mechanistic understanding of auxin effects on endocytic trafficking. Thus, given the potential importance of these processes and their auxin regulations for feedback control of auxin homeostasis (Paciorek et al. 2005) or coordinated polarization and auxin channel formation (Wabnik et al. 2010; Mazur et al. 2020a), it is paramount to revisit these questions using state-of-the art visualization and genetic tools.

Here we clarify the previously observed auxin effects and their interpretations, and further present new insights into auxin regulation of endocytosis and constitutive endocytic trafficking.

We used the synthetic auxin NAA and the natural auxin, IAA, for all our studies. To differentiate between specific and nonspecific auxin effects, we chose incremental concentrations from 10 nM to 100 µM and treatment durations of 5 min to 2 h. We further provide: (i) a better characterization of the effects of NAA and IAA on different cellular processes including CME and intracellular trafficking; (ii) comparisons of the effects between NAA and IAA on different cargoes; and (iii) the identification of a rapid, specific endocytic auxin effect; during which NAA and IAA, even at very low concentrations, specifically promote internalization of PIN2.

2.1.2 Results

2.1.2.1 Both NAA and IAA interfere with BFA-induced intracellular cargo accumulation and endosomal aggregation

It has been shown that co-treatment of different auxins and auxin-analogues, such as IAA, NAA, 2,4-dichlorophenoxyacetic acid (2,4-D), α-(phenyl ethyl-2-one)-indole-3-acetic acid (PEO-IAA), 2-naphthalene acetic acid (2-NAA) and pin static acid (PISA) with BFA leads to reduced intracellular cargo (typically exemplified by PIN1 or PIN2 accumulation), in BFA bodies (Paciorek et al. 2005; Robert et al. 2010; Jasik et al. 2016; Oochi et al. 2019; Paponov et al. 2019). Since neither auxin, nor BFA has been shown to inhibit transcription and translation of PINs (Paciorek et al. 2005; Vieten et al. 2005), reduced PINs and other cargoes in BFA bodies implies that auxin inhibits overall endocytosis. The visualization of a protein of interest, be it endocytosed cargo, *de novo* synthesized, secretory or recycled protein, is facilitated by a general aggregation of the endomembrane system in response to BFA, resulting in accumulation and concentration of the protein (Satiat-Jeunemaitre and Hawes 1994; Geldner et al. 2003; Kleine-Vehn et al. 2008a; Feraru et al. 2012; Kania et al. 2018). Already the earlier studies noted that the natural auxin, IAA, is significantly less effective than the synthetic auxin, NAA in reducing the intracellular endocytosed cargo accumulation (Paciorek et al. 2005; Paponov et al. 2019) and other studies using photo-convertible tag showed specifically for PIN2, a major contribution of the *de novo* synthesized proteins to BFA bodies formation in presence of auxin (Jasik et al. 2016). These observations do not support a specific, regulatory auxin effect on endocytosis. Therefore, we decided to resolve the contradictions by evaluating BFA as a tool for studying auxin effects. We first aimed to better characterize the NAA and IAA effects on BFA-induced endomembrane aggregation and further evaluate their effects on the intracellular accumulation of the endocytic cargo, PIN2.

Using confocal microscopy, we observed the endosomal system aggregation simultaneously with a cargo after BFA and auxin treatments. We used high BFA concentrations, such as 37.5 or 50 μM for the duration of 30-60 min in order to mediate the formation of bigger and more pronounced BFA bodies (Paciorek et al. 2005; Jasik et al. 2016; Paponov et al. 2019). And we used high NAA and IAA concentrations such as 10 μM and 20 μM to emulate the previously studied auxin-BFA effects (Paciorek et al. 2005; Robert et al. 2010; Jasik et al. 2016). First we followed the aggregation of the EE/TGN marked by VHA-a1-RFP (Dettmer et al. 2006) and the protein, PIN2-GFP that includes both *de novo* synthesized and the endocytosed cargo pools (Figure S1B-D). To make sure that high concentrations of IAA and NAA do not affect the localization of VHA-a1 at the EE/TGN, we performed co-localization studies of VHA-a1-GFP with ARF1, a marker of Golgi and EE/TGN (Robinson et al. 2011). The study confirmed that treatment with 10 μM of neither IAA nor NAA for 1.5 h period modified the VHA-a1 localization (Figure S1A).

Under mock conditions (DMSO/EtOH + BFA) BFA bodies consisted of pronounced endosomal VHA-a1-RFP aggregations, and corresponding strong accumulation of PIN2-GFP (both *de novo* synthesized and endocytosed) in the same structures (Figure S1B). In combination with high concentrations of either IAA or NAA (IAA/NAA 10 μM + BFA), there was a substantial decrease in the size of the VHA-a1 aggregations. Cells contained smaller bodies of around 3 μm^2 and the PIN2 signal in the partial aggregates was diffuse and less intense (Figure S1B-D). We further tested the NAA and IAA effects specifically on the endocytic PIN2 pool by co-treating with the protein synthesis inhibitor, cycloheximide (CHX) (Obrig et al. 1971) (Figure 1A-C). The accumulation of PIN2 in the BFA bodies in the mock condition (CHX + DMSO + BFA) despite the inhibition of protein synthesis confirmed that the observed PIN2 pool is largely derived from endocytosed PM PIN2 pool and pre-existing endosomal PIN2. Consistent to the previous observations, we saw that high IAA and NAA concentrations (CHX + IAA/NAA + BFA), such as 10 μM or more, interfered with the EE/TGN aggregation to form BFA bodies leading to a decreased PIN2 signal (Figure 1A-C). We made similar observations using yet another EE/TGN marker - CLC2-GFP (Konopka et al. 2008), where co-treatment of BFA and NAA (10 μM) resulted in smaller CLC2-GFP marked aggregates and concomitantly less anti-PIN2 signal in these aggregates (Figure S1E).

These observations were further corroborated by experiments using the late endosomal (LE) marker, ARA7-RFP (Jia et al. 2013), which showed clear co-localization with PIN2-GFP already in the absence of BFA or auxin treatment (Figure S2A). We tested the BFA-induced

aggregation of LE and PIN2 cargo in the presence of both NAA and IAA with and without CHX treatment (Figure 1D-F, S2B-D). Consistent with the EE/TGN markers, we clearly observed a concentration-dependent IAA effect on the ARA7-RFP-marked LE aggregations and concomitantly on the PIN2 cargo. At higher IAA and NAA concentrations, such as 10-20 μM, the LE aggregated only partially or not at all, and the PIN2 intensity in the BFA bodies was correspondingly low. However, at a lower IAA concentration, 50 nM, the ARA7 aggregates remained whole and aggregated and the PIN2 intensity was high and on par with the mock condition (Figure 1D-F).

Finally, we observed the Golgi apparatus, whose stacks arrange at the periphery of BFA bodies around the tightly packed endosomes in their center (Satiat-Jeunemaitre et al. 1996; Naramoto et al. 2014). In the presence of 20 μM NAA or IAA (BFA + NAA/IAA), one could clearly observe disarrayed Golgi apparatus (marked by ST-YFP and anti-ARF1 (Boevink et al. 1998; Robinson et al. 2011)) around loosely dispersed EE/TGN structures (also marked by ARF1 (Robinson et al. 2011)) in less compact BFA bodies (Figure S2E).

These observations show that high concentrations of NAA and IAA nonspecifically interfere with the aggregation of different types of endosomes and the Golgi apparatus during the formation of BFA bodies, thus leading to reduced accumulation of protein pools – be it *de novo* synthesized proteins or endocytosed cargo. Therefore, cargo endocytic rates are underestimated by the inability to concentrate the endocytosed cargoes in BFA bodies. Thus, the identified auxin effect on BFA-induced endosomal aggregation makes it difficult to distinguish between contributions of endomembrane aggregations and endocytic internalization of cargoes. So previous reports that auxin inhibits cargo internalization from the PM, which was based on auxin inhibiting the cargo accumulation in the BFA bodies (Paciorek et al. 2005; Robert et al. 2010) needs to be re-evaluated, preferentially using other approaches.

2.1.2.2 NAA but not IAA inhibits the internalization of FM4-64

The inhibitory effect of auxin has so far been inferred using BFA as an indirect tool. Given the inhibitory effects of NAA and IAA on the BFA-mediated endomembrane aggregation, the interpretation of the effect of auxin on cargo endocytosis gets more complicated, hence the question whether auxin inhibits endocytosis still remains. An alternative tool to BFA to evaluate the endocytic rate is to quantify the intracellular signal of an amphiphilic styryl dye, such as FM4-64 that stains the PM and gets inside the cell only by membrane internalization (Jelínková et al. 2010). The internalized FM4-64 stained membranes reach the EE/TGN and

over time spread over the entire endomembrane system (Rigal 2015). Previous studies have shown that auxin decreases FM4-64 internalization into the cells, supporting the conclusion that auxin inhibits the overall endocytosis of the cell (Paciorek et al. 2005; Zwiewka et al. 2015). However, the reports were predominantly based on NAA or NAA + BFA co-treatment; and the effects of IAA have not been analyzed extensively. Therefore, we decided to evaluate the NAA ad IAA concentration-dependent effects on FM 4-64 internalization.

We quantified FM4-64 internalization in the root epidermal cells at increasing NAA and IAA concentrations from 10 µM to 100 µM for 0.5 h (Figure 2A-C, S3A). We detected a decrease in the intracellular FM4-64 signal at 10 µM NAA (Figure 2A,C) and the signal got progressively weaker as the NAA concentration increased (Figure S3A). At 100 µM there was almost no observable intracellular FM4-64 signal (Figure 2A,C). However, the natural auxin IAA had no effect on FM4-64 internalization even at a concentration as high as 100 µM (Figure 2B,C). FM4-64 stained PM still got internalized and reached EE/TGN with no obvious defects/delays.

In summary the synthetic auxin NAA inhibits FM4-64 labeling of endosomes in a concentration-dependent manner. Nonetheless, IAA, even at high concentrations elicits no such effect.

2.1.2.3 NAA but not IAA interferes with the structure and identity of the endomembrane system

We further investigated the observed disparity between the effects of NAA and IAA on FM4-64 internalization (Figure 2A-C, S3A). Less intracellular FM4-64 staining after NAA could be attributed to either or a combination of: (i) inhibited endocytosis, (ii) defective transport of endocytosed vesicles and endosomes along actin network, (iii) affected endomembrane system. The scenarios (ii) and (iii) may prove that FM4-64 internalization would not be an ideal tool to study the effect of NAA on endocytosis.

We first tested the effect of NAA on endosomal movement and transport, as defective vesicular transport could result in less FM4-64 dye reaching the EE/TGN (Video S1, Figure S3B). Auxin has been suggested to modify actin bundling (Rahman et al. 2007). Thus, NAA may potentially alter the transport efficiency along the cytoskeletal network as observed for the auxin transport inhibitor, triiodobenzoic acid (TIBA) (Dhonukshe et al. 2008). Therefore, we tested the trafficking of ARA7-RFP marked endosomes in root epidermal cells after 20 µM NAA treatment. We observed no obvious endosomal mobility defect after NAA application and the

endosomal transport speed was comparable to that of mock condition; whereas blebbistatin, a potent myosin inhibitor (Kovács et al. 2004), significantly reduced the speed (Video S1, Figure S3B).

Next, we tested the effects of varying NAA and IAA concentrations on the endomembrane system itself (Figure 2D-F, S3C). We first tested their effects on the number and the distribution of EE/TGN structures in root epidermal cells, marked by VHA-a1-RFP. We observed that at very high NAA concentration (100 µM) there were far less EE/TGN structures in the cells compared to the mock condition (Figure 2D). However, at lower NAA concentrations, like 10 and 50 µM, there was no obvious decrease in the number of these structures (Figure S3C). In contrast, IAA, even at high concentration of 100 µM, did not affect the EE/TGN, which is also reflected by the unchanged FM4-64 signal (Figure 2B-D). This indicates that higher concentrations of the synthetic auxin NAA have a profound impact on EE/TGN structures.

To further explore the auxin effect on the EE/TGN structures, we looked at phosphatidylinositols, the molecules that confer basic identity to the endomembrane system and that are therefore important for its efficient functioning (Noack and Jaillais 2017). It was reported that NAA increases the amount of phosphatidylinositol-4,5-bisphosphate ($PIns(4,5)P_2$) while decreasing the amount of phosphatidylinositol-4-monophosphate (PIns(4)P), thus altering their ratio at the PM (Tejos et al. 2014). We, therefore, tested if the observed loss of EE/TGN structures could correspond to changes in endomembrane composition (Figure 2E,F). To that end, we applied 20 µM NAA for 1 to 2 h and observed the cellular PIns(4)P levels with FAPP1-Citrine biosensor (Simon et al. 2014). There was a significant increase in intracellular intensity (Figure 2E,F) suggesting increased PIns(4)P levels at the EE/TGN. Importantly, after 50 µM NAA treatment, we observed a similar increase in intracellular intensity already after 30 min of treatment; and notably there were far less EE/TGN structures with high PIns(4)P levels (Figure 2E,F). After 2 h of treatment, the structures completely disappeared (data not shown), similar to the observations made in the VHA-a1 marker line (Figure 2D). However, IAA treatment, even after 2 h at 10 µM, had no effect on the PIns(4)P levels (Figure 2E,F). These results indicate that NAA significantly affects the phosphatidylinositols of the EE/TGN system, and at higher concentrations, degenerates the number and distribution of EE/TGN structures, which was also observed in the VHA-a1 marker line and by FM4-64 staining (Figure 2A-D).

In summary, NAA, at high concentrations, has a profound effect on the endomembrane system, its morphology and phosphatidylinositol composition; but IAA does not. This suggests that the observed NAA-mediated decrease in the intracellular FM4-64 staining, albeit observed already at lower concentrations, may be, at least in part, due to the affected EE/TGN structures. This effect, presumably, also contributes to the NAA effects on the BFA body formation and may provide an explanation for the previously reported auxin-mediated decrease in endocytosed cargo and intracellular FM4-64 at the EE/TGN (Paciorek et al. 2005). In order to unambiguously evaluate the effects of NAA on the overall endocytic rate of the cell, alternative tools, which do not involve imaging at the affected EE/TGN system, should be used. Hence, we opted to directly visualize and measure endocytosis at the PM.

2.1.2.4 IAA and NAA do not affect the individual CME events at the PM

The synthetic auxin NAA, besides inhibiting endocytic internalization of cargoes, has also been shown to decrease the incidence of the key components of CME, like the coat protein clathrin at the cell surface (Robert et al. 2010; Grones et al. 2015). We re-evaluated these observations to determine possible direct effects of auxin on CME at the PM.

First, we have re-evaluated the NAA effects on clathrin localization at the PM by visualizing CLC1-GFP (Wang et al. 2013) in root epidermal cells using confocal microscopy. After 1 h of 10 μM NAA application, we confirmed a decrease in the PM clathrin signal (Figure S4A,B) that potentially indicates lower density of CME events.

To assess a possible auxin effect on CME, we tested the effects of both NAA and IAA by directly looking at individual endocytic events at the PM of root epidermal cells using TIRF microscopy (Johnson and Vert 2017). We observed the endocytic foci, marked by CLC2-GFP, after short-term NAA treatment (5-10 min) at a concentration (10 μM) that showed a significant decrease in FM4-64 internalization (Figure 2A,C) but did not cause visible endomembrane defects (Figure S3C), thus avoiding nonspecific effects. We saw no significant changes in the overall lifetime distribution of the endocytic foci or their density (Figure 3A-C). Furthermore, we observed the clathrin intensity profile of all the PM foci and saw no obvious difference in the presence or absence of NAA treatment (Figure 3D,E). The clathrin-coated pit (CCP) progressively develops as clathrin polymerizes at the pit, which can be classified into the following developmental phases: assembly, maturation and scission. By observing the clathrin foci intensity over time, we could trace the CCP developmental profile (Loerke et al. 2009; Narasimhan et al. 2020). We analyzed the developmental profile of the foci with the average

lifetime population (18-24 s) after NAA and mock treatments. The analysis did not reveal any significant differences in the duration or other characteristics of any of those phases (Figure S4C). We further performed the same experiment with IAA (10 µM; 5 min). We observed no significant differences in CCP density, lifetime distribution or intensity and developmental profile (Figure 3F-J, S4D). This shows that short-term treatments of neither NAA nor IAA alter the individual clathrin endocytic foci at the PM; and by extension, the overall capacity of CME.

In summary, NAA, over long-term, decreases clathrin incidence at the PM and consequently, could potentially alter the overall endocytic rate of the cell. However, observation of short-term effects of both NAA and IAA on large number of individual CME events at the PM did not reveal any alterations in the incidence or dynamics of the CME machinery. Nonetheless, we cannot exclude the possibility that auxin regulates endocytosis of specific cargoes under specific conditions, for example regulatory mechanisms such as phosphorylation or ubiquitination (Mettlen et al. 2018; Zwiewka et al. 2019) instead of targeting the entire clathrin machinery at the PM.

2.1.2.5 Both NAA and IAA promote endocytosis of PIN2 but not of other cargoes

Our analysis did not reveal any effects of NAA or IAA on the overall CME. However, we wanted to test if auxin has the potential to regulate the internalization of specific cargoes. Notably, we chose alternative tools and imaging techniques to follow the cargoes directly at the PM and not rely on their indirect observation post-endocytosis in the endosomal system (EE/TGN or LE). We first analyzed PIN2, as diverse effects of auxin on the internalization and stability of this protein are well-described (Abas et al. 2006; Baster et al. 2013). We employed the photo-convertible PIN2-Dendra (Jásik et al. 2013; Salanenka et al. 2018), which allows imaging of the pre-existing PIN2 in the red channel and the newly synthesized PIN2 pool in green after photo-conversion. Following the photo-converted PIN2 over time provides a cleaner evaluation of the rate of endocytosis.

We treated the roots with varying NAA (5 µM, 10 µM, 20 µM) and IAA (50 nM, 200 nM, 10 µM) concentrations and followed the photo-converted PIN2 signal in the epidermal cells of the entire root tip using confocal microscopy (Figure 4A-F, S5A-C). With all these different concentrations of both IAA and NAA, we consistently observed a pronounced decrease in PIN2 PM signal over time compared to the mock condition (45 min to 3 h) (Figure 4A-D, S5A-C). This suggests that auxin promotes the rate of PIN2 endocytosis from the PM, which is consistent with earlier observations (Abas et al. 2006). We further examined the lowest IAA

concentration that could elicit the same response. We saw that a concentration as low as 10 nM could promote PIN2 endocytosis, albeit not as pronounced as at 50 nM or higher (Figure S5A,B). Next, we tested how early IAA and NAA can trigger a significant response. We used the microfluidic RootChip set-up (Fendrych et al. 2018), which allows for a controlled and fast drug application during imaging. We observed that as early as 5 min (until ≥30 min) after IAA and NAA application promotion of PIN2 endocytosis was significant (Figure 4E,F). These results were further confirmed by Western blots showing that the total PIN2 amount decreases substantially within 5 min of 1 μM IAA treatment (Figure S5D,E), meaning that PIN2 was not only endocytosed but also degraded in a rapid manner.

We then tested if auxin mediates endocytosis of only PIN2 or other efflux carriers, such as PIN1. PIN1 is localized in root endodermis and stele (Friml et al. 2002); however, we used the line PIN2::PIN1-Dendra to express PIN1 in epidermal cells like in the case of PIN2. This ensures observing the protein-specific effects eliminating the tissue-associated effects of auxin. We applied 10 μM IAA and followed the photo-converted PIN1 signal. Surprisingly, unlike PIN2, we observed no decrease in PIN1 PM intensity over time (Figure 4G,H). Even at high IAA concentrations (10 μM), there was no increase or decrease over the basal constitutive endocytic rate; meaning auxin did not influence PIN1 endocytosis.

Next, we investigated if auxin generally influences PM cargoes, or has a specific effect only on PIN2. To that end, we tested a cargo unrelated to auxin or its signaling: PEP Receptor1 (PEPR1). PEPR1 is an immune response receptor localized at the PM of the root meristem. Following binding of its signal peptide pep1, it undergoes endocytosis and subsequent degradation (Huffaker et al. 2006; Ortiz-morea et al. 2016). After a brief pep1 pulse, we followed the PEPR1 PM signal in the presence of mock and IAA treatments (Figure 4I,J, S5F). 1 h after the pulse we observed a substantial PEPR1 loss from the PM (untreated vs pep1 pulsed), however, there was no significant increase or decrease between the treatments (mock vs IAA) (Figure 4I,J). This implies that IAA does not alter the endocytic rate of PEPR1. Furthermore, we evaluated the long-term auxin effect on PEPR1 endocytosis by pre-treating the seedlings with NAA, IAA or mock, followed by a pep1 pulse to internalize PEPR1 in the presence of mock and auxin treatments. Once again, there was no difference in PEPR1 internalization between treatments 1 h after the pep1 pulse (Figure S5F). This shows consistently that both endogenous and synthetic auxins (IAA and NAA) do not regulate the overall endocytosis of all cargoes but specifically affect the PIN2 auxin transporter. This is in line with IAA not influencing the overall FM4-64 internalization (Figure 2B,C).

In summary, by directly following a cargo unrelated to auxin – PEPR1 and two auxin-related cargoes, PIN1 and PIN2 efflux carriers, we observed that auxin promotes the endocytosis of PIN2 but does not influence other cargoes. This effect is clearly distinct from less specific effects of higher concentrations of synthetic auxins on BFA- and FM4-64 visualized endocytosis (Paciorek et al. 2005). Instead, this specific, pronounced effect on PIN2 endocytosis is elicited by both synthetic and natural auxins rapidly and at low concentration.

2.1.2.6 Constitutive clathrin-mediated PIN2 internalization maintains apical PIN2 polarity

Inhibition of PIN endocytosis by auxin has been proposed to be a central mechanism for establishing auxin transport channels (Wabnik et al. 2010; Robert et al. 2010; Mazur et al. 2020a) and for asymmetric auxin distribution during gravitropic response (Abas et al. 2006; Baster et al. 2013). However, the physiological role of the identified auxin-mediated promotion of PIN2 internalization remains unclear.

It has been shown that PINs undergo constitutive endocytosis and recycling, thus maintaining their polar distribution (Kleine-Vehn et al. 2011; Glanc et al 2018). Previous studies have indicated that constitutive basal-rate of PIN2 internalization from the PM is clathrin-mediated (Dhonukshe et al. 2007; Kitakura et al. 2011). To that end, we monitored the basal endocytic rate of PIN2-Dendra and, furthermore, analyzed the rate after blocking CME by using the inducible over-expression line *XVE::AUXILIN-LIKE2* (Adamowski et al. 2018) (Figure 5A). After inducing *AUXILIN-LIKE2 (AXL2)* over-expression for ~24 h, we observed a significant decrease in the basal PIN2 endocytosis rate (Figure 5A); this is consistent with PIN2 constitutive endocytosis being clathrin-mediated (Dhonukshe et al. 2007; Narasimhan et al. 2020). Furthermore, when we looked at the PIN2 polarity after *AXL2* overexpression, the apical polarity was lost and there we observed an aploarPIN2 localization along the lateral sides (Figure 5B,C). This shows that maintaining a basal rate of constitutive PIN2 endocytosis is vital for PIN2 apical polarity maintenance, as suggested before (Kleine-Vehn et al. 2011).

Then, we investigated if auxin mediates PIN2 internalization specifically through the CME pathway (Figure 5D-F). After 24 h *AXL2* induction, we applied high IAA and NAA (10 µM) concentrations. We observed that both auxins no longer promoted PIN2 internalization (Figure 5D-F), proving that auxin indeed promotes PIN2 internalization via CME. In parallel, we also investigated if PIN1 internalization happens through CME and further assessed if it is influenced by auxin (Figure S6A). To this end, we quantified the interaction between PIN1 and

μ2 adaptin, which is necessary for cargo recognition during CME (Marcote et al. 2016), using pull-down experiments with and without NAA treatment. We observed a positive μ2-PIN1 interaction, however there was no increase or decrease in the interaction in the presence of NAA. This proves that the constitutive endocytosis of PIN1 is clathrin-mediated, but unlike PIN2 endocytosis, it is not enhanced by auxin. Unfortunately, we failed to perform similar experiments with PIN2, presumably due to the low stability of the PIN2 protein.

Based on these results, it is conceivable that cellular auxin levels specifically regulate the basal rate of constitutive, CME-mediated PIN2 endocytosis presumably to uphold apical PIN2 polarity, and possibly contribute to polarity re-establishment.

2.1.3 Discussion

In this study, we have explored the effects of both natural and synthetic auxins, IAA and NAA, on endocytosis and related trafficking processes. We show that high auxin concentrations, particularly of the synthetic auxin, NAA, which interfere with uptake of the lipophilic endocytic tracer FM4-64 or with intracellular accumulation of endocytic cargoes in response to trafficking inhibitor, BFA, also affect the identity and the distribution of the endomembrane system and interfere with its aggregation after BFA treatment. This renders these commonly used approaches, such as FM4-64 uptake or BFA treatment with their ineffectuality of observing the endocytosed cargo indirectly together with the endomembrane system, problematic for assessing auxin effects. By state-of-the-art imaging techniques that enable direct monitoring of the individual endocytic events or the amount of cargoes at the PM, we did not observe any general and direct effects on endocytosis but detected that both NAA and IAA, rapidly promote endocytosis of PIN2 auxin transporter only. This rapid positive effect of auxin on PIN2 endocytosis may be relevant for the auxin regulation and maintenance of its polar distribution.

2.1.3.1 Nonspecific auxin effects on the endomembrane system and BFA-sensitive trafficking

BFA treatment in Arabidopsis leads to aggregation of endosomes and other endomembrane organelles together with their endocytic, secretory and vacuolar-targeted cargoes to form BFA bodies (Geldner et al. 2003; Paciorek et al. 2005; Kleine-Vehn et al. 2008a; Feraru et al. 2012; Kania et al. 2018). Our re-evaluation of auxin effects revealed that NAA and IAA at different concentrations interfere with BFA-induced cargo aggregations and modify the endomembrane system to a different extent. While the natural auxin IAA shows mild effects, the synthetic

auxin NAA is more effectual (Simon et al. 2013). The underlying cause of this difference remains unclear.

Several mutants have been described for their decreased sensitivity to the NAA inhibition of BFA-induced PIN aggregation. For example mutations in the Callosin-like protein BIG cause auxin-insensitive BFA-induced PIN aggregations (Paciorek et al. 2005) but the underlying mechanism remains unclear. Notably, many of these mutants have defects in the homeostasis and distribution of lipid components in the endomembrane system, including sterol biosynthesis mutants (Pan et al. 2009; Carland et al. 2010), phosphatidylserine biosynthesis (Platre et al. 2019) and aminophospholipid flippase mutants (Zhang et al. 2020). The phosphatidylserine biosynthesis mutant *pss1-3* has prominent BFA bodies, which are resistant to NAA. Additionally, *pss1-3* and ROP6^{7Q} (which has abolished phospholipid interaction) show mislocalization of ROP6 in the endosomes (Platre et al. 2019). The phospholipid translocator – ALA3 flippase is localized at the EE/TGN and its mutants also have NAA-resistant prominent BFA bodies. Consistently, we found that NAA modifies the ratio of lipids, PIns (4)P and PIns(4,5)P_2 (Figure 2E,F) (Tejos et al. 2014). The components of the endomembrane system that are associated to the membrane lipids - PSST, ROP6, ALA3, Pins(4)P etc., could potentially be important contributors to the BFA-induced endomembrane aggregation.

Another set of experiments showed that pH might modify the BFA effect (Figure S7). When we incubated the roots in medium of pH 5.7, we observed PIN1-GFP in BFA bodies. The aggregates in general were smaller; additionally, the NAA effect on BFA body disaggregation was stronger. However, at pH 7.0, the BFA bodies were more pronounced and the NAA effect on disaggregation of the BFA bodies was not significant. The pH was shown to affect the membrane properties (Petelska et al. 2000). pH and ionic homeostasis are vital for the effective functioning of the endomembrane system and also for the BFA body formation (Dejonghe et al. 2016; Sze et al. 2018). These results suggest that NAA may affect the endomembrane system through pH changes.

Jointly, these observations suggest a tight interplay between effects of auxin analogues and the endomembrane lipid composition. This could explain some effects of NAA, such as reduced number of functional endosomes, possibly also the reduced internal FM4-64 fluorescence due to a shift in spectral properties caused by a distinct membrane composition (Zal et al. 2006) and changes in the membrane potential (Dombeck et al. 2005). NAA (at 100 μM) was also

found to destabilize artificial membranes, an effect that was stronger for NAA than for IAA at the same concentration (Hac-Wydro et al. 2015). That is in line with a general observation from pharmacological studies showing that synthetic compounds have often a broader activity spectrum than their natural counterparts (Feher et al. 2003).

Together, these data provide a plausible mechanistic explanation for auxin effects on the inhibition of BFA-induced endosomal aggregation, the endomembrane composition and the observed variability between IAA and NAA effects. For additional insights, it will be of interest to dissect the mode of action and the range of effects in mutants with reported auxin-resistance in terms of the BFA effect, such as *spk1* (Lin et al. 2012), *rop6*, *ric1* (Xu et al. 2010) and *big/doc1/tir3* (Paciorek et al. 2005). Particularly tantalizing observations were linked to genetic manipulation of the ABP1 function. Two types of conditional *abp1* knock-down lines (antisense and immunomodulation) show decreased BFA body formation. Consistently, ABP1 overexpression (whether transient in tobacco cultured cells or in stable Arabidopsis transgenic lines) leads to enhanced and NAA-resistant BFA body formation (Robert et al. 2010). Nonetheless, the conditional knock-down lines may produce off target effects (Michalko et al. 2016) and verified *abp1* knock-outs show normal NAA sensitivity (Paponov et al. 2019; Gelová et al. 2020). Thus, the possible involvement of ABP1 in auxin effect on BFA body formation remains unclear.

2.1.3.2 Absence of direct auxin effects on clathrin-mediated endocytic events

The original observations that auxin treatment diminishes BFA-induced intracellular accumulation of endocytic cargoes, as well as, reduces the uptake of endocytic tracers (e.g. FM4-64) or typical CME cargoes, such as transferrin suggested that auxin somehow targets the endocytic clathrin machinery (Paciorek et al. 2005; Robert et al. 2010). Reevaluation of this conception shows that auxin effects are much broader, including alteration of the endomembrane system. Hence, neither BFA treatment nor observing transferrin or FM4-64 dye at the EE/TGN can be used as reliable approaches to address the auxin effects on endocytosis. Hence following the individual endocytic events at the PM directly is vital to make robust conclusions.

The notion of auxin effect on endocytosis was further supported by the observation that prolonged NAA treatment leads to a significant decrease in the clathrin density at the PM. However the physiological relevance of this effect remains unclear. One possibility is that auxin affects the phosphatidylinositol membrane composition. For example, PIns(4,5)P2 :

PIns(4)P ratio at the PM increases after NAA treatment (Tejos et al. 2014) and mutants defective in PInsP metabolism, such as *pip5k1 pip5k2* also show strongly reduced clathrin density at the PM (Ischebeck et al. 2013). Thus, membrane PInsPs are vital in maintaining the endocytic processes, and NAA, by modifying their ratios, might cause adverse effects on the CME machinery and, in extension, on the overall endocytic rate.

To address direct auxin effects on CME, we directly followed individual CME events at the PM using TIRF microscopy but did not observe any auxin effects on density or lifetime of individual endocytic foci. This suggests that auxin, despite globally influencing clathrin association with the cell surface, has no direct effects on the individual CME events, their incidence or behavior.

2.1.3.3 Specific, promoting auxin effect on clathrin-mediated PIN2 endocytosis

Our analyses revealed not only the nonspecific global effects of high auxin concentrations on endocytic processes and endomembrane functionality but also a specific effect on endocytosis of PIN2. This is clearly a regulation distinct from the general auxin effects since also the natural auxin IAA, at concentrations as low as 10 nM, rapidly within minutes, promotes clathrin-mediated PIN2 internalization from the PM.

The potential physiological role of such auxin regulation remains unclear but may be linked to maintenance of PIN polarity, which requires constitutive PIN2 endocytosis (Dhonukshe et al. 2007; Kleine-Vehn et al. 2008c; Kleine-Vehn et al. 2011; Adamowski et al. 2015) and auxin-mediated PIN2 degradation (Abas et al. 2006; Baster et al. 2013). Both processes have been associated with physiological responses, such as root gravitropism, phototropism and halotropism (Abas et al. 2006; Laxmi et al. 2008; Galvan-Ampudia et al. 2013) and their regulation occurs via many endogenous signals, such as calcium (Zhang et al. 2011) and hormones like auxin (Baster et al. 2013), gibberellic acid (Löfke et al. 2013; Salanenka et al. 2018), salicylic acid (Du et al. 2013; Tan et al. 2020), abscisic acid (Li et al. 2020) or brassinosteroids (Retzer et al. 2019). These responses typically involve not only polar cellular PIN2 distribution but also asymmetric PIN2 abundance with PIN2 stabilized on one side of the root and increased degradation on the other (Abas et al. 2006; Baster et al. 2013; Galvan-Ampudia et al. 2013). It remains to be seen how the identified auxin promotion on PIN2 internalization is connected to the regulations of gravitropic/halotropic root bending and other PIN2-mediated processes.

The signaling mechanisms underlying the auxin-mediated promotion of PIN2 endocytosis remain unclear. The less specific auxin effects on endocytosis and endomembranes do not require the canonical $SCF^{TIR1/AFB}$ auxin pathway (Robert et al. 2010; Oochi et al. 2019), but the long-term auxin-mediated PIN2 degradation (Baster et al. 2013) or auxin effect on PIN polarity (Sauer et al. 2006; Han et al. 2020; Mazur et al. 2020b) have been shown to require $SCF^{TIR1/AF}$ signaling. Recently, it has been shown that $SCF^{TIR1/AFB}$ signaling, which has been considered purely transcriptional for decades (Leyser 2018), mediates also a non-transcriptional rapid regulation of root growth rate (Fendrych et al. 2018; Gallei et al. 2020). It is therefore possible that rapid PIN2 endocytosis and degradation is also mediated by the $SCF^{TIR1/AFB}$ mechanism, but this remains to be seen.

2.1.4 Material and Methods

Gene codes

The Arabidopsis thaliana genes studied and their corresponding accession numbers are listed: ARA7 – AT4G19640, CLC1 - AT2G20760, CLC2 - AT2G40060, ADAPTIN μ2 - AT5G46630, VHA-a1 - At2g28520, PIN1 - AT1G73590, PIN2 - AT5G57090, AUXILIN-LIKE2 - AT4G12770, PEPR1 - AT1G73080, PEPR2 - AT1G17750.

Plant Material

All the plant material is from the model organism Arabidopsis thaliana. The marker lines used are: pVHA-a1::VHA-a1-GFP (Dettmer et al. 2006), pCLC2::CLC2-GFP (Konopka et al. 2008), p35S::CLC1-GFP (Wang et al. 2013), p35S::N-ST-YFP (Grebe et al. 2003), pPIN2::PIN2-Dendra eir1-1 (Salanenka et al. 2018), pPIN2::PIN2-GFP x p35S::ARA7-RFP (Ueda et al. 2004; J. Xu 2005; C. Zhang et al. 2016), pUBQ10::CITRINE-1xPH(FAPP1) (Simon et al. 2014), pPEPR1::PEPR1-GFP pepr1 pepr2 (Ortiz-morea et al. 2016), XVE::AUXILIN-LIKE2 x pPIN2::PIN2-Dendra eir1-1 (Adamowski et al. 2018); pVHA-a1::VHA-a1-RFP x pPIN2::PIN2-GFP eir1-1 was made by crossing pVHA-a1::VHA-a1-RFP (Dettmer et al. 2006) and eir1-1 pPIN2::PIN2-GFP (J. Xu 2005).

Reagents used

IAA (Indole 3-Acetic Acid, Duchefa Biochemie, I0901.0025), dissolved in ethanol (EtOH) or DMSO to a stock concentration of 10 mM (in DMSO), 1 mM (in DMSO), 100 μM (in EtOH) or 10 μM (in EtOH). NAA (1-Naphthalene Acetic Acid, Sigma-Aldrich N0640) dissolved in DMSO to a stock concentration of 10 mM. BFA (Brefeldin-A, Sigma-Aldrich, B7651) dissolved in DMSO to a stock concentration of 50 mM. CHX (Cycloheximide, Sigma-Aldrich, C1988) dissolved in DMSO to a stock concentration of 10 mM. FM4-64 (N-(3-

Triethylammoniumpropyl)-4-(6-(4-(Diethylamino) Phenyl) Hexatrienyl) Pyridinium Dibromide, Life Technology, T-13320) dissolved in water to a stock concentration of 2 mM. Blebbistatin (Santa Cruz Biotechnology, sc-204253) dissolved in DMSO to a stock concentration of 1 M. pep1 (peptide sequence: ATKVKAKQRGKEKVSSGRPGQHN (Ortiz-Morea et al., 2016), commercially synthesized by EZbiolab) dissolved in water to a stock concentration of 200 µM. β-estradiol (Sigma-Aldrich, E8875) dissolved in DMSO to a stock concentration of 50 mM. For Western blot analysis the following antibodies were used: primary rabbit anti-PIN2 1:2000 (produced and processed in lab, Abas et al., 2006), mouse anti-actin 1:5000 (Sigma-Aldrich, A0480), mouse anti-His 1:1000 (GE Healthcare) and secondary anti-rabbit IgG antibody conjugated to horseradish peroxidase (HRP) 1:10000 (GE Healthcare, NA934). Membranes were developed using the SuperSignal Chemiluminiscence solutions (SuperSignal West Femto, Thermo Scientific). For immunolocalization the following primary and secondary antibodies were used: rabbit anti-ARF1 1:500 (Agrisera, AS08325), goat anti-PIN1 1:600 (SantaCruz technologies, sc-27163), mouse anti-GFP 1:500 (Sigma, G6539) and rabbit anti-PIN2 1:1000 (produced and processed in lab, Abas et al., 2006), donkey anti-goat antibody coupled to Alexa Fluor 488 1:600 (Thermo Fisher Scientific, A11055), goat anti-mouse antibody coupled to Alexa Fluor 594 1:600 (Abcam, 150116) goat anti-rabbit antibody coupled to Alexa Fluor 488 (Invitrogen, A11034), and sheep anti-rabbit antibody coupled to Cy3 1:600 (Sigma-Aldrich, C2306).

Seedling growth conditions

Seeds were surface sterilized by chlorine gas and sown on ½MS 0.8% agar (w/v) medium supplemented with 1% (w/v) sucrose. After stratification for 2 days in the dark at 4°C, the seedlings were grown at 21°C in a 16 h/8 h day/night cycle for 3-4 days. 7-day-old seedlings were used for the observation of endocytic foci in roots. 5-day-old seedlings were used for PIN2 Western blot analysis. For the CLC1 PM localization experiment, 4-5-day-old seedlings grown under continuous light were used.

Pharmacological treatments

All the treatments were carried out at room temperature (RT) by diluting the drugs in liquid ½MS medium containing 1% (w/v) sucrose to the working concentrations. Throughout the imaging time course, the seedlings were kept in treatment conditions, except for the FM4-64 internalization and CLC1 PM localization experiments. For the latter, imaging was done with seedlings settled flatly on a solid agar block containing the drugs dissolved to the working concentration.

BFA treatments: For Figure S1B-D and S2B, seedlings were pre-treated with either DMSO, 10 µM NAA (10 mM stock) or 10 µM IAA (10 mM stock) for 30 min and then co-treated with 37.5 µM BFA (50 mM stock) and mock or the original auxin for 60 min. For Figure 1, seedlings were pre-treated with ethanol, DMSO, 50 nM (100 µM stock), 10 µM (10 mM stock) or 20 µM (10 mM stock) IAA or NAA for 30 min and then co-treated with 50 µM BFA for 30 min. 10 µM CHX (10 mM stock) treatment was present throughout the experiments. For Figure S2E seedlings were pre-treated with either DMSO, 20 µM NAA (10 mM stock) or210 µM IAA (10 mM stock) for 30 min and then co-treated with 50 µM BFA (50 mM stock) and mock or the original auxin for 60 min. FM4-64 staining: seedlings were stained with 2 µM FM4-64 in liquid ½MS medium. The seedlings were incubated for 2 min in the dye and washed twice before imaging. For Figure 2A-B and Figure S3A, seedlings were pre-treated with DMSO, ethanol, 10 µM or 100 µM IAA (10 mM stock) or varying concentrations of NAA for 30 min. Blebbistatin treatment: seedlings were pre-treated with DMSO or 500 µM Blebbistatin (1 M stock) before imaging. For Figure 4 I,J roots were pulse-treated with 200 nM (200 µM stock) pep1 for 1 min and then treated with 20 µM NAA (10 mM stock) or the corresponding mock for 60 min. As control, seedlings were not pep1 pulsed (untreated). For Figure S5F, roots were pre-treated with 10 µM NAA, 10 µM IAA (10 mM stock) or DMSO (control) for 30 min before the pep1 pulse, followed by the same post-treatment for 60 min. As control, seedlings were incubated with DMSO/mock throughout pep1 pulse (untreated). For PIN2 Western blots, seedlings were treated with 1 µM IAA (1 mM stock) or the corresponding mock for varying durations. For β-estradiol induction, 2 day-old seedlings were transferred to plates containing 2 µM β-estradiol for 24 h. The seedlings were maintained continuously under chemical induction during subsequent imaging. Mock treatments in all experiments contained an equivalent amount of solvent in the treatment conditions.

Immuno staining

For immuno staining of the roots, the InsituPro VSi robot was used as described in (Sauer et al. 2006). Used antibodies are described in the section ‘reagents used’.

Protein extraction and Western blot

Seedlings on plates were treated by spraying them with liquid ½MS medium containing DMSO (mock) or 1 µM IAA. At the indicated time intervals, roots were harvested and flash frozen in liquid nitrogen. These root samples were ground using a Retsch mill for 2x 1 min at 20 Hz and the resulting root powder was re-suspended in a 1:1 (w/v) ratio of protein extraction buffer (50 mM Tris-HCl (pH 7.5), 150 mM NaCl, 1% (v/v) Triton X-100, 1x Roche complete™ Mini

Protease Inhibitor Cocktail, 1x Roche PhosSTOPTM, 1 mM EDTA, 1 mM DTT, 10 µM MG-132 and 0.5 mM PMSF). The samples were incubated on ice for 30 min, with intermediate vortexing to mix root powder and extraction buffer, followed by a centrifugation step at 10,000 g to sediment the plant debris. The cleared supernatant containing the proteins of interest was collected and the total protein content was determined using Quick Start Bradford reagent (Bio-Rad). The protein extracts were all diluted in extraction buffer to the same concentration (30 µg/25 µL) to allow equal loading of the samples. Proteins were separated by SDS-PAGE in a 12% (v/v) acrylamide gel (Protean® TGXTM, Bio-Rad) and were transferred to PVDF membranes by electroblotting (wet-transfer, Towbin transfer buffer, Bio-Rad system). The membranes were then incubated in blocking buffer (0.05% (v/v) Tween-20, 5% (w/v) milk powder or 3% (w/v) BSA, 20 mM Tris-HCl (pH 7.5), 150 mM NaCl) for at least 60 min and reacted with anti-PIN2 or anti-actin antibodies in TBS-T buffer + 3% BSA. This was followed by an anti-rabbit IgG secondary antibody conjugated to HRP incubation and chemiluminescence reaction. To allow multiple antibody detections using the same PVDF membrane, mild stripping was performed using 15 g/L glycine, 1 g/L SDS, 10 mL/L Tween-20 buffer at pH 2.2 for 2-5 min.

GST pull-down assay

GST and GST-PIN1CL recombinant proteins were expressed in bacteria and purified with glutathione sepharose beads, as described previously (Sancho-Andrés et al. 2016). The receptor binding domain (RBD) of Arabidopsis µ2-adaptin was expressed in bacteria as an histidine-tagged protein (His)6x-RBD-µ2-adaptin and purified with a Nickel column. Buffer exchange was performed using a PD-10 column (Amersham Pharmacia Biotech) to binding buffer (100 mM Tris-HCl (pH 7.5), 5 mM EDTA, 0.1% (v/v) Triton X-100) as described previously (Sancho-Andrés et al. 2016). Purified µ2-adaptin protein was pre-incubated for 1 h at RT in the absence or presence of 10 µM NAA, 2,4-D, 2-NAA or BA and then for 2 h at RT with 30 µL glutathione sepharose beads containing GST or GST-PIN1CL, which also had been pre-incubated with or without the respective auxin analogues. The beads were washed three times with 0.5 mL binding buffer and re-suspended in two-fold sample buffer (Laemmli, 1970). The samples were boiled at 95°C for 3 min and subjected to SDS–PAGE and Western blotting with a His-antibody. Each pull-down assay was independently performed three times and similar results were obtained.

Confocal microscopy

To determine the PIN2 endocytic rate, photo-conversion and subsequent imaging of photo-converted PIN2-Dendra at the PM was done with a Zeiss LSM700 vertical confocal microscope using a Plan-Apochromat 20x/NA 0.8 air objective and PMT/T-PMT detectors. The whole root expressing PIN2-Dendra was photo-converted as described in Jasik et al (2013). The growing root was tracked with the 'Tip-Tracker' software as described in von Wangenheim et al. (2017). The time interval between subsequent measurements was 15 min, except for the early time point studies, where the interval was 5 min. For controlling the treatment environment during determination of the PIN2 endocytic rate (Figure 4 E-F) the roots were grown in the RootChip, as described in Fendrych et al. (2018). An alternative device, named Chip'n'Dale was designed to allow drug application during live imaging as in Figure 4J. The Chip'n'Dale device consists of a cylindrical well, a permeable polyester membrane insert and a nylon mesh in between. The cylindrical well was constructed in house. It consists of a cover glass at the bottom, four springs to allow adjustment of the depth of the well and a notch on the edge to fit the commercial permeable polyester membrane insert (Corning). Before mounting the seedlings, a piece of nylon mesh was placed on the polyester membrane of the insert and made wet by a drop of liquid ½MS medium. On the liquid medium, 4-day-old seedlings were mounted. The mounted seedlings with the insert was then flipped and clipped into the cylindrical well. Afterwards, the Chip'n'Dale with samples was mounted onto the vertical confocal microscope. The drug was injected during imaging.

Imaging of FM4-64 internalization, BFA treatment (except Figure 1A), PtdIns(4)P quantifications and VHA-a1-RFP distribution was done with a Zeiss LSM700 inverted confocal microscope using a Plan-Apochromat 40x/NA 1.3 water objective and PMT/T-PMT detectors. Imaging of PEPR-GFP internalization was performed with a Zeiss LSM880 inverted confocal microscope using Plan-Apochromat 40x/NA 1.2 water objective and GaAsP/PMT detectors. To make the time-lapse movie of the endosomal movement and to observe the BFA effect (Figure 1A), a LSM800 inverted confocal microscope with a 40x/NA 1.3 water objective and GaAsP/PMT detectors was used. For observing the CLC1-GFP PM localization, a Zeiss LSM710 confocal microscope with a C-Apochromat 63x/NA 1.20 oil objective was used. For Figure S7 images were taken with a Leica SP2 confocal microscopes using a 63x water objective.

TIRF microscopy

Roots of 7-day-old seedlings were imaged with an Olympus IX83 inverted microscope equipped with a Cell^TIRF module and Hamamatsu EM-CCD C9100-13 camera, using OLYMPUS Uapo N 100x/NA 1.49 Oil TIRF objective at 1.6X magnification. Single channel imaging was done sequentially with the mentioned time interval. Time-lapse imaging in roots was done in the epidermal cells of the transition zone in TIRF mode (Johnson et al. 2020).

Quantification of endosomal aggregation size

'Particle analysis' was performed using ImageJ to determine the sizes of the ARA7 and VHA-a1 endosome aggregates.

Analysis of late endosomal movement

The time-lapse movie of LE movement was processed using ImageJ. The frames were stabilized and then subjected to temporal color-coding (Magenta Hot).

Quantification of endocytic foci at the PM

Time lapse data sets of CLC2-GFP were processed as using the unbiased automated single channel endocytosis analysis in Matlab, as described in Narasimhan et al. 2020. The detections were made using the values of the experimental setup. The developmental profile of the endocytic foci marked by CLC2-GFP was processed as described in Narasimhan et al. 2020. Post processing of the data and the subsequent plots were made in GraphPad Prism6.

PIN2 endocytic rate test

The time series were processed using ImageJ. Maximum intensity Z-projection of the epidermal PIN2 signal was made and a ROI covering the majority of the epidermal cells of the root tip was drawn. Within this ROI, the mean intensity of photo-converted PIN2-Dendra was measured over time using the multi-measure option.

Other intensity quantifications

PM and/or cytosolic signal intensity measurements for analyzing PEPR-GFP localization, FM4-64 staining, PIN2 polarity and PIN2 visualization in the aggregates were done by drawing free-hand lines at the PM and polygons internally in the individual cells, followed by measuring the mean intensity values in these regions using ImageJ. The number of cells with strong PM CLC1-GFP signal was visually evaluated and counted.

A logistic regression was performed to compare the presence of CLC1-GFP at the plasma membrane in root cells of roots treated with DMSO versus roots treated with 10 μM NAA. A random effect was added to the model for the experiments with multiple repeats to take into account the correlation between measurements done at the same time. The analysis was

performed with the glimmix procedure from SAS (Version 9.4 of the SAS System for windows 7 64bit. Copyright 2002-2012 SAS Institute Inc. Cary, NC, USA (www.sas.com)). Maximum likelihood estimation was done with the default estimation method. A Wald-type test was performed to estimate the effect of the treatment on the localization of CLC1-GFP at the PM.

Statistical analyses for differences in PIN2 internalization rate between treatments were carried out using R (version 1.1.383). A linear mixed effects regression (LMER) was used to test for the effect on the PIN2 internalization rate. We modeled PIN2 PM intensity values as a function of two predictors: time and treatment and their interaction, and we included a random intercept for each root, which is common for longitudinal studies (Bolker et al 2009). We assessed the model's significance comparing it to a null (mean) model and the significance of the interaction comparing to a model without interaction using likelihood ratio tests. The modeling package lme4 was used (Bates et al. 2014). The model assumptions were checked by 1) testing for equal variance of the residuals 2) testing for normality of the residuals and 3) testing the normality of the random effects. For statistical analysis of the immunolocalization of PIN2 in BFA bodies, a logistic regression was performed to compare the presence of BFA bodies in root cells of untreated roots versus treated roots or wild type versus mutant. A random effect was added to the model for the experiments with multiple repeats to consider the correlation between measurements done at the same time. The analysis was performed with the glimmix procedure from SAS (Version 9.4 of the SAS System for windows 7 64bit. Copyright 2002-2012 SAS Institute Inc. Cary, NC, USA (www.sas.com)). Maximum likelihood estimation was done with the default estimation method. A Wald-type test was performed to estimate the treatment/genotype effect on the presence of BFA bodies in the root cells.

The endosomal aggregation size was analyzed in R. The statistical tests for all the other experiments were made in GraphPad Prism 6. Significance is defined by $p<0.05$. The number of samples, the repetitions and the type of statistical tests are described in the respective Figure legends.

2.1.5 Acknowledgments

We thank Ivan Kulik for developing the Chip'n'Dale apparatus with Lanxin Li; the IST machine shop and the Bioimaging facility for their excellent support; Matouš Glanc and Matyáš Fendrych for their valuable discussions and help; Barbara Casillas-Perez for her help with statistics. This project has received funding from the European Research Council (ERC) under the European Union's Horizon 2020 research and innovation program (grant agreement No

742985). A.J. is supported by funding from the Austrian Science Fund (FWF): I3630B25 to J.F.

2.1.6 Figures

Figure 1 - Effect of NAA and IAA on the endosomal aggregation response to BFA

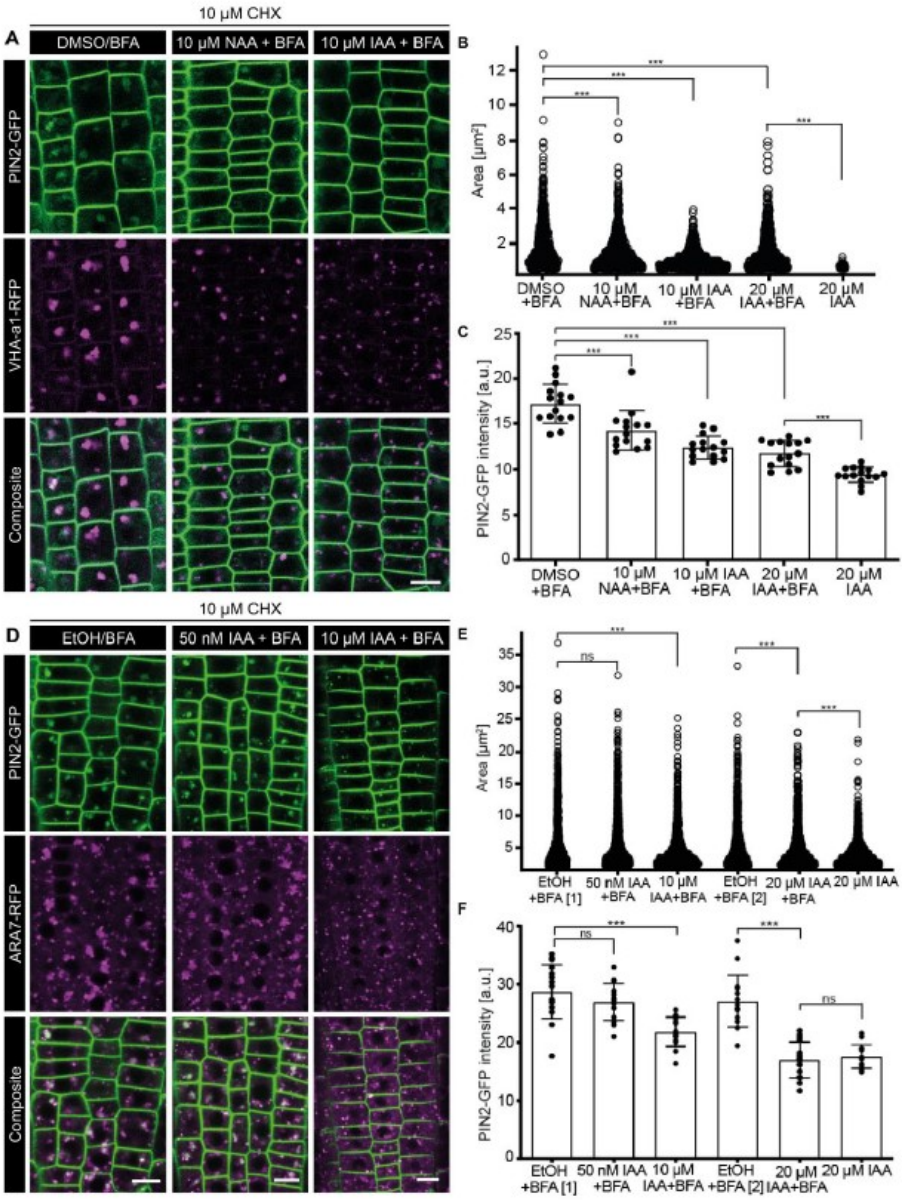

Figure 3 Section 2.1.6 - Effect of NAA and IAA on the endosomal aggregation response to BFA

A) Confocal images of the root epidermis expressing VHA-a1-RFP and PIN2-GFP. Endosomal aggregation after 30 min pre-treatment with DMSO (mock), 10 µM IAA, 20 µM IAA or 10 µM NAA, followed by 30 min co-treatment with 50 µM BFA. 20 µM IAA treatment is the internal control. Throughout the experiment, seedlings were treated with 10 µM CHX. **B)** Sina plot of the EE/TGN aggregation size in μm^2. Each point is a measurement of an aggregate. N=6 roots in each condition; all the epidermal cells in the imaging plane of the root tip were measured. One-sided Mann-Whitney U test (653, 898, 691, 842 and 50 measurements from each condition). DMSO+BFA (mock) > 10 µM NAA+BFA, p=9.646e-09***; DMSO+BFA (mock) > 20 µM IAA+BFA, p=6.982e-09***;

DMSO+BFA (mock) > 10 µM IAA+BFA, p<2.2e-16***; 20 µM IAA+BFA > 20 µM IAA (control), p < 4.59e-16***. **C)** Scatter dot plots of PIN2 intracellular intensity. The error bars represent mean with SD. N=5 roots in each condition; 15 cells per root. One-sided t test (with Welch's correction). DMSO+BFA (mock) > 10 µM NAA+BFA, p=0.0010***; DMSO+BFA (mock) > 20 µM IAA+BFA, p<0.0001***; DMSO+BFA (mock) > 10 µM IAA+BFA, p<0.0001***; 20 µM IAA+BFA > 20 µM IAA (control), p<0.0001***. **D)** Confocal images of root epidermal cells expressing ARA7-RFP and PIN2-GFP. Endosomal aggregation after 30 min pre-treatment with Ethanol (mock), 50 nM IAA or 10 µM IAA followed by 30 min co-treatment with 50 µM BFA. 20µM IAA treatment is the internal control. Throughout the experiment, seedlings were treated with 10 µM CHX. **E)** Sina plot of the LE aggregation size in μm^2. Each point is a measurement of an aggregate. N≥6 roots in each condition; all the epidermal cells in the imaging plane of the root tip were measured. EtOH+BFA [1] is the corresponding mock for 50 nM and 10 µM IAA and EtOH+BFA [2] corresponds to 20 µM IAA. One-sided Mann-Whitney U test (1122, 1552, 1397, 1048, 1197 and 1229 measurements from each condition). EtOH+BFA (mock) > 10 µM IAA+BFA, p=3.789e-09***; EtOH+BFA (mock) > 20 µM IAA+BFA, p=0.000241***; EtOH+BFA (Mock) > 50 nM IAA+BFA, p=0.2; 20 µM IAA+BFA > 20 µM IAA (control), p=0.001**. **F)** Scatter dot plots of PIN2 intracellular intensity. EtOH+BFA [1] is the corresponding mock for 50 nM and 10 µM IAA and EtOH+BFA [2] corresponds to 20 µM IAA. The error bars represent mean with SD. N≥6 roots in each condition; 15 cells per root. One-sided t test (with Welch's correction). EtOH+BFA (mock) > 20 µM IAA+BFA, p<0.0001***; EtOH+BFA (mock) > 10 µM IAA+BFA, p<0.0001***; EtOH+BFA (Mock) > 50 nM IAA+BFA, p=0.11; 20 µM IAA+BFA < 20 µM IAA (control), p=0.26. Scale bars: 10 µm.

Figure 2 - Effects of NAA and IAA on the endomembrane system

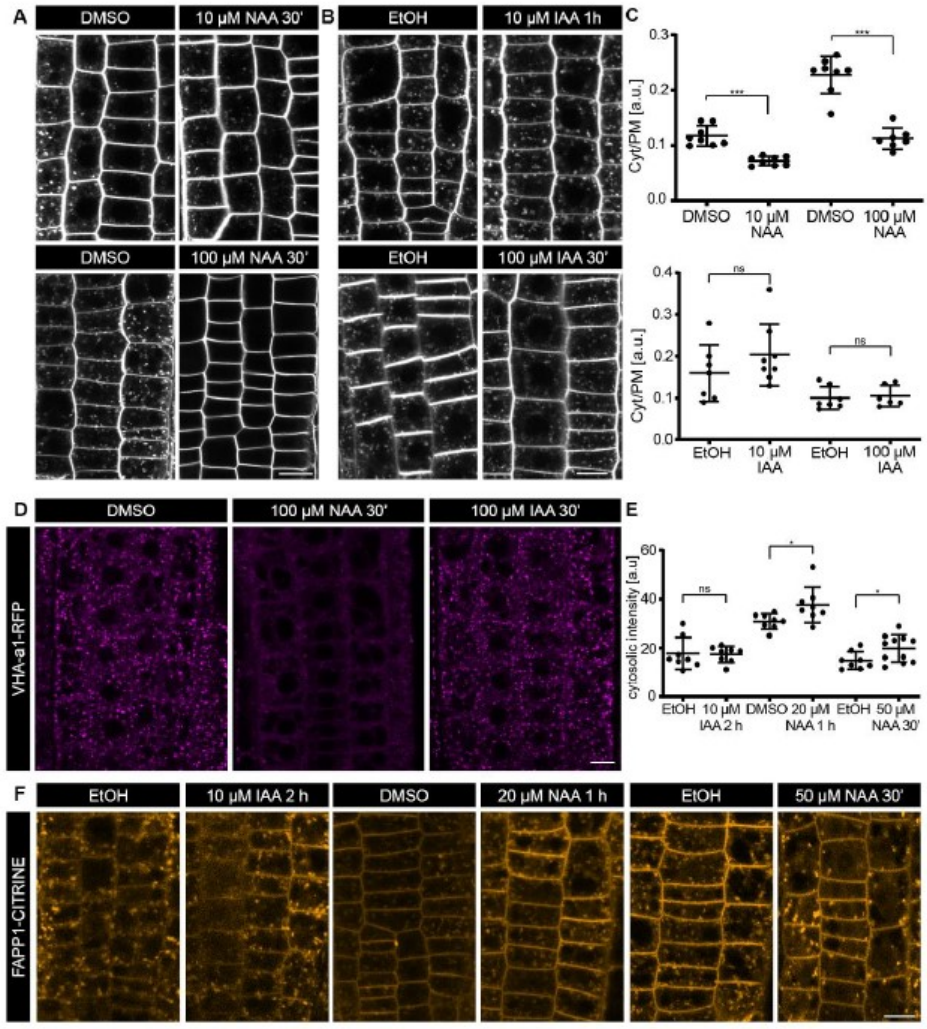

Figure 4 Section 2.1.6 - Effects of NAA and IAA on the endomembrane system

A-B) Representative confocal images of FM4-64 internalization after treatment with NAA (A) or IAA (B) (10 µM or 100 µM for 30 min). **C)** Scatter dot plots of the amount of endosomal FM4-64 signal measured as the ratio between the mean cytosolic intensity to the mean PM intensity. The error bars represent mean with SD. 10 µM and 100 µM NAA: N≥7 roots per condition; at least 10 cells per root. Two-sided t test. DMSO (mock) vs. NAA (10 µM/100 µM), p<0.0001***. 10 µM IAA: N≥6 roots; at least 7 cells per root. Two-sided t test. EtOH (mock) vs. 10 µM IAA, p=0.25. 100 µM IAA: N=8 roots; at least 10 cells per root. Two-sided t test. EtOH (mock) vs. 100 µM IAA, p=0.74. **D)** Confocal images of EE/TGN at the root epidermis expressing VHA-a1-RFP after treatment with 100 µM NAA or 100 µM IAA for 30 min. **E)** Scatter dot plots of the intracellular FAPP1-CITRINE intensity. The error bars represent the mean with SD. N=8 roots per condition; 8 cells per root. One-sided t test. EtOH 2 h (mock) < 10 µM IAA 2 h, p=0.445; DMSO 1 h (mock) < 20 µM NAA 1 h, p=0.0183* (with Welch's correction); EtOH 30' (mock) < 50 µM NAA 30', p=0.02*. Scale bars: 10 µm. **F)** Confocal images of the endomembrane system marked by FAPP1-CITRINE after mock, NAA or IAA treatment.

Figure 3 – Effect of NAA and IAA on the CME machinery

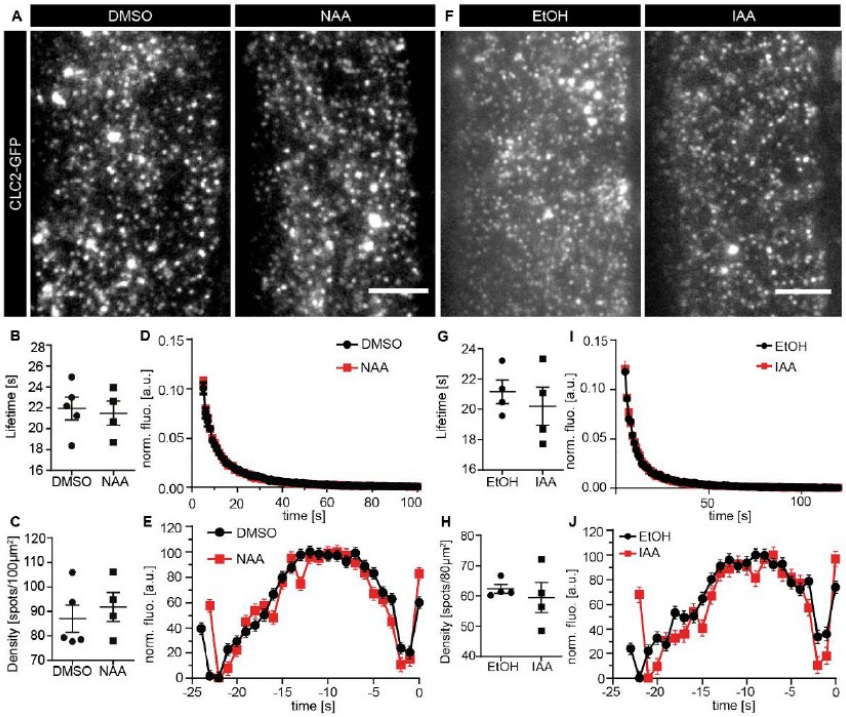

Figure 5 Section 2.1.6 – Effect of NAA and IAA on the CME machinery

A) Representative TIRF-M images of root epidermal cells expressing CLC2-GFP after treatment with DMSO (mock) or NAA (10 µM, 5-10 min). **B)** Mean lifetimes, **C)** mean density, **D)** normalized lifetime histogram and **E)** the fluorescence intensity profile of all tracks. All plots represent the mean +/- SEM. N: DMSO=5 cells from independent roots, 32990 tracks; N: NAA=4 cells from independent roots, 32534 tracks. Two-sided t tests: mean lifetimes: p=0.58; mean density: p=0.78. **F)** Representative TIRF-M images of root epidermal cells expressing CLC2-GFP after treatment with DMSO (mock) or IAA (10 µM, 5-10 min). **G)** Mean lifetimes, **H)** mean density, **I)** normalized lifetime histogram and **J)** the fluorescence intensity profile of all tracks. All plots represent the mean +/- SEM. N: DMSO=4 cells from independent roots, 22786 tracks; N: IAA=4 cells from independent roots, 28618 tracks. Two-sided t tests: mean lifetimes: p=0.54; mean density: p=0.6. Scale bars: 5 µm.

Figure 4 - Effect of NAA and IAA on the internalization of different cargoes

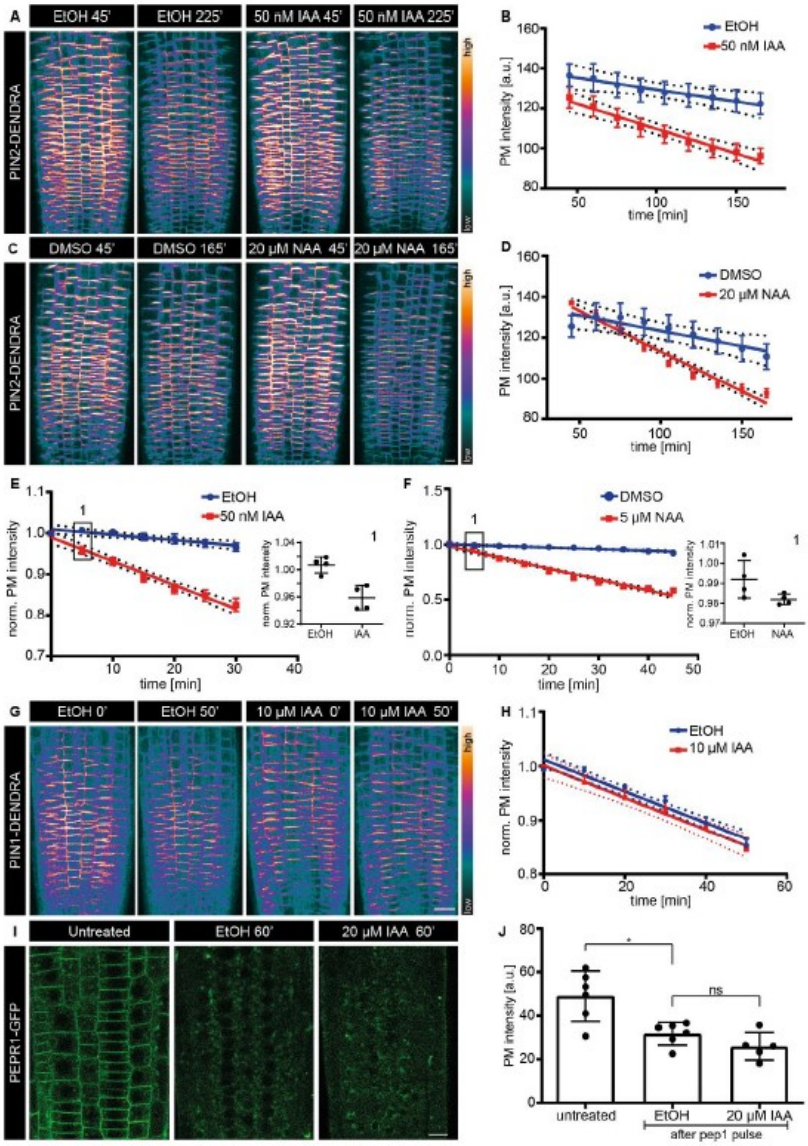

Figure 6 Section 2.1.6 - Effect of NAA and IAA on the internalization of different cargoes

A, C) Representative confocal images of the root epidermis expressing PIN2-Dendra at two isolated time-points after treatments: EtOH (mock) or 50 nM IAA (A), DMSO (mock) or 20 µM NAA (C) and their corresponding intensity measurements over-time in (B) and (D) **B)** Regression analysis (mock vs. 50 nM IAA). N≥3 roots per condition; 2 independent experiments. $\chi 2$- 56.897; df=1; p=4.594e-14 ***. **D)** Regression analysis (mock vs. 20 µM NAA). N=4 roots per condition. $\chi 2$- 62.216; df=1; p=3.078e-15 ***. **E)** Regression analysis (mock vs. 50 nM IAA). N=4 roots per condition. $\chi 2$- 69.418; df=1; p=2.2e-16 ***. **F)** Regression analysis (mock vs. 5 µM NAA). N=4 roots per condition. $\chi 2$- 75.878; df=1; p=2.2e-16 ***. The scatter plot in the inset 1 (representing the 1st data point of graph F) shows intensity difference 5 minutes after IAA (E) or NAA (F) treatment. One-sided t test. EtOH (mock) > 50 nM IAA, p=0.0021**; DMSO (mock) > 5 µM NAA, p=0.043*. **G)** Representative confocal images of root epidermal cells expressing PIN1-Dendra at two isolated time-points after EtOH (mock) or 10 µM IAA treatments. **H)** Regression analysis (mock vs. 10 µM IAA). N≥5 roots per condition. $\chi 2$- 0.65; df=1; p=0.42. All the regression analyses of the PIN PM intensity were performed by fitting a linear mixed model on the intensity values measured from all the cells in the imaging plane of the epidermis. Each dot represents the mean intensity and the dotted lines depict the 95% CI. LMER - random effects for position. **I)** Representative confocal images of root epidermal cells expressing PEPR1-GFP; before

pep1 pulse (untreated – control); and after pep1 pulse and treatments with EtOH (mock) or 20 µM IAA for 1 h. **J)** Scatter dot plots of PM PEPR intensity. The error bars represent the mean with SD. N≥5 roots per condition; 10 cells per root. Two-sided Mann-whitney U test. EtOH vs. 20 µM IAA, p=0.24. One-sided Mann-Whitney U-test. Untreated > EtOH, p=0.013*. Scale bars: 10 µm.

Figure 5 - Auxin-mediated promotion of PIN2 internalization and its polarity are clathrin dependent

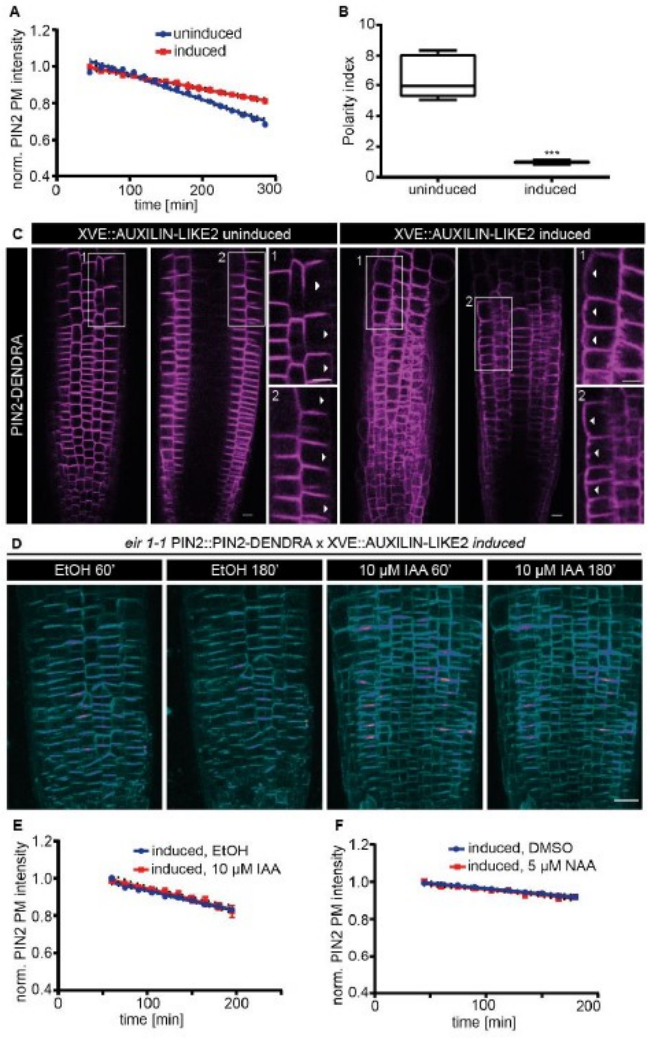

Figure 7 Section 2.1.6 - Auxin-mediated promotion of PIN2 internalization and its polarity are clathrin dependent

A) Regression analysis (uninduced vs. induced). N=4 roots per condition; χ2- 65.82; df=1; p=4.931e-16 ***. **B)** PIN2 polarity index in *AXL2* uninduced vs. induced conditions measured as the ratio of apical PIN2 intensity to lateral PIN2 intensity. N=5 roots per condition; 10 cells per root; 3 independent experiments. Mann-Whitney U test, p<0.0001 ***. **C)** Representative confocal images of root epidermal cells expressing PIN2-Dendra; *AXL2* uninduced (left) and induced (right) conditions. The inset 1 in each condition shows the front of the epidermis and the inset 2 shows the middle of the epidermis. White arrowheads indicate the lateral PIN2 distribution. **D)** Representative confocal images of root epidermal cells expressing PIN2-Dendra at two isolated time-points after EtOH (Mock) or 10 µM IAA treatments in *AXL2*-induced condition. **E)** Regression analysis (mock vs. 10 µM IAA). N≥5 roots per condition; LM; F=0.88; p=0.34. **F)** Regression analysis (mock vs. 5 µM NAA). N=5 roots per condition; LMER - random effects for position; χ2- 0.0027; df=1; p= 0.95. The regression analysis of the PIN2 PM intensity shown in plots A and F were performed by fitting a linear mixed model on the intensity values measured from all the epidermal cells in the imaging plane of the root tip. Each dot

represents the mean intensity and the dotted lines depict the 95% CI. LMER - random effects for position. Scale bar: 20 µm.

2.1.7 Supplemental Figures

Figure S1: Effect of NAA and IAA on EE/TGN system and its BFA-induced aggregation

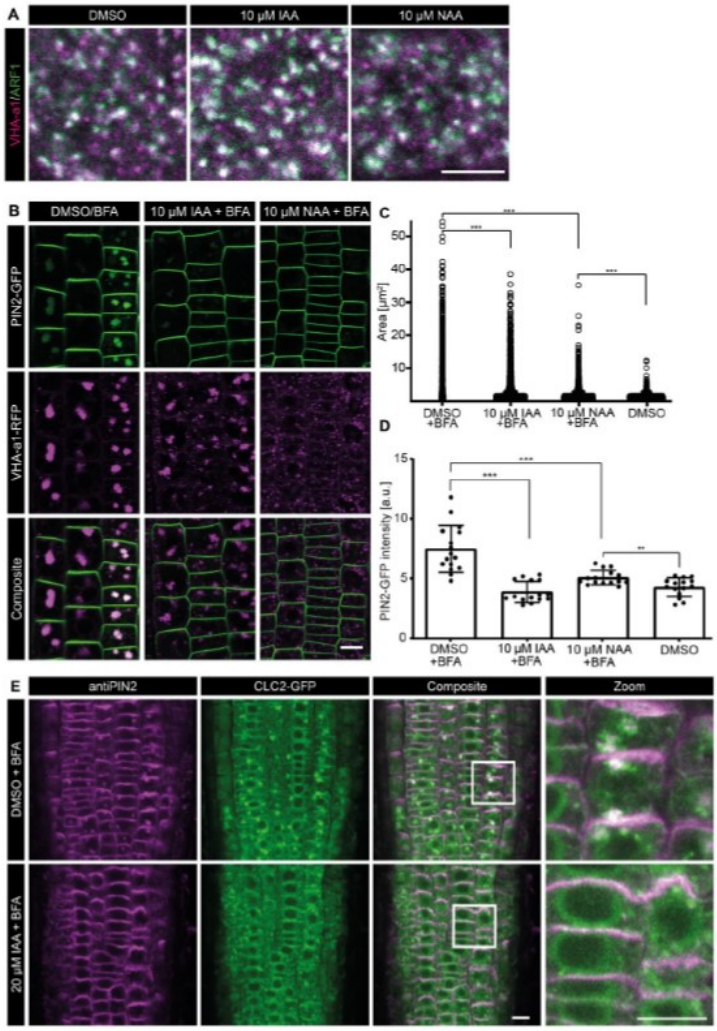

Figure 8 Section 2.1.7 - Effect of NAA and IAA on EE/TGN system and its BFA-induced aggregation

A) Representative confocal images of the root epidermis expressing VHA-a1-GFP, immunolabeled with anti-GFP to visualize VHA-a1 and anti-ARF1 antibody. The zoomed-in images show co-localization of ARF1 and VHA-a1 in the EE/TGN system in DMSO (mock) or auxin-treated conditions (10 µM IAA and 10 µM NAA; 1.5 h). N=4 roots per condition. B) Representative confocal images of the root epidermis expressing VHA-a1-RFP and PIN2-GFP. EE/TGN aggregation after 30 min pre-treatment with DMSO (mock), 10 µM IAA or 10 µM NAA, followed by 60 min co-treatment with 37.5 µM BFA. C) Sina plot representing the EE/TGN aggregation size in μm^2. Each point is a measurement of an aggregate. N=5 roots in each condition; all the epidermal cells in the imaging plane of the root tip were measured. One-sided Mann-Whitney U test (858, 2064, 2220 and 2550 measurements from each condition). DMSO+BFA (mock) > 10 µM IAA+BFA, p<2.2e-16***; DMSO+BFA (Mock) > 10 µM NAA+BFA, p<2.2e-16***; 10 µM NAA+BFA > DMSO (control), p<2.2e-16*** . D) Scatter dot plots representing the PIN2 intracellular intensity. The error bars represent mean with SD. N=5 roots in each condition; 15 cells per root. One-sided t test (with Welch's correction). DMSO+BFA (mock) > 10 µM IAA+BFA, p<0.0001***; DMSO+BFA (mock) > 10 µM NAA, p<0.0001***; 10 µM NAA+BFA > DMSO (control), p=0.002**. E) Representative confocal images of root epidermal cell expressing CLC2-GFP immunolabeled with anti-PIN2 antibody. The roots were pre-treated with DMSO (mock)

or 20 µM IAA for 30 min, followed by a co-treatment with 50 µM BFA for 30 min, and then immunolabeled. N=8 roots per condition. Scale bars: A) 5 µm B, E) 10 µm.

Figure S2: Effect of NAA and IAA on BFA-induced aggregation of LE and Golgi bodies

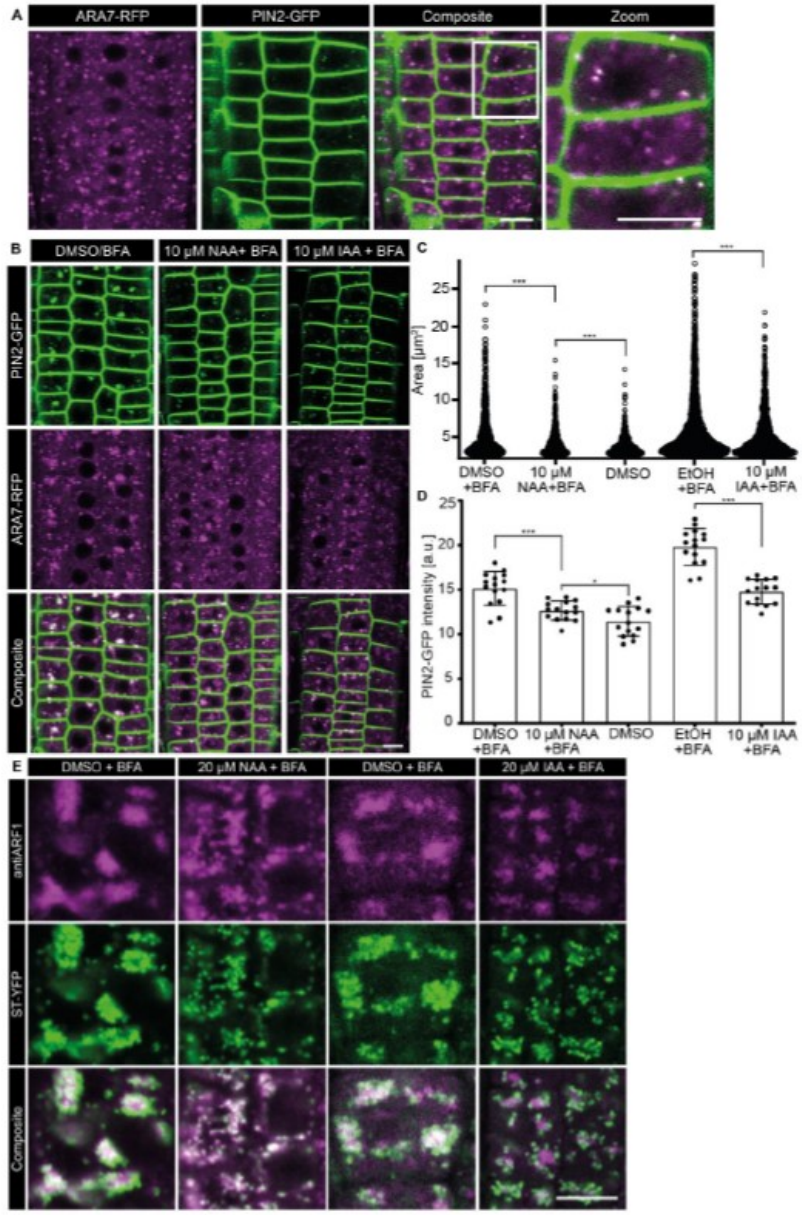

Figure 9 Section 2.1.7 - Effect of NAA and IAA on BFA-induced aggregation of LE and Golgi bodies

A and B) Representative confocal images of root epidermal cells expressing ARA7-RFP and PIN2-GFP. A) The image shows the co-localisation of PIN2-GFP with ARA7-RFP under no external treatment. B) LE aggregation after 30 min pre-treatment with DMSO (mock), 10 µM IAA or 10 µM NAA, followed by 30 min co-treatment with 50 µM BFA. C) Sina plot representing the LE aggregation size in µm2. Each point is a measurement of an aggregate. N=8 roots in each condition; all the epidermal cells in the imaging plane of the root tip were measured. One-sided Mann-Whitney U test (869, 603, 578, 1585 and 1403 measurements from each condition). DMSO+BFA (mock) > 10 µM NAA+BFA, p-value = 7.997e-06***; EtOH+BFA (Mock) > 10 µM IAA+BFA, p-value = 1.606e-10 ***; 10 µM NAA+BFA > DMSO (control), p-value = 0.0001922 ***. D) Scatter dot plots representing the PIN2 intracellular intensity. The error bars represent mean with SD. N=8 roots in each condition; 15 cells per root. One-sided t test (with Welch's correction). DMSO+BFA (mock) > 10 µM NAA, p<0.0001***;

EtOH+BFA (mock) > 10 µM IAA +BFA, p<0.0001***; 10 µM NAA+BFA > DMSO (control), p=0.01*. E) Representative confocal images of the root epidermal cells expressing ST-YFP, immunolabeled with anti-ARF1 antibody. The roots were pre-treated with DMSO (mock) or 20 µM IAA or 20 µM NAA for 30 min, followed by a co-treatment with 50 µM BFA for 30 min, and then immunolabeled. N=8 roots per condition. Scale bars: A,B,E) 10 µm.

Figure S3: Effects of NAA and IAA on the endomembrane system

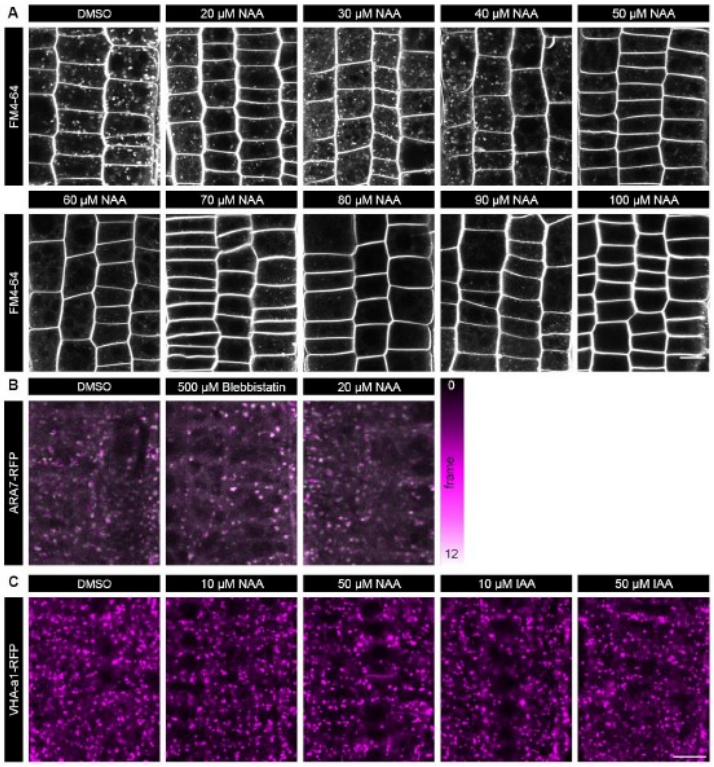

Figure 10 Section 2.7.1 - Effects of NAA and IAA on the endomembrane system

A) Representative confocal images of epidermal cells of the root with internalized FM4-64 dye marking the endomembrane after 30 min pre-treatments with DMSO (mock) or NAA: 10 to 100 µM. N=10 roots for each condition. B) Temporal color code of the time-lapse movie (Movie S1) of the LE movements in the roots expressing ARA7-RFP, after DMSO (mock), 500 µM blebbistatin or 20 µM NAA for 60 min. The frames are color-coded as the color-scale bar indicates. The whiter the endosomes are, the lesser the movement. C) Representative confocal images of root epidermal cells expressing VHAa1-RFP after treatments with DMSO (mock), NAA or IAA for 30 min. N≥7 roots per condition. Scale bars: 10 µm.

Figure S4: Effects of NAA and IAA on PM clathrin

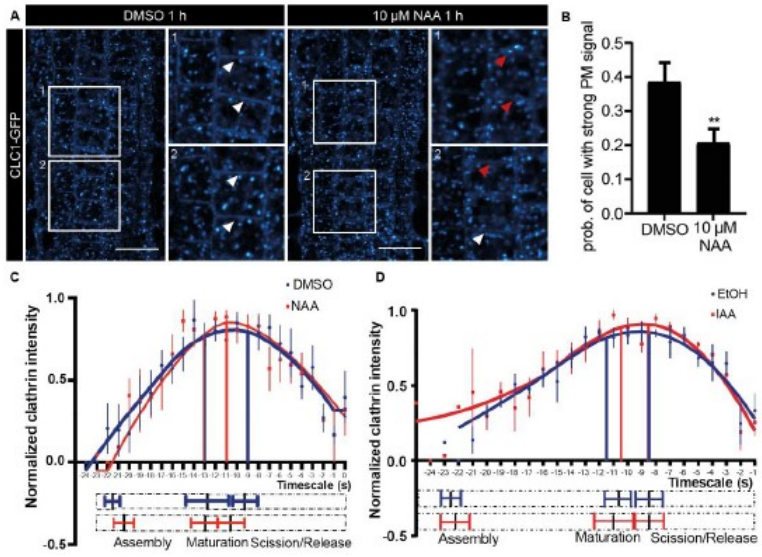

Figure 11 Section 2.7.1 - Effects of NAA and IAA on PM clathrin

A) Representative confocal images of the root epidermal cells expressing CLC1-GFP. Red arrows indicate weak/loss of PM CLC1 signal and the white arrows indicate a strong signal. B) Bar graph showing the frequency of cells with strong CLC1 PM signal (10 µM NAA, 1 h). Error bars indicate 95% CI. N=4-12 roots; 6-33 cells per root; 4 independent experiments. Two-sided t test. $p<0.01$*. C and D) Smoothened intensity profile of clathrin tracks of the mean lifetime (18-24 s) after mock and auxin (10 µM NAA or IAA; 5-10 min). Each dot represents the mean intensity with SEM. CCP developmental profile classified into 'Assembly', 'Maturation' and 'Scission/Release' phases (bottom). The extrapolation lines mark the different CCP development phases. The dotted bars represent the whole time course of CCP development; the solid lines with error bars mark the mean ± SD of the transition point between phases. C) N: DMSO=4 cells from independent roots, 397 tracks; NAA=4 cells from independent roots, 783 tracks. Two-sided t tests. Assembly p=0.69; Maturation p=0.48. D) N: EtOH=4 cells from independent roots, 247 tracks; IAA=4 cells from independent roots, 431 tracks. Two-sided t tests. Assembly p=0.58; Maturation p=0.73. Scale bar: 20 µm.

Figure S5: Effect of NAA and IAA on internalization of different cargoes

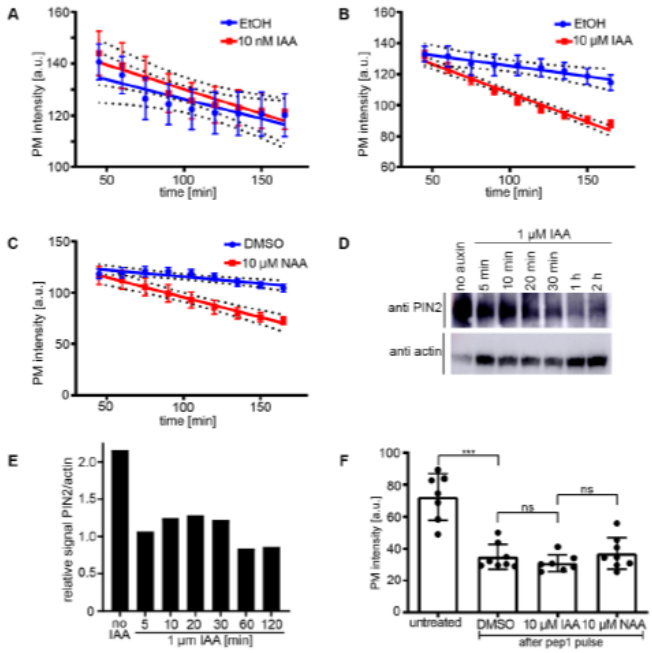

Figure 12 Section 2.7.1 - Effect of NAA and IAA on internalization of different cargoes

A-C) All the regression analysis of the photo-converted PIN2 PM intensity were performed by fitting a linear mixed model on the intensity values measured from all the epidermal cells in the imaging plane of the root tip. Each dot represents the mean intensity and the dotted lines depict the 95% CI. LMER - random effects for position. A) Regression analysis (mock vs. 10 nM IAA): N=5 roots per condition; χ2- 15.70; p=7.187e-05 ***. B) Regression analysis (10 µM IAA): N=5 roots per condition; χ2- 96.703; p=2.2e-16 ***. C) Regression analysis (mock vs. 10 µM NAA): N=3 roots per condition; χ2- 50.17; p=1.41e-12 ***. D) Western blot showing the total amount of PIN2 without auxin treatment (control) and after different incubation times with 1 µM IAA. Anti-actin was used as a loading control. E) Bar graph representing the relative amount of PIN2 intensity to intensity of the anti actin loading control. F) The scatter dot plot of the mean PM PEPR intensity with no pep1 pulse (untreated – control) or after pep1 pulse in the presence DMSO (mock) or auxin treatment (30 min pretreatment followed by pep1 pulse and then 1 h treatment with DMSO, 10 µM IAA or 10 µM NAA). N≥ 7 seedlings per condition; 20 cells per root. Two-sided Mann-Whitney U test. DMSO (mock) vs. 10 µM IAA, p = 0.27; DMSO (mock) vs. 10 µM NAA, p=0.56; One-sided Mann-Whitney U test. Untreated > DMSO (mock), p=0.003**.

Figure S6: Effect of auxin analogues on binding of µ2-adaptin to the cytosolic loop of PIN1

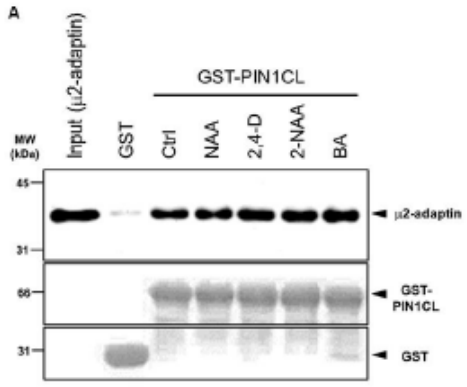

Figure 13 Section 2.7.1 - Effect of auxin analogues on binding of µ2-adaptin to the cytosolic loop of PIN1

A) GST Pull-down assays showing the binding of the cytosolic loop of PIN1 fused with GST (GST-PIN1CL) and the receptor binding domain (RBD) of Arabidopsis µ2-adaptin, with an N-terminal (His)6-tag used for purification and detection, in the absence (control) or presence of BA (mock) or auxin analogs (10 µM of NAA, 2,4-D, 2-NAA). GST was used as a control. Pull-downs were analyzed by Western blotting with an anti-His antibody, which detected His-tagged µ2-adaptin (upper panel), and Ponceau staining (medium and bottom panels) showing the loaded amount of GST and GST-PIN1CL in the pull-down assays. The input lane contains 5% of the amount of the µ2-adaptin used in the pull-down assay. Arrowheads point at the expected positions of the RBD of µ2-adaptin, GST and GST-PIN1CL.

Figure S7: Effect of pH on BFA body formation

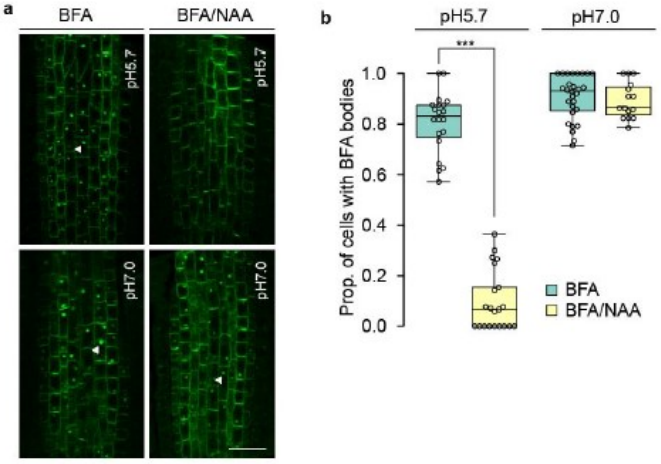

Figure 14 Section 2.7.1 - Effect of pH on BFA body formation

A) Representative confocal images of root endodermal and stele cells with PIN1 immunolocalization after 1 h treatment with with 25 µM BFA or co-treatment with 25 µM BFA and 10 µM NAA in liquid medium set at pH 5.7 and pH 7.0. White arrows indicate PIN1 in BFA bodies. Scale bar: 20 µm. B) Quantification of the probability of BFA bodies in the root cells. Center-lines show the medians; box limits indicate the 25th and 75th percentiles; whiskers extend 1.5 times the interquartile range from the 25th and 75th percentiles. pH 5.7: N=21 roots; 28 cells; $p \leq 0.0005$***. pH 7.0: N=29 roots; 28 cells; p=n.s. 5 independent experiments.

2.1.8 References

1. Abas, Lindy, René Benjamins, Nenad Malenica, Tomasz Paciorek, Justyna Wiřniewska, Jeanette C Moulinier Anzola, Tobias Sieberer, Jiří Friml, and Christian Luschnig. 2006. "Intracellular Trafficking and Proteolysis of the Arabidopsis Auxin-Efflux Facilitator PIN2 Are Involved in Root Gravitropism," no. November 2005. https://doi.org/10.1038/ncb1369.
2. Adamowski, Maciek, and Jiří Friml. 2015. "PIN-Dependent Auxin Transport: Action, Regulation, and Evolution." The Plant Cell Online 27 (1): 20–32. https://doi.org/10.1105/tpc.114.134874.
3. Adamowski, Maciek, Geert De Jaeger, Madhumitha Narasimhan, and Urszula Kania. 2018. "A Functional Study of AUXILIN-LIKE1 and 2 , Two Putative Clathrin Uncoating Factors in Arabidopsis" 30 (March): 700–716. https://doi.org/10.1105/tpc.17.00785.
4. Balla, Jozef, Petr Kalousek, Vilém Reinöhl, Jiåí Friml, and Stanislav Procházka. 2011. "Competitive Canalization of PIN-Dependent Auxin Flow from Axillary Buds Controls Pea Bud Outgrowth." Plant Journal 65 (4): 571–77. https://doi.org/10.1111/j.1365-313X.2010.04443.x.
5. Barbosa, Inês C R, Ulrich Z Hammes, and Claus Schwechheimer. 2018. "Activation and Polarity Control of PIN- FORMED Auxin Transporters by Phosphorylation," 523–38. https://doi.org/10.1016/j.tplants.2018.03.009.
6. Bargmann, Bastiaan O.R., Steffen Vanneste, Gabriel Krouk, Tal Nawy, Idan Efroni, Eilon Shani, Goh Choe, et al. 2013. "A Map of Cell Type-Specific Auxin Responses." Molecular Systems Biology 9 (1): 1–13. https://doi.org/10.1038/msb.2013.40.
7. Baster, Pawe, Steffen Vanneste, Urszula Kania, Wim Grunewald, Bert De Rybel, and Tom Beeckman. 2013. "-Auxin Signalling Regulates PIN Vacuolar Trafficking and Auxin Fluxes during Root Gravitropism" 32 (2): 260–74. https://doi.org/10.1038/emboj.2012.310.
8. Bates, Douglas, Martin Mächler, Benjamin M. Bolker, and Steven C. Walker. 2014. "Fitting Linear Mixed-Effects Models Using Lme4." Journal of Statistical Software 67 (1). https://doi.org/10.18637/jss.v067.i01.
9. Belda-Palazon, Borja, Lesia Rodriguez, Maria A. Fernandez, Mari Cruz Castillo, Erin M. Anderson, Caiji Gao, Miguel Gonzalez-Guzman, et al. 2016. "FYVE1/FREE1 Interacts with the PYL4 ABA Receptor and Mediates Its Delivery to the Vacuolar Degradation Pathway." Plant Cell 28 (9): 2291–2311. https://doi.org/10.1105/tpc.16.00178.
10. Benkova, Eva, Marta Michniewicz, Michael Sauer, Thomas Teichmann, and Molekularbiologie Der Pflanzen. 2003. "Local , Efflux-Dependent Auxin Gradients as a Common Module for Plant Organ Formation" 115: 591–602.
11. Berleth, Thomas, and Tsvi Sachs. 2001. "Plant Morphogenesis: Long-Distance Coordination and Local Patterning." Current Opinion in Plant Biology 4 (1): 57–62. https://doi.org/10.1016/S1369-5266(00)00136-9.
12. Boevink, Petra, Karl Oparka, Simon Santa Cruz, Barry Martin, Alan Betteridge, and Chris Hawes. 1998. "Stacks on Tracks: The Plant Golgi Apparatus Traffics on an Actin/ER Network." Plant Journal 15 (3): 441–47. https://doi.org/10.1046/j.1365-313X.1998.00208.x.
13. Carland, Francine, Shozo Fujioka, and Timothy Nelson. 2010. "The Sterol Methyltransferases SMT1, SMT2, and SMT3 Influence Arabidopsis Development through Nonbrassinosteroid Products." Plant Physiology 153 (2): 741–56. https://doi.org/10.1104/pp.109.152587.
14. Dejonghe, Wim, Sabine Kuenen, Evelien Mylle, Mina Vasileva, Olivier Keech, Corrado Viotti, Jef Swerts, et al. 2016. "Mitochondrial Uncouplers Inhibit Clathrin-Mediated Endocytosis Largely through Cytoplasmic Acidification." Nature Communications 7. https://doi.org/10.1038/ncomms11710.
15. Dettmer, Jan, Anne Hong-Hermesdorf, York-Dieter Stierhof, and Karin Schumacher. 2006. "Vacuolar H+-ATPase Activity Is Required for Endocytic and Secretory Traf Cking in Arabidopsis." The Plant Cell 18 (March): 715–30. https://doi.org/10.1105/tpc.105.037978.null.
16. Dhonukshe, Pankaj, Fernando Aniento, Inhwan Hwang, David G Robinson, and Jozef Mravec. 2007. "Report Clathrin-Mediated Constitutive Endocytosis of PIN Auxin Efflux Carriers in Arabidopsis," 1–8. https://doi.org/10.1016/j.cub.2007.01.052.
17. Dhonukshe, Pankaj, Ilya Grigoriev, Rainer Fischer, Motoki Tominaga, David G. Robinson, Jiří Hašek, Tomasz Paciorek, et al. 2008. "Auxin Transport Inhibitors Impair Vesicle Motility and Actin Cytoskeleton Dynamics in Diverse Eukaryotes." Proceedings of the National Academy of Sciences of the United States of America 105 (11): 4489–94. https://doi.org/10.1073/pnas.0711414105.

18. Dombeck, Daniel A., Leonardo Sacconi, Mireille Blanchard-Desce, and Watt W. Webb. 2005. “Optical Recording of Fast Neuronal Membrane Potential Transients in Acute Mammalian Brain Slices by Second-Harmonic Generation Microscopy.” Journal of Neurophysiology 94 (5): 3628–36. https://doi.org/10.1152/jn.00416.2005.
19. Du, Yunlong, Ricardo Tejos, Martina Beck, Ellie Himschoot, Hongjiang Li, Silke Robatzek, Steffen Vanneste, and Jiří Friml. 2013. “Salicylic Acid Interferes with Clathrin-Mediated Endocytic Protein Trafficking.” Proceedings of the National Academy of Sciences of the United States of America 110 (19): 7946–51. https://doi.org/10.1073/pnas.1220205110.
20. Eliasson, Lennart, Gertrud Bertell, and Eva Bolander. 1989. “Inhibitory Action of Auxin on Root Elongation Not Mediated by Ethylene.” Plant Physiology 91 (1): 310–14. https://doi.org/10.1104/pp.91.1.310.
21. Feher, Miklos, and Jonathan Schmidt. 2003. “Property Distributions: Differences between Drugs, Natural Products, and Molecules from Combinatorial Chemistry.” ACS Chemical BiologyS 43: 2003.
22. Fendrych, Matyáš, Maria Akhmanova, Jack Merrin, Matouš Glanc, Shinya Hagihara, Koji Takahashi, Naoyuki Uchida, Keiko U Torii, and Jiří Friml. 2018. “Rapid and Reversible Root Growth Inhibition by TIR1 Auxin Signalling.” Nature Plants 4 (July). https://doi.org/10.1038/s41477-018-0190-1.
23. Feraru, Elena, Mugurel I. Feraru, Rin Asaoka, Tomasz Paciorek, Riet De Rycke, Hirokazu Tanaka, Akihiko Nakano, and Jiří Frimla. 2012. “BEX5/RabA1b Regulates Trans-Golgi Network-to-Plasma Membrane Protein Trafficking in Arabidopsis.” Plant Cell 24 (7): 3074–86. https://doi.org/10.1105/tpc.112.098152.
24. Friml, Jiří, Eva Benková, Ikram Blilou, Justyna Wisniewska, Thorsten Hamann, Karin Ljung, Scott Woody, et al. 2002. “AtPIN4 Mediates Sink-Driven Auxin Gradients and Root Patterning in Arabidopsis.” Cell 108 (5): 661–73. https://doi.org/10.1016/S0092-8674(02)00656-6.
25. Gallei, Michelle, Christian Luschnig, and Jiří Friml. 2020. “Auxin Signalling in Growth: Schrödinger’s Cat out of the Bag.” Current Opinion in Plant Biology 53: 43–49. https://doi.org/10.1016/j.pbi.2019.10.003.
26. Galvan-Ampudia, Carlos S., Magdalena M. Julkowska, Essam Darwish, Jacinto Gandullo, Ruud A. Korver, Geraldine Brunoud, Michel A. Haring, Teun Munnik, Teva Vernoux, and Christa Testerink. 2013. “Halotropism Is a Response of Plant Roots to Avoid a Saline Environment.” Current Biology 23 (20): 2044–50. https://doi.org/10.1016/j.cub.2013.08.042.
27. Gao, Yangbin, Yi Zhang, Da Zhang, Xinhua Dai, Mark Estelle, and Yunde Zhao. 2015. “Auxin Binding Protein 1 (ABP1) Is Not Required for Either Auxin Signaling or Arabidopsis Development” 1. https://doi.org/10.1073/pnas.1500365112.
28. Geldner, Niko, Nadine Anders, Hanno Wolters, Jutta Keicher, Wolfgang Kornberger, Philippe Muller, Alain Delbarre, et al. 2003. “The Arabidopsis GNOM ARF-GEF Mediates Endosomal Recycling , Auxin Transport , and Auxin-Dependent Plant Growth” 112: 219–30.
29. Geldner, Niko, and Klaus Palme. 2001. “Auxin Transport Inhibitors Block PIN1 Cycling and Vesicle Traf ® Cking” 413 (SEPTEMBER): 425–28.
30. Gelová, Zuzana, Michelle Gallei, Marketa Pernisov, Geraldine Brunoud, Xixi Zhang, Matouš Glanc, Lanxin Li, et al. 2020. “Developmental Roles of Auxin Binding Protein 1 in Arabidopsis Thaliana.” Plant Science. https://doi.org/https://doi.org/10.1016/j.plantsci.2020.110750.
31. Glanc, Matouš, Matyáš Fendrych, and Jiří Friml. 2018. “Mechanistic Framework for Cell-Intrinsic Re-Establishment of PIN2 Polarity after Cell Division.” Nature Plants 4 (12): 1082–88. https://doi.org/10.1038/s41477-018-0318-3.
32. Grebe, Markus, Jian Xu, Wiebke Moebius, Takashi Ueda, Akihiko Nakano, Hans Geuze, Martin B. Rook, and Ben Scheres. 2003. “Arabidopsis Sterol Endocytosis Involves Actin-Mediated Trafficking via ARA6-Positive Early Endosomes.” Current Biology 13: 654–58. https://doi.org/10.1016/S.
33. Grones, Peter, Melinda Abas, Jakub Hajný, Angharad Jones, Sascha Waidmann, Jürgen Kleine-Vehn, and Jiří Friml. 2018. “PID/WAG-Mediated Phosphorylation of the Arabidopsis PIN3 Auxin Transporter Mediates Polarity Switches during Gravitropism.” Scientific Reports 8 (1): 1–11. https://doi.org/10.1038/s41598-018-28188-1.
34. Grones, Peter, Xu Chen, Sibu Simon, Walter A. Kaufmann, Riet De Rycke, Tomasz Nodzyński, Eva Zažímalová, and Jiří Friml. 2015. “Auxin-Binding Pocket of ABP1 Is Crucial for Its Gain-of-Function Cellular and Developmental Roles.” Journal of Experimental Botany 66 (16): 5055–65. https://doi.org/10.1093/jxb/erv177.

35. Grones, Peter, and Jiří Friml. 2015. “Auxin Transporters and Binding Proteins at a Glance.” Journal of Cell Science 128 (1): 1–7. https://doi.org/10.1242/jcs.159418.
36. Hac-Wydro, Katarzyna, and Michał Flasiński. 2015. “The Studies on the Toxicity Mechanism of Environmentally Hazardous Natural (IAA) and Synthetic (NAA) Auxin - The Experiments on Model Arabidopsis Thaliana and Rat Liver Plasma Membranes.” Colloids and Surfaces B: Biointerfaces 130: 53–60. https://doi.org/10.1016/j.colsurfb.2015.03.064.
37. Han, Huibin, Hana Rakusova, Inge Verstraeten, Yuzhou Zhang, and Jiří Friml. 2020. “SCFTIR1/AFB Auxin Signaling for Bending Termination during Shoot Gravitropism.” Plant Physiology 1: pp.00212.2020. https://doi.org/10.1104/pp.20.00212.
38. Huffaker, Alisa, Gregory Pearce, and Clarence A Ryan. 2006. “An Endogenous Peptide Signal in Arabidopsis Activates Components of the Innate Immune Response.”
39. Irani, Niloufer G., Simone Di Rubbo, Evelien Mylle, Jos Van Den Begin, Joanna Schneider-Pizoń, Jaroslava Hniliková, Miroslav Šíša, et al. 2012. “Fluorescent Castasterone Reveals BRI1 Signaling from the Plasma Membrane.” Nature Chemical Biology 8 (6): 583–89. https://doi.org/10.1038/nchembio.958.
40. Ischebeck, Till, Irene Stenzel, Christian Löfke, Theresa Wiessner, Ju Im, Imara Y Perera, Tim Iven, et al. 2013. “Phosphatidylinositol 4 , 5-Bisphosphate In Fl Uences PIN Polarization by Controlling Clathrin-Mediated Membrane Traf Fi Cking in Arabidopsis” 25 (December): 4894–4911. https://doi.org/10.1105/tpc.113.116582.
41. Jásik, Ján, Barbara Boggetti, František Baluška, Dieter Volkmann, Thomas Gensch, Twan Rutten, Thomas Altmann, and Elmon Schmelzer. 2013. “PIN2 Turnover in Arabidopsis Root Epidermal Cells Explored by the Photoconvertible Protein Dendra2.” PLoS ONE 8 (4). https://doi.org/10.1371/journal.pone.0061403.
42. Jasik, Jan, and Elmon Schmelzer. 2016. “Effects of Auxins on PIN-FORMED2 (PIN2) Dynamics Are Not Mediated by Inhibiting PIN2 Endocytosis 1” 172 (October): 1019–31. https://doi.org/10.1104/pp.16.00563.
43. Jelínková, Adriana, Kateřina Malínská, Sibu Simon, Jürgen Kleine-Vehn, Markéta Pařezová, Přemysl Pejchar, Martin Kubeš, et al. 2010. “Probing Plant Membranes with FM Dyes: Tracking, Dragging or Blocking?” Plant Journal 61 (5): 883–92. https://doi.org/10.1111/j.1365-313X.2009.04102.x.
44. Jia, Tianran, Caiji Gao, Yong Cui, Junqi Wang, Yu Ding, Yi Cai, Takashi Ueda, Akihiko Nakano, and Liwen Jiang. 2013. “ARA7(Q69L) Expression in Transgenic Arabidopsis Cells Induces the Formation of Enlarged Multivesicular Bodies.” Journal of Experimental Botany 64 (10): 2817–29. https://doi.org/10.1093/jxb/ert125.
45. Johnson, Alexander, Nataliia Gnyliukh, Walter A. Kaufmann, Madhumitha Narasimhan, Grégory Vert, Sebastian Y. Bednarek, and Jiří Friml. 2020. “Experimental Toolbox for Quantitative Evaluation of Clathrin-Mediated Endocytosis in the Plant Model Arabidopsis.” Journal of Cell Science 133 (15). https://doi.org/10.1242/jcs.248062.
46. Johnson, Alexander, and Grégory Vert. 2017. “Single Event Resolution of Plant Plasma Membrane Protein Endocytosis by TIRF Microscopy.” Frontiers in Plant Science 8 (April): 1–11. https://doi.org/10.3389/fpls.2017.00612.
47. Kania, Urszula, Tomasz Nodzyński, Qing Lu, Glenn R. Hicks, Wim Nerinckx, Kiril Mishev, François Peurois, et al. 2018. “The Inhibitor Endosidin 4 Targets Sec7 Domain-Type Arf Gtpase Exchange Factors and Interferes with Subcellular Trafficking in Eukaryotes[Open].” Plant Cell 30 (10): 2553–72. https://doi.org/10.1105/tpc.18.00127.
48. Kitakura, Saeko, Steffen Vanneste, Stéphanie Robert, Christian Löfke, Thomas Teichmann, Hirokazu Tanaka, and Jiří Friml. 2011. “Clathrin Mediates Endocytosis and Polar Distribution of PIN Auxin Transporters in Arabidopsis.” Plant Cell 23 (5): 1920–31. https://doi.org/10.1105/tpc.111.083030.
49. Kleine-Vehn, Jürgen, Pankaj Dhonukshe, Michael Sauer, Philip B Brewer, Justyna Wiśniewska, Tomasz Paciorek, Eva Benkova, and Jiří Friml. 2008. “ARF GEF-Dependent Transcytosis and Polar Delivery of PIN Auxin Carriers in Arabidopsis,” 526–31. https://doi.org/10.1016/j.cub.2008.03.021.
50. Kleine-Vehn, Jürgen, Łukasz Łangowski, Katrin Willig, Satoshi Naramoto, Christian Luschnig, Willy Govaerts, Stefan W Hell, Johannes Leitner, Hirokazu Tanaka, and Stefan Jakobs. 2011. “Recycling , Clustering , and Endocytosis Jointly Maintain PIN Auxin Carrier Polarity at the Plasma Membrane,” no. 540: 1–13. https://doi.org/10.1038/msb.2011.72.
51. Kleine-Vehn, Jürgen, Łukasz Łangowskia, Jystina Wisniewska, Pankaj Dhonuske, Philip B Brewer, and Jiří Friml. 2008. “Cellular and Molecular Requirements for Polar PIN Targeting and Transcytosis in Plants,” no. July: 1–11. https://doi.org/10.1093/mp/ssn062.

52. Kleine-Vehn, Jürgen, Johannes Leitner, Marta Zwiewka, Michael Sauer, Lindy Abas, Christian Luschnig, and Jiří Friml. 2008. “Differential Degradation of PIN2 Auxin Efflux Carrier by Retromer-Dependent Vacuolar Targeting.” Proceedings of the National Academy of Sciences of the United States of America 105 (46): 17812–17. https://doi.org/10.1073/pnas.0808073105.
53. Konopka, C. A., S. K. Backues, and S. Y. Bednarek. 2008. “Dynamics of Arabidopsis Dynamin-Related Protein 1C and a Clathrin Light Chain at the Plasma Membrane.” The Plant Cell Online 20 (5): 1363–80. https://doi.org/10.1105/tpc.108.059428.
54. Kovács, Mihály, Judit Tóth, Csaba Hetényi, András Málnási-Csizmadia, and James R. Seller. 2004. “Mechanism of Blebbistatin Inhibition of Myosin II.” Journal of Biological Chemistry 279 (34): 35557–63. https://doi.org/10.1074/jbc.M405319200.
55. Lavy, Meirav, and Mark Estelle. 2016. “Mechanisms of Auxin Signaling.” Development (Cambridge) 143 (18): 3226–29. https://doi.org/10.1242/dev.131870.
56. Laxmi, Ashverya, Jianwei Pan, Mustafa Morsy, and Rujin Chen. 2008. “Light Plays an Essential Role in Intracellular Distribution of Auxin Efflux Carrier PIN2 in Arabidopsis Thaliana.” PLoS ONE 3 (1): 1–11. https://doi.org/10.1371/journal.pone.0001510.
57. Leyser, Ottoline. 2018. “Auxin Signaling.” Plant Physiology 176 (1): 465–79. https://doi.org/10.1104/pp.17.00765.
58. Li, Yang, Yaping Wang, Shutang Tan, Zhen Li, Zhi Yuan, Matouš Glanc, David Domjan, et al. 2020. “Root Growth Adaptation Is Mediated by PYLs ABA Receptor-PP2A Protein Phosphatase Complex.” Advanced Science 7 (3). https://doi.org/10.1002/advs.201901455.
59. Lin, Deshu, Shingo Nagawa, Jisheng Chen, Lingyan Cao, Xu Chen, Tongda Xu, Hongjiang Li, et al. 2012. “A ROP GTPase-Dependent Auxin Signaling Pathway Regulates the Subcellular Distribution of PIN2 in Arabidopsis Roots.” Current Biology 22 (14): 1319–25. https://doi.org/10.1016/j.cub.2012.05.019.
60. Loerke, Dinah, Marcel Mettlen, Defne Yarar, Khuloud Jaqaman, Henry Jaqaman, Gaudenz Danuser, and Sandra L. Schmid. 2009. “Cargo and Dynamin Regulate Clathrin-Coated Pit Maturation.” PLoS Biology 7 (3): 0628–39. https://doi.org/10. 1371/journal.pbio.1000057.
61. Löfke, Christian, Marta Zwiewka, Ingo Heilmann, Marc C.E. Van Montagu, Thomas Teichmann, and Jiří Friml. 2013. “Asymmetric Gibberellin Signaling Regulates Vacuolar Trafficking of PIN Auxin Transporters during Root Gravitropism.” Proceedings of the National Academy of Sciences of the United States of America 110 (9): 3627–32. https://doi.org/10.1073/pnas.1300107110.
62. Marcote, María Jesús, Gloria Sancho-Andrés, Esther Soriano-Ortega, and Fernando Aniento. 2016. “Sorting Signals for PIN1 Trafficking and Localization.” Plant Signaling & Behavior 11 (8): e1212801. https://doi.org/10.1080/15592324.2016.1212801.
63. Mazur, Ewa, Eva Benková, and Jiří Friml. 2016. “Vascular Cambium Regeneration and Vessel Formation in Wounded Inflorescence Stems of Arabidopsis.” Scientific Reports 6: 1–15. https://doi.org/10.1038/srep33754.
64. Mazur, Ewa, Michelle Gallei, Maciek Adamowski, Huibin Han, Hélène S. Robert, and Jiří Friml. 2020. “Clathrin-Mediated Trafficking and PIN Trafficking Are Required for Auxin Canalization and Vascular Tissue Formation in Arabidopsis.” Plant Science 293 (November 2019). https://doi.org/10.1016/j.plantsci.2020.110414.
65. Mazur, Ewa, Ivan Kulik, Jakub Hajný, and Jiří Friml. 2020. “Auxin Canalization and Vascular Tissue Formation by TIR1/AFB-mediated Auxin Signaling in Arabidopsis.” New Phytologist. https://doi.org/10.1111/nph.16446.
66. Mettlen, Marcel, Ping-hung Chen, Saipraveen Srinivasan, Gaudenz Danuser, and Sandra L Schmid. 2018. “Regulation of Clathrin-Mediated Endocytosis.” Annu. Rev. Biochem, no. 87: 871–96.
67. Michalko, Jaroslav, Matouŝ Glanc, Catherine Perrot-Rechenmann, and Jirí Friml. 2016. “Strong Morphological Defects in Conditional Arabidopsis Abp1 Knock-down Mutants Generated in Absence of Functional ABP1 Protein.” F1000Research 5 (0): 1–13. https://doi.org/10.12688/f1000research.7654.1.
68. Naramoto, Satoshi, Jürgen Kleine-Vehn, Stéphanie Robert, Masaru Fujimoto, Tomoko Dainobu, Tomasz Paciorek, Takashi Ueda, et al. 2010. “ADP-Ribosylation Factor Machinery Mediates Endocytosis in Plant Cells.” Proceedings of the National Academy of Sciences of the United States of America 107 (50): 21890–95. https://doi.org/10.1073/pnas.1016260107.
69. Naramoto, Satoshi, Marisa S. Otegui, Natsumaro Kutsuna, Riet de Rycke, Tomoko Dainobu, Michael Karampelias, Masaru Fujimoto, et al. 2014. “Insights into the Localization and Function of the

Membrane Trafficking Regulator GNOM ARF-GEF at the Golgi Apparatus in Arabidopsis." Plant Cell 26 (7): 3062–76. https://doi.org/10.1105/tpc.114.125880.
70. Narasimhan, Madhumitha, Alexander Johnson, Roshan Prizak, Walter Anton Kaufmann, Shutang Tan, Barbara Casillas-Pérez, and Jiří Friml. 2020. "Evolutionarily Unique Mechanistic Framework of Clathrin-Mediated Endocytosis in Plants." ELife 9: 1–30. https://doi.org/10.7554/eLife.52067.
71. Noack, Lise C., and Yvon Jaillais. 2017. "Precision Targeting by Phosphoinositides: How PIs Direct Endomembrane Trafficking in Plants." Current Opinion in Plant Biology 40: 22–33. https://doi.org/10.1016/j.pbi.2017.06.017.
72. Obrig, T. G., W. J. Culp, W. L. McKeehan, and B. Hardesty. 1971. "The Mechanism by Which Cycloheximide and Related Glutarimide Antibiotics Inhibit Peptide Synthesis on Reticulocyte Ribosomes." Journal of Biological Chemistry 246 (1): 174–81.
73. Oochi, Akihiro, Jakub Hajny, Kosuke Fukui, Yukio Nakao, Michelle Gallei, Mussa Quareshy, Koji Takahashi, et al. 2019. "Pinstatic Acid Promotes Auxin Transport by Inhibiting Pin Internalization." Plant Physiology 180 (2): 1152–65. https://doi.org/10.1104/pp.19.00201.
74. Ortiz-morea, Fausto Andres, Daniel V Savatin, Wim Dejonghe, Rahul Kumar, and Yu Luo. 2016. "Danger-Associated Peptide Signaling in Arabidopsis Requires Clathrin." https://doi.org/10.1073/pnas.1605588113.
75. Paciorek, Tomasz, Nadia Ruthardt, Jan Petra, David A Morris, Neil Emans, and Gerd Ju. 2005. "Auxin Inhibits Endocytosis and Promotes Its Own Efflux from Cells," no. June 2014. https://doi.org/10.1038/nature03633.
76. Pan, Jianwei, Shozo Fujioka, Jianling Peng, Jianghua Chen, Guangming Li, and Rujin Chen. 2009. "The E3 Ubiquitin Ligase SCF TIR1 / AFB and Membrane Sterols Play Key Roles in Auxin Regulation of Endocytosis , Recycling , and Plasma Membrane Accumulation of the Auxin Efflux Transporter PIN2 in Arabidopsis Thaliana" 21 (February): 568–80. https://doi.org/10.1105/tpc.108.061465.
77. Paponov, Ivan A., William Teale, Daniel Lang, Martina Paponov, Ralf Reski, Stefan A. Rensing, and Klaus Palme. 2009. "The Evolution of Nuclear Auxin Signalling." BMC Evolutionary Biology 9 (1): 1–16. https://doi.org/10.1186/1471-2148-9-126.
78. Paponov, Ivan, and Klaus Palme. 2019. "Natural Auxin Does Not Inhibit Brefeldin A Induced PIN1 and PIN2 Internalization in Root Cells" 10 (May): 1–7. https://doi.org/10.3389/fpls.2019.00574.
79. Petelska, Aneta D., and Zbigniew A. Figaszewski. 2000. "Effect of PH on the Interfacial Tension of Lipid Bilayer Membrane." Biophysical Journal 78 (2): 812–17. https://doi.org/10.1016/S0006-3495(00)76638-0.
80. Platre, Matthieu Pierre, Vincent Bayle, Laia Armengot, Joseph Bareille, Maria del Mar Marquès-Bueno, Audrey Creff, Lilly Maneta-Peyret, et al. 2019. "Developmental Control of Plant Rho GTPase Nano-Organization by the Lipid Phosphatidylserine." Science 364 (6435): 57–62. https://doi.org/10.1126/science.aav9959.
81. Prát, Tomáš, Jakub Hajný, Wim Grunewald, Mina Vasileva, Gergely Molnár, Ricardo Tejos, Markus Schmid, Michael Sauer, and Jiří Friml. 2018. "WRKY23 Is a Component of the Transcriptional Network Mediating Auxin Feedback on PIN Polarity." PLoS Genetics 14 (1): 1–18. https://doi.org/10.1371/journal.pgen.1007177.
82. Rahman, Abidur, Alex Bannigan, Waheeda Sulaman, Priit Pechter, Elison B Blancaflor, Tobias I Baskin, Plant Biology Division, Samuel Roberts, and Noble Foundation. 2007. "Auxin , Actin and Growth of the Arabidopsis Thaliana Primary Root," 514–28. https://doi.org/10.1111/j.1365-313X.2007.3068.x.
83. Rakusová, Hana, Mohamad Abbas, Huibin Han, Siyuan Song, Hélène S. Robert, and Jiří Friml. 2016. "Termination of Shoot Gravitropic Responses by Auxin Feedback on PIN3 Polarity." Current Biology 26 (22): 3026–32. https://doi.org/10.1016/j.cub.2016.08.067.
84. Rakusová, Hana, Huibin Han, Petr Valošek, and Jiří Friml. 2019. "Genetic Screen for Factors Mediating PIN Polarization in Gravistimulated Arabidopsis Thaliana Hypocotyls." Plant Journal 98 (6): 1048–59. https://doi.org/10.1111/tpj.14301.
85. Ravichandran, Sree Janani, Nguyen Manh Linh, and Enrico Scarpella. 2020. "The Canalization Hypothesis - Challenges and Alternatives." New Phytologist. https://doi.org/10.1111/nph.16605.
86. Retzer, Katarzyna, Maria Akhmanova, Nataliia Konstantinova, Kateřina Malínská, Johannes Leitner, Jan Petrášek, and Christian Luschnig. 2019. "Brassinosteroid Signaling Delimits Root Gravitropism via Sorting of the Arabidopsis PIN2 Auxin Transporter." Nature Communications 10 (1). https://doi.org/10.1038/s41467-019-13543-1.

87. Rigal, Adeline. 2015. “Live Cell Imaging of FM4-64, a Tool for Tracing the Endocytic Pathways in Arabidopsis Root Cells.” Plant Cell Expansion: Methods and Protocols 1242: 1–227. https://doi.org/10.1007/978-1-4939-1902-4.
88. Robert, Hélène S., Peter Grones, Anna N. Stepanova, Linda M. Robles, Annemarie S. Lokerse, Jose M. Alonso, Dolf Weijers, and Jiří Friml. 2013. “Local Auxin Sources Orient the Apical-Basal Axis in Arabidopsis Embryos.” Current Biology 23 (24): 2506–12. https://doi.org/10.1016/j.cub.2013.09.039.
89. Robert, Hélène S, Chulmin Park, Carla Loreto Guitérrez, and Barbara Wójcikowska. 2018. “Maternal Auxin Supply Contributes to Early Embryo Patterning in Arabidopsis” 4 (8): 548–53. https://doi.org/10.1038/s41477-018-0204-z.Maternal.
90. Robert, Stephanie, Elke Barbez, Michael Sauer, Tomasz Paciorek, Pawel Baster, Kenichiro Hayashi, Pankaj Dhonukshe, et al. 2010. “ABP1 Mediates Auxin Inhibition of Clathrin-Dependent Endocytosis in Arabidopsis,” 111–21. https://doi.org/10.1016/j.cell.2010.09.027.
91. Robinson, David G., David Scheuring, Satoshi Naramoto, and Jirí Friml. 2011. “ARF1 Localizes to the Golgi and the Trans-Golgi Network.” Plant Cell 23 (3): 846–49. https://doi.org/10.1105/tpc.110.082099.
92. Rubbo, Simone Di, Niloufer G. Irani, Soo Youn Kim, Zheng Yi Xu, Astrid Gadeyne, Wim Dejonghe, Isabelle Vanhoutte, et al. 2013. “The Clathrin Adaptor Complex AP-2 Mediates Endocytosis of Brassinosteroid INSENSITIVE1 in Arabidopsis.” Plant Cell 25 (8): 2986–97. https://doi.org/10.1105/tpc.113.114058.
93. Salanenka, Yuliya, Inge Verstraeten, Christian Löfke, Kaori Tabata, Satoshi Naramoto, Matouš Glanc, and Jirí Friml. 2018. “Gibberellin DELLA Signaling Targets the Retromer Complex to Redirect Protein Trafficking to the Plasma Membrane.” Proceedings of the National Academy of Sciences of the United States of America 115 (14): 3716–21. https://doi.org/10.1073/pnas.1721760115.
94. Satiat-Jeunemaitre, B., L. Cole, T. Bourett, R. Howard, and C. Hawks. 1996. “Brefeldin A Effects in Plant and Fungal Cells: Something New about Vesicle Trafficking?” Journal of Microscopy 181 (2): 162–77. https://doi.org/10.1046/j.1365-2818.1996.112393.x.
95. Satiat-Jeunemaitre, Beatrice, and Chris Hawes. 1994. “G.A.T.T. (A General Agreement on Traffic and Transport) and Brefeldin A in Plant Cells.” The Plant Cell 6 (4): 463. https://doi.org/10.2307/3869925.
96. Sauer, Michael, Jozef Balla, Christian Luschnig, Justyna Wis, Vilém Reinöhl, and Eva Benková. 2006. “Canalization of Auxin Flow by Aux / IAA-ARF-Dependent Feedback Regulation of PIN Polarity,” 2902–11. https://doi.org/10.1101/gad.390806.integrated.
97. Sauer, Michael, Jozef Balla, Christian Luschnig, Justyna Wiśniewska, Vilém Reinöhl, Jiří Friml, and Eva Benková. 2006. “Canalization of Auxin Flow by Aux/IAA-ARF-Dependent Feedback Regulation of PIN Polarity.” Genes and Development 20 (20): 2902–11. https://doi.org/10.1101/gad.390806.
98. Scarpella, Enrico, Danielle Marcos, Jiří Friml, and Thomas Berleth. 2006. “Control of Leaf Vascular Patterning by Polar Auxin Transport.” Genes and Development 20 (8): 1015–27. https://doi.org/10.1101/gad.1402406.
99. Shinohara, Naoki, Catherine Taylor, and Ottoline Leyser. 2013. “Strigolactone Can Promote or Inhibit Shoot Branching by Triggering Rapid Depletion of the Auxin Efflux Protein PIN1 from the Plasma Membrane.” PLoS Biology 11 (1). https://doi.org/10.1371/journal.pbio.1001474.
100. Simon, Mathilde Laetitia Audrey, Matthieu Pierre Platre, Sonia Assil, Ringo Van Wijk, William Yawei Chen, Joanne Chory, Marlène Dreux, Teun Munnik, and Yvon Jaillais. 2014. “A Multi-Colour/Multi-Affinity Marker Set to Visualize Phosphoinositide Dynamics in Arabidopsis.” Plant Journal 77 (2): 322–37. https://doi.org/10.1111/tpj.12358.
101. Simon, Sibu, Martin Kubeš, Pawel Baster, Stéphanie Robert, Petre Ivanov Dobrev, Jiří Friml, Jan Petrášek, and Eva Zažímalová. 2013. “Defining the Selectivity of Processes along the Auxin Response Chain: A Study Using Auxin Analogues.” New Phytologist 200 (4): 1034–48. https://doi.org/10.1111/nph.12437.
102. Sze, Heven, and Salil Chanroj. 2018. “Plant Endomembrane Dynamics: Studies of K+/H+ Antiporters Provide Insights on the Effects of PH and Ion Homeostasis.” Plant Physiology 177 (3): 875–95. https://doi.org/10.1104/pp.18.00142.
103. Tan, Shutang, Melinda Abas, Inge Verstraeten, Matouš Glanc, Gergely Molnár, Jakub Hajný, Pavel Lasák, et al. 2020. “Salicylic Acid Targets Protein Phosphatase 2A to Attenuate Growth in Plants.” Current Biology 30 (3): 381-395.e8. https://doi.org/10.1016/j.cub.2019.11.058.
104. Tejos, Ricardo, Michael Sauer, Steffen Vanneste, Miriam Palacios-Gomez, Hongjiang Li, Mareike Heilmann, Ringo van Wijk, et al. 2014. “Bipolar Plasma Membrane Distribution of Phosphoinositides

and Their Requirement for Auxin-Mediated Cell Polarity and Patterning in Arabidopsis." Plant Cell 26 (5): 2114–28. https://doi.org/10.1105/tpc.114.126185.
105. Ueda, Takashi, Tomohiro Uemura, Masa H. Sato, and Akihiko Nakano. 2004. "Functional Differentiation of Endosomes in Arabidopsis Cells." Plant Journal 40 (5): 783–89. https://doi.org/10.1111/j.1365-313X.2004.02249.x.
106. Vieten, Anne, Steffen Vanneste, Justyna Wiśniewska, Eva Benková, René Benjamins, Tom Beeckman, Christian Luschnig, and Jiří Friml. 2005. "Functional Redundancy of PIN Proteins Is Accompanied by Auxin-Dependent Cross-Regulation of PIN Expression." Development 132 (20): 4521–31. https://doi.org/10.1242/dev.02027.
107. Wabnik, Krzysztof, Jürgen Kleine-Vehn, Jozef Balla, Michael Sauer, Satoshi Naramoto, Vilém Reinöhl, Roeland M.H. Merks, Willy Govaerts, and Jiří Friml. 2010. "Emergence of Tissue Polarization from Synergy of Intracellular and Extracellular Auxin Signaling." Molecular Systems Biology 6 (447). https://doi.org/10.1038/msb.2010.103.
108. Wabnik, Krzysztof, Hélène S. Robert, Richard S. Smith, and Jiří Friml. 2013. "Modeling Framework for the Establishment of the Apical-Basal Embryonic Axis in Plants." Current Biology 23 (24): 2513–18. https://doi.org/10.1016/j.cub.2013.10.038.
109. Wang, C., X. Yan, Q. Chen, N. Jiang, W. Fu, B. Ma, J. Liu, C. Li, S. Y. Bednarek, and J. Pan. 2013. "Clathrin Light Chains Regulate Clathrin-Mediated Trafficking, Auxin Signaling, and Development in Arabidopsis." The Plant Cell 25 (2): 499–516. https://doi.org/10.1105/tpc.112.108373.
110. Wangenheim, Daniel von, Robert Hauschild, Matyáš Fendrych, Vanessa Barone, Eva Benková, and Jiří Friml. 2017. "Live Tracking of Moving Samples in Confocal Microscopy for Vertically Grown Roots." ELife 6. https://doi.org/10.7554/eLife.26792.
111. Xu, J. 2005. "Dissection of Arabidopsis ADP-RIBOSYLATION FACTOR 1 Function in Epidermal Cell Polarity." The Plant Cell Online 17 (2): 525–36. https://doi.org/10.1105/tpc.104.028449.
112. Xu, Tongda. 2010. "Cell Surface- and Rho GTPase-Based Auxin Signaling Controls Cellular Interdigitation in Arabidopsis." Cell 23 (1): 1–7. https://doi.org/10.1161/CIRCULATIONAHA.110.956839.
113. Zal, Tomasz, M. Anna Zal, Carina Lotz, Craig J. Goergen, and Nicholas R.J. Gascoigne. 2006. "Spectral Shift of Fluorescent Dye FM4-64 Reveals Distinct Microenvironment of Nuclear Envelope in Living Cells." Traffic 7 (12): 1607–13. https://doi.org/10.1111/j.1600-0854.2006.00498.x.
114. Zhang, Chunhua, Michelle Q. Brown, Wilhelmina van de Ven, Zhi-Min Zhang, Bin Wu, Michael C. Young, Lukáš Synek, et al. 2016. "Endosidin2 Targets Conserved Exocyst Complex Subunit EXO70 to Inhibit Exocytosis." Proceedings of the National Academy of Sciences 113 (1): E41–50. https://doi.org/10.1073/pnas.1521248112.
115. Zhang, Jing, Steffen Vanneste, Philip B. Brewer, Marta Michniewicz, Peter Grones, Jürgen Kleine-Vehn, Christian Löfke, et al. 2011. "Inositol Trisphosphate-Induced Ca2+ Signaling Modulates Auxin Transport and Pin Polarity." Developmental Cell 20 (6): 855–66. https://doi.org/10.1016/j.devcel.2011.05.013.
116. Zhang, Xixi, Maciek Adamowski, Petra Marhava, Shutang Tan, Yuzhou Zhang, Lesia Rodriguez, Marta Zwiewka, et al. 2020. "Arabidopsis Flippases Cooperate with ARF GTPase Exchange Factors to Regulate the Trafficking and Polarity of PIN Auxin Transporters." The Plant Cell 12: tpc.00869.2019. https://doi.org/10.1105/tpc.19.00869.
117. Zwiewka, Marta, Veronika Bilanovičová, Yewubnesh Wendimu Seifu, and Tomasz Nodzyński. 2019. "The Nuts and Bolts of PIN Auxin Efflux Carriers." Frontiers in Plant Science 10 (July). https://doi.org/10.3389/fpls.2019.00985.
118. Zwiewka, Marta, Tomasz Nodzyński, Stéphanie Robert, Steffen Vanneste, and Jiří Friml. 2015. "Osmotic Stress Modulates the Balance between Exocytosis and Clathrin-Mediated Endocytosis in Arabidopsis Thaliana." Molecular Plant 8 (8): 1175–87. https://doi.org/10.1016/j.molp.2015.03.007.

2.2 Clathrin-mediated trafficking and PIN trafficking are required for auxin canalization and vascular tissue formation in Arabidopsis

Adapted and modified from:

Mazur E, **Gallei M**, Adamowski M, Han H, Robert HS, Friml J. *Clathrin-mediated trafficking and PIN trafficking are required for auxin canalization and vascular tissue formation in Arabidopsis*. Plant Sci. 2020;293. doi:10.1016/j.plantsci.2020.110414

This study aims to answer the question which cellular processes related to PIN subcellular dynamics are involved in the establishment of auxin conducting channels and the formation of vascular tissue, both processes important for auxin canalization. We combined the well-established experimental models of vascular tissue regeneration after wounding and *de novo* vasculature formation from an exogenous auxin source with genetic and pharmacological methods to answer the question. We involved mutants defective in CME, actin cytoskeleton and in polar auxin transport regulation and PIN trafficking. Further we employed different auxin analogues and an inhibitor of actin polymerization. We found that clathrin-mediated and actin-dependent trafficking of PIN proteins is crucial for auxin canalization and vascular strand formation.

Contributions Michelle Gallei:

- Writing and correcting the manuscript
- Correcting the figures
- Revising the manuscript according to reviewer comments

2.2.1 Introduction

The development of plants is a very flexible and dynamic process, which is characterized, among others, by post embryonic organ formation of new leaves, flowers and roots and a high capability of regeneration after wounding [1]. *De novo* tissue patterning and re-patterning typically depend on the coordinated polarization of individual cells leading to polarization of the whole tissues. The important driver for polarity and patterning in plant development is the intercellular morphogen-like plant signaling molecule auxin, which, in some developmental contexts, is able on its own to establish polarized auxin transporting channels [2]. The canalization hypothesis describes the unique property of auxin being transported actively from

cell to cell in a directional manner by regulating the polarity of its own flow [3,4,5]. This feed-back regulation has been proposed to be a key prerequisite for a spontaneous formation of these auxin transport channels [6]. The direction and throughput of the auxin flow depend on the polar localization of the auxin transport proteins PIN (PIN-FORMED) at the plasma membrane (PM) [7,8]. During venation in leaves [9], shoot apical meristem organogenesis [10,11], shoot branching [12] or regeneration of wounded vasculature [13] it has been shown that localized and polarized PIN1 expression and thus directional auxin transport routes demarcate the position of future vascular strands. To ensure correct tissue patterning and vascular development PIN subcellular localization must be tightly regulated. PIN proteins have the ability to change their subcellular localization dynamically thus allowing for a flexible rise of new, polarized routes for auxin. Especially when the polar auxin flow is disrupted by wounding they can adapt dynamically and re-establish auxin flow by the formation of new channels and ultimately leading to the formation of new vasculature strands [5,12].

The dynamic changes in the subcellular PIN localization are presumably related to the constitutive cycling of PINs from and to the PM [14], involving clathrin-mediated endocytosis (CME) [15]. Additionally, auxin itself can increase its own efflux by stabilizing PINs at the PM by interfering with their internalization [16,17]. Mutations within the clathrin heavy chain (CHC), an essential protein for CME and some intracellular trafficking pathways[18], interfere with polar PIN distribution, auxin distribution patterns and lead to auxin transport-related phenotypes linking PIN polar localization with endocytosis [19]. Further it was shown that many post-endocytic processes and trafficking of cargoes, amongst others PINs, strongly depend on an intact actin cytoskeleton [20] despite the CME can operate [21] and PIN polarity itself can be generated at least within polarized tissues also without intact actin cytoskeleton [22].

Even though major progress was made in the last years to understand how PINs can change their polarity and thus guide auxin flow through the plant it still remains elusive, which cellular processes related to PIN subcellular dynamics are involved in the establishment of auxin conducting channels and the formation of vascular tissue.

Elegant ways to study canalization is to observe vasculature regeneration after wounding or vasculature formation from a place of local auxin application. This allows to follow *de novo* auxin channel and vasculature formation, which are either formed around the wound or

between an external auxin source and pre-existing vasculature. Performing this in the model *Arabidopsis thaliana*, allows to exploit the large genetic and pharmacological toolbox [13,23].

By the use of genetic and pharmacological methods applied to the model of vascular tissue regeneration after wounding or *de novo* vasculature formation from an artificial auxin source, this work demonstrates that clathrin-mediated and actin-dependent trafficking of PIN proteins are crucial for auxin canalization and vascular strands formation.

2.2.2 Results

2.2.2.1 Vasculature regeneration after wounding in endocytosis-defective mutants

Stem vasculature regeneration after wounding is associated with the induction of polarized PIN1-expressing auxin transport channels, however, it is not clear yet, which cellular processes are involved in the establishment of these channels.

Given that PIN proteins undergo clathrin-mediated constitutive endocytic recycling, and this was proposed to be important for various PIN relocations [15], we first tested the involvement of CME in vasculature regeneration. To this end, we wounded inflorescence stems of Col-0, *chc2-1* and *chc2-2* mutants defective in the **c**lathrin **h**eavy **c**hain, a critical component for CME and some intracellular trafficking pathways [18, 19, 28]. Wounding was performed in the basal part of the stems, which were stimulated mechanically to obtain secondary growth [13] (Fig. 1A). In analyzed control stems regenerated vasculature developed 6 days after wounding around the inner side of the wound connecting the incised pre-existing vasculature (Fig. 1B). Regenerated vasculature exhibited all features recognized in mature vessels; they were arranged in continued strands and connected together by perforation plates (Fig. 1B, inset). Secondary cell wall patterning was recognizable (Fig. 1B, inset). In contrast, both of the analyzed clathrin heavy chain-defective mutants *chc2-1* and *chc2-2* either did not show any signs of vasculature regeneration near the wound (Fig.1C) or the regenerated vasculature was highly defective as seen in case of *chc2-2* (Supplementary Fig. S1A).

Next, we tested the line *XVE>>AUXILIN-LIKE2*, where clathrin-mediated endocytosis is conditionally inhibited by the overexpression of AUXILIN-LIKE2, a putative uncoating factor in clathrin-mediated processes [25]. Also in this case, development of vasculature was completely stopped following AUXILIN-LIKE2 induction (Fig. 1D). In the non-induced *XVE>>AUXILIN-LIKE2* stems vasculature developed in the neighborhood of the wound (Supplementary Fig. S1B). To evaluate the effect of β-estradiol alone on vasculature

regeneration, Col-0 wild type plants were treated and the regeneration of vasculature after wounding was observed and quantified (Supplementary Fig. S1C, D).

Quantification of the regeneration capacity revealed no vasculature formation around a wound in *chc2-1* (0% regeneration, N=15) and β-estradiol induced *XVE>>AUXILIN-LIKE2* stems (0%, N=15) and only limited regeneration in incised *chc2-2* stems (40%, N=15) compared to the Col-0 control (100%, N=15) (Fig. 1E-F).

These results show that mutants interfering with clathrin and therefore with CME are defective in stem vasculature regeneration after wounding.

2.2.2.2 Vasculature formation from external auxin sources in endocytosis-defective mutants

Next we tested requirement of clathrin-mediated trafficking in canalization processes more directly by looking at the vasculature formation from the place of local auxin application. In these experiments we applied auxin and inhibitors in a droplet of lanolin paste at the side of the stem below the wound as established previously [29] (Fig. 2A).

Natural auxin (IAA, indole-3-acetic acid, 10 μM water solution) externally applied onto the Col-0 inflorescence stems led to the formation of vascular strands, extending from the site of auxin application to the pre-existing vasculature (Fig. 2B). Mature vessels, recognized by the features typical for the tracheary elements, such as secondary cell wall patterning and open perforation plates, developed 6 days after application (DAA) (Fig. 2B, inset). In turn, in all of the analyzed endocytosis-defective mutants (*chc2-1*, *chc2-2*, induced *XVE>>AUXILIN-LIKE2*), no vasculature developed in response to the locally applied auxin (0%, N=15 for each of analyzed samples; Fig. 2C-D, Supplementary Fig. S2A). In contrast, in almost all analyzed Col-0 (90%, N=15) and in non-induced *XVE>>AUXILIN-LIKE2* stems (70%, N=10) vascular strands developed from the sites of auxin application (Fig. 2E-F, Supplementary Fig. S2B). To evaluate the effect of β-estradiol alone on vasculature formation from an external source of auxin, Col-0 wild type plants were co-treated with and the vasculature formation was observed and quantified (Supplementary Fig. S2C, D).

These results show that formation of the vascular strands from the place of the local auxin application, similar to vasculature regeneration, requires functioning clathrin-mediated trafficking.

2.2.2.3 Auxin channel formation from external auxin sources in endocytosis-defective mutants

Next we tested whether the defects in vasculature formation in endocytosis mutants are due to defects in the establishment of auxin-conducting channels which can be visualized by the auxin response and auxin transport reporters *DR5rev::GFP* and *pPIN1::PIN1-GFP*, respectively.

Local application of natural auxin onto wounded inflorescence stems of *DR5rev::GFP* and *pPIN1::PIN1-GFP* transgenic plants is accompanied by the formation of PIN1-mediated, DR5-positive channels from the exogenous source, 4 DAA (Fig. 3A-B). Moreover, application of natural auxin onto the surface of these stems led to the development of vascular strands extending from the sites of auxin application to the pre-existing vasculature (Supplementary Fig. S3A). In addition to these, in the non-induced *XVE>>AUXILIN-LIKE2* x *DR5rev::GFP* transgenic lines, we also observed establishment of DR5-positive channels 4 DAA (Supplementary Fig. S3B) resulting in vascular strand formation in the following 2 days, like it was shown in Supplementary Fig. S2B. In contrast, in the β-estradiol induced *XVE>>AUXILIN-LIKE2* x *DR5rev::GFP* stems, neither DR5-positive auxin channels nor vasculature development was observed (Fig. 3C, F).

Next, we tested the effect of PISA, a synthetic auxin analog, which stabilizes PINs at the PM by inhibiting their internalization [30]. In these experiments we locally applied PISA together with auxin or without auxin onto stems of *DR5rev::GFP* and *pPIN1::PIN1-GFP* plants and analyzed them 4 DAA. No formation of auxin-channels from the site of locally applied PISA was observed (Fig. 3D-E and Supplementary Fig. S3C-D). Elevated auxin response in the outer tissues, neighboring the application sites, but no auxin channel formation was visible when PISA+IAA were applied (Fig. 3D, inset). A similar situation was observed in the *pPIN1::PIN1-GFP* stems. In this case, application of PISA together with IAA shows no PIN1-positive channel formation from the sources of local applications (Fig. 3E). Non-polar PIN1 expression was found only in the cells of the outer tissue neighboring the sites of the compound application (Fig. 3E, inset). Definitely, in both of the experiments performed with PISA + IAA application, neither PIN1-mediated auxin channels nor vascular strand development was observed (0% in each of tested samples) (Fig. 3G).

These results reveal that already PIN1-expressing, DR5-positive auxin channel formation from the local auxin source is defective in mutants or following treatments interfering with clathrin-mediated trafficking in general or PIN1 internalization more specifically. Overall, this suggests

that it is specifically the functional PIN internalization, which is required for formation of auxin channels leading to vasculature formation.

2.2.2.4 Vasculature regeneration and auxin canalization in actin-defective mutants

Next we tested whether also subcellular trafficking is required for vascular tissue regeneration and canalization. Given that not endocytosis itself but post-endocytic processes and trafficking of PIN proteins and other cargoes in plants is strongly dependent on the actin cytoskeleton [20,21], we tested *actin2, actin7, actin8* (*act2, act7, act8*) mutants for their capacity to regenerate vasculature and to form auxin channels from an external auxin source.

We observed that *act7* and *act8* mutants exhibited a complete block of vasculature regeneration (0% of analyzed *act7* and *act8* stems; N=10), whereas *act2* showed some regeneration, by forming defective vascular strands around the wound (50%, N=10) comparing to Col-0 controls (90%, N=10) (Fig. 4A-C, Fig.4J and Supplementary Fig. S4A).

Next, we locally applied auxin onto the stems of actin-defective mutants and Col-0 controls and analyzed vasculature formation 6 DAA. The vasculature formation from the sites of auxin application was highly defective in *act2*, *act7* and *act8* mutants (Fig. 4D-F), characterized by unshaped vessels arranged in disorganized and typically non-continued vascular-like strands (Fig. 4D, inset) whereas in analyzed Col-0 controls, continuous vascular strands developed from the sites of local auxin application (100%; N=10) (Supplementary Fig. S4B). In this experimental set-up, vasculature formation was not completely stopped, but strongly defective development was observed in the tested mutants (80% in *act2*; 30% in *act8* and 20% in *act7* samples; N=10 for each of the actin-defective mutants) (Fig. 4K).

To complement these observations, we also interfered with actin cytoskeleton pharmacologically using Latrunculin B (LatB), a well-established drug depolymerizing actin cytoskeleton [22,31]. When LatB together with IAA was applied at the stem side of either Col-0, *DR5rev::GFP* or *pPIN1::PIN1-GFP*, vasculature formation and formation of DR5-positive and PIN1-GFP-positive auxin channels was also completely inhibited by the co-treatment (0% in both *DR5rev::GFP* and *pPIN1::PIN1-GFP* samples, N=10 for each of the lines)(Fig. 4G-I, L). In addition, we tested Col-0, *DR5rev::GFP* and *pPIN1::PIN1-GFP* stems treated with LatB without auxin and analyzed 6 DAA. Also here, neither PIN1-mediated, DR5-positive auxin channels nor vascular strand development was observed (Supplementary Fig. S4C-E).

Altogether, these observations reveal that an intact actin cytoskeleton is required for establishment of PIN1-expressing, DR5-positive auxin channels and for vascular tissue formation from an external auxin source as well as for vasculature regeneration after wounding.

2.2.2.5 Vasculature regeneration and auxin canalization in big mutants

To test the requirement of PIN trafficking more specifically and by an independent method, we tested mutants in the Callosin-like protein, BIG that have been shown to have defects in polar auxin transport regulation and PIN trafficking [16, 26].

Two independent alleles of *big*, i.e. *doc1* and *tir3,* were tested for their capability of vasculature regeneration and auxin channel formation. The *tir3* mutant failed to regenerate vasculature after wounding and to form vasculature from an external source of auxin (0% for both experiments, N=15) (Fig. 5A, E-G). Also *doc1* x *pPIN1::PIN1-GFP* failed to regenerate vasculature or to form vasculature from an external source of auxin. Additionally no PIN1-mediated auxin channels could be observed (0% for both experiments, N=15) (Fig 5B, C, E-G). Only in the control line *pPIN1::PIN1-GFP* PIN1-positive channels and new vasculature strands developed from the external source of auxin (Fig 5D, E-G).

The analysis of these mutants confirmed that polar auxin transport and PIN trafficking is important for auxin channel establishment and vasculature formation as well as regeneration after wounding.

2.2.3 Discussion

Formation and regeneration of auxin-conducting channels demarcating vascular strands in plants is a spectacular example of the plant's flexible and self-organizing development. These processes involve tightly regulated intercellular communication, hormonal signaling and coordinated tissue repolarization. Experimental data have proven a key role of auxin in these processes [32]. Nonetheless, the molecular and cellular mechanisms underlying auxin channel formation and vasculature patterning remain mostly unrevealed. Our study is part of the decades long efforts aimed to elucidate the so-called canalization hypothesis [3]. The observations show the crucial importance of subcellular, actin-mediated PIN mobility and PIN internalization by clathrin-mediated trafficking mechanisms in processes linked to canalization including auxin channel formation, *de novo* vascular formation and vascular regeneration after wounding.

2.2.3.1 Subcellular PIN dynamics are important for auxin canalization and vasculature formation

PIN proteins undergo constitutive subcellular dynamics of repeated steps of clathrin-mediated endocytosis and recycling back to the PM [15,19,20]. The physiological role of this dynamics remains unclear but it can be important for both, maintaining PIN polar distribution at the PM [22,33] or dynamically changing PIN polarity, for example in response to environmental signals such as gravity or endogenous signals, presumably including auxin [14,27,34]. Here we tested whether this PIN dynamics is also required in auxin canalization-related contexts such as vasculature formation from an auxin source or vasculature regeneration since these processes require coordinated PIN polarization in individual cells [5,13,35].

Indeed, if correct trafficking of PINs is impaired either genetically, for example by a mutation in the gene coding for the PIN trafficking and polar auxin transport regulator BIG or pharmacologically, by PISA, which stabilizes PINs at the PM, plants display phenotypes associated with a decrease in polar auxin transport [26,30]. This suggests that PINs need to be in a state where they are, on the one hand, mobile or capable of a re-localization and, on the other hand, this mobility must be coordinated in a way that the proteins end up in the right location. By the stabilization of PINs at the PM by the use of PISA, we could show that no auxin channel formation from an external source is initiated, indicating that PINs at the PM are not sufficient and need to undergo subcellular dynamics to allow for this process. Further we show that in *big*, a mutant with a defect in polar auxin transport which is affecting the localization of PIN1, neither channel formation nor vascular regeneration is occurring, further suggesting that not only subcellular dynamics itself but coordinated trafficking is necessary for auxin canalization and vasculature formation.

2.2.3.2 Endocytosis in auxin canalization and vasculature formation

The key process in auxin canalization – formation of polarized auxin channels away from the localized auxin source is conceptually unclear. How is the auxin signal propagated across the tissue and how does it allow for coordinated PIN polarization in individual cells? Studies in the shoot apical meristem proposed mechanical transmission of the signal [36] or other modelling efforts proposed that auxin-mediated PIN polarization can be theoretically realized by cooperation of intracellular and extracellular auxin perception with the latter inhibiting PIN internalization leading to selective retention of PINs on the cell side away from the auxin source [37]. A possible experimental support for this model provided observations that auxin interferes with endocytosis and thus also internalization of PINs from the cell surface [15,16,17,38]. The

PIN internalization is mediated by a clathrin-mediated mechanism and it has been experimentally shown that CME plays a key role in the regulation of PIN polarity and its interference significantly disturbs plant development [14,25].

Therefore, we tested whether functional CME is required for auxin canalization. We show that interference with endocytosis, shown by the use of mutants with defects in the coat protein clathrin and over-expression of the uncoating factor AUXILIN-LIKE2, significantly blocks auxin canalization, *de novo* vascular formation and regeneration. Due to their cell toxicity in long term experiments, the use of specific CME inhibitors, like IKA and Dyngo [39], was not possible for this study. So mutants interfering with clathrin itself or processes associated with clathrin-mediated endocytosis were used. Clathrin is, however, not only involved in processes at the PM but also in intracellular trafficking from the TGN [18], which makes the mutants not necessarily specific to CME. However, the interference with clathrin is blocking the major route for cargo internalization from the PM in plants [15], therefore the used mutants highlight the importance of clathrin-mediated trafficking and most likely also endocytosis for the processes analyzed in this study. As shown, the process of regeneration is blocked in one of the very first steps, the formation of PIN1-expressing auxin channels, presumably due to failure of PIN polarity establishment but this would require detailed observations of PIN polarities, which is in the stem system not easily possible. Nonetheless, the observations that clathrin-mediated trafficking is required during formation of auxin channels and ultimately for vascular strand formation support the model that auxin feed-back on PIN endocytosis is a part of the canalization mechanism.

2.2.3.3 Actin-mediated trafficking in auxin canalization and vasculature formation

After proving that endocytosis, the first step of PIN internalization and thus polarity establishment, is crucial for the formation of PIN1-expressing auxin channels and vasculature regeneration we aimed to test whether also post-endocytic trafficking is required. To this end, we decided to genetically and pharmacologically interfere with the actin cytoskeleton since the CME does not require intact actin whereas post-endocytic processes and trafficking of PIN proteins do [20,21]. We used several actin defective mutants and the actin depolymerizing drug Latrunculin B and these manipulations consistently show that not only endocytosis but also an intact actin cytoskeleton are a prerequisite for both, the formation of auxin-conducting channels and the regeneration of vasculature. Similar to the endocytosis mutants, regeneration is also blocked already in the step of auxin-conducting channel formation which could be arguably due to a failure in the establishment of PIN polar localization. Thus, whereas in stably polarized

tissues such as root tip, the cytoskeleton is not needed for PIN polarity establishment, for example after cell division [20], the dynamic establishment of PIN-conducting channels for vasculature formation and regeneration strictly depends on the intact actin cytoskeleton.

2.2.4 Conclusions

In conclusion, our observations provide novel insights regarding the cellular mechanisms underlying auxin canalization-mediated vascular tissue formation and regeneration. With the present work, we show that the formation of PIN1-expressing auxin channels either in context of vascular tissue regeneration or *de novo* vascular strand formation from the place of local auxin application requires intact subcellular dynamics of PIN auxin transporters; functional clathrin-mediated trafficking and an intact actin cytoskeleton. If one if these steps is impeded, canalization and vascularization are blocked at an early stage of auxin channel formation highlighting the importance of a properly functioning trafficking machinery in these processes. These observations support a model in which auxin feed-back on endocytosis and trafficking of PIN auxin transporters is a crucial part of the mechanism of coordinated PIN polarization underlying auxin channel formation.

2.2.5 Material and Methods

Plant material and plant growth condition

Wild-type Col-0 (NASC, The Nottingham Arabidopsis Stock Centre; http://www.arabidopsis.info, N1092) and reporter lines: *DR5rev::GFP* [24], *pPIN1::PIN1-GFP* [10] were used as controls. All mutants and transgenic lines used in this study are in the *Arabidopsis thaliana* ecotype Columbia (Col-0) background. Endocytosis-defective mutants: *chc2-1* (SALK 028826) and *chc2-2* (SALK 042321) [19], *XVE>>AUXILIN-LIKE2 x DR5rev::GFP, XVE>>AUXILIN-LIKE2* (At4g12770) [25], *tir3*, [26], *doc1 x PIN1::PIN1-GFP* and actin filament mutants: *act2* (SALK_048987), *act7* (SALK_131610), *act8* (GABI_480B07) [27] were used for the experiments. All seeds were sterilized with 70% aqueous ethanol solution (2 minutes) and in 10% sodium hypochlorite solution (15 minutes), washed 3 times in water (2 minutes in each change) and next refrigerated at 4ºC for stratification for 48 hours. Seeds were germinated in pots with soil and seedlings with second pair of leaves were individually planted and grown in pots with soaked peaty rings in a growth chamber with 16-hours light/8-hours dark cycle at 20°C. For the experiments, plants with 10 cm tall inflorescence stem were chosen.

Experimental design

Inflorescence stems (10 cm tall) having primary tissue architecture were used for experiments with vasculature regeneration after wounding and with local application of compounds. The flowering parts of the stems were dissected (stems were 7cm tall after decapitation) and an external weight (a leaden ball, 2.5 g) was applied to them for subsequent 6 days, to obtain secondary growth on the stem circumference. Finally, the mechanically stimulated stems were incised transversally in the basal parts (above the leaf rosette) as described previously [13]. An incision was made with a razor blade in the transversal plane to disturb basipetal transport of endogenous auxin. Six days after compound application auxin canalization and vasculature formation from the local sites of application were analyzed. Experiments were conducted two times for each line, with at least 15 plants analyzed.

Treatment conditions

All the treatments were carried out with mechanically stimulated inflorescence stems, which remained under the external weight during the experiments.

Dependent on the experiment, material was analyzed either 6 days after wounding (tests for vasculature regeneration around wounds) or a droplet of lanolin paste with natural auxin (IAA, Indole-3-Acetic Acid, Sigma-Aldrich, cat. no 15148-2G), synthetic auxin (PISA, Pinstatic Acid, Alfa Aesar, Santa Cruz Biotechnology and Cross Organics, CAS Registry Number: 4919-33-9), or actin cytoskeleton inhibitor Latrunculin B (LatB, Sigma-Aldrich, cat. no L5288) was applied locally together with auxin below the cut (tests for auxin channels and vascular strand formation from the local sites of application). The applied compounds were replaced during the experiments every 2 days in a fresh droplet of lanolin paste. For the local application, 10 µM water solutions of all compounds mixed with a droplet of lanolin paste were used. Stock solutions of auxin and compounds (LatB, PISA) were dissolved in DMSO (Sigma, cat. no. D5879-500ML).To induce the overexpression of AUXILIN-LIKE2, inflorescence stems of *XVE>> AUXILIN-LIKE2* mutants were sprayed with 2 µM β-estradiol (Sigma-Aldrich, cat. no E8875) aqueous solution. The stems were under chemical induction 3 days before the experiment and during the whole duration of the experiments. Plants were sprayed once *per* day. Non-induced *XVE>>AUXILIN-LIKE2* mutants were used as controls.

Imaging and image analysis

The samples of wounded inflorescence stems after treatments were collected under a stereomicroscope (NIKON MSZ1500), manually sectioned with a razor blade and mounted in a 50% glycerol aqueous solution onto microscopy slides. Visualization of the auxin response

reporter *DR5rev::GFP* and PIN1 protein *pPIN1::PIN1-GFP* was performed using a Zeiss Observer.Z1 or an Olympus FLUOVIEW FV1000 confocal laser-scanning microscope. GFP fluorescence was excited by an argon-ion laser light of 488 nm and detected at 510 nm. Acquired images were processed with ZEN 2012 Light Edition and FLUOVIEW software. Figures were created by CorelDraw X6.

Quantification and statistical analysis
All calculations and graphs were made with Microsoft Office Excel software (Microsoft 2010).

2.2.6 Acknowledgements

We thank Mark Estelle, José M. Alonso and Arabidopsis Stock Centre for providing seeds and Alexander Johnson for valuable scientific input. This project has received funding from the European Research Council (ERC) under the European Union's Horizon 2020 research and innovation program (grant agreement No 742985), the Czech Science Foundation GAČR (GA13-40637S and GA18-26981S) to JF, and the Ministry of Education, Youth and Sports of the Czech Republic within CEITEC 2020 (LQ1601) project (to HSR). We acknowledge the core facilities PLANT Science and CELLIM of CEITEC MU supported by the MEYS CR (LM2015062 Czech-BioImaging). The authors declare no competing interests.

2.2.7 Author Contribution

E.M., M.G., H.H. and J.F. designed and conducted experiments and analyzed data. M.A. and H.S.R. contributed with the generation of the genetic material used in the study. E.M., M.G. and J.F. wrote the manuscript, with the assistance of H.H.

2.2.8 Figures

Figure 1 - Vasculature regeneration after wounding in endocytosis-defective mutants

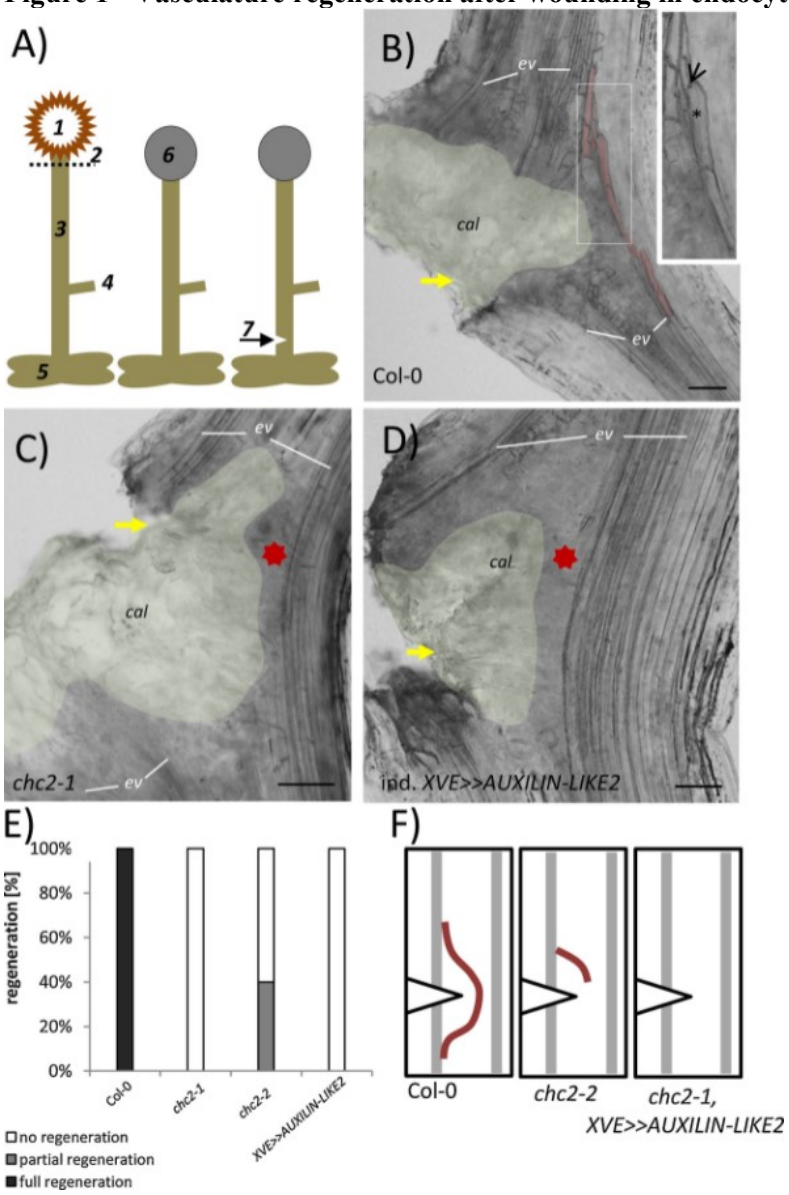

Figure 15 Section 2.2.8 - Vasculature regeneration after wounding in endocytosis-defective mutants

A) Schematic view of the wounding experimental design in mechanically stimulated inflorescence stems: 1 – inflorescence, 2 – place of inflorescence decapitation, 3 - stem, 4 – axillary bud, 5 – leaf rosette, 6 – external weight (2.5g), 7 – wounding. B) Development of regenerated vascular strands in wounded regions. Healing vasculature, with typical vascular features, extending between wound and pre-existing vasculature (*red*). Regenerated vessels with secondary cell wall patterning (*asterisk*, inset) are connected by perforations (*arrowhead*, inset). C-D) No regeneration of vascular tissue around a wound in *chc2-1* and *XVE>>AUXILIN-LIKE2* mutants (*red asterisks*). Extended callus developed in place of the wound in both of the mutants. E) Comparison of the vasculature regeneration in analyzed mutants. Vascular regeneration was stopped in *chc2-1* and *XVE>>AUXILIN-LIKE2* mutants (0% of analyzed plants in comparison to control regenerated). Defective vasculature developed only in *chc2-2* mutant (40%), but still in 60% of the analyzed plants no regeneration around a wound was observed. F) Schematic visualization of vasculature regeneration and defective regeneration around a wound. Abbreviations: *cal* – callus, *ev* – pre-existing vasculature. Yellow arrows indicate wounds. Red colors indicate regenerated vasculature around a wound.Scale bars: 50 µm (B, D), 100 µm (C).

Figure 2 - Vasculature formation from local, external sources of auxin in endocytosis-defective mutants

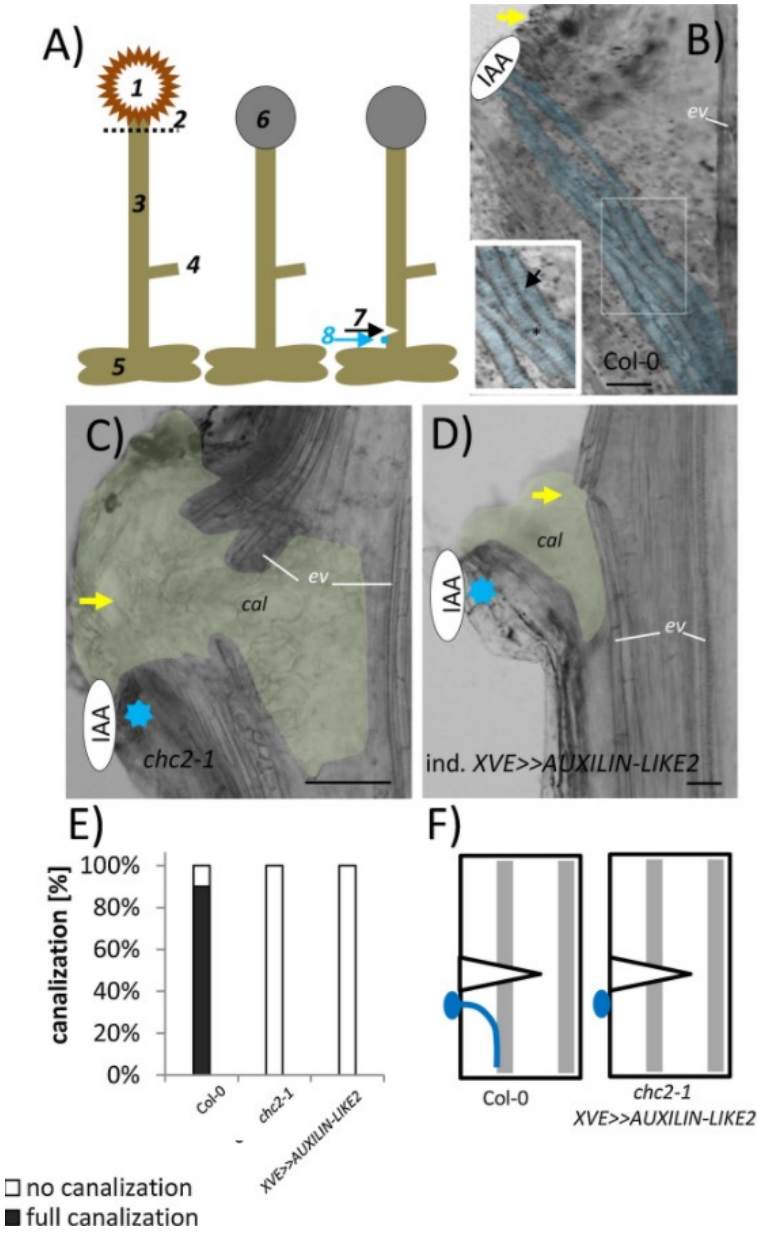

Figure 16 Section 2.2.8 - Vasculature formation from local, external sources of auxin in endocytosis-defective mutants

A) Schematic view of the local auxin application experiments : 1 – inflorescence, 2 – place of inflorescence decapitation, 3 - stem, 4 – axillary bud, 5 – leaf rosette, 6 – external weight (2.5g), 7 – wounding, 8 – local application of a droplet of lanolin paste together with auxin. B) Vasculature formation from auxin application site (*blue outlines*). Vessels with typical vascular features, such as secondary cell walls and perforations connecting vessel elements (inset, *arrowhead* and *asterisk*, respectively), extending from the external auxin source to pre-existing stem vasculature. C-D) No vascular strand formation from the local source of auxin in analyzed *chc2-1* and *XVE>>AUXILIN-LIKE2* mutants (*blue asterisks*), 6 days after application [DAA]. Abundant callus is observed in both of the mutants. E) Quantification of the results shows complete stop of vasculature formation from external auxin sources in each of the analyzed mutants compared to the control (0% developed vasculature in mutants and 90% developed vasculature in control). F) Schematic visualization of vasculature formation from local, external auxin sources. Abbreviations: *cal* – callus, *ev* –existing vasculature.

Yellow arrows indicate wounds. Blue colors indicate developed vasculature from the local auxin application sites. Scale bars: 50 µm (B, D), 100 µm (C).

Figure 3 - Auxin channel formation from a local, external auxin source in endocytosis-defective mutants and after PISA treatment

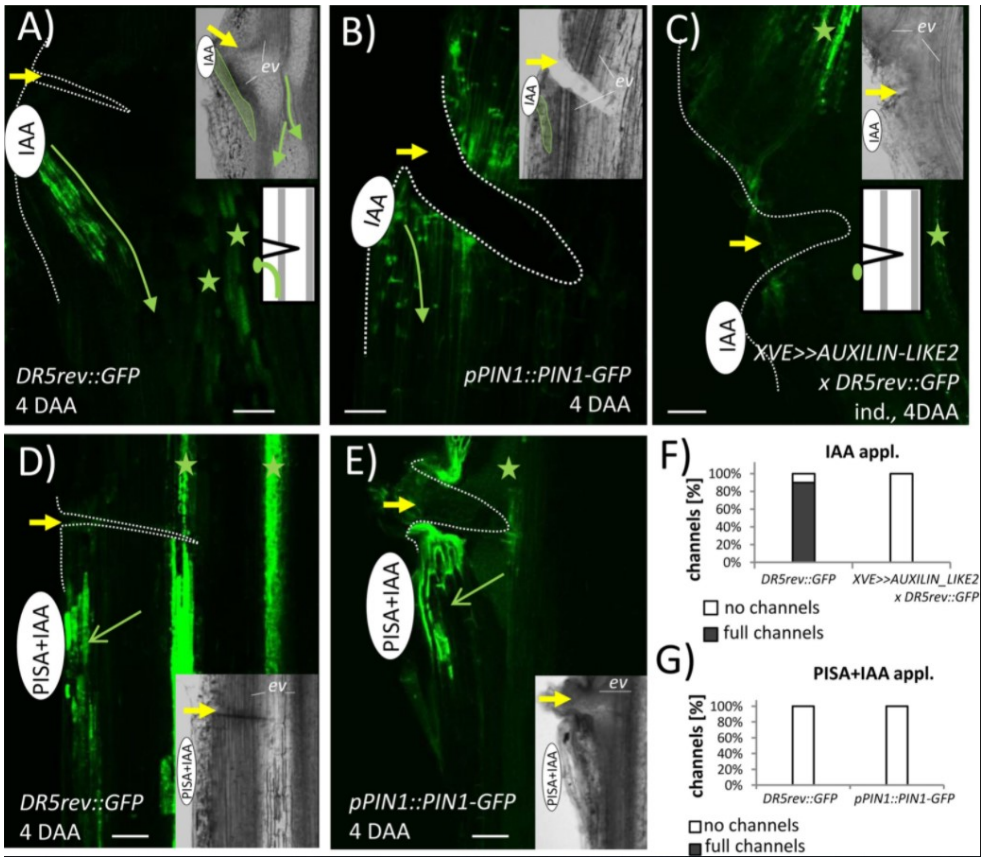

Figure 17 Section 2.2.8 - Auxin channel formation from a local, external auxin source in endocytosis-defective mutants and after PISA treatment

A) Formation of an auxin channel in *DR5rev::GFP* stems (*green arrow*), 4 DAA. Channels developed from the external sources of auxin and connected with pre-existing vasculature (inset, *green outline* and scheme). Elevated auxin response is also observed in regenerating vasculature around a wound (*green asterisks* and *green arrows* in inset). Development of the auxin channel is schematically visualized. B) Development of PIN1-positive channel from source of auxin application towards the pre-existing vasculature (*green arrow* and *green outline* in inset). C) No auxin-channel formation from the source of locally applied auxin in induced *XVE>>AUXILIN-LIKE2* x *DR5rev::GFP* mutant (inset and scheme). Elevated auxin response is visible in pre-existing vasculature (*green asterisks*). D) Application of PISA together with auxin, 4 DAA. No auxin-channel formation from the source of locally applied compounds was observed in *DR5rev::GFP* stems. Elevated auxin response extending in the outer tissues (*green arrow* and inset), but no auxin canalization was visible at the site of PISA+IAA application. High auxin response was also observed in pre-existing vasculature (*green asterisks*). E) Application of PISA together with auxin, 4 DAA. No PIN1-positive channel formation from the source of locally applied compounds was observed in *pPIN1::PIN1-GFP* stems (*green arrow*). Non-polar PIN1 localization was found in the outer tissues neighboring the sites of the compounds application (inset). Elevated auxin response was observed in pre-existing vasculature (*green asterisk*). F) Quantification of the results shows complete stop of auxin channel formation from external auxin sources in induced *XVE>>AUXILIN-LIKE2 x DR5rev::GFP* line compared to the control (0% channel formation and 90% in control). G) Co-treatment with IAA and PISA resulted in complete block of auxin channel formation in *DR5rev::GFP* and *pPIN1::PIN1-GFP* lines. Abbreviations: *ev* – pre-existing

vasculature. Yellow arrowheads indicate wounds. Contours of wounded stems are indicate with dotted lines. Green colors indicate formation of PIN1-positive auxin channels. Scale bars: 50 µm.

Figure 4 - Vasculature regeneration and auxin channel formation in actin-defective mutants

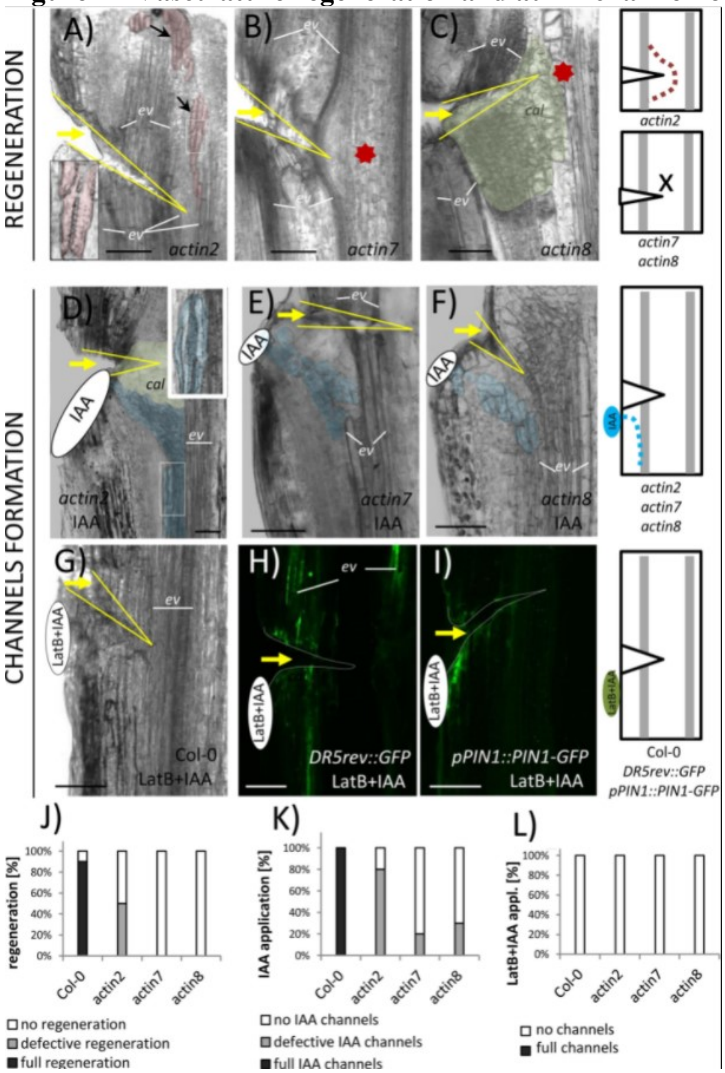

Figure 18 Section 2.2.8 - Vasculature regeneration and auxin channel formation in actin-defective mutants

A) Defective vasculature regeneration in *actin2* mutants. Development of discontinuous vessel strands in the neighborhood of the wound was observed (*black arrows* and *red outlines*). Vasculature was recognized with secondary cell wall patterning (inset). Defective vasculature regeneration is visualized on the scheme. B-C) No vascular strand formation around the wound in analyzed *actin7* and *actin8* mutants (*red asterisks*). Defective vasculature regeneration is visualized on the schemes. D-F) Defective vasculature formation from local source of external auxin in all analyzed actin defective mutants (*blue outlines* and scheme). Vessels developed in the mutants are strongly defective visible by the shapes and connections. However, the secondary cell wall patterning is recognizable in the *act2* mutant (D, inset). Defective vasculature formation is visualized on the scheme. G-I) No vasculature development in Col-0 stems (G) and no positive auxin channel formation in *DR5rev::GFP* and *pPIN1::PIN1-GFP* stems (H, I) after local application of Latrunculin B together with auxin. Experimental results are visualized on scheme. J-L) Quantification of the results shows defective regeneration of vasculature around the wound in *actin2* (in 50% of analyzed plants comparing to control), and absent regeneration in *actin 7* and *actin 8* mutants (0%, N=10) (J), defective vasculature formation after local IAA application (80% in *act2*; 30% in *act8* and 20% in *act7* samples; N=10) or no vasculature formation after local IAA application (20% in *act2*; 70% in *act8* and 80% in *act7* samples; N=10) (K) and no vasculature and

channel formation after local LatB+IAA application (L) in all analyzed mutants. Abbreviations: *cal* – callus, *ev* –existing vasculature. Yellow lines and arrows indicate wounds. Red colors indicate regenerated vasculature around a wound. Blue colors indicate developed vasculature from the local auxin application sites. Contours of wounded stems are indicate with dotted lines (H, I). Scale bars: 100 µm.

Figure 5 - Vasculature regeneration and auxin channel formation in *big* PIN trafficking-defective mutants

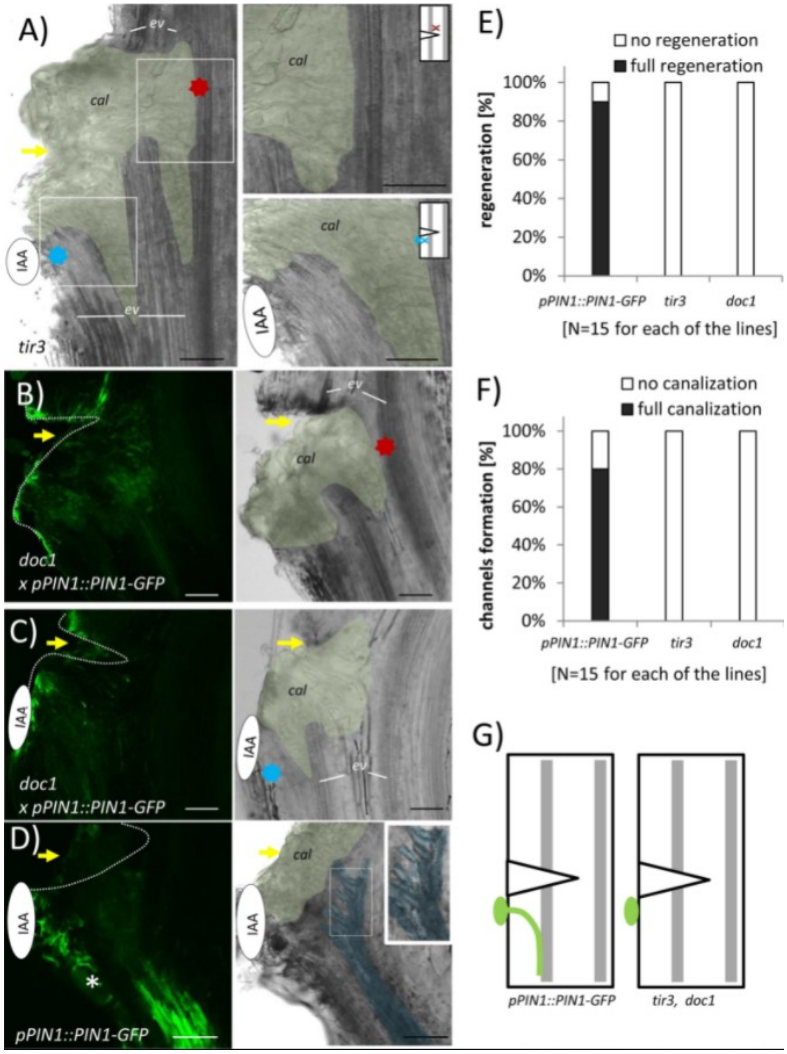

Figure 19 Section 2.2.8 - Vasculature regeneration and auxin channel formation in big *PIN trafficking-defective mutants*

A) No regeneration around a wound and no vasculature formation from a local auxin source in *tir3* (*red* and *blue asterisk*, respectively). Frames are shown with magnification. B-C) No regeneration around a wound (B, *red asterisk*), no vasculature formation and no PIN1-positive channel formation from local auxin source (C, *blue asterisk*) in the *doc1* mutant. D) PIN1-positive channels (*asterisk*) and new vessel strands developed from the external source of auxin in stems of *pPIN1::PIN1-GFP*. New vessels developed extending from the site of auxin application to the pre-existing vasculature (*blue outlines* and inset). E-F) Quantification shows no vasculature formation and no auxin channel formation from the sources of local auxin application in both of the tested alleles of *big*: *doc1* and *tir3* (0% in *tir3* and *doc1*). G) Schematic visualization of PIN1 channel formation in analyzed *pPIN1::PIN1-GFP* stems and PIN trafficking-defective mutants.Abbreviations: *cal* – callus, *ev* – existing vasculature. Yellow arrows indicate wounds. Contours of wounded stems are indicated with dotted lines. Scale bars: 100 µm.

2.2.9 Supplemental Figures

Figure S1 - Vasculature regeneration in *chc2-2* and non-induced *XVE>>AUXILIN-LIKE2* mutants, 6 DAW

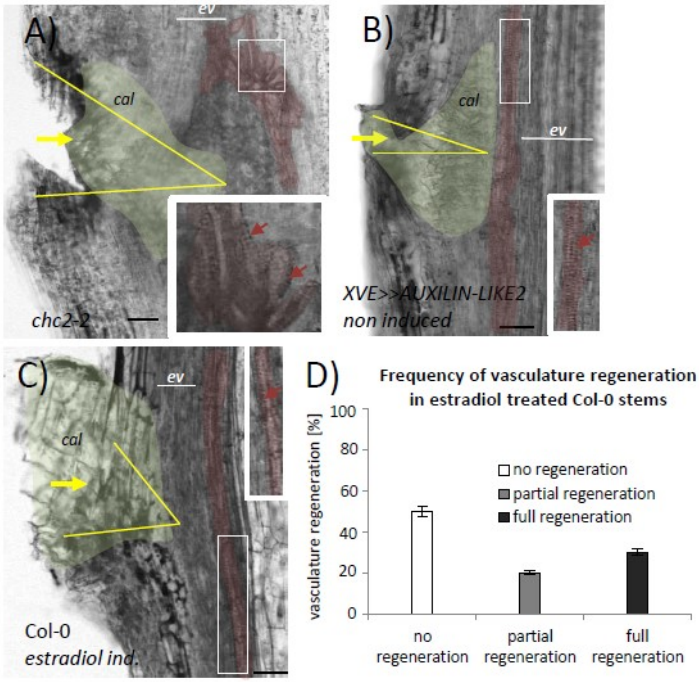

Figure 20 Section 2.2.9 - Vasculature regeneration in chc2-2 *and non-induced* XVE>>AUXILIN-LIKE2 *mutants, 6 DAW*

A) Defective vasculature formation around a wound in the *chc2-2* mutant (*red outlines*). Developed vessels are unshaped and not connected together in continuous strands. The secondary cell walls are recognizable (inset, *red arrowheads*). B) Non induced stem of *XVE>>AUXILIN-LIKE2* mutant, 6 DAW. Regenerated vasculature developed around a wound (*red outline*). Vessels are arranged in continuous strands (inset). Secondary cell wall is visible (inset, *arrowhead*). C) Wounded stem of the wild type Col-0, induced with β-estradiol, 6 DAW. Regeneration of vasculature around a wound is completed (*red outline*). Vessels are arranged in continuous strands. Secondary cell wall is visible (inset, *arrowhead*). D) Statistical analysis of the β-estradiol induced Col-0 controls shows completed or partial vasculature regeneration around a wound in half of the analyzed plants (in 30% and 20% of the β-estradiol induced stems respectively, N=10). Abbreviations: *cal* – callus, *ev* – existing vasculature. Yellow lines and arrows indicate wounds. Red colors indicate regenerated vasculature around a wound. Scale bars: 100 µm (A), 50 µm (B).

Figure S2 - Vasculature formation from the local auxin sources in *chc2-2* and non-induced *XVE>>AUXILIN-LIKE2* mutants, 6 DAA

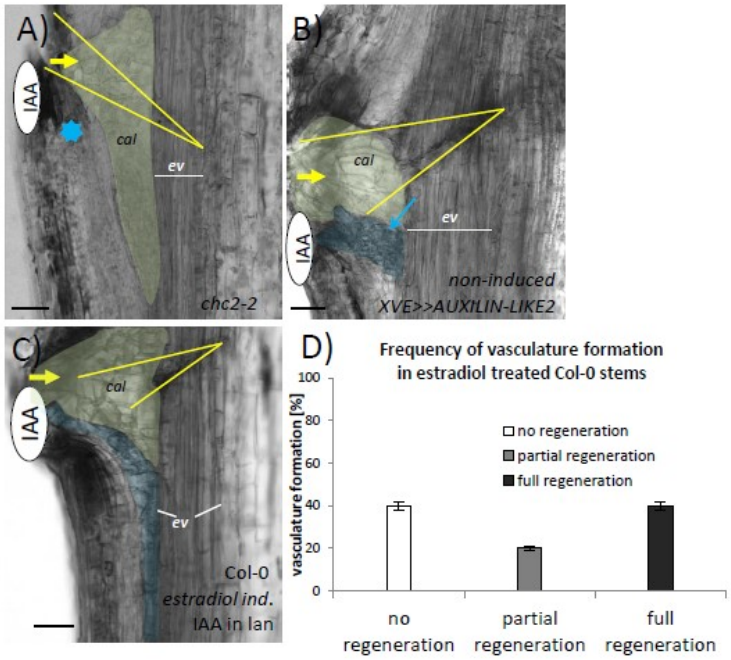

Figure 21 Section 2.2.9 - Vasculature formation from the local auxin sources in chc2-2 *and non-induced* XVE>>AUXILIN-LIKE2 *mutants, 6 DAA*

A) No vascular strand formation from the local source of auxin in *chc2-2* mutant, 6 DAA (*blue asterisk*). B) Development of vascular-like group of cells in non-induced *XVE>>AUXILIN-LIKE2* mutant after local auxin application (*blue outline* and *arrow*). Vasculature formed from the source of auxin and extended to pre-existing vasculature. C) Wounded stem of the wild type Col-0 induced with β-estradiol. Vasculature developed from the local auxin source (*blue outline*). D) Quantification of the β-estradiol induced Col-0 controls shows vasculature formation from the source of locally applied auxin in 60% of induced control stems (completely or partially developed vasculature in 40% and 20% of the analyzed plants respectively, N=10). Abbreviations: *cal* – callus, *ev* –existing vasculature. Yellow lines and arrows indicate wounds. Blue colors indicate developed vasculature from the local auxin application sites. Scale bars: 50 μm

Figure S3 - Formation of auxin channels in *XVE>>AUXILIN-LIKE2* x *DR5rev::GFP* mutant and after PISA application

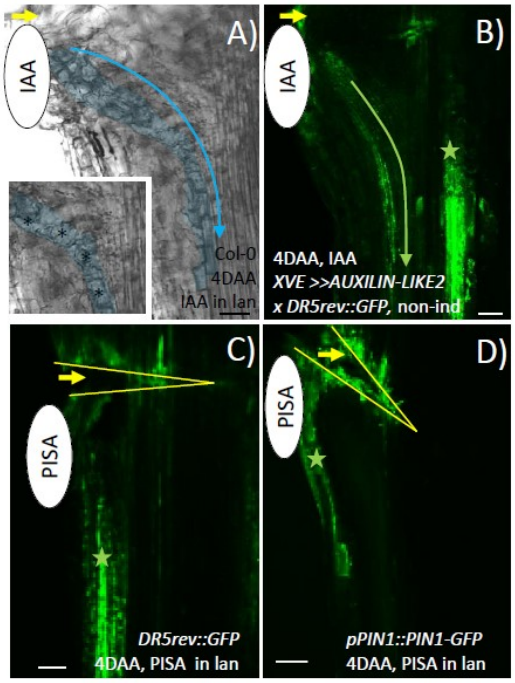

Figure 22 Section 2.2.9 - Formation of auxin channels in XVE>>AUXILIN-LIKE2 *x* DR5rev::GFP *mutant and after PISA application*

A) Col-0, 4 DAA. Development of vessel strands from source of auxin application (*blue outlines* and *arrow*). Vasculature extending from the site of auxin application to existing vasculature. Vessels are recognized by the secondary cell walls (*asterisks*, inset). B) Non-induced stem of *XVE>>AUXILIN-LIKE2* x *DR5rev::GFP*, 4 DAA. Application of auxin in droplet of lanolin paste resulted in auxin channel formation (*green arrow*). Channels extending from the site of auxin application to existing vasculature show elevated auxin response (*green star*). C-D) Local application of PISA without auxin onto *DR5rev::GFP* and *pPIN1::PIN1-GFP* stems, 4 DAA. In both of the tested lines no development of auxin channels was observed. Increased auxin level (*green stars*) was found in tissues neighboring the place of synthetic auxin application. Yellow lines and arrows indicate wounds. Blue colors indicate developed vasculature from the local auxin application sites. Scale bars: 50 µm

Figure S4 - Influence of Latrunculin B on regeneration and auxin channel formation

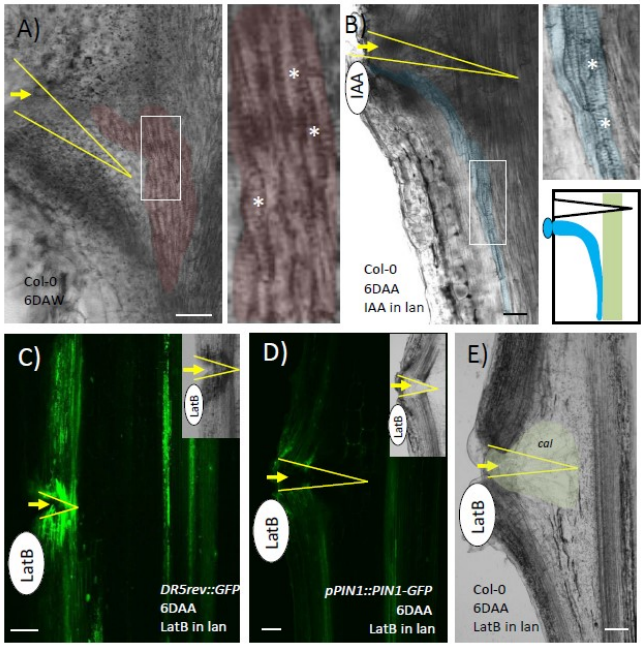

Figure 23 Section 2.2.9 - Influence of Latrunculin B on regeneration and auxin channel formation

A) Col-0, 6 DAW. Vascular tissue which regenerated around the wound is connected with continued strands around a wound (*red outlines*). Vessels with secondary cell wall are recognizable (*asterisks,* magnification). B) Col-0, 6 DAA. Application of auxin in droplet of lanolin paste results in development of vessels (*blue outlines* and *asterisks* in magnification). The scheme shows new vasculature extending between source of auxin and existing vasculature. C-E) Application of Latrunculin B without auxin shows no PIN1-mediated DR5-positive auxin channel formation from the source of application, *DR5rev::GFP* and *pPIN1::PIN1-GFP* (C-D) and no vasculature formation in Col-0 stems (E). Tissues arrangement is shown with bright field images (C, D, insets). Yellow lines and arrowheads and lines indicate wounds. Red colors indicate regenerated vasculature around a wound. Blue colors indicate developed vasculature from the local auxin application sites. Scale bars: 100 µm (A, C-E), 50 µm (B)

2.2.10 References

1. T.A. Steeves, I.M. Sussex, Patterns in plant development, Cambridge University Press; Cambridge, UK, 1989
2. P. Grones, J. Friml, Auxin transporters and binding proteins at a glance, J. Cell Sci. 128 (2015) 1-7
3. T. Sachs, The Control of the Patterned Differentiation of Vascular Tissues, Adv. Bot. Res. 9 (1981) 151–262
4. T.Sachs, Cell Polarity and Tissue Patterning in Plants, Development 112 (1991) 83–93
5. M. Sauer, J. Balla, C. Luschnig, J. Wiśniewska, V. Reinöhl, J. Friml, E. Benková, Canalization of Auxin Flow by Aux/IAA-ARF-Dependent Feedback Regulation of PIN Polarity, Gen. Dev. 20 (2006) 2902–2911
6. T. Berleth, T. Sachs, Plant Morphogenesis: Long-Distance Coordination and Local Patterning, Curr. Opinion Plant Biol. 4 (2001) 57–62
7. J. Wiśniewska, J. Xu, D. Seifertová, P.B. Brewer, K. Růžička, I. Blilou, D. Rouquié, E. Benková, B. Scheres, J. Friml, Polar PIN localization directs auxin flow in plants, Science 312 (2006) 883-883
8. M. Adamowski, J. Friml, PIN-Dependent Auxin Transport: Action, Regulation and Evolution, Plant Cell 27 (2015) 20-32
9. E. Scarpella, D. Marcos, J. Friml, T. Berleth, Control of Leaf Vascular Patterning by Polar Auxin Transport, Gen. Dev. 20 (2006) 1015–1027
10. E. Benkova, M. Michniewicz, M. Sauer, T. Teichmann, D. Seifertova, G. Jürgens, J. Friml, Local, Efflux-Dependent Auxin Gradients as a Common Module for Plant Organ Formation, Cell 115 (2003) 591-602
11. M.G. Heisler, C. Ohno, P. Das, P. Sieber, G.V. Reddy, J.A. Long, E.M. Meyerowitz, Patterns of Auxin Transport and Gene Expression during Primordium Development Revealed by Live Imaging of the Arabidopsis Inflorescence Meristem, Curr. Biol. 15 (2005) 1899-1911
12. J. Balla, P. Kalousek, V. Reinöhl, J. Friml, S. Procházka, Competitive Canalization of PIN-Dependent Auxin Flow from Axillary Buds Controls Pea Bud Outgrowth, Plant J. 65 (2011) 571–577
13. E. Mazur, E. Benková, J. Friml, Vascular Cambium Regeneration and Vessel Formation in Wounded Inflorescence Stems of Arabidopsis, Sci. Rep. 6 (2016) 1–15
14. J. Kleine-Vehn, Z. Ding, A.R. Jones, M. Tasaka, M.T. Morita, J. Friml, Gravity-induced PIN transcytosis for polarization of auxin fluxes in gravity-sensing root cells, Proc. Natl. Acad. Sci. USA 107 (2010) 22344-22349
15. P. Dhonukshe, F. Aniento, I. Hwang, D.G. Robinson, J. Mravec, Y.D. Stierhof, J. Friml, Clathrin-Mediated Constitutive Endocytosis of PIN Auxin Efflux Carriers in Arabidopsis, Curr. Biol. 17 (2007) 520–527
16. T. Paciorek, E. Zažímalová, N. Ruthardt, J. Petrášek, Y.D. Stierhof, J. Kleine-Vehn, D.A. Morris, N. Emans, G. Jürgens, N. Geldner, J. Friml, Auxin inhibits endocytosis and promotes its own efflux from cells, Nature 435 (2005) 1251-1256
17. P. Grones, X. Chen, S. Simon, W.A. Kaufmann, R. De Rycke, T. Nodzynski, E. Zazimalova, J. Friml, Auxin-binding pocket of ABP1 is crutial for its gain-of-function cellular and developmental roles, J. Exp. Bot. 66 (2015) 5055-5065
18. D.G. Robinson, P.Pimpl, Clathrin and post-Golgi trafficking: a very complicated issue, Trends in Plant Sci. 19 (2014) 134-139
19. S. Kitakura, S. Vanneste, S. Robert, K. Lofke, T. Teichmann, H. Tanaka, J. Friml, Clathrin Mediates Endocytosis and Polar Distribution of PIN Auxin Transporters in Arabidopsis, Plant Cell 23 (2011) 1920-1931
20. N. Geldner, J. Friml, Y.D. Stierhof, G. Jürgens, K. Palme, Auxin Transport Inhibitors Block PIN1 Cycling and Vesicle Trafficking, Nature 413 (2001) 425–428
21. M. Narasimhan, A. Johnson, R. Prizak, W.A. Kauffman, S. Tan, B. Casillas-Perez, J. Friml, Evolutionary unique mechanistic framework of clathrin-mediated endocytosis in plants, in press
22. M. Glanc, M. Fendrych, J. Friml, PIN2 Polarity Establishment in Arabidopsis in Absence of an Intact Cytoskeleton, Biomolecules 9 (2019) doi:10.3390/biom9060222
23. Flaishman, A. Moshe, K. Loginovsky, S. Lev-Yadun, Regenerative Xylem in Inflorescence Stems of Arabidopsis thaliana, J. Plant Growth Reg. 22 (2003) 253–258

24. J. Friml, A. Vieten, M. Sauer, D. Weijers, H. Schwarz, T. Hamann, R. Offringa, G. Jürgens, Efflux-dependent auxin gradients establish the apical-basal axis of Arabidopsis, Nature 426 (2003) 147-153
25. M. Adamowski, M. Narasimhan, U. Kania, M. Glanc, G. De Jaeger, J. Friml, A Functional Study of AUXILIN-LIKE1 and 2, Two Putative Clathrin Uncoating Factors in Arabidopsis, The Plant Cell 30 (2018) 700-716
26. P. Gil, E. Dewey, J. Friml, Y. Zhao, K.C. Snowden, J. Putterill, K. Palme, M. Estelle, J. Chory, BIG: a calossin-like protein required for polar auxin transport in Arabidopsis. Gen. Dev. 15 (2001) 1985-1997
27. H. Rakusová, H. Han, P. Valošek, J. Friml, Genetic screen for factors mediating PIN polarization in gravistimulated Arabidopsis thaliana hypocotyls, Plant J. 98 (2019) 1048-1059
28. Fotin, Y. Cheng, P. Sliz, N. Grigorieff, S.C. Harrison, T. Kirchhausen, T. Waltz, Molecular model for a complete clathrin lattice from electron cryomicroscopy, Nature 432 (2004) 573-579
29. E. Mazur, I. Kulik, J. Hajny, J. Friml, Auxin Canalization and Vascular Tissue Formation by TIR1/AFB-Mediated Auxin Signaling in Arabidopsis, in revision
30. Oochi, J. Hajny, K. Fukui, Y. Nakao, M. Gallei, M. Quareshy, K. Takahashi, T. Kinoshita, S.R. Harborough, S. Kepinski, H. Kasahara, R. Napier, J. Friml, K.I. Hayashi, Pinstatic Acid Promotes Auxin Transport by Inhibiting PIN Internalization, Plant Phys. 180 (2019) 1152-1165
31. W.M. Morton, K.R. Ayscough, P.J. McLaughlin, Latrunculin alters the actin-monomer subunit inteface to prevent polymerization, Nat. Cell Biol. 2 (2000) 376-378
32. S. Vanneste, J. Friml, Auxin: a trigger for change in plant development, Cell 136 (2009) 1005-1006
33. J. Kleine-Vehn, K. Wabnik, A. Martiniere, Ł. Łangowski, K. Willig, S. Naramoto, J. Leitner, H. Tanaka, S. Jakobs, S. Robert, C. Luschnig, W. Govaerts, S.W. Hell, J. Runions, J. Friml, Recycling, clustering, and endocytosis jointly maintain PIN auxin carrie polarity at the plasma membrane, Mol. Syst. Biol. 7 (2011) 540
34. H. Rakusova, M. Abbas, H. Han, S. Song, H. Robert, J. Friml, Termination of shoot gravitropic responses by auxin feedback on PIN3 polarity, Curr. Biol. 26 (2016) 3026-3032
35. T. Prat, J. Hajny, W. Grunewald, M.K. Vasileva, G. Molnar, R. Tejos, M. Schmid, M. Sauer, J. Friml, WRKY23 is a component of the transcriptional network mediating auxin feedback on PIN polarity, PLoS Genetics 14 (2018)
36. M.G. Heisler, O. Hamant, P. Krupinski, M. Uyttewaal, C. Ohno, H. Jonsson, J. Traas, E.M. Meyerowitz, Alingement between PIN1 Polarity and Microtubule Orientation in Shoot Apical Meristem Reveals a Tight Coupling between Morphogenesis and Auxin Transport, PLos Biology 8 (2010)
37. K. Wabnik, J. Kleine-Vehn, J. Balla, M. Sauer, S. Naramoto, V. Reinohl, R.M. Merks, W. Govaerts, J. Friml, Emergence of tissue polarization from synergy of intracellular and extracellular auxin signaling, Mol. Syst. Biol. 6 (2010) 447
38. S. Robert, J. Kleine-Vehn, E. Barbez, M. Sauer, T. Paciorek, P. Baster, S. Vanneste, J. Zhang, S. Simon, M. Covanova, K. Hayashi, P. Dhonukshe, Z. Yang, S.Y. Bednarek, A.M. Jones, C. Luschnig, F. Aniento, E. Zazimalova, J. Friml, ABP1 Mediates Auxin Inhibition of Clathrin-Dependent Endocytosis in Arabidopsis, Cell 143 (2010) 111-121
39. S.R. Elkin, N.W. Oswald, D.K. Reed, M. Mettlen, J.B. MacMillan, S.L. Schmid. Ikarugamycin: A Natural Product Inhibitor of Clathrin-Mediated Endocytosis, Traffic 17 (2016) 1139-1149

2.3 ABP1-TMK auxin perception mediates ultrafast global phosphorylation and auxin canalization

Adapted and modified from:

Friml J, **Gallei M**, Gelová Z, et al. *ABP1-TMK auxin perception mediates rapid phosphorylation for regeneration and auxin canalization*. Nature. 2021 - under revision

In the previous section ABP1 was mentioned several times in the context of rapid, non-canonical and non-transcriptional auxin signaling, involving responses like stabilization of PINs at the PM. Next to the canonical auxin receptor TIR1/AFB proteins, ABP1 was proposed to be another auxin receptor, binding auxin at the apoplastic pH 5.5 (Tian 1995, Neblec 1999, Woo 1993) and presumably acting in the endoplasmic reticulum (ER) together with the receptor-like kinase TRANSMEMBRANE KINASE 1 (TMK1). The auxin-promoted TMK1-ABP1 interaction at the PM was proposed to form an auxin receptor complex, responsible for the activation of downstream cellular processes (Dai 2013, Xu 2014). ABP1 was thought to be essential for various developmental processes like embryogenesis (Chen et al., 2001) and postembryonic shoot and root development (Braun et al., 2008; Tromas et al., 2009). However, auxin binding has not yet been confirmed for the *Arabidopsis thaliana* ABP1. Moreover all the above mentioned studies were called in question after the original *abp1* loss-of-function mutants were found erroneous, as they were harboring a disruption of a neighboring gene rather than *ABP1* itself (Gao 2015, Grones 2015, Michalko 2015). Thus ABP1, and its eventual physiological and developmental roles remain largely unknown and are awaiting re-evaluation.

After the detailed phenotypical analysis of the ABP1 gain- and loss-of-function mutant lines in Gelova et al 2020 (see Apendix) we aimed for a more mechanistically characterization of ABP1 in terms of auxin binding potential, TMK1 receptor complex formation and cellular functions.

The following study could finally confirm that Arabidopsis ABP1 binds auxin at apoplastic pH and it also confirms the necessary prerequisite of the protein being secreted to the apoplast/cell surface where it could potentially interact with TMK1 to facilitate cellular downstream responses. Further we show that indeed both, ABP1 and TMK1 are required for a rapid auxin phospho-response. Next to that both proteins are also found to have a common role in auxin canalization processes mediating vasculature regeneration. This results assign ABP1 a role in auxin perception important to plant growth and development.

Contributions Michelle Gallei:

- Interaction studies of ABP1 and TMK1 (data not shown)
- Regeneration studies of ABP1 and TMK1 (data not shown)
- Corrections of the manuscript
- Designing and assembling figures

2.3.1 Introduction

The plant hormone auxin is a key regulator of growth and development[1]. The best-characterized auxin signalling mechanism operates in the nucleus and relies on canonical TIR1/AFB receptors, Aux/IAA repressors and ARF transcriptional regulators, which mediate global transcriptional changes leading to developmental reprogramming[2,3]. Some classical auxin activities including regulation of root growth also depend on TIR1/AFBs[4,5] but are too fast to involve transcription, suggesting existence of an unknown non-transcriptional branch of TIR1/AFB signalling[6,7]. Other transcriptional mechanisms involve direct binding of auxin to transcription factors[8] or auxin-triggered cleavage and nuclear translocation of plasma membrane-localized TMK1[9].

Very rapid cellular auxin effects have been known for decades; e.g. plasma membrane (PM) hyperpolarization, PM H^+-fluxes, cytosolic Ca^{2+}-transients or protoplast swelling[10]. Another rapid, TIR1/AFB-independent auxin effect is regulation of endocytic trafficking of PIN auxin transporters[11–13], which is a possible mechanism of auxin feedback on its own transport, the main prerequisite of so called auxin canalization[14]. Recently, an ultrafast, TIR1/AFB-independent auxin-triggered phospho-response has been identified targeting about a thousand of proteins involved in diverse cellular functions[15]. Those include PM H^+-ATPases, which mediate growth regulation[16,17] or Myosin XI and associated proteins, mediating the above-mentioned trafficking and polarization of PIN transporters[15]. All these observations support the existence of fast, non-transcriptional responses involving so far unknown auxin perception and signalling mechanisms[6,7]. Cell surface-localized TMK receptor-like kinases are candidates to contribute to this uncharacterized auxin signalling since they mediate auxin effects on growth, lateral root formation and auxin biosynthesis[18]. Nonetheless, this remains ambiguous, mainly due to the lack of an established auxin perception mechanism for this pathway.

Auxin Binding Protein 1 (ABP1), already identified in the early 1970s[19] as a protein potentially binding auxin, is a candidate protein for mediating auxin input into the TMK pathway; not the

least on account of its association with TMK1[20]. Nonetheless, auxin binding has not been confirmed for *Arabidopsis thaliana* ABP1, for which all genetic studies have been conducted and, more importantly, these studies were called in question after the original *abp1* loss-of-function mutants were found erroneous[21–23]. Thus ABP1 and its eventual physiological roles remain controversial[24] and the mechanism of auxin perception for TMK signalling and for rapid auxin responses in general, remains obscure.

Here, we critically evaluated potential of the ABP1-TMK auxin perception module to act in fast auxin responses, such as proteome-wide phosphorylation, as well as in developmental regulations. Analysis of loss-of-function alleles and their complementation by ABP1 variants confirm that auxin binding to ABP1 is crucial for its function, establishing ABP1 as auxin receptor for TMK1-mediated signalling upstream of a range of rapid auxin effects and auxin canalization-mediated development.

2.3.2 Results

2.3.2.1 *Arabidopsis* ABP1 binds auxin at apoplastic pH

Members of the leucine-rich repeat receptor-like kinase (LRR-RLK) family, to which TMKs belong, are known to act as receptors for various ligands via their extracellular domain[25]. Nonetheless, we did not find any supporting evidence for direct auxin association to TMKs (exemplified by TMK1) *in planta* or to the TMK1 extracellular domain *in vitro* (Extended Data Fig. 1a-c). Therefore, we focused on *Arabidopsis* ABP1, which has been associated with TMK-based signalling[20] and its homologue from maize (*Zea mays*) has been shown to bind the synthetic auxin, 1-napthalene acetic acid (NAA)[26].

First we verified a possible binding of natural auxin (indole-3-acetic acid, IAA) to *Arabidopsis* ABP1 using Drug Affinity Responsive Target Stability (DARTS). Both, *in planta* studies using a *35S::ABP1-GFP* transgenic line and *in vitro* experiments using heterologously expressed ABP1, suggested IAA association with ABP1 (Fig. 1a and Extended Data Fig. 1d,e). Next, we used Grating-Coupled Interferometry (GCI)-assisted analysis with purified ABP1, which detected binding of IAA to ABP1. This binding occurred at pH 5.5 but with a far smaller affinity at pH 7.6 (Fig. 1b), and was specific since no interaction was found with benzoic acid (BA) (Extended Data Fig. 1f). We also used Microscale Thermophoresis (MST) to assess binding of IAA to ABP1. Again, the binding occurred at pH 5.5 but not at pH 7 or 7.5 (Extended Data Fig. 1g-i), and no interaction was found with BA or L-Trp (Fig. 1c).

These observations show that *Arabidopsis* ABP1 specifically binds IAA, preferentially at the acidic pH 5.5.

2.3.2.2 ABP1 is partly secreted to the cell surface

IAA binding to ABP1 preferentially at the apoplast-like pH 5.5 reopened the question about extracellular localization of ABP1, which has remained a matter of debate since decades. Previously, maize ABP1 was shown to localize mainly to the endoplasmic reticulum (ER), consistent with the ER-retention signal in the ABP1 sequence and, to a minor extent, to the extracellular space[27]. This was also suggested for *Arabidopsis* ABP1 based on staining with heterologous antibodies[20].

To determine the localization of ABP1, we utilized immunostaining and Electron Microscopy (EM). We optimized fixation protocols and used pre-embedding labelling on intact samples, which preserved the PM and thus ensured the unequivocal localization of the immunogold signals to the intra- or extra-cellular areas. We used anti-GFP antibodies in *RPS5A::ABP1-GFP* roots with chemical fixation and in combinations with high-pressure freezing techniques. Both approaches revealed consistent signals that were absent in the non-transgenic controls. Intracellular ABP1 was detected in ER-like structures and absent from other organelles, for example the mitochondria or Golgi apparatus (Fig. 1e and Extended Data Fig. 2a-c). Besides intracellular signals, we detected ABP1 in the apoplast, which was slightly increased by IAA. Interestingly, we observed regularly the apoplastic immunogold signal formed clusters (ranging from 3-20 particles) with their appearance increasing upon auxin treatment (Fig. 1e and Extended Data Fig. 2a-c). Similar EM analysis was conducted using the shoot apical meristem of the *ABP1::GFP-ABP1* lines expressing functional GFP-ABP1 under the endogenous promotor[28] . Samples were fixed using high pressure freezing and subjected to post-embedding labelling. We found a similar pattern of ABP1 localisation as in roots, where we reliably detected ABP1 in the extracellular space, which significantly increased upon auxin treatment (Fig. 1d,f and Extended Data Fig. 2d).

Thus, different immunostaining EM approaches on different ABP1 tagged lines confirmed that *Arabidopsis* ABP1, besides residing predominantly in the ER, is also secreted to the apoplast, which is in line with IAA binding at acidic pH and ABP1 association with PM-localized TMKs[20].

2.3.2.3 ABP1 and TMK1 are required for rapid auxin phospho-response

Recently we showed that auxin, within 2 minutes, induces phosphorylation of about a thousand proteins in *Arabidopsis* roots by a mechanism largely independent of the TIR1/AFB auxin receptors[15]. We therefore tested whether TMK1 as a kinase and the associated ABP1 may be required for this ultrafast, global auxin-triggered phospho-response.

We compared this phospho-response in WT to *tmk1* and *abp1* mutants across 4 biological replicates for each genotype for both 100 nM IAA and solvent control treatments. In WT, over 1000 individual phospho-sites (P-sites) were hyper-phosphorylated after IAA treatment. Conversely, in the *tmk1-1* and *abp1-TD1* mutants, this hyper-phosphorylation response was almost completely abolished with the majority of P-sites being very moderately hypo-phosphorylated, when compared to the distribution of hyper-phosphorylation in WT (Fig. 2a). This opposite tendency to hypo-phosphorylation in the mutants may be in part due to large differences in steady-state phosphorylation in the mutants (Extended Data Fig. 3a), as well as to the potential feedback regulations.

When comparing phospho-proteomes of untreated WT, *tmk1* and *abp1* roots, we found 2104 hypo-phosphorylated P-sites in the *tmk1-1* mutant, constituting potential substrates of the TMK1 kinase. Similar hypo-phosphorylation was found in the *abp1-TD1* mutant with 2589 hypo-phosphorylated P-sites as compared to WT (Extended Data Fig. 3a). The identified P-sites showed a significant overlap (Fisher's Exact Test: Odds Ratio = 9.53, 95% Confidence Interval = 8.28 – 11.00, $p < 2.2e-16$) between the *tmk1-1* and *abp1-TD1* mutants (Fig. 2c; Extended Data Fig. 3b,c) suggesting that TMK1 and ABP1 act together in mediating this rapid phospho-response. This is further substantiated by a high co-linearity between *tmk1-1* and *abp1-TD1* effects on the phosphorylation levels of individual sites. Notably, whereas a majority of the P-sites were co-regulated in *abp1* and *tmk1* mutants, about 5% showed an opposite regulation (Fig. 2b).

These observations suggest that ABP1 and TMK1 together mediate the ultrafast auxin effect on global protein phosphorylation, with ABP1 required also for phosphorylation of TMKs and other targets dependent on TMKs.

2.3.2.4 ABP1 and TMK1 are required for subset of rapid cellular responses

Prominent among the hypo-phosphorylated or systematically non-detectable P-sites in the *abp1* mutant under mock conditions were TMK1, TMK3, and TMK4 (TMK2 was not detected at all, presumably due to its low expression in roots) (Fig. 2d), suggesting that ABP1 is required

for the auxin-induced phosphorylation and thus activation of TMKs. This is also supported by a common requirement of both these regulators for auxin-induced phosphorylation of many targets, prominent among them PM H^+-ATPases, the established direct targets of TMK1[16,17].

PM H^+-ATPase generate H^+ gradient across the PM, which acidifies apoplast and contributes to membrane potential (MP); both classical rapid cellular auxin responses[10]. Indeed, consistent with lower phosphorylation of PM H^+-ATPases (Fig. 2e), roots of *abp1-c1* and *abp1-TD1* have lower PM ATPase activity than WT (Fig. 2f), similar to *tmk1* roots[16]. This diminished auxin-induced PM ATPase activity correlates well with a previously shown inability of *abp1* mutant protoplasts to undergo auxin-induced swelling[29]. On the other hand, electrophysiological[30] and growth measurements[16] detected normal auxin-triggered MP depolarization in the *abp1* roots[31] along with normal auxin sensitivity of their growth (Extended data Fig. 3e-g), consistent with a dominant role of TIR1/AFB signalling mechanism in this rapid auxin responses[4,32].

Other prominent targets of ABP1-TMK1 auxin phospho-response are cytoskeletal motor protein Myosin XI and MadB Myosin-binding proteins[15] (Fig. 2g and Extended Data Fig. 3d). A known cellular process dependent on Myosin XI function is cytoplasmic streaming[33]. We monitored this essential cellular process in root elongation zone by quantifying movement of small intracellular organelles. This revealed that IAA treatment promotes cytoplasmic streaming in concentration-dependent manner (Extended Data Fig. 3h), which occurs in WT and complemented lines but not in *abp1-c1*, *abp1-TD1*, *tmk1-1* or *tmk4-1* roots (Fig. 2h; Extended Data Fig. i,j). This shows involvement of ABP1 and TMK1 in auxin-triggered acceleration of cytoplasmic streaming consistent with a decrease of auxin-triggered Myosin XI phosphorylation in the mutants (Fig. 2g).

Overall, these observations suggest that ABP1 mediates auxin-triggered activation of the TMK1 signalling and they both are required for a subset of rapid cellular auxin responses such as PM H^+-ATPase activation and cytoplasmic streaming acceleration, providing examples of cellular targets for the ultrafast auxin phospho-response mediated by the ABP-TMK1 module.

2.3.2.5 ABP1 and TMKs are required for vascular tissue regeneration after wounding

Notably, Myosin XI also plays a role in the auxin feedback on its own transport and formation of auxin channels[15], which is part of the auxin canalization processes underlying self-organizing aspects of plant development[14]. A classic example of these canalization-mediated processes is vasculature regeneration after wounding when new vasculature is generated to circumvent the wound[34–37] (Fig. 3a).

We first evaluated ABP1 expression during vasculature regeneration after wounding in *ABP1::GUS* inflorescence stems. Staining 1–7 days after wounding (daw) induced by a horizontal cut revealed localized *ABP1::GUS* expression during vasculature regeneration. Early after wounding (before 2 daw), the GUS signal was strongly and specifically expressed above and below the wound; followed by a gradually weaker expression over time (Fig. 3b). Similar expression pattern was observed also in the *ABP1::GFP-ABP1* stems (Extended Data Fig. XX) confirming upregulation of ABP1 expression during vasculature regeneration.

Next, we assessed the efficiency of vasculature regeneration after wounding. As visualized by toluidine blue (TBO) staining in WT or in the complemented lines (*comp-c1*, *comp-TD1*), the vasculature fully developed, and both newly regenerated vessel cells and lignified parenchyma cells stained in blue were visibly circumventing the wound. In contrast, in *abp1-c1* and *abp1-TD1* mutant stems, regeneration was defective, with cells either failing to form a continuous strand of regenerated tissue or only partially (Fig. 3c, e and Extended Data Fig. 5b). Notably, the gain-of-function *35S::ABP1-GFP* line showed more efficient regeneration (Fig. 3c, e).

We analysed, in a similar way, the role of TMK in vasculature regeneration. *TMK::GUS* transgenic lines revealed the strongest expression of *TMK4* above and below the wound (2 daw) with gradually forming a channel-like pattern around the wound (4–6 daw), similar but weaker expression of *TMK3* and even weaker expression of *TMK1* (Extended Data Fig. 5a). Analysis of the corresponding loss-of-function mutants (*tmk1-1*, *tmk2-1*, *tmk3-1* and *tmk4-1*) revealed the strongest regeneration defects in *tmk4-1*, followed by *tmk3-1* and *tmk1-1*, whereas *tmk2-1* showed normal regeneration capacity consistent with the lack of TMK2 expression during regeneration (Fig. 3d, e).

These results show that both ABP1 and various TMKs are expressed following wounding and their function is crucial for the stem's capacity to regenerate vasculature around the wound.

2.3.2.6 ABP1 and TMKs are required for auxin canalization from external source

A direct manifestation of auxin canalization processes, is the formation of auxin-transporting channels followed by vasculature differentiation originating at a local, exogenous auxin source[37] (Fig. 5a).

Application of an IAA droplet on the stem side led to the formation of a distinct, new vascular strand connecting the external auxin source to the pre-existing vasculature (Fig. 5b). Similar experiments in *PIN1::PIN1-GFP* auxin transporter and *DR5rev::GFP* auxin response marker lines confirmed that PIN1-expressing, DR5-positive auxin channels already formed 2 days

after application (daa), thus, preceding the differentiation of new vasculature (Fig. 5c, d). All these processes related to auxin channel and vasculature formation were defective in *abp1* and *tmk* loss-of-function mutants. *abp1-c1* and *abp1-TD1* mutant alleles failed to form channels, as seen by PIN1-GFP and DR5 markers as well as TBO staining, whereas their corresponding complemented lines (*comp-c1*, *comp-TD1*) formed channels normally. As observed for vasculature regeneration, *tmk4-1* showed the strongest defects followed by *tmk3-1* and *tmk1-1* (Fig. 5b–e and Extended Data Fig. 6).

Overall, these experiments revealed a crucial role for ABP1 and TMKs in the formation of auxin transporting channels for vasculature formation originating from a local auxin source.

2.3.2.7 Auxin binding to ABP1 is crucial for its role in regeneration and auxin canalization

The strong defects of *abp1* mutants in vasculature regeneration and auxin canalization allowed us to test importance of IAA binding to ABP1 for its function. To this end, we engineered the ABP1^{M2X} version with a mutation in the predicted auxin-binding site[22]. Heterologously expressed and purified ABP1^{M2X} behaved similarly to the ABP1^{WT} in terms of (*i*) stability as shown by Western blot; (*ii*) dimerization assessed by Mass photometry; and (*iii*) protein folding as inferred from thermal melts and Circular Dichroism (CD) spectra (Fig. 5b; Extended Data Fig. 6a,b). This ABP1^{M2X} protein variant, however, did not associate with IAA in the DARTS assay (Extended Data Fig. 6c) and did not bind to IAA as confirmed by MST and GCI analysis (Fig. 5a and Extended Data Fig. 6d).

We introduced *ABP1::GFP-ABP1* or *ABP1::GFP-ABP1^{M2X}* into *abp1-c1* mutants and compared their ability to complement the defects in the vasculature regeneration (visualized by TBO staining) and in the formation of auxin channels from the external auxin source (visualized by TBO and *DR5rev::GFP* expression). *ABP1::GFP-ABP1* fully complemented the defects in both processes, whereas no complementation was observed in any of the four tested independent lines (Fig. 5c; Extended Data Fig. 6e-h), which verifiably expressed stable GFP-ABP1^{M2X} protein (Extended Data Fig. 6b).

The non-functionality of ABP1^{M2X} variant shows that ability of ABP1 to bind auxin is crucial for its developmental roles providing strong support for action of ABP1 as the auxin receptor mediating auxin canalization.

2.3.3 Conclusions

In this study we addressed a long-debated role of ABP1 in auxin perception and its relevance to plant development. We show that *Arabidopsis* ABP1 binds natural auxin IAA at a pH typical for the apoplast and a fraction of ABP1 is secreted. This provides a possibility for extracellular ABP1 to mediate auxin input into the cell surface TMK receptor like kinase-dependent signalling. This is supported by their auxin-induced interaction[20] and diminished auxin-triggered TMK phosphorylation in *abp1* mutants.

The ABP1-TMK1 signalling module is required for a large part of the ultrafast, global auxin phospho-response[15] as evidenced by its diminishment and largely overlapping hypo-phosphorylation detected in *abp1* and *tmk1* mutant roots. Among the common targets are previously established direct substrates of TMK1, PM H^+-ATPases[16,17], or Myoxin XI and Myosin-binding proteins[15]. Accordingly, *abp1* mutants show defects in a relared subset of auxin-triggered cellular responses, such as H^+-ATPase activation, protoplast swelling[29] or cytoplasmic streaming. In contrast, other rapid auxin responses, such as plasma membrane depolarization[32], Calcium transients[5] and root growth inhibition[4] are mediated by a non-transcriptional branch of TIR1/AFB signalling.

It is remarkable that the massive misregulation of protein phosphorylation is reflected by only mild developmental defects reported for *abp1* and *tmk1* mutants grown under standard conditions[28,38]. Nonetheless, rigorous analysis of loss-of-function alleles and corresponding complemented lines revealed crucial roles of both, ABP1 and TMKs in the auxin-triggered *de novo* formation and regeneration of vasculature in the shoot, a classical example of the auxin canalization, a mechanism behind many aspects of self-organizing plant development[39]. It remains unclear why canalization-related processes, which can take days to complete, involve ultrafast phosphorylation but one of its obvious rapid phospho-targets is Myosin XI, also required for canalization[15]. The strong defects in auxin canalization-dependent processes suggest that ABP1-TMK cell surface signalling provides a long sought mechanism for auxin input into the feedback regulation of auxin transport, the main pre-requisite of coordinated tissue polarization during canalization[14,40], which is also targeted by the CAMEL-CANAR receptor complex acting upstream of PIN auxin transporters[41].

abp1 mutants show more pronounced defects as compared to the single *tmk1* mutant. This is likely due to the redundant action of TMKs in this process, as suggested by their overlapping expression around the wound and similar defects in other *tmk* mutants. On the other hand,

multiple *tmk* mutants such as *tmk1,4* have much stronger developmental phenotypes than observed in *abp1*[28,38]. This is either due to an ABP1-independent role of TMKs or it is possible that ABP1 acts redundantly with other members of the large cupin family[26].

A long contested role of ABP1 as an auxin receptor is now strongly supported by the verified defects in multiple auxin-triggered rapid cellular processes and developmental defects in auxin canalization-related processes. Additional strongr support comes the ABP1^{M2X} variant, which does not bind auxin and is consequently non-functional to mediate auxin canalization. Thus ABP1-TMK auxin perception complex at the cell surface mediates auxin phospho-response and provides now a means how to interrogate genetically biological roles of this novel, global regulation in auxin canalization and beyond.

2.3.4 Materials and Methods

Genetic material and growth conditions

All *Arabidopsis thaliana* lines are in Columbia-0 (Col-0) background with exception of *abp1-TD1*, which is in Col-4. The following lines were described previously: *abp1-c1* and *abp1-TD1*[21]; *tmk1-1* (SALK_016360), *tmk2-1* (SAIL_1242_H07), *tmk3-1* (SALK_129759) and *tmk4-1* (GABI_348E01)[9]; *TMK1::GUS, TMK2::GUS, TMK3::GUS,* and *TMK4::GUS* transgenic lines (unpublished); *DR5rev::GFP*[42]*, PIN1::PIN1-GFP*[43]*, ABP1::GUS*[44] and *abp1* complemented lines: *comp-TD1 = ABP1::ABP1/abp1-TD1*; *comp-c1 = ABP1::GFP-ABP1/abp1-c1*[28]. The ABP1-M2X variant was generated by substitutions of two Histidines (H59V, H61V) by Valines[22] into *pABP1::GFP-ABP1* construct[28] using QuikChange Lightning Site-Directed Mutagenesis Kit (Agilent Technologies) and following primers: M2X_Val-F (5'-aaaaacctcttcacaggagaccctgacaattggtgtctctgaacctggag-3') and M2X_Val-R (5'-ctccaggttcagagacaccaattgtcagggtctcctgtgaagaggttttt-3'). Those constructs were introduced to *abp1-c1* and *abp1-TD1* mutant backgrounds. *RPS5A::ABP1-GFP* plasmid was constructed with the Gateway cloning technology (Invitrogen). The *ABP1-GFP* coding sequence[13] and the *pRPS5* promoter region were recombined into the expression vector *pB7m24GW,3*. The resulting constructs were transformed into *Arabidopsis* (Col-0) plants by floral dipping in *Agrobacterium tumefaciens* liquid cultures.

Seeds were sterilized overnight by chlorine gas, sown on solid *Arabidopsis* medium (half-strength Murashige and Skoog basal salts, 1% sucrose, and 0.8% phyto-agar, pH 5.7) and stratified at 4 °C for at least 2 days prior to transfer to a growth room with 16 h-light/8 h-dark light cycle at 21 °C. Seedlings were grown vertically for 4 or 6 days, depending on the assay. The root growth assays were performed as described[16].

Heterologous expression and purification of recombinant proteins

To express the extracellular domain (ECD) of TMK1 the ECD residues determined as described[25] were cloned in the pECIA2 and pECIA14 plasmids[45]. To enhance expression and ease purification, the ER-retaining C-term KDEL sequence in the full-length coding sequence of ABP1 was replaced by KEQL. ABP1-M2X mutations in the Zn^{2+}-associated predicted auxin binding pocket were introduced as described[22]. Both ABP1 and ABP1-M2X were also introduced into pECIA2 and pECIA14. All sequences were N-terminally fused with the TEV pronase site, StrepII- and 9xHis-tag. These purified plasmids were transformed into DH10EMBacY *E. coli*. Selected colonies contained the recombinant bacmids from which recombinant bacmid DNA could be stored. 3 µg of this recombinant DNA was then transfected into Sf9 baculovirus cell cultures. Yellow fluorescent protein (YFP) indicated the efficiency of the transfection. Hi5 insect cells were infected with the three generated baculovirus stocks following the published protocol[46]. Due to the initial plasmids used, protein purification could proceed from the medium of the expression cultures. For all three proteins, 2 L cell culture was used. ABP1 and ABP1-M2X proteins were purified from Hi5 insect cells using a HisTrap Excel column (Cytiva) with gradual washes up to 50 mM imidazole in 50 mM HEPES/NaOH, 500 mM NaCl buffer at pH 7.5. Elution from the column was performed with 500 mM imidazole and the eluted fractions were pooled, concentrated (Vivaspin 20, 10 kDa MWCO) and loaded onto a Superdex 200 16/60 column. Size exclusion (SEC) was performed in 50 mM citrate buffer pH 5.5 containing 250 mM NaCl and 0.05 mM $ZnCl_2$. Fractions were analysed on SDS-PAGE and based on size and purity selected and pooled for another concentration step. Aliquots were frozen and stored at -80 °C. TMK1 ECD protein was purified from Hi5 insect cells using a cOmplete His-tag purification column (Roche) with gradual washes up to 50 mM imidazole in 50 mM HEPES/NaOH, 500 mM NaCl buffer at pH 7.5. Elution from the column was performed with 500mM imidazole and the eluted fractions were pooled, concentrated (Vivaspin 20, 10 kDa MWCO). To exchange the buffer, the concentrated His-eluted fraction was loaded onto a HiPrep 16/10 desalting column, equilibrated with 10% 50 mM HEPES/NaOH, 1 M NaCl buffer at pH 7.5. To increase the purity of the target protein, sample was loaded onto a 5 mL ANX FF high sub ion exchange (IEX) column. Bound protein was eluted with 100% 50 mM HEPES/NaOH, 1 M NaCl buffer, pH 7.5 buffer. The flow-through from IEX was concentrated (Vivaspin, MWCO 10 kDa) and loaded onto a Superdex 200 16/60 column. Size exclusion (SEC) was performed in 50 mM NaH_2PO_4/Na_2HPO_4 buffer containing 200 mM NaCl and 5% glycerol at pH 7.5. Fractions were analysed on SDS-PAGE and based

on size and purity selected and pooled for another concentration step. Aliquots were frozen and stored at -80 °C.

Drug Affinity Responsive Target Stability (DARTS)

The DARTS assay, for testing the binding of IAA to ABP1 or TMK1, was performed as previously reported[47]. Roots of 7 day old *TMK1::TMK1-GFP* seedlings or full 7 day old seedlings expressing *35S::ABP1-GFP* were used for total protein extraction. After harvesting, the samples were ground in liquid nitrogen, resuspended at a 1:2 (w/v) ratio in protein extraction buffer (25 mM Tris-HCl, pH 7.5; 150 mM NaCl; 0.1% IGEPAL CA-630, Roche cOmplete protease inhibitor cocktail, EDTA free) and spun down to discard the cell debris. After quantifying the protein concentration (Quick Start™ Bradford Reagent, Bio-Rad), the cell lysate was aliquoted and incubated with 0, 1, 10 or 50 µM IAA or benzoic acid (BA) respectively. As both IAA and BA were dissolved in DMSO, the equivalent volume DMSO was added in one mock aliquot. Cell lysate plus small molecule were incubated for 1h at 4°C while mixing at a low speed. Subsequently, the treated extracts were further aliquoted and mixed with different concentrations of Pronase (Roche) in Pronase buffer (25 mM Tris-HCl, pH 7.5; 150 mM NaCl). After incubation at 25 °C for 30 min, the proteolytic digestion was terminated by adding protease inhibitor cocktail (cOmplete, Roche) and the samples were kept on ice for 10 min. The protein samples were then analysed by Western blot. Band intensity was quantified using the Plot lane function in ImageJ. GFP-fused proteins were detected by an anti-GFP antibody (JL8, Clontech, 1:2000) or using anti-His-HRP for the *in vitro* experiments (Agrisera, AS15-2930, 1:5000). Anti-actin (Sigma-Aldrich A0480, 1:5000) was used as loading control on the blots from the plant extracts. HRP activity was detected by the SuperSignal Western Detection Reagents (Thermo Scientific) and imaged with a GE Healthcare Amersham 600RGB system.

Microscale Thermophoresis (MST)

IAA binding affinities were analysed by Microscale Thermophoresis (MST) [48]. All recombinant proteins were fluorescently labelled using Monolith Protein Labeling Kit RED-NHS 2nd Generation (Cat# MO-L011, NanoTemper Technologies) according to the manufactured manual including the buffer exchange step. ABP1 and ABP1-M2X were labelled in NHS labelling buffer (130 mM $NaHCO_3$, 50 mM NaCl, pH 8.2-8.3) followed by elution in either 50 mM citrate buffer pH 5.5 containing 250 mM NaCl, 0.05 mM $ZnCl_2$, 0.01% (w/v) TWEEN®20 for measurements at pH5.5 or in HEPES buffer pH 7.5 or pH 7 supplemented with 250 mM NaCl, 50 µM $ZnCl_2$, 0.01% (w/v) TWEEN®20 to perform measurements at pH

7.5 or pH 7. TMK1 was labelled using the same kit, but elution was performed in 50mM NaH_2PO_4/Na_2HPO_4 buffer containing 200mM NaCl and 0.01% (w/v) TWEEN®20 at pH 7.5.

All experiments were carried out on a Monolith NT.115 Blue/Green system (NanoTemper Technologies) and were performed in premium glass capillaries (Cat# MO-K025, NanoTemper Technologies). The target protein concertation was kept constant in the reaction as following: 100 nM or 75 nM ABP1 or ABP1-M2X respectively for binding study at pH 5.5, 100 nM ABP1 for binding study at pH 7.5 and pH 7 and 150 nM for TMK1 ECD. IAA, BA and L-Trp as ligands were serially diluted 1:1 from 2 mM to 61 nM in the ABP1 experiments. IAA, 1-naphthalene acetic acid (NAA), BA and L-Trp as ligands were serially diluted from 200 µM to 3 nM and MST power 80% with excitation power 80% was used for binding measurements of ABP1 at pH 5.5, pH 7 and pH 7.5; MST power 80% with excitation power 40% was used for binding measurements of ABP1-M2X at pH 5.5 and MST power 40% with excitation power 20% was used for binding measurements of TMK1 ECD. All ABP1-related MST measurements were running in 3/3/3/25 seconds intervals. For TMK1 ECD 5/30/25 seconds intervals were used. The capillaries were measured repetitively 10 times in each experiment. ABP1 binding at pH 5.5 was performed in 3 independent replicates, all other experiments in 2 independent replicates. The evaluation of TMK1 ECD binding to auxin was repeated four times. MST traces were analysed in MO. Affinity Analysis software (NanoTemper Technologies) at time point 1.5 s on time. Data were fitted to Kd model assuming a 1:1 stoichiometry per binding partner and the confidence interval of the Kd was calculated from the variance of the fitted parameter using standard fitting mode.

Grating-coupled interferometry (GCI) (Creoptix® WAVEsystem)

GCI measurements were done on the WAVEsystem (Creoptix, Waedenswil, Switzerland). All experiments were performed on 4PCH WAVEchips (polycarboxylate hydrogel chips, Creoptix). Proteins were immobilised on the chip surface with standard amine-coupling (7 min activation [1:1 mix of 400 mM N-(3-dimethylaminopropyl)-N′-ethylcarbodiimide hydrochloride and 100 mM N-hydroxysuccinimide] (Xantec), followed by the injection of ABP1 on channel 2 (50 µg/ml in 10 mM sodium acetate pH 5); ABP1-M2X on channel 3 (50 µg/ml in 10 mM sodium acetate pH 5) and TMK1 on channel 4 (120 µg/ml in 10 mM sodium acetate pH 4.5). High protein density was reached for each protein and mentioned in the Results table. Finally, the surface was deactivated with 1 M ethanolamine pH 8 for 7 min (Xantec). Channel 1 was also activated/deactivated and served as a reference channel. All kinetic analyses were performed at 25 °C with 8 dilutions in a 1:3 dilution series from 200 µM of either

IAA or BA, diluted in a 50 mM citrate buffer of pH5.5 (250 mM NaCl, 50 µM $ZnCl_2$ and 1% DMSO) or HBS buffer of pH 7.6 (250 mM NaCl, 50 µM $ZnCl_2$ and 1% DMSO). Blank injections were used for double referencing and a dimethyl sulfoxide (DMSO) calibration curve for bulk correction. Data Analysis was performed using the Creoptix WAVE control software and a 1:1 Langmuir model was applied.

Electron microscopy

Wild type and transgenic lines expressing *pABP1::ABP1-GFP* or *RPS5A::ABP1-GFP*, were grown for 4–5 days on *Arabidopsis* medium (AM) plates, incubated in a mock or 1 µM IAA solution for 3 hours and subjected to immuno-electron microscopy.

I) Pre-embedding immunometal electron microscopy: samples were fixed with 4% formaldehyde and 0.05% glutaraldehyde in phosphate buffer (PB; 0.1 M, pH 7.4) for 1 h at room temperature (RT) under vacuum. The samples were washed with PB, incubated in increasing gradients of sucrose in PB (10% and 20%) and then 20% sucrose plus 5% glycerol in PB for 1 h each at RT. They were then rapidly frozen on liquid nitrogen and thawed in hand-warm PB containing 20% sucrose to increase penetration of reagents. This freeze-thawing cycle was repeated three times. Samples were then washed with phosphate buffered saline (PBS; 0.1 M, 0.9% NaCl, pH 7.4) and MilliQ water briefly, and incubated with 2% Driselase in PBS for 30 min at 37 °C. They were then washed with Tris-buffered saline (TBS; 0.05 M, 0.9% NaCl, pH 7.4) and 50 mM glycine in TBS for 1 hour at RT to quench free aldehyde groups, followed by incubation in 10% normal goat serum (NGS), 2% bovine serum albumin (BSA) and 0.2% fish-skin gelatin (FSG) in TBS for 90 min at RT to block nonspecific binding sites. An anti-GFP antibody raised in rabbit (Abcam, ab6556) was then applied in TBS containing 2% BSA at a concentration of 0.2 µg/ml for 48 hours at 15 °C with gentle agitation. After consecutive washes with TBS and TBS containing 2% BSA, 1.4 Nanogold® conjugated Fab' fragments (Nanoprobes Inc.; 1:100 in TBS containing 2% BSA) were applied for 16 h at 15 °C. The samples were washed with MilliQ water and postfixed with 2% glutaraldehyde in 0.1 M PB. Nanogold particles were then amplified with silver using the HQ SilverTM Enhancement kit (Nanoprobes Inc.) for 7–8 min at RT under light microscopy control, and amplification stopped by wash with MilliQ water. Samples were fixed again with 2% glutaraldehyde in PB for 20 min at RT, and incubated in PB. For conventional resin embedding, samples were contrast enhanced by applying 0.5% (w/v) tannic acid in 0.1 M PB for 1 hour at 4 °C, 1% (w/v) osmium tetroxide for 30 min at 4 °C and 1% (w/v) uranyl acetate in 50% ethanol (aqueous) for 30 min at 4 °C in the dark. Samples were dehydrated in graded ethanol (50%,

70%, 90%, 96%, 100%), incubated in propylene oxide two times 10 min each, and embedded in epoxy resin (Durcupan ACM, Fluka). For polymerization, the samples were transferred to BEEM capsules (EMS; Hatfield), the capsules filled with freshly prepared Durcupan and cured for 48 h at 60 °C. For samples subjected to high-pressure freezing fixation, root tips were rapidly frozen and freeze-substituted after the immunolabeling to minimize structural impairments during the dehydration and embedding steps. For this, root tips were dissected, immersed in 5% (w/v) sucrose in water and placed into aluminium carriers (2 mm inner diameter, indentation 200 µm; Wohlwend). The flat side of a carrier with a 300 µm indentation was used as a lid. The sandwiched samples were high-pressure frozen using an HPM 010 (Leica Microsystems). Freeze substitution was carried out in an EM AFS I device (Leica Microsystems). The following protocol was applied: 24 h substitution in 0.1% (w/v) tannic acid in anhydrous acetone at -85 °C, followed by 3 times 20 min washes in acetone at -85 °C, 6 h substitution in 1% (w/v) osmium tetroxide plus 0.2% (w/v) uranyl acetate in acetone at -85 °C, raising of the temperature 15 °C/h to -60 °C, 6 h incubation at -60 °C, raising of the temperature 15 °C/h to -20 °C, 2 h incubation at -20 °C, raising of the temperature 15 °C/h to 4 °C, 30 min incubation at 4 °C. Samples were washed in acetone 3 times 20 min each at 4 °C, removed from the carriers and embedded in epoxy resin (Durcupan ACM, Fluka) as described above. Ultrathin sections (70–80 nm) were cut from the blocks using an ultramicrotome UC7 (Leica Microsystems), collected onto Formvar-coated copper slot grids, and stained with 1% uranyl acetate in water and 0.3% lead citrate. Sections were examined under a Tecnai 10 TEM (Thermo Fisher) at 80 kV and imaged with a side-mounted camera Megaview G3 (EMSIS).

II) Post-embedding immunogold electron microscopy: samples were grown on AM plates as described above. After incubation in mock or IAA, samples were immersed in 15% (w/v) polyvinylpyrrolidone (Sigma) in growth medium, high-pressure frozen in the HPM 010 (Leica Microsystems) and freeze-substituted in the EM AFS I (Leica Microsystems). The following protocol was applied to the samples: substitution in anhydrous acetone containing 0.2% (w/v) uranyl acetate, 2% (v/v) methanol, 0.15% (v/v) glutaraldehyde and 1% (w/v) paraformaldehyde for 32 h at -85 °C, raising of the temperature 15 °C/h to -60 °C, 6 h incubation at -60 °C, raising of the temperature 15 °C/h to -20 °C, 2 h incubation at -20 °C, and raising of the temperature 15 °C/h to 4 °C. Samples were removed from the substitution chamber immediately, rinsed in dry ethanol 3 times 20 min each at 4 °C, and embedded in LR-White resin (Hard grade acrylic resin; London Resin Company Ltd.). Then the following was applied to the samples: infiltration in 1:1 dry ethanol to LR White for 30 min at RT, 1:2 dry ethanol to LR White for 30 min at RT

and mere LR White overnight at RT. Samples were transferred to gelatin capsules, the capsules fully filled with fresh resin, tightly capped, and polymerized for 24 h at 50 °C. Ultrathin sections (80 nm) were cut using the ultramicrotome UC7 (Leica Microsystems), collected onto Formvar-coated nickel slot grids and processed for immunogold labeling. Samples were first washed in drops of TBS containing 0.1% Triton X-100 (T-TBS) for 20 min at RT. Then they were incubated in 50 mM glycine in TBS to quench free aldehyde groups for 1 h at RT, and T-TBS containing 10% NGS plus 2% BSA and 1% FSG for 90 min at RT to block nonspecific binding sites. The rabbit anti-GFP antibody (Abcam) was applied at a concentration of 1 µg/ml in T-TBS containing 2% BSA overnight at 4 °C. After consecutive washes with TBS and T-TBS containing 2% BSA and 1% FSG, goat anti-rabbit immunoglobulins conjugated to 10-nm gold particles were applied (British BioCell Int.) at a dilution of 1:50 in TBS-T containing 2% BSA and 0.05% polyethylene glycol for 90 min at RT. Sections were then rinsed in TBS and air dried. Sections were contrast enhanced applying 1% aqueous uranyl acetate for 20 min at RT and 0.3% lead citrate for 6 min at RT. Sections were examined under a Tecnai 10 TEM (Thermo Fisher) at 80 kV and imaged with a side-mounted camera Megaview G3 (EMSIS).

Sampling and analysis of data: For root samples, 5–7 seedlings of each line were included per immunolabeling experiment, and three experimental runs were performed For quantitation of the immunoreaction product, sections were selected randomly per seedling and per experiment. For shoot apical meristem samples, at least 2 repetitions were performed, and the experimenter was blinded during acquisition and analysis. The density of the immunoparticles in the apoplast was calculated by counting the visible particles clearly visible in the apoplastic areas and dividing this by the area of the plasma membrane manually measured using ImageJ. For the post-embedded samples, for each particle the distance to the PM was determined. If this distance was greater than 19 nm (the size of the immuno complex), it was classified as such. Particles greater than this distance were classified as *bona fide* apoplastic signals.

Phospho-proteomic analysis

For rapid auxin-dependent phosphorylation analysis, Arabidopsis Col-0, *tmk1-1* or *abp1*-TD1 seeds were surfaced-sterilized, suspended in 0.1% agarose and stratified for 48 hours. Seeds were sowed in two lines on half-strength Murashige and Skoog (MS) plates covered with sterile nylon mesh with 100 µm pore size. Plates were grown vertically in a growth chamber at 22ºC in long-day lighting (16 h:8 h light:dark). Five days after germination, root tips were locally treated for 2 minutes by applying liquid half strength MS medium with 100 nM IAA, or

equivalent volume DMSO solvent control, directly to the root tips. After exactly two minutes, each row of root tips (~10mm) was cut with a surgical blade and frozen in liquid nitrogen. Plates were treated one by one to stay within a 2 minute time frame. In total, 4 biological replicates per condition were harvested on consecutive days, in total pooling 10-15 plates per biological replicate.

For protein extraction, frozen root tips were ground to a fine powder in liquid nitrogen using a mortar and pestle. Proteins were subsequently extracted in SDS lysis buffer (100mM Tris pH 8.0, 4% SDS and 10mM DTT) and sonicated in a cooled CupHorn sonicator (QSonica) for 10 minutes at 90% amplitude with 30 seconds on / 30 seconds off cycle. The lysate was cleared by centrifugation at maximum speed (13,000xg) in a table-top centrifuge for 30 minutes. Protein concentrations were determined using Bradford reagent (Bio-Rad).

For all samples, 500 µg protein was used for filter aided sample preparation FASP[49]. For FASP, 30 kDa cut-off amicon filter units (Merck Millipore) were used. Filters were first tested by applying 1000 µl UT buffer (8 M Urea and 100mM Tris, pH 8.5) and centrifuging for 20 minutes at 6,000 RPM at 20ºC. All further centrifugation steps were at this speed and temperature. The desired amount of protein sample was next mixed with UT buffer to a volume of 5000 µl, applied to the filter and centrifuged for 20 minutes. Filters were washed with UT buffer and centrifuged for 20 minutes. Retained proteins were alkylated with 50 mM acrylamide (Sigma) in UT buffer for 30 minutes at 20ºC while gently shaking. The filter was centrifuged and afterwards washed three times with UT buffer for 20 minutes. Next, filters were washed three times with 50 mM Ammonium BiCarbonate buffer (ABC). After the last wash, proteins were cleaved overnight by adding Trypsin (Roche) in a 1:100 trypsin: protein ratio. The filter was transferred to a new tube and peptides were eluted by 20 minutes centrifugation. Further elution was completed by twice adding (500µl) 50 mM ABC buffer and centrifuging.

For peptide desalting and concentrating, C18 Stagetips were used. 1000 µl pipette tips were fitted with 2 plugs of C18 octadecyl 47mm Disks 2215 (Empore™) material and 10 µg of LiChroprep® RP-18 peptides (Merck). Tips were sequentially equilibrated with 100% methanol, 80% Acetonitrile in 0.1% formic acid and twice with 0.1% formic acid with intermittent centrifugation for 4 minutes at 1,500xg. After equilibration, peptides were loaded and centrifuged for 20 minutes at 400xg. Bound peptides were washed with 0.1% formic acid and eluted with 80% ACN in 0.1% formic acid by spinning for 4 minutes at 1,500xg. Eluted

peptides were subsequently concentrated using a vacuum concentrator for 30 minutes at 45ºC and resuspended in 50 µl Ti^{4+}-IMAC loading buffer (Resyn Biosciences).

Phosphopeptide enrichment was performed using Ti^{4+}-IMAC magnetic beads as per manufacturer's instruction (Resyn Biosciences). After phosphopeptide enrichment, peptides were desalted and concentrated using C18 Stagetips. Eluted peptides were subsequently concentrated using a vacuum concentrator for 30 minutes at 45ºC and resuspended in 50 µl 0.1% formic acid. For LC-MS/MS analysis, maximally 5 µl prepared sample was injected into a 0.10 × 250 mm ReproSil-Pur 120 C18-AQ 1.9 µm beads analytical column (prepared in-house) at a constant pressure of 825 bar using a 1 hour gradient from 9 to 34% acetonitrile in water with 0.1% formic acid in 50 min by a nanoLC-MS/MS (Thermo nLC1000 coupled to a Q Exactive-HFX). MS and MSMS AGC targets were set to 3.106, 50,000, respectively, or maximum ion injection times of 50 ms (MS) and 25 ms (MS/MS) were used. HCD-fragmented (isolation width 1.2 m/z, 24% normalized collision energy) MS/MS scans of the 25 most abundant 2–5+ charged peaks in the MS scan were recorded in data-dependent mode (threshold 1.2e5, 15 s exclusion duration for the selected m/z +/− 10 ppm).

The MaxQuant quantitative proteomics software package was used to analyse LCMS data with all MS/MS spectra. The following settings were used; FDR≤0.01, the proteome of *Arabidopsis thaliana* (UniProt ID UP000006548) was used as protein database, maximum missed cleavage was set at 2, variable modifications Oxidation (M);Acetyl (Protein N-term);Deamidation (NQ);Phospho (STY), fixed modification AcrylAmide (C), match between runs was selected.

Perseus was employed for filtering and further bioinformatics and statistical analysis of the MaxQuant ProteinGroups files[50]. The data was filtered on reverse and potential contaminant hits. P-site localisation probability was filtered using a cut-off of ≥0.75. Data was further filtered on a minimum of 75% valid values in at least one condition. From the phosphopeptides passing this filtering, normality was checked using histograms. Data was normalized using median subtraction. Missing values were imputed from a normal distribution using standard settings in Perseus. FDR permutation-based t-tests were done in a pairwise comparisons (i.e. WT IAA vs Mock or *tmk1-1* IAA vs Mock etc.). Phosphopeptides passing an FDR cut-off ≤0.05 were used for further analysis. Data was visualized using R and Adobe illustrator.

The mass spectrometry proteomics data, protein lists and intensity values of all samples have been deposited to the ProteomeXchange Consortium via the PRIDE[51] partner repository with the dataset identifier PXD031063.

ATPase assays

The excised roots from 7-day-old seedlings, which are pre-treated with 30 μM kynurenine for 24 h under dark condition, were homogenized in the homogenization buffer (50 mM MOPS-KOH [pH 7.0], 100 mM KNO_3, 2 mM sodium molybdate, 0.1 mM NaF, 2 mM EGTA, 1 mM PMSF and 20 μM leupeptin) and were centrifuged at 10,000*g* for 10 min. The supernatant was centrifuged at 45,000 rpm for 60 min. The resultant precipitate was resuspended in the homogenization buffer, and was addressed as a microsomal fraction. ATP hydrolytic activity in the microsomal fraction was measured in a vanadate-sensitive manner following the method[52] of with some modifications. Briefly, the microsomal fraction (22.5 μL) was mixed with the equal volume of the reaction buffer (60 mM Mes-Tris [pH 6.5], 6 mM $MgSO_4$, 200 mM KNO_3, 1 mM ammonium molybdate, 10 μg/mL oligomycin, 2 mM NaN_3, 0.1% Triton X-100, 1 mM PMSF and 20 μM leupeptin) with or without 1 μL of 10 mM sodium orthovanadate. The sample solution was incubated with 5 μL of 20 mM ATP at 30ºC, and was added with 50 μL of the stop solution (2.6% [w/v] SDS, 0.5% [w/v] sodium molybdate and 0.6 N H_2SO_4) after 30 min. The inorganic phosphate released from ATP was measured.

Membrane potential measurements

The Arabidopsis seedlings were grown at constant light at 22 °C. Four- to five-days old seedlings were used for membrane potential measurements. Seedlings were attached to the glass slide in air together with agar growing medium taken from Petri Dish above the hypocotyl, while the root was free and immersed into electrophysiological solution (BSM-basic salt medium: 0.1 mM CaCl2, 0.5 mM KCl, pH 5.5 non-buffered). The root was immobilized in an experimental chamber by a silicon tube and the seedling was conditioned for 20 min before the onset of the measurements. The experimental chamber with the seedling was transferred on the stage in Faraday cage and the membrane potential measurements were performed with the conventional glass microelectrodes inserted into the epidermal cells of mature root zone with a manually operated 3D-micromanipulator, under a visual observation with a horizontal Leitz stereomicroscope (×160 magnification) using a Leitz micromanipulator (Leitz, Wetzlar, Germany). The glass microelectrodes were pulled (a tip diameter of ~0.5 μm) from capillaries with an internal filament (GB150F, Science Products, Hofheim, Germany) on a vertical pipette puller (700C, David Kopf Instruments, Tujunga, CA) and filled with 1 M KCl. The reference electrode was an Ag/AgCl wire in a small glass tube, also filled with 1 M KCl, contacting the BSM via a piece of porous ceramic, as previously described[53]. The microelectrode was connected to a custom made high-input impedance (›1015 Ω) amplifier BBA18 (OP Amplifier LMC 6081, National Instruments, USA) via an Ag-AgCl half-cell, and

recorded by data acquisition card (DAQ, LabJack U3-LV, National Instruments, USA) and LabVIEW 7.1 program with sampling rate of 12 ms. Once the root is impaled with the microelectrode, the membrane potential was recorded for several minutes to provide a stable level. The root was treated with auxin (100 nM IAA) that was added into the experimental chamber when the membrane potential reached a steady-state level and the membrane potential was recorded for at least 20-30 min after the start of treatment.

Cytoplasmic streaming

Cytoplasmic streaming was recorded under widefield microscope (Nikon Ti2E) with bright field module via Plan Apo λ 40×/0.95 air objective. 4–5 days old seedlings were taken into microscope room 30 minutes in advance to make seedling adapt to the environment. To further ensure equal experimental condition, Col-0, mutants and complemented lines were placed in the same square of media (1/2 MS containing 1% agar), with or without IAA (10 mM IAA stock in ethanol) and then moved to a coverglassed chamber for 30 minutes before imaging. Cytoplasmic streaming was recorded in the epidermal cells of the root elongation zone at 1 second interval for 30 seconds. The maximal velocities of cytoplasm streaming were determined by tracing particles of 0.5 - 1.0 μm in diameter that were smoothly moving for at least 3 seconds by using Fiji manual tracking (3 fastest particle per cell, 3 cells per seedling and 7 seedlings per treatment).

Vasculature regeneration after wounding in inflorescence stems

The regeneration experiments were performed as described previously [35,37]. Plants with immature inflorescence stems (9 to 10 cm tall) were used. Stems were decapitated with a sharp razor blade, the apical floral parts (1 to 2 cm) were removed, and the artificial weight, a 2.5 g lead ball connected with a plastic tube was applied. Decapitated stems covered by the artificial weight were additionally supported by a wood stick to avoid their bending. With this method, secondary tissue architecture could be obtained 6 days after weight application in the basal parts of previously immature *Arabidopsis* stems (5 mm segments above the rosette).

For observation of regeneration, inflorescence stems were wounded precisely with a sharp razor blade, in distance of approximately 5 mm from the rosette in the transversal plane of the basal sectors with vascular cambium and secondary tissues to interrupt their longitudinal continuum. During all experimental steps, plants were still covered with the artificial weights. Axillary buds grown above the rosette leaves were not removed, thus remaining the source of endogenous auxin. After 0, 4 and 6 days after wounding (daw), stem segments were cut with an automated vibratome (Leica VT1200 S, Leica Microsystems Ltd., Wetzlar, Germany) and

70 µm-thick native sections were prepared. The native sections were stained with a 0.025% Toluidine Blue O aqueous solution and regeneration was analysed in stems with fully developed, closed cambial rings, and secondary tissues in their basal parts. The native sections were observed using a bright field microscope (Zeiss Axioscope.A1) and pictures of vasculature were photographed with a camera (Axiocam 506) at 10x magnification.

For observation of GUS activity after wounding, the same technique of plant preparation was used as described previously for the regeneration analysis. After 0, 4 and 6 daw, stem segments were incubated with X-Gluc solution at 37 °C, overnight, and fixed with a 70% ethanol solution at room temperature. The samples with positive GUS reaction were cut with an automated vibratome and 70 µm-thick native sections were prepared. The native sections were cleared in a solution containing 4% HCl and 20% methanol for 15 min at 65 °C, followed by a 15-min incubation in 7% NaOH and 70% ethanol at room temperature. In the next step, seedlings were rehydrated by successive incubations in 70%, 50%, 25%, and 10% ethanol for 10 min at room temperature, followed by an incubation in a solution containing 25% glycerol and 5% ethanol for 10 min at room temperature. Finally, seedlings were mounted in 50% glycerol and observed using a bright field microscope. Pictures of GUS activity were photographed with a camera at 10x magnification.

Auxin-induced canalization in inflorescence stems

The auxin canalization experiments were performed as before[37]. *Arabidopsis* plants with young, 10 cm tall inflorescence stems were chosen for exogenous auxin application. Stems were wounded by a transversal incision 3–4 mm above the rosette to interrupt the vascular cambium and secondary tissues and hence also the polar, basipetal transport of endogenous auxin. We then applied 10 µM IAA (Sigma-Aldrich, cat. no 15148-2G) in a droplet of lanoline paste below the cut. This droplet was replaced every 2 days to ensure the constant presence of auxin. Samples were collected and the manual longitudinal stem sections were obtained using a NIKON SMZ1500 stereomicroscope. Sections were stained in 0,05% Toluidine Blue O and mounted in a 50% glycerol aqueous solution. Images of these sections were obtained using an Olympus BX43 microscope equipped with an Olympus SC30 Camera. Number of analysed stems were >10, typically, =20.

Characterization of $ABP1^{WT}$ and $ABP1^{M2X}$ proteins

The behaviour of $ABP1^{WT}$ and $ABP1^{M2X}$ proteins was analysed by mass photometry. Landing assays, data acquisition and image processing were performed with Refeyn TwoMP mass photometer and software. The instrument was calibrated by running standard proteins, such as

bovine serum albumin (BSA) and immunoglobulin G (IgG) (from Sigma-Aldrich) diluted to 10 nM concentration. The resulting calibration parameters were used as a conversion between measured contrast and mass of $ABP1^{WT}$ and $ABP1^{M2X}$ proteins. $ABP1^{WT}$ and $ABP1^{M2X}$ were measured at a concentration of 40 nM in ABP1 buffer (50mM citrate pH 5.5; 250 mM NaCl; 0.05 mM $ZnCl_2$).

For Circular Dichroism (CD) spectral measurement, $ABP1^{WT}$ and $ABP1^{M2X}$ were diluted in ABP1 buffer to 0.3 mg/ml. A Chirascan Plus CD Spectrophotometer by Applied Photophysics was used to generate CD spectra. The ellipticity (Circular Dichroism [mdeg]) was recorded with a spectral scan from 190-260 nm at 20 ˚C. Three repeats of spectrum were collected for each sample.

Accession Numbers

Sequence data from this article can be found in the *Arabidopsis* Genome Initiative databases under the following accession numbers: At4g02980 for ABP1, At1g66150 for TMK1, At1g24650 for TMK2, At2g01820 for TMK3, At3g23750 for TMK4, At2g18960 for AHA1, At4g30190 for AHA2, At5g20490 for Myosin XIK, At1g62390 for MadB2/PHOX2, At2g25290 for MadB1/PHOX1, At5g20360 for MadB/PHOX3.

2.3.5 References Material and Methods

1. Gao, Y. *et al.* Auxin binding protein 1 (ABP1) is not required for either auxin signaling or Arabidopsis development. *Proc. Natl. Acad. Sci.* **112**, 2275–2280 (2015).
2. Cao, M. *et al.* TMK1-mediated auxin signalling regulates differential growth of the apical hook. *Nature* **568**, 240–243 (2019).
3. Friml, J. *et al.* Efflux-dependent auxin gradients establish the apical-basal axis of Arabidopsis. *Nature* **426**, 147–153 (2003).
4. Benková, E. *et al.* Local, Efflux-Dependent Auxin Gradients as a Common Module for Plant Organ Formation. *Cell* **115**, 591–602 (2003).
5. Klode, M., Dahlke, R. I., Sauter, M. & Steffens, B. Expression and Subcellular Localization of Arabidopsis thaliana Auxin-Binding Protein 1 (ABP1). *J. Plant Growth Regul.* **30**, 416–424 (2011).
6. Gelová, Z. *et al.* Developmental roles of Auxin Binding Protein 1 in Arabidopsis thaliana. *Plant Sci.* **303**, 110750 (2021).
7. Grones, P. *et al.* Auxin-binding pocket of ABP1 is crucial for its gain-of-function cellular and developmental roles. *J. Exp. Bot.* **66**, 5055–5065 (2015).
8. Robert, S. *et al.* ABP1 Mediates Auxin Inhibition of Clathrin-Dependent Endocytosis in Arabidopsis. *Cell* **143**, 111–121 (2010).
9. Li, L. *et al.* Cell surface and intracellular auxin signalling for H + fluxes in root growth. *Nature* **599**, 273–277 (2021).
10. Smakowska-Luzan, E. *et al.* An extracellular network of Arabidopsis leucine-rich repeat receptor kinases. *Nature* **553**, 342–346 (2018).
11. Özkan, E. *et al.* XAn extracellular interactome of immunoglobulin and LRR proteins reveals receptor-ligand networks. *Cell* **154**, 228 (2013).
12. Wasilko, D. J. *et al.* The titerless infected-cells preservation and scale-up (TIPS) method for large-scale production of NO-sensitive human soluble guanylate cyclase (sGC) from insect cells infected with recombinant baculovirus. *Protein Expr. Purif.* **65**, 122–132 (2009).

13. Tan, S. *et al.* Salicylic Acid Targets Protein Phosphatase 2A to Attenuate Growth in Plants. *Curr.Biol.* **30**, 381-395.e8 (2020).
14. Jerabek-Willemsen, M., Wienken, C. J., Braun, D., Baaske, P. & Duhr, S. Molecular interaction studies using microscale thermophoresis. *Assay and Drug Development Technologies* vol. 9 342–353 (2011).
15. Wiśniewski, J. R., Zougman, A., Nagaraj, N. & Mann, M. Universal sample preparation method for proteome analysis. *Nat. Methods* **6**, 359–362 (2009).
16. Tyanova, S. *et al.* The Perseus 445 computational platform for comprehensive analysis of (prote)omics data. *Nat. Methods* **13**, 731–740 (2016).
17. Vizcaíno, J. A. *et al.* 2016 update of the PRIDE database and its related tools. *Nucleic Acids Res.* **44**, D447–D456 (2016).
18. Okumura, M. & Kinoshita, T. Measurement of ATP Hydrolytic Activity of Plasma Membrane H+-ATPase from Arabidopsis thaliana Leaves. *BIO-PROTOCOL* **6**, (2016).
19. Živanovic, B., Köhler, K., Galland, P. & Weisenseel, M. MEMBRANE POTENTIAL AND ENDOGENOUS ION CURRENT OF PHYCOMYCES SPORANGIOPHORES. *http://dx.doi.org/10.1081/JBC-100108575* **20**, 343–362 (2009).
20. Mazur, E., Benková, E. & Friml, J. Vascular cambium regeneration and vessel formation in wounded inflorescence stems of Arabidopsis. *Sci. Rep.* **6**, 33754 (2016).
21. Mazur, E., Kulik, I., Hajný, J. & Friml, J. Auxin canalization and vascular tissue formation by TIR1/AFB-mediated auxin signaling in Arabidopsis. *New Phytol.* **226**, 1375–1383 (2020).
22. Young, G. *et al.* Quantitative mass imaging of single biological macromolecules. *Science* **360**, 423–427 (2018).
23. Kelly, S. M., Jess, T. J. & Price, N. C. How to study proteins by circular dichroism. *Biochim. Biophys. Acta - Proteins Proteomics* **1751**, 119–139 (2005).
24. Anthis, N. J. & Clore, G. M. Sequence-specific determination of protein and peptide concentrations by absorbance at 205 nm. *Protein Sci.* **22**, 851–858 (2013).

2.3.6 Acknowledgments

We would like to acknowledge Jana Neuhold, Anita Lehner and Arthur Sedivy for technical assistance at Vienna Biocenter Core Facilities (VBCF) for recombinant protein production and purification; Creoptix for performing the GCI; Bioimaging, Electron microscopy and Life Science Facilities at IST Austria as well as Plant Sciences Core Facility of CEITEC Masaryk University and Core Facility CELLIM (MEYS CR, LM2018129 Czech-BioImaging) and Joris Sprakel (Laboratory of Biochemistry, Wageningen University) for their invaluable assistance. We thank all past and present members of Friml group for their much valued moral support and other contributions over past six years to this collective endeavour to clarify the controversial role of ABP1.

This project received funding from the European Research Council (ERC) under the European Union's Horizon 2020 research and innovation program (grant agreement No 742985 to J.F. and 833867 to D.W.), the Austrian Science Fund (FWF): I 3630-B25 to J.F and the Netherlands Organization for Scientific Research (NWO, VICI grant 865.14.001 to D.W. and VENI grant VI.Veni.212.003 to A.K.), and the Ministry of Education, Science and Technological Development of the Republic of Serbia (Contract No. 451-03-68/2022-14/200053 to B.D.Ž.), the MEXT/JSPS KAKENHI to K.T. (20K06685) and T.K. (20H05687 and 20H05910).

2.3.7 Author contributions

J.F. conceived the experiments and wrote the paper. J.F., D.W. interpreted the results. Following persons conducted the experiments, analyzed the data and contributed to their design and interpretation: M.G., Z.G., A.J., E.M., A.M., M.P., M.R., I.V., L.F., P.G., J.H., W.A.K., N.R., S.T., H.R., B.D.Ž.

2.3.8 Competing interests

The authors declare that they have no competing interests.

2.3.9 Figures

Figure 1. Auxin binding to *Arabidopsis thaliana* ABP1 and its apoplastic localization

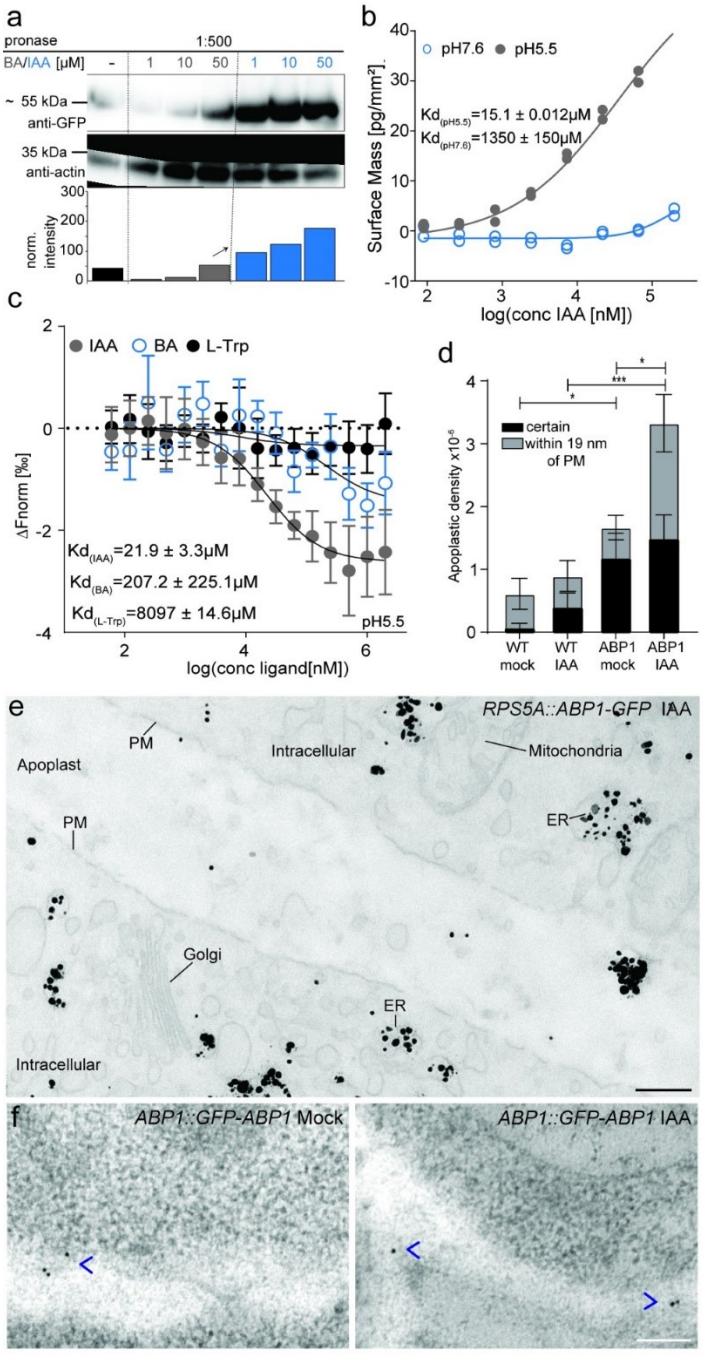

Figure 24 Section 2.3.9 - Auxin binding to Arabidopsis thaliana *ABP1 and its apoplastic localization*

a, DARTS assay on *35S::ABP1-GFP* plants. Protein extracts were incubated with same concentrations of IAA (in blue) or BA (in grey). Afterwards, different pronase quantities were added. As visualized in the blots and quantifications (normalized to the actin levels) less degradation was observed in the presence of IAA suggesting that ABP1 binds IAA as opposed to BA *in vivo*.
b, GCI-assisted analysis of binding properties of ABP1 to IAA using the Creoptix® WAVEsystem. Binding kinetics of immobilized ABP1 to different concentrations of IAA in running buffer revealed IAA binding to ABP1 at pH 5.5 as opposed to pH 7.6. Values of two independent experiments plotted.

c, MST analysis of ABP1 binding properties at pH 5.5. The inferred Kd values show strong binding of IAA compared to much weaker binding of both BA and L-Trp. Error bars represent the ± SD from 3 independent experiments.
d, Quantification of the apoplastic-localized GFP-ABP1 by TEM. anti-GFP gold particles densities in shoot apical meristem cells of WT (Extended Data Fig. 3d) and *ABP1::GFP-ABP1* (Fig. 1f) plants subjected to either mock or 1 µM IAA incubation for 3 hours. Gray bars denote gold particles detected within 19 nm (the size of the immuno-gold complex) of the PM, black bars are spots localised in the apoplast greater than 19 nm away from the PM. Plots are mean ± SEM. N; WT mock, 2 repetitions, 16 images; WT IAA, 3 repetitions, 16 images; ABP1 Mock, 4 repetitions, 16 images; ABP1 IAA, 2 repetitions, 18 images. t-tests, * $P \leq 0.05$, *** $P \leq 0.001$.
e, Example TEM image of a IAA-treated *RPS5A::ABP1-GFP* root cell labelled with anti-GFP immunogold particles (dark black spots) using a high-pressure freezing/freeze-substitution. PM, plasma membrane; Scale bar, 200 nm.
f, Example TEM images of *ABP1::GFP-ABP1* shoot apical meristem cells labelled with anti-GFP immunogold particles (arrows) subjected to either mock or 1 µM IAA incubation for 3 hours. Scale bar. 200 nm.

Figure 2. ABP1 and TMK1 in global auxin phospho-response and downstream cellular effects

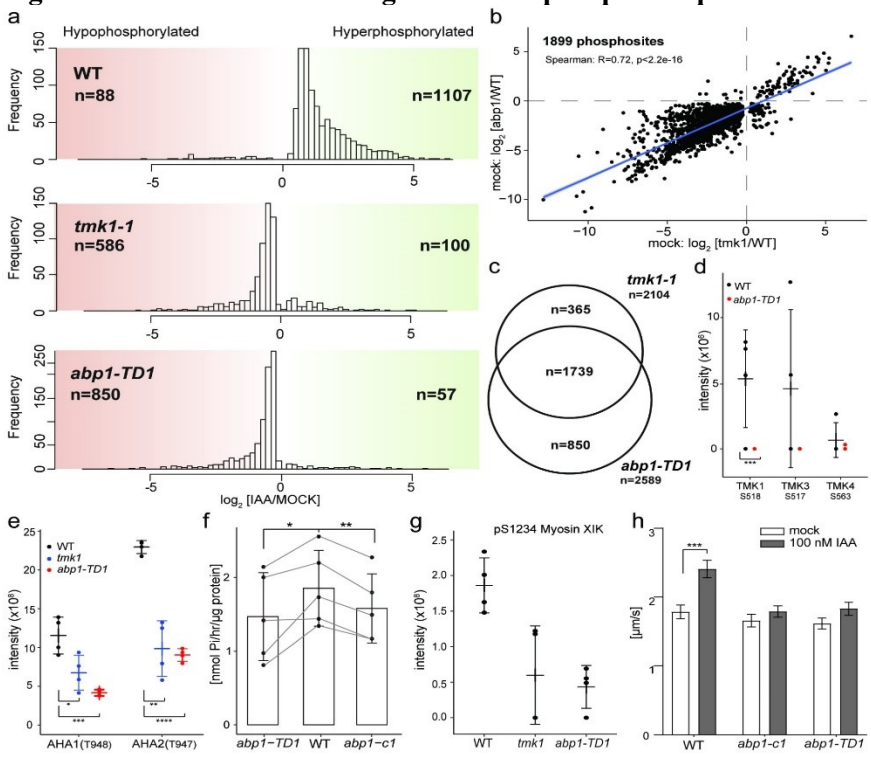

Figure 25 Section 2.3.9 - ABP1 and TMK1 in global auxin phospho-response and downstream cellular effects

a, Auxin (IAA, 100 nM; 2 min) treatment of *Arabidopsis* roots. Distributions of $\log_2$ fold changes for P-sites with significantly differential phosphorylation (FDR<0.05) after IAA treatment compared to mock in WT, *tmk1-1*, and *abp1-TD1*. The global auxin-triggered hyper-phosphorylation is absent in both mutants.
b, P-sites which are significantly regulated (FDR<0.05) in both mock-treated *tmk1-1*, and in *abp1-TD1* (compared to mock-treated WT), exhibit strong positive correlation in $\log_2$ fold change magnitudes of the respective mutants. Blue indicates a line of best fit with 95 % confidence interval as grey shading. Co-regulated sites are in bottom left and upper right quadrants. Oppositely regulated sites (5 % of total) are in bottom right and upper left quadrants – the majority of these are hypo-phosphorylated in *abp1-TD1* and hyper-phosphorylated in *tmk1-1*.

c, Considerable overlap between significantly downregulated (FDR<0.05) P-sites from mock-treated *tmk1-1*, and *abp1-TD1* (compared to mock-treated WT).
d, Relative MS intensities of TMK1^{S518}, TMK3^{S517} and TMK4^{S563} P -sites are lower in *abp1-TD1* mutants suggesting that TMK phosphorylation is dependent on ABP1. Mock treatment, 4 independent biological replicates, mean ± SD. Asterisks represent FDR contrasts.
e, Relative MS intensity for P-sites known to activate plasma membrane AHA H^+-ATPases. Auxin (IAA, 100 nM; 2 min) treatment, 4 independent biological replicates, mean ± SD. Asterisks represent FDR contrasts.
f, ATP hydrolysis activity in WT and *abp1* mutant roots after 100 nM IAA treatment. Grey lines connect paired data from five independent experiments. Asterisks represent two-sided paired t-tests.
g, Relative MS intensity for previously identified auxin-regulated Myosin XIK phospho-site. Auxin (IAA, 100 nM; 2 min) treatment, 4 independent biological replicates, mean ± SD.
h, Auxin-induced cytoplasmic streaming (IAA, 100 nM, 30 min) in *abp1* mutants. Fast moving particles were tracked in root elongation zone epidermal cells. N>50 for each treatment, Error bars represent mean ± SEM. Asterisks are from a two-way ANOVA with Tukey's multiple comparisons test. *P ≤ 0.05, **P ≤ 0.01, ***P ≤ 0.001, ****P ≤ 0.0001.

Figure 3. ABP1 and TMKs in vasculature regeneration following wounding

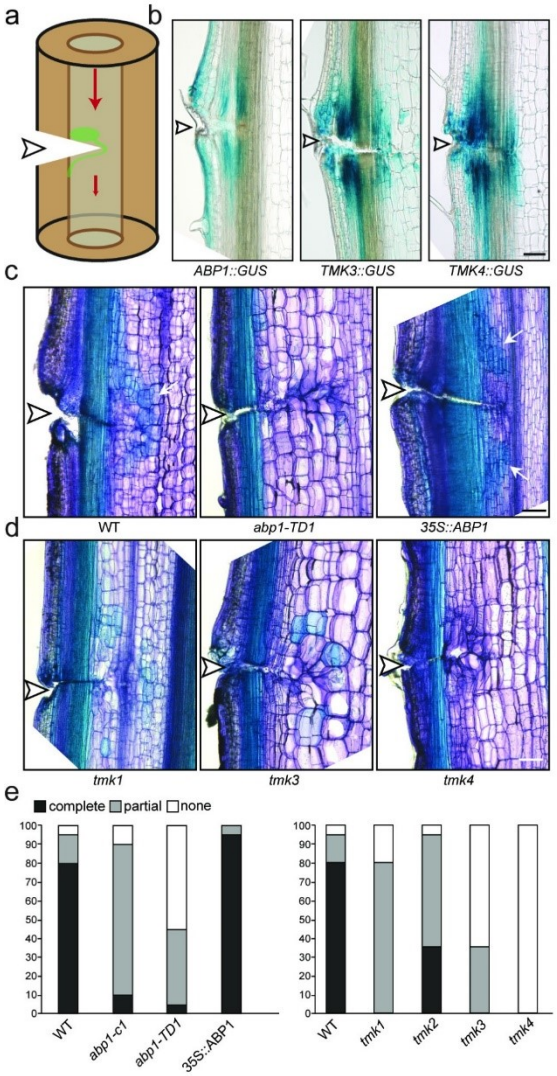

Figure 26 Section 2.3.9 - ABP1 and TMKs in vasculature regeneration following wounding

a, Schematics of vasculature regeneration in wounded *Arabidopsis* stems. The incision site is marked by an arrowhead. Red arrows indicate auxin flow. Green depicts auxin accumulation above the wound and regenerated vasculature circumventing it.
b, GUS staining revealed specific upregulation of *ABP1::GUS*, *TMK3::GUS* and *TMK4::GUS* expression around the wound 2 days after wounding (daw). Scale bar, 100 µm.
c, Vasculature regeneration 4 daw. All WT stems regenerated vascular tissue around the wound which is almost completed, as visualized by toluidine blue staining (TBO), while in the *abp1-TD1* mutant, this regeneration did not occur but in *35S::ABP1* more massive vasculature developed (indicated by white arrows).
d, *tmk* mutants show defective vasculature regeneration. *tmk1* regenerates only partially with fragmented vasculature; *tmk3* shows stronger defects and in *tmk4* the vasculature regeneration is blocked. Scale bar, 100 µm.
e, Quantification of vasculature regeneration in wounded *Arabidopsis* stems of WT and *abp1* and *tmk* mutants 6 daw. Total number of samples for each observation N > 40.

Figure 4. ABP1 and TMKs in auxin channel formation

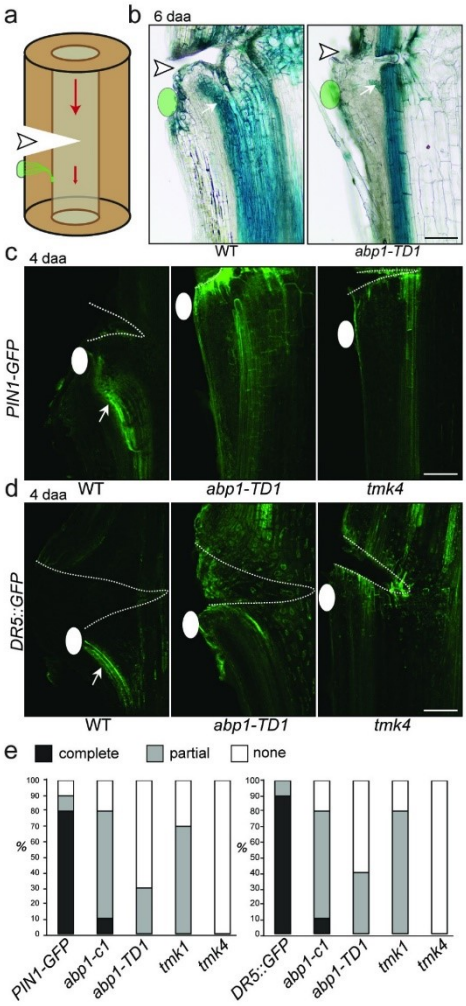

Figure 27 Section 2.3.9 - ABP1 and TMKs in auxin channel formation

a, Schematics of canalization and vasculature formation from local auxin application in wounded *Arabidopsis thaliana* stems. The incision site is marked by a white arrowhead. Red arrows indicate auxin flow. Green depicts local auxin application and *de novo* formed vasculature.

b, Exogenous IAA application (green oval shape) on stems triggered the formation of a channel (visualized by toluidine blue; indicated by white arrow) from this local source to the existing vascular tissue in WT but not *abp1-TD1* mutant 6 days after application (daa). Scale bar, 100 µm.
c, Exogenous IAA application (white oval) on *PIN1::PIN1-GFP* stems triggered the formation of a PIN1-expressing channel (indicated by the white arrow) from this source in WT but not in *abp1-TD1* or *tmk4* mutants. Scale bar; 100 µm.
d, Exogenous IAA application (white oval) on *DR5rev::GFP* stems triggered the formation of a DR5-visualized high auxin response channel (indicated by white arrow) from the source in WT but not in *abp1-TD1* or *tmk4* mutants. Scale bar, 100 µm.
e, Quantification of *de novo* vasculature formation from local auxin source in *PIN1::PIN1-GFP* and *DR5rev::GFP* lines. Total number of samples for each observation N > 30.

Figure 5. Importance of auxin binding to ABP1 for its role in canalization

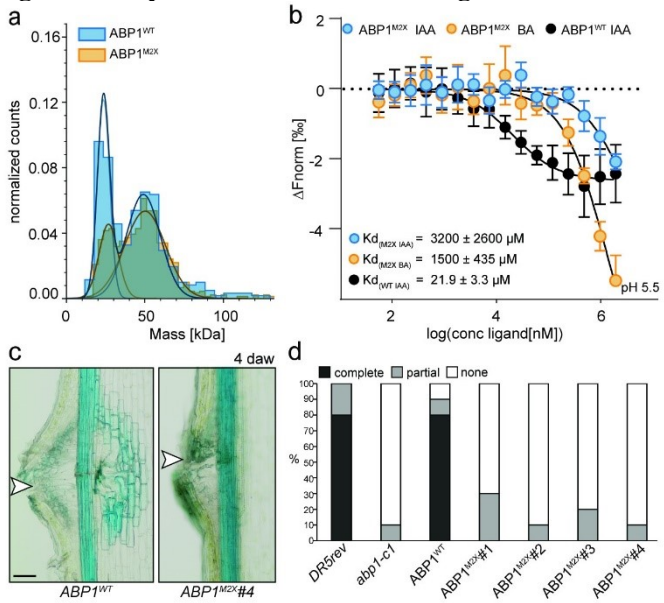

Figure 28 Section 2.3.9 - Importance of auxin binding to ABP1 for its role in canalization

a, Histograms and respective fitted Gaussians showed a similar behaviour for ABP1WT (blue profile) and ABP1M2X (orange profile) proteins. The two overlapping profiles indicate that both proteins are mainly found as homodimer (around 50 kDa), while approximately 30% are in solution as a monomer (around 25 kDa).
b, MST analysis of ABP1 binding properties at pH 5.5. The inferred Kd values show strong binding of IAA to ABP1WT compared to much weaker binding to ABP1M2X. Error bars represent the ± SD calculated from 2 independent experiments.
c, Examples of vasculature regeneration 4 days after wounding as visualized by the TBO staining. abp1-c1 mutant transformed with ABP1::GFP- ABP1WT, but not with ABP1::GFP- ABP1M2X, regenerated vascular tissue around the wound.
d, Quantification of vasculature regeneration from (c) shows inability of ABP1::GFP- ABP1M2X to rescue abp1-c1 regeneration in four characterized lines. Total number of samples for each observation N > 40.

2.3.10 Supplemental Figures

Extended Data Figure S1. No IAA binding to TMK1 and additional data on auxin binding to *Arabidopsis thaliana* ABP1

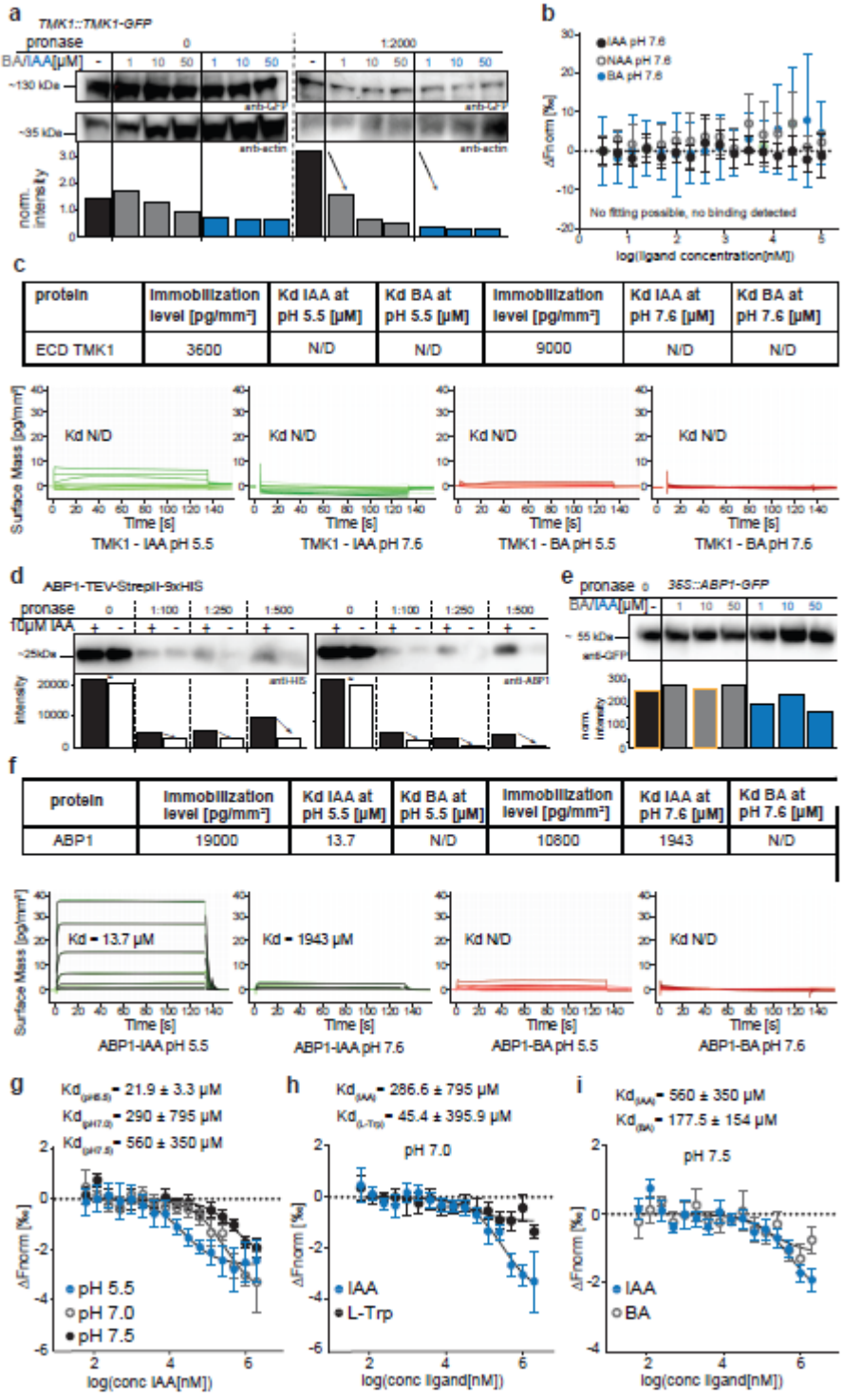

Figure 29 Section 2.3.10 - No IAA binding to TMK1 and additional data on auxin binding to Arabidopsis thaliana *ABP1*

a, DARTS assay on protein extracts from *TMK1::TMK1-GFP* expressing plants. Extracts were incubated with 1-10 or 50 µM benzoic acid (BA, in grey) or IAA (in blue) at the same concentration. Afterwards, different pronase quantities were mixed into the extracts. As visualized in the blots and

quantification (normalized to the actin levels) comparable pronase-induced degradation was observed in the presence of both IAA and BA compared, suggesting no specific IAA binding to TMK1 *in vivo*.
b, MST analysis of auxin binding to TMK1. Normalized binding curves of IAA, NAA and BA in presence of 150 nM TMK1 heterologously expressed and purified extracellular domain (ECD). Error bars represent the ± SD calculated from 4 independent experiments, but no fitting curves to determine binding kinetics were obtained.
c, GCI-assisted analysis of binding properties of TMK1 ECD to IAA or BA as a control ligand, using the Creoptix® WAVEsystem. Heterologously expressed and purified TMK1 ECD was immobilized to the surface at the indicated levels, following which the response to different concentrations of IAA/BA in running buffer at different pH (resp. 5.5 and 7.6) was monitored for analysis of binding kinetics. No binding of IAA to TMK1 ECD was detected.
d, DARTS assay on heterologously expressed and purified ABP1. Purified protein was mixed with different quantities of pronase enzyme mixture and proteolysis was stopped after 30 minutes. The resulting degraded protein samples were run on SDS-PAGE and blotted for antibody-aided visualization. Pronase-induced proteolysis of tagged ABP1 occurred less in the presence of 10 µM IAA, which was consistent for multiple pronase dilutions, indicating IAA association with ABP1. This was verified both by the anti-HIS-HRP and anti-ABP1 antibody to ensure specificity of the visualized band. The intensity profiles are plotted in the graph below the blots.
e, Control samples for DARTS results represented in Figure 1a. Protein extracts from *35S::ABP1-GFP* expressing plants were incubated with 1-10 or 50 µM benzoic acid (BA, in grey) or indole-3-acetic acid (IAA, in blue) at the same concentration. Blots intensities were quantified and normalized to actin levels). Since these samples were aliquoted from the same extract, no differences in actin levels were expected. However, for the yellow marked bands, we observed decreased amount of actin. In order not artificially affect their representation, they were normalized to the average actin intensity for the no pronase samples. In these no pronase control samples, we visualize that the presence of the respective small molecule at their concentration did not affect target protein stability as such.
f, Overview table and graphs of all ABP1 GCI-binding analysis. The potential ligands IAA and BA were evaluated in serial dilution ranging from 91.449 nM to 200 µM. IAA binding kinetics could be observed, resulting in a Kd estimate of 13.7 µM at pH 5.5 and 1943 µM at pH 7.6.
g, MST analysis of IAA binding to ABP1 at different pH. Normalized binding curve of IAA in presence of 75 nM ABP1 at pH 5.5 (blue), 100 nM ABP1 at pH 7.0 (grey) or 100 nM ABP1 pH 7.5 (black). The IAA concentration varied from 61 nM to 2 mM. Error bars represent the ± SD calculated in 3 and 2 independent experiments respectively. The estimated Kd values demonstrate more efficient (10x) IAA-binding at the apoplastic pH of 5.5 in comparison to binding at the other pHs evaluated.
h, MST analysis of ligand binding to ABP1 at pH 7.0. Normalized binding curve of IAA (blue) and L-Trp (black) to 100 nM ABP1 at pH 7.0. The ligand concentration varied from 61 nM to 2 mM. Error bars represent the ± SD calculated in 3 independent experiments. The estimated Kd values with big SD indicate no binding of these ligands at this pH.
i, MST analysis at pH 7.5. Normalized binding curve of IAA (blue, same as black in Extended Data Fig. 1g) and control ligand BA (grey) to 75 nM ABP1. The ligand concentration varied from 61 nM to 2 mM. Error bars represent the ± SD calculated in 3 independent experiments. The estimated Kd values are much higher than those obtained for pH 5.5 and indicate no binding of these ligands at this pH.

Extended Data Figure S2. TEM analysis of apoplastic ABP1 localization

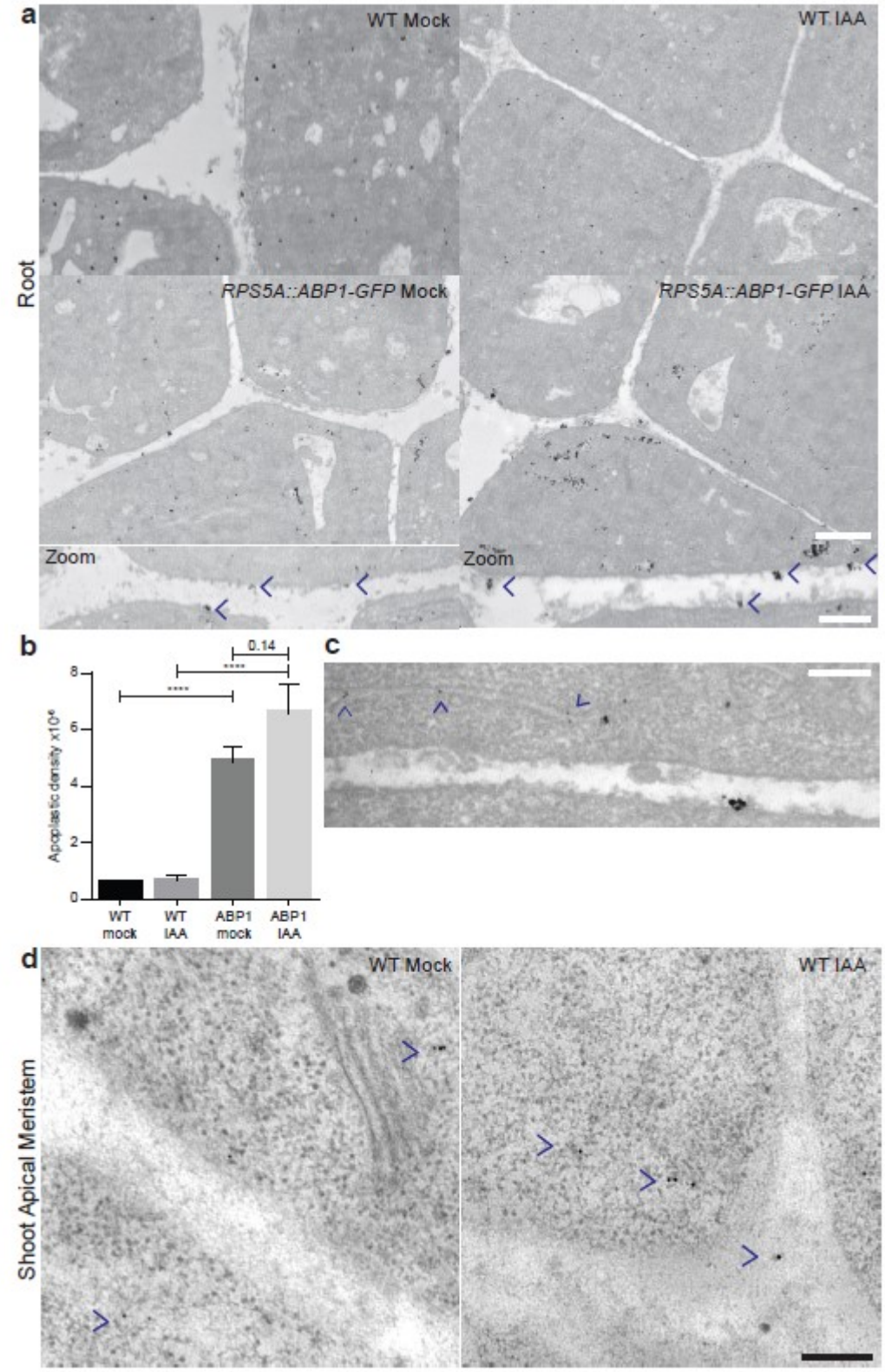

Figure 30 Section 2.3.10 - TEM analysis of apoplastic ABP1 localization

a, Example TEM images of *RPS5A::ABP1-GFP* root cells after mock and IAA (1 μM) incubation for 3 hours. Lower 'Zoom' panels are higher magnification images of apoplastic areas from *RPS5A::ABP1-GFP* cells incubated with IAA. Arrows note gold particles. Scale bars; upper, 1 μm; lower, 500 nm.
b, Quantification of the densities of apoplastic localized anti-GFP gold particles in root cells of WT and *RPS5A::ABP1-GFP* plants subjected to either mock or 1 μM IAA incubation for 3 hours, as detected by TEM. Plots are mean ± SEM. N; 3 experimental repeats; WT Mock, 37 images; WT IAA, 43 images; ABP1 mock, 45 images; ABP1 IAA 47 images. Comparisons were made via t-tests, **** $P \leq 0.0001$, or p value is reported.
c, Example TEM image of an *RPS5A::ABP1-GFP* root cell showing anti-GFP gold labeling of the ER (arrows). Scale bar, 200 nm.
d, Example TEM images of wild type shoot apical meristem cells labelled with anti-GFP immunogold particles (magenta arrows) subjected to either mock or 1 μM IAA incubation for 3 hours. Scale bar. 200 nm.

Extended Data Figure S3. Global, ultrafast auxin phospho-response and rapid cellular effects

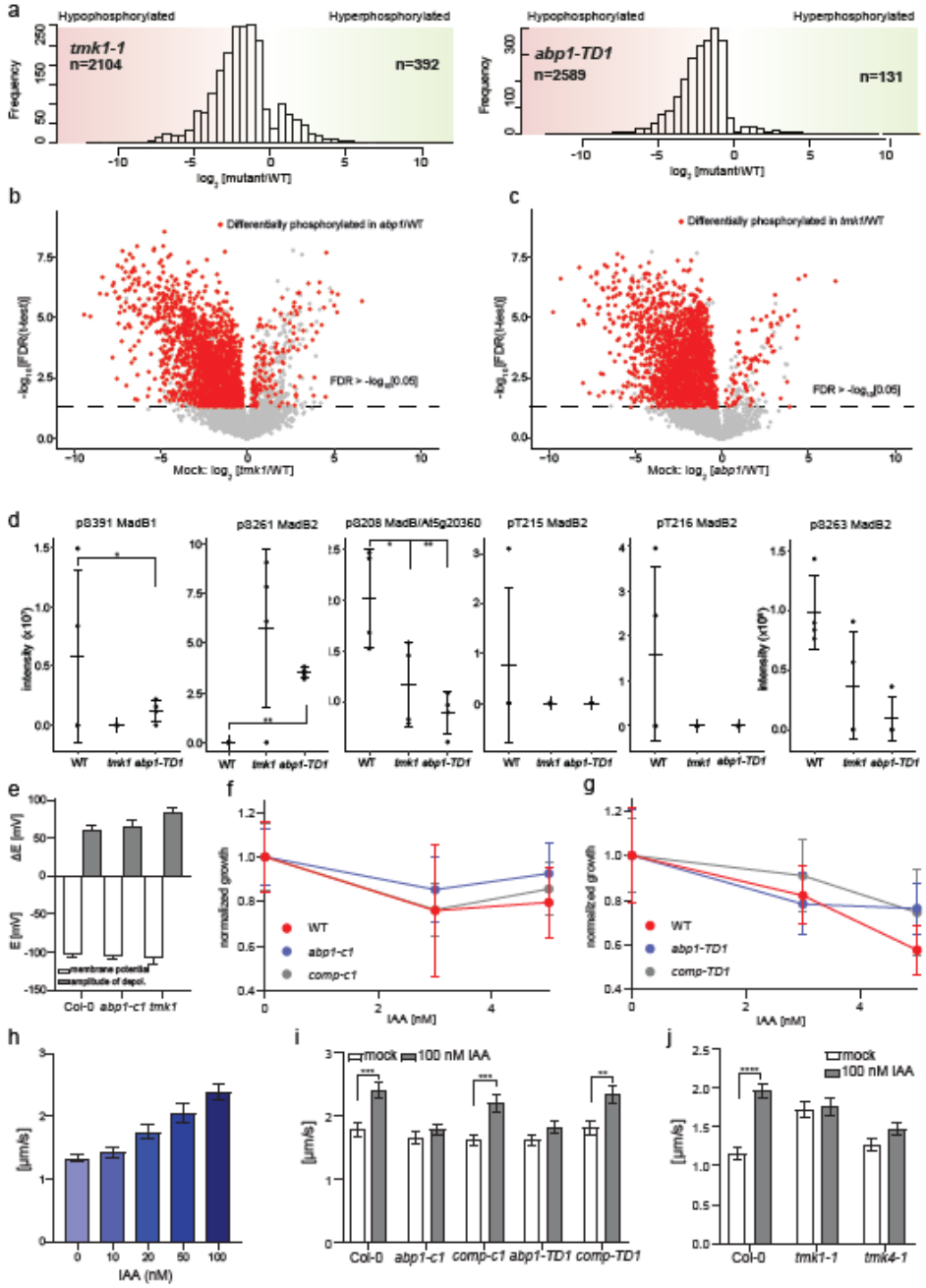

Figure 31 Section 2.3.10 - Global, ultrafast auxin phospho-response and rapid cellular effects

a, Mock treatment (2 min) of *Arabidopsis* roots. Distributions of $\log_2$ fold changes for phospho-peptides with significantly differential phosphorylation (FDR<0.05) in *tmk1-1* and *abp1-TD1* as compared to WT. Both mutants exhibit global hypo-phosphorylation.
b, Mock treatment (2 min) of *Arabidopsis* roots. Volcano plot depicts $\log_2$ fold changes (x-axis; *tmk1-1* versus WT) and statistical significance (y-axis). Highlighted in red is the subset of significantly regulated phospho-peptides (FDR<0.05), which are also significantly regulated in *apb1-TD1*/WT. This shows global hypo-phosphorylation in *tmk1-1* and extensive functional overlap between the two mutants.
c, Mock treatment (2 min) of *Arabidopsis* roots. Volcano plot depicts $\log_2$ fold changes (x-axis; *abp1-TD1* versus WT) and statistical significance (y-axis). Highlighted in red is the subset of significantly regulated phospho-peptides (FDR<0.05) which are also significantly regulated in *tmk1-1*/WT. This

shows global hypo-phosphorylation in *abp1-TD1* and extensive functional overlap between the two mutants.
d, Relative MS intensity for phospho-peptides pertaining to various *Arabidopsis* MadB paralogs (MadB1, MadB/At5g20360, MadB2/PHOX2). Auxin (IAA, 100 nM, 2 min) treatment, 4 independent biological replicates, mean ± SD. Asterisks represent FDR contrasts.
e, Steady-state membrane potentials and IAA-induced depolarization of MP (in mV) measured in the mature root zone of 4-5-day-old seedlings of WT, *abp1-c1* and *tmk1-1* mutants. Values are means ± SE (n = 3-11 seedlings).
f, Auxin sensitivity of *abp1-c1* root growth. Data on the graph represent the normalized growth rate of *abp1-c1* mutant in comparison to *comp-c1* line and WT, mean ± SD (n = 8-12 seedlings) for each genotype. No statistically significant difference in sensitivity of growth rate to auxin was detected with one-way ANOVA.
g, Auxin sensitivity of *abp1-TD1* root growth. Data on the graph represent the normalized growth rate of *abp1-TD1* mutant in comparison to *comp-TD1* line and Col-4, mean ± SD (n = 8-12 seedlings) for each genotype. No statistically significant difference in sensitivity of growth rate to auxin was detected with one-way ANOVA.
h, Cytoplasmic streaming velocity increases with concentration of IAA treatment. Col-0 seedlings were treated with 0, 10, 20, 50 and 100 nM IAA for 30 min. Fast-moving particles in epidermal cells of the root elongation zone were recorded. N>50 for each treatment. Error bars represent mean ± SEM. Asterisks are from a two-way ANOVA with Tukey's multiple comparisons test. *P ≤ 0.05, **P ≤ 0.01, ***P ≤ 0.001, ****P ≤ 0.0001.
i, Auxin-mediated induction of cytoplasmic streaming is lacking in *abp1* mutants but becomes restored in complemented *abp1* lines. Error bars represent mean ± SEM. N>50 for each genotype. Asterisks are from a two-way ANOVA with Tukey's multiple comparisons test. *P ≤ 0.05, **P ≤ 0.01, ***P ≤ 0.001, ****P ≤ 0.0001.
j. Auxin-mediated induction of cytoplasmic streaming is lacking in *tmk* mutants. Unlike *tmk4*, *tmk1* appears to have already accelerated cytoplasmic streaming but both mutants are largely auxin insensitive. Error bars represent mean ± SEM. N>50 for each genotype. Asterisks are from a two-way ANOVA with Tukey's multiple comparisons test. *P ≤ 0.05, **P ≤ 0.01, ***P ≤ 0.001, ****P ≤ 0.0001.

Extended Data Figure S4. ABP1 and TMKs in vasculature formation and regeneration

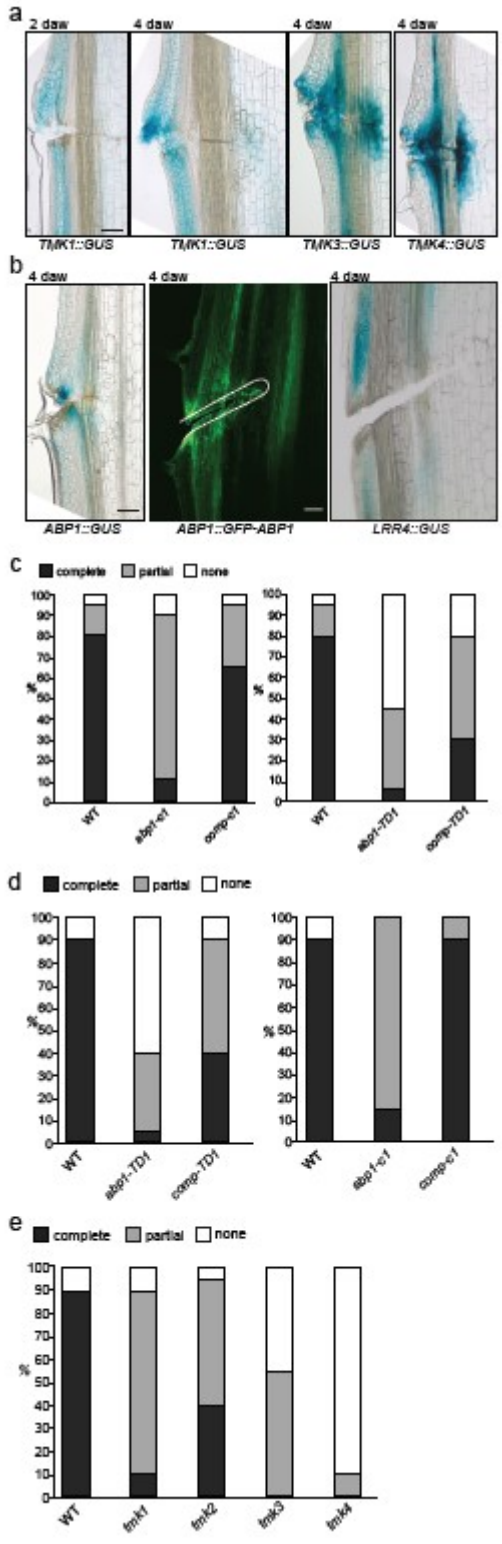

Figure 32 Section 2.3.10 - ABP1 and TMKs in vasculature formation and regeneration

a, GUS staining revealed specific upregulation of *TMK1::GUS*, *TMK3::GUS* and *TMK4::GUS* expression around the wound 2 or 4 days after wounding (daw). Scale bar, 100 µm.
b, GUS staining revealed specific upregulation of *ABP1::GUS* but not *LRR4::GUS* expression around the wound. *ABP1::GFP-ABP1* confirmed the GUS staining. Scale bar, 100 µm.

c, Quantification of vasculature regeneration in wounded *Arabidopsis* stems in *abp1-c1* and *abp1-TD1* mutants as well as corresponding complemented lines (*comp-c1* and *comp-TD1*) confirms that the vasculature regeneration defects are due to disruption of the *ABP1* locus. Total number of samples for each observation, N = 20.
d, Quantification of *de novo* vasculature formation from local auxin source (as visualized by TBO) in *abp1-c1* and *abp1-TD1* mutants as well as corresponding complemented lines confirms that the vasculature regeneration defects are due to the *ABP1* locus disruption. Total number of samples for each observation, N = 20.
e, Quantification of *de novo* vasculature formation from local auxin source (as visualized by TBO) in *tmk* mutants. *tmk4* shows stronger defects followed by *tmk3* and *tmk1* whereas *tmk2* has almost normal vasculature formation. Total number of samples for each observation N = 20.

Extended Data Figure S5. ABP1 and ABP1^{M2X} protein characterization, IAA binding analysis and role in regeneration and auxin canalization

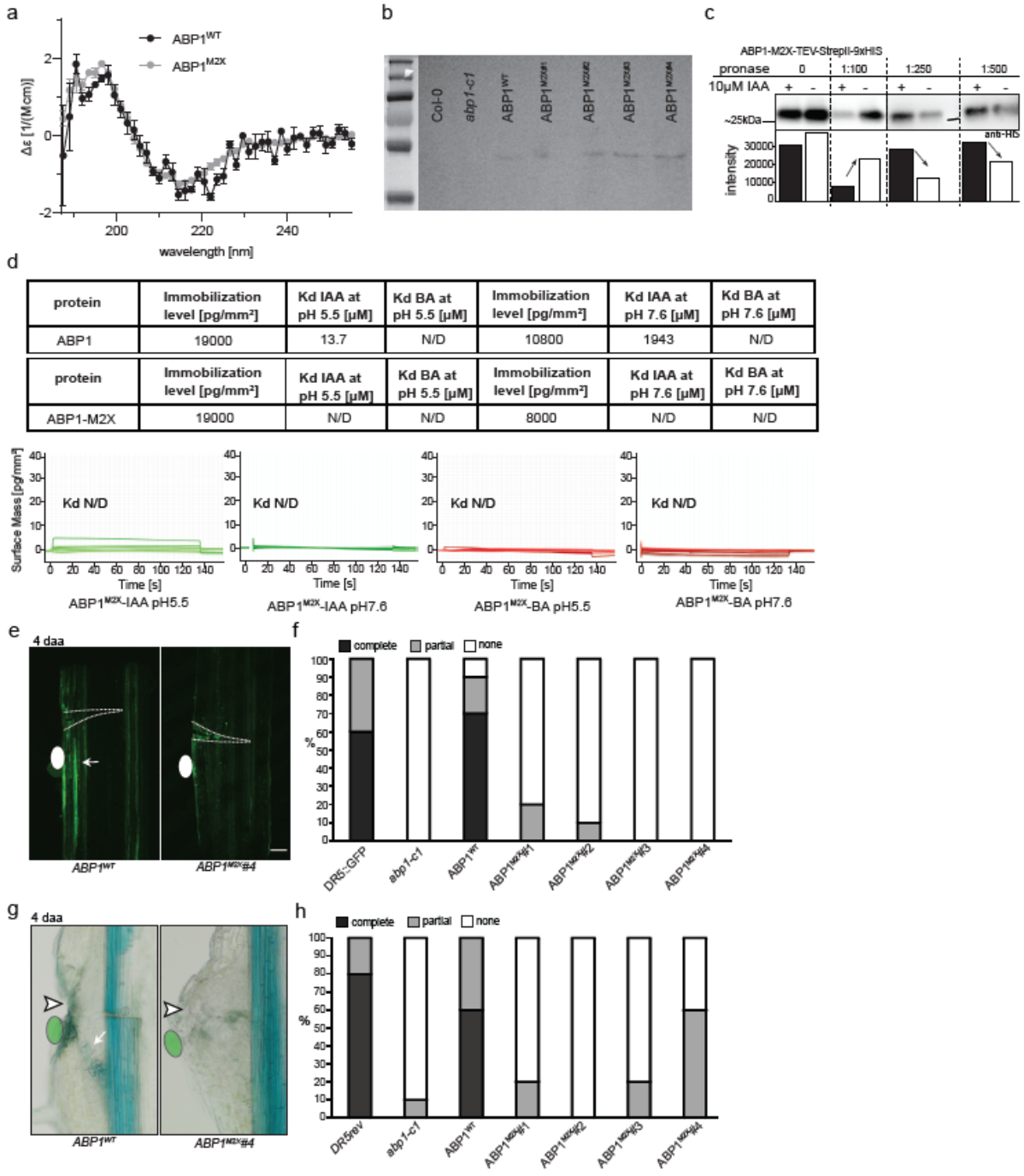

protein	Immobilization level [pg/mm²]	Kd IAA at pH 5.5 [μM]	Kd BA at pH 5.5 [μM]	Immobilization level [pg/mm²]	Kd IAA at pH 7.6 [μM]	Kd BA at pH 7.6 [μM]
ABP1	19000	13.7	N/D	10800	1943	N/D

protein	Immobilization level [pg/mm²]	Kd IAA at pH 5.5 [μM]	Kd BA at pH 5.5 [μM]	Immobilization level [pg/mm²]	Kd IAA at pH 7.6 [μM]	Kd BA at pH 7.6 [μM]
ABP1-M2X	19000	N/D	N/D	8000	N/D	N/D

Figure 33 Section 2.3.10 - ABP1 and ABP1^{M2X} protein characterization, IAA binding analysis and role in regeneration and auxin canalization

a, Nearly identical Circular Dichroism (CD) spectra of ABP1^{WT} and ABP1^{M2X} proteins. This and temperatures of transition midpoints as derived from Prometheus thermal stability measurements ((ABP1^{WT} , 58.3 ºC; ABP1^{M2X} , 61.4 ºC) suggest similar folding of both protein variants.
b, Western blot detection of ABP1^{WT} and ABP1^{M2X} proteins in different transgenic lines showing similar size and expression levels.
c, DARTS assay on heterologously expressed and purified ABP1^{M2X}. Purified protein was mixed with different quantities of pronase enzyme mixture and proteolysis was stopped after 30 minutes. The resulting degraded protein samples were run on SDS-PAGE and blotted for antibody-aided

visualization. Pronase-induced proteolysis of tagged ABP1^{M2X} was very variable in the presence of 10 µM IAA not supporting any binding of IAA to ABP1^{M2X}. The intensity profiles are plotted in the graph below the blots.
d, Overview table and graphs of all ABP1^{M2X} GCI-binding analysis. The potential ligands IAA and BA were evaluated in serial dilution ranging from 91.449 nM to 200 µM. Albeit ABP1 and ABP1^{M2X} could be immobilized at the surface to the same level (compared to Extended Data Figure 1f), only for ABP1^{WT}, IAA binding kinetics could be observed while for the analyses using ABP1^{M2X} no Kd could be estimated.
e, Exogenous IAA application (white oval) on *DR5rev::GFP* stems triggered the formation of a DR5-visualized auxin channels (indicated by white arrow) from the source in *abp1-c1* transformed with *ABP1::GFP- ABP1^{WT}* but not in any of the *ABP1::GFP- ABP1^{M2X}* lines. Scale bar, 100 µm.
f, Quantification of *de novo* vasculature formation from local auxin source in *DR5rev::GFP* lines as in (e). Total number of samples for each observation N > 30.
g, Exogenous IAA application (green oval shape) on stems triggered the formation of a channel (visualized by TBO; indicated by white arrow) from this local source 6 days after application (daa) in *abp1-c1* transformed with *ABP1::GFP- ABP1^{WT}* but not in any of the *ABP1::GFP- ABP1^{M2X}* lines. Scale bar, 100 µm.
h, Quantification of *de novo* vasculature formation from (g). Total number of samples for each observation N > 30.

2.3.11 References

1. Friml, J. Fourteen Stations of Auxin. *Cold Spring Harb. Perspect. Biol.* a039859 (2021) doi:10.1101/cshperspect.a039859.
2. Lavy, M. & Estelle, M. Mechanisms of auxin signaling. *Development* **143**, 3226–3229 (2016).
3. Morffy, N. & Strader, L. C. Structural Aspects of Auxin Signaling. *Cold Spring Harb. Perspect. Biol.* a039883 (2021) doi:10.1101/cshperspect.a039883.
4. Fendrych, M. *et al.* Rapid and reversible root growth inhibition by TIR1 auxin signalling. *Nat. Plants* **4**, 453–459 (2018).
5. Dindas, J. *et al.* AUX1-mediated root hair auxin influx governs SCFTIR1/AFB-type Ca2+ signaling. *Nat. Commun.* **9**, (2018).
6. Gallei, M., Luschnig, C. & Friml, J. Auxin signalling in growth: Schrödinger's cat out of the bag. *Curr. Opin. Plant Biol.* **53**, 43–49 (2020).
7. Li, L., Gallei, M. & Friml, J. Bending to auxin: fast acid growth for tropisms. *Trends Plant Sci.* (2021) doi:10.1016/J.TPLANTS.2021.11.006.
8. Kuhn, A. *et al.* Direct ETTIN-auxin interaction controls chromatin states in gynoecium development. *Elife* **9**, (2020).
9. Cao, M. *et al.* TMK1-mediated auxin signalling regulates differential growth of the apical hook. *Nature* **568**, 240–243 (2019).
10. Dubey, S. M., Serre, N. B. C., Oulehlová, D., Vittal, P. & Fendrych, M. No Time for Transcription-Rapid Auxin Responses in Plants. *Cold Spring Harb. Perspect. Biol.* (2021) doi:10.1101/cshperspect.a039891.
11. Adamowski, M. & Friml, J. PIN-dependent auxin transport: Action, regulation, and evolution. *Plant Cell* **27**, 20–32 (2015).
12. Narasimhan, M. *et al.* Systematic analysis of specific and nonspecific auxin effects on endocytosis and trafficking. *Plant Physiol.* (2021) doi:10.1093/plphys/kiab134.
13. Robert, S. *et al.* ABP1 Mediates Auxin Inhibition of Clathrin-Dependent Endocytosis in Arabidopsis. *Cell* **143**, 111–121 (2010).
14. Sachs, T. The induction of transport channels by auxin. *Planta* **127**, 201–206 (1975).
15. Han, H. *et al.* Rapid auxin-mediated phosphorylation of Myosin regulates trafficking and polarity in Arabidopsis. *bioRxiv* 439603 (2021) doi:10.1101/2021.04.13.439603.
16. Li, L. *et al.* Cell surface and intracellular auxin signalling for H + fluxes in root growth. *Nature* **599**, 273–277 (2021).

17. *acidification in Arabidopsis*. http://10.0.82.211/rs.3.rs-203621/v1 (2021) doi:10.21203/rs.3.rs-203621/v1.
18. McLaughlin, H. M., Ang, A. C. H. & Østergaard, L. Noncanonical Auxin Signaling. *Cold Spring Harb. Perspect. Biol.* **13**, (2021).
19. Hertel, R., Thomson, K. S. & Russo, V. E. In-vitro auxin binding to particulate cell fractions from corn coleoptiles. *Planta* **107**, 325–340 (1972).
20. Xu, T. *et al.* Cell Surface ABP1-TMK Auxin-Sensing Complex Activates ROP GTPase Signaling. *Science (80-.).* **343**, 1025–1028 (2014).
21. Gao, Y. *et al.* Auxin binding protein 1 (ABP1) is not required for either auxin signaling or Arabidopsis development. *Proc. Natl. Acad. Sci.* **112**, 2275–2280 (2015).
22. Grones, P. *et al.* Auxin-binding pocket of ABP1 is crucial for its gain-of-function cellular and developmental roles. *J. Exp. Bot.* **66**, 5055–5065 (2015).
23. Michalko, J., Dravecká, M., Bollenbach, T. & Friml, J. Embryo-lethal phenotypes in early abp1 mutants are due to disruption of the neighboring BSM gene. *F1000Research* **4**, 1104 (2015).
24. Napier, R. The Story of Auxin-Binding Protein 1 (ABP1). *Cold Spring Harb. Perspect. Biol.* a039909 (2021) doi:10.1101/cshperspect.a039909.
25. Smakowska-Luzan, E. *et al.* An extracellular network of Arabidopsis leucine-rich repeat receptor kinases. *Nature* **553**, 342–346 (2018).
26. Woo, E. J. *et al.* Crystal structure of auxin-binding protein 1 in complex with auxin. *EMBO J.* **21**, 2877–2885 (2002).
27. Tian, H., Klambt, D. & Jones, A. M. Auxin-binding protein 1 does not bind auxin within the endoplasmic reticulum despite this being the predominant subcellular location for this hormone receptor. *J. Biol. Chem.* **270**, 26962–26969 (1995).
28. Gelová, Z. *et al.* Developmental roles of Auxin Binding Protein 1 in Arabidopsis thaliana. *Plant Sci.* **303**, 110750 (2021).
29. Dahlke, R. I. *et al.* Protoplast Swelling and Hypocotyl Growth Depend on Different Auxin Signaling Pathways. *Plant Physiol.* **175**, 982–994 (2017).
30. Jayakannan, M., Bose, J., Babourina, O., Rengel, Z. & Shabala, S. Salicylic acid improves salinity tolerance in Arabidopsis by restoring membrane potential and preventing salt-induced K+ loss via a GORK channel. *J. Exp. Bot.* **64**, 2255–2268 (2013).
31. Paponov, I. A. *et al.* Auxin-Induced Plasma Membrane Depolarization Is Regulated by Auxin Transport and Not by AUXIN BINDING PROTEIN1. *Front. Plant Sci.* **9**, (2019).
32. Serre, N. B. C. *et al.* AFB1 controls rapid auxin signalling through membrane depolarization in Arabidopsis thaliana root. *Nat. Plants* (2021) doi:10.1038/s41477-021-00969-z.
33. Tominaga, M. & Ito, K. The molecular mechanism and physiological role of cytoplasmic streaming. *Curr. Opin. Plant Biol.* **27**, 104–110 (2015).
34. Sauer, M. *et al.* Canalization of auxin flow by Aux/IAA-ARF-dependent feedback regulation of PIN polarity. *Genes Dev.* **20**, 2902–2911 (2006).
35. Mazur, E., Benková, E. & Friml, J. Vascular cambium regeneration and vessel formation in wounded inflorescence stems of Arabidopsis. *Sci. Rep.* **6**, 33754 (2016).
36. Mazur, E. *et al.* Clathrin-mediated trafficking and PIN trafficking are required for auxin canalization and vascular tissue formation in Arabidopsis. *Plant Sci.* **293**, 110414 (2020).
37. Mazur, E., Kulik, I., Hajný, J. & Friml, J. Auxin canalization and vascular tissue formation by TIR1/AFB-mediated auxin signaling in Arabidopsis. *New Phytol.* **226**, 1375–1383 (2020).
38. Young, G. *et al.* Quantitative mass imaging of single biological macromolecules. *Science* **360**, 423–427 (2018).
39. Dai, N., Wang, W., Patterson, S. E. & Bleecker, A. B. The TMK Subfamily of Receptor-Like Kinases in Arabidopsis Display an Essential Role in Growth and a Reduced Sensitivity to Auxin. *PLoS One* **8**, (2013).
40. Hajný, J., Tan, S. & Friml, J. Auxin canalization: From speculative models toward molecular players. *Curr. Opin. Plant Biol.* **65**, (2022).
41. Wabnik, K. *et al.* Emergence of tissue polarization from synergy of intracellular and extracellular auxin signaling. *Mol. Syst. Biol.* **6**, (2010).
42. Hajný, J. *et al.* Receptor kinase module targets PIN-dependent auxin transport during canalization. *Science* **370**, 550–557 (2020).

43. Lin, W. *et al. TMK-based cell surface auxin signaling activates cell wall*

2.4 Auxin and strigolactone crosstalk

The studies from the previous chapters aimed to broaden our understanding of auxin canalization with the involvement of the different branches of auxin signaling, together with processes necessary for canalization like endocytosis and as well as components involved like ABP1 and TMK1. Based on the observations that various other plant hormones can influence PIN-dependent auxin transport (eg Marhavy 2014, Retzer 2019 and Du 2013) and hence canalization the next studies will focus on the cross-talk between auxin and strigolactones (SLs). We decided to focus on SL as this hormone was shown to be in cross-talk with auxin in processes linked to auxin canalization before (Crawford 2010, Sinohara 2013).

Strigolactones are carotenoid-derived molecules found for the first time around 50 years ago as germination stimulants for the parasitic weed *Striga lutea* (Cook et al. 1966). Further they are involved in promotion of hyphal branching of arbuscular mycorrhizal fungi (Akiyama, Matsuzaki, and Hayashi 2005) and the repression of shoot branching (Gomez-Roldan et al. 2008). More recently it was shown that SLs influence an even more versatile range of plant traits ranging from shoot gravitropism (Sang et al. 2014), secondary growth (Agusti et al. 2011), adventitious root formation (Rasmussen et al. 2012), lateral rooting to root hair elongation (Koltai 2015). Additionally strigolactones can induce changes in transcription by a short nuclear signaling pathway which is usually referred to as canonical strigolactone signaling or MAX2-dependent signaling and most responses were until now assigned to depend on transcription (Marzec 2016).

2.5 Strigolactones inhibit auxin feedback on PIN-dependent auxin transport canalization

Adapted and modified from:

Zhang J, Mazur E, Balla J, **Gallei M**, et al. *Strigolactones inhibit auxin feedback on PIN-dependent auxin transport canalization*. Nat Commun. 2020;11(1). doi:10.1038/s41467-020-17252-y

Many of the mentioned responses mediated by SLs require functional auxin transport and hence its canalization, a process especially important in shoot branching (Sinohara 2013). In this

response SL is interfering with the PM localization of PIN1 specifically which leads to changes in auxin flux and in further consequence to regulation of shoot branching (Crawford 2010, Sinohara 2013). However the mechanisms by which SLs might impact on the localization of PINs still remains enigmatic.

In the following study we show that SL is very strongly interfering with auxin canalization in pea and Arabidopsis stems using again the well-established experimental models of vascular tissue regeneration after wounding and *de novo* vasculature formation from an exogenous auxin source. We also found the formation of leaf venation to be interrupted by SL treatment. At the cellular level, we show that SLs can interfere with auxin effect on PIN polar localization and BFA body formation. Those ways of SL regulation of auxin canalization-mediated processes have been shown to be MAX2-depedent but non-transcriptional. This provides a comprehensive and mechanistic picture of SL action in many auxin canalization but also opens up new questions about non-transcriptional SL signaling.

Contribution Michelle Gallei:

- immunolocalization for PIN polar localization after pharmacological treatments and data analysis (Figure S4F)
- leaf venation analysis after SL treatment (Figure S3C,D)
- BFA body formation for PINs after pharmacological treatments and data analysis (Figure 3H, Figure S4K, Figure S5A,B,G, Figure S6D)
- Correction of the manuscript

2.5.1 Introduction

Plant development is characterized by self-organized processes, such as the regular patterns of organ initiation at the shoot apical meristem, branching of roots and shoots, as well as the connection of newly formed organs with pre-existing vasculature or the spontaneous occurrence of vasculature veins in developing leaves. The plant hormone auxin and its directional transport through tissues has been implicated in all of these traits[1]. The process of so-called auxin canalization establishes narrow auxin transport routes between cells and tissues of relatively high auxin concentration (source), to locations where auxin is being depleted (sink) [2-4]. A self-reinforcing system has been proposed to drive canalization. In this system, auxin feeds back on PIN-FORMED (PIN) auxin transporters by promoting the expression of *PIN* genes in channels and localizing PINs to the side of the cell towards

the sink[3,5]. These polarly localized PIN protein transport auxin out of cells towards the sink, leading to intensified polar localization of PINs in downstream cells and gradually focused auxin movement. Canalization is particularly prominent where auxin channels promote the formation of new vasculature connections along channel routes[2,6]. For example, vein patterns in leaves result from the interplay of auxin source-sink relationships. New vein connections occur as auxin builds up at locations, triggering PINs to shift auxin flow towards established auxin channels[6]. Auxin feed-back on PIN polarization also accompanies developmental processes that are not directly linked with vasculature formation along auxin channels, such as the embryonic apical-basal axis establishment[7,8], shoot and root organogenesis[9-11], and even the termination of shoot gravitropic bending[12].

Although much is now known about PIN proteins; their action in auxin export, the developmental roles and their regulations[1]; the mechanism by which auxin controls PINs, and in particular their polarization, is conceptually unclear. The modelling of auxin-mediated polarization[13] has linked auxin feed-back on PIN polarity with the effect of auxin on PIN subcellular trafficking[14-16]. In cells, membrane-bound PINs are internalized in clathrin-coated vesicles in a process called endocytosis[17,18], and may be relocated by vesicle movement to other membranes[19,20]. Various compounds and genetic factors act on specific cellular events in auxin transport and have been crucial to building the picture of cellular mechanisms that are involved[1]. For example, the use of brefedin A (BFA) revealed the constitutive endocytic recycling of PIN proteins. BFA represses GNOM ARFGEF, auxin-specific vesicle movement between the interior of the cell and the plasma membrane, causing plasma membrane proteins to aggregate in cells[17]. Auxin itself appears to act specifically by inhibiting the opposite process of endocytosis (internalization) and can counteract the effect of BFA[14]. In addition to the effect that auxin has on PINs, various other plant hormones can influence PINdependent auxin transport such as cytokinins[21], gibberellins[22-24], salicylic acid[25] and strigolactones (SLs)[26]. Much is still to be uncovered about exactly how other plant hormones regulate PINs and consequently how their interaction with the auxin distribution machinery regulates plant development. SLs are a recently discovered class of plant growth regulators and their developmental roles and signaling mechanisms are not yet fully characterized. They have been shown to influence a range of plant traits including shoot branching[27], shoot gravitropism[28], secondary growth[29], adventitious rooting[30], and lateral rooting and root hair elongation[31]. Many of the processes targeted by SLs also require auxin transport, or more specifically auxin transport canalization as proposed, for example, for the classical SL effect - shoot branching.

At the cellular level, SLs can inhibit PIN plasma membrane localization and reduce auxin transport[26,32-34], but the underlying molecular mechanism and developmental relevance of these effects is not clear.

Our observations in this study broaden the spectrum of the physiological effects of SLs to include processes traditionally associated with auxin transport canalization such as leaf venation, vascular tissue regeneration and PIN-dependent auxin transport channel formation from external auxin sources. At the cellular level, we show that SLs specifically interfere with the feedback of auxin on PIN polarization and clathrin-mediated internalization, providing a mechanistic framework for the action of SLs in many developmental processes.

2.5.2 Results

2.5.2.1 SLs interfere with canalization of PIN-dependent auxin transport in pea

A classical physiological role of SLs is in the inhibition of shoot branching. This is also a process that involves canalization, because when buds are released from dormancy they initiate PIN1-expressing channel connections with the main vasculature[5]. These channels appear similar to those that form after adding exogenous auxin to the side of the stem[3,5]. Both canalization events can be inhibited by auxin produced from shoot apices, providing one possible mechanism of how dominant shoot tips control branching[5]. When SLs are applied directly to buds after decapitation, they inhibit bud outgrowth[35,36] and can reduce transport of auxin (indole-3-acetic acid, [^{3}H]-IAA) from buds into the stem (Supplementary Fig. 1a-d).

However, the precise action of SLs on auxin canalization and vascularization is less obvious[37]. Therefore, we explored the effect of synthetic SL, *rac*-GR24 (hereafter called GR24) on auxin (indole-3-acetic acid; IAA) to partly or fully decapitated pea plants. Firstly, we analyzed PIN1 channel and subsequent vasculature formation from an artificial lateral auxin source. Local auxin application in lanolin paste to the side of the pea (*Pisum sativum*) stem just below a cut (Fig. 1a) was sufficient to induce the formation of PIN1-expressing auxin channels and subsequent vascular connections to the stem vasculature[3,38]. In our control situation, strong PIN1 expression in the vicinity of the local IAA application was observed with a predominantly lateral PIN1 localization away from the auxin source (Fig. 1b). This initially broad field of PIN1 expression became gradually narrow and more polarized until about 5 days after application when fully defined and strongly polarized narrow PIN1 channels formed, which were already often accompanied by differentiated xylem vessels (Fig. 1b). This is in a full agreement with the auxin canalization process as proposed by the classical canalization

hypothesis in the absence of competing auxin sources[2]. In contrast, co-application of GR24 prevented strongly polarized PIN1 expression and the formation of both PIN1 channels and continuous de novo vasculature; only occasional fragmented xylem cells appeared instead (Fig. 1b). Analogous observations were made when we analyzed PIN1 expression in fully decapitated stems. IAA application on the stump (Fig. 1c) led to a massive increase of PIN1 expression in the polarized field below the place of application in the first 3 days and a gradual formation of narrow PIN1-expressing channels accompanied with differentiated xylem strands at the day 5 (Fig. 1d). The simultaneous application of GR24 strongly inhibited this process. There was no strong increase in polarized PIN1 and no channel formation either (Fig. 1d).

These observations are the first to show that SLs can inhibit the new formation of auxinconducting, PIN-expressing channels induced from auxin sources. This SL effect on auxin canalization provides a plausible explanation for how SLs regulate auxin transport, vascularization and branching.

2.5.2.2 SLs inhibit vasculature formation and regeneration in Arabidopsis

To further explore the role of SLs in other canalization processes, we examined the classical process of canalization-dependent vasculature regeneration following wounding[2], which has recently been established in *Arabidopsis* stems[39] (Fig. 2a). This allowed us to use the extensive genetic toolkit in this model species, and also allowed us to test plant-produced endogenous SLs rather than relying on synthetic GR24.

In control experiments, we observed that vascular regeneration was characterized by initial auxin accumulation above the wound, broad PIN1 expression and gradual establishment of narrow, polarized PIN1-expressing, auxin-conducting channels circumventing the wound[39] (Supplementary Fig. 2a). In the SL biosynthesis defective mutants *more axillary growth (max)1-1* and *max4-1*, the regeneration occurred about as fast as in controls (Supplementary Fig. 2b), but the regenerated vasculature was much more abundant than in the controls (Fig. 2b). To test for the effect of increased endogenous SLs, we used conditional overexpression of SL biosynthetic enzyme MAX1 in the *max1* mutant background (*DEX>>MAX1 max1-1* – hereafter named *DEX>>MAX1*). In the control (uninduced) plants, the first vessels around the wound appeared after 4 days and fully regenerated vasculature appeared after 6 days (Fig. 2c, Supplementary Fig. 2c). In contrast, while we detected the groups of isolated vessel-like cells developed from callus in both untreated and dexamethasone (Dex)-treated plants (Fig. 2c), there was no regeneration of vasculature around the wound observed after Dex induction (Fig.

2c, Supplementary Fig. 2c). These results are in line with the observations from the pea plants and show that SLs negatively regulate canalization-mediated vasculature regeneration processes.

We also examined the efficiency of vasculature regeneration in mutants affected in SL/karrikin-related (KR) signaling, including mutants for the MAX2 F-box protein (*max2-3*) and the double mutant for the SL/KR receptors *dwarf14-1 hyposensitive to light*-3 (*d14-1 htl3*)[40]. In both genotypes, regeneration occurred much faster (Fig. 2d) and the regenerated strands were more abundant compared to wild type controls (Supplementary Fig. 2d), suggesting that SL/KR signaling normally restricts vasculature regeneration.

To directly test whether SL signaling is involved in auxin channel formation, we analyzed the expression of the DR5 auxin response reporter (*DR5rev::GFP*) during regeneration. Comparison between control and *max2-3* mutant revealed that indeed the DR5positive channels formed much faster and more abundantly when SL/KR signaling was compromised (Fig. 2e, f). Consistently, in the *max2-3* mutant, the layer of regenerated vasculature was also formed earlier and thicker (Fig. 2e, f).

Together these results identify SLs as a crucial regulator of regeneration after wounding increased SL levels inhibit whereas decreased SL biosynthesis or compromised signaling promote canalization-mediated vasculature regeneration. Another presumably auxin canalization-dependent process that involves vasculature formation along auxin channels is the de novo vasculature formation during the leaf venation[2,6,41-43]. Therefore, we examined vascular development in leaves and found simplified venation patterns with occasional discontinuities after growth on GR24 or induction of endogenous SL production by Dex (Supplementary Fig. 3a-d). This supports the notion that SLs are not only regulating regeneration of vasculature, but also the de novo formation of vasculature during venation in leaves.

2.5.2.3 SLs interfere auxin-mediated PIN polarization in Arabidopsis seedlings

The mechanism, by which a local auxin source promotes formation of auxin channels and vascularization is largely unknown. The classical canalization hypothesis proposes a positive auxin feed-back on auxin transport directionality[13], which can be realized at the cellular level by the effect of auxin on PIN polarity distribution. This can be visualized by the auxinmediated PIN polarity rearrangements in *Arabidopsis* roots[3,44]. In primary roots, PIN2 localizes to the apical cell side in epidermal cells, and preferentially to the basal cell side in young cortex

cells[20], and auxin (synthetic 1-naphthaleneacetic acid, NAA or natural, IAA) treatment leads to PIN2 rearrangements to the outer lateral sides in cortex cells[3] (Fig. 3a). This auxin PIN lateralization effect was consistently counteracted by induced production of endogenous SLs in *DEX>>MAX1* plants (Fig. 3a, b) or by co-treatment with exogenous NAA and GR24 in wild type (Fig. 3c). Notably, this inhibitory effect of GR24 on auxin-mediated PIN lateralization was significantly impaired in *max2-3* (Fig. 3d).

These observations suggest that SLs, through the MAX2-dependent pathway, not only negatively regulate canalization processes at the organ and tissue levels, but also auxinmediated polarization of PIN transporters at the level of individual cells.

2.5.2.4 SLs interfere with auxin feed-back on PIN endocytic recycling

How auxin can regulate PIN polarity and, in particular, how a localized auxin source can lead to the coordinated polarity changes in a whole field of cells, is conceptually unclear. Modelling of canalization and PIN polarization suggests that auxin feed-back on PIN polarity can be related to the known inhibitory auxin effect on dynamic PIN internalization in individual cells[13]. PIN proteins are known to constitutively cycle between the plasma membrane (PM) and the endosomes[17,45]. This cycling is sensitive to the fungal inhibitor brefeldin A (BFA)[17], which more strongly inhibits trafficking to the PM, than from the PM to the endosomes[20,46] leading to the intracellular accumulation of constitutively cycling PIN proteins[17]. Previous studies have shown that PIN endocytosis and constitutive recycling are important in determining PIN polarity[47-49]. Intracellular PIN accumulation is rapidly and transiently inhibited by auxin itself [14], providing a possible mechanism of how auxin can influence PIN polarity[13].

Therefore, we investigated the SL effect on auxin-mediated inhibition of PIN endocytic recycling. As shown previously[14], PIN proteins accumulated intracellularly after BFA treatment and these BFA-induced PIN internalizations were inhibited by the synthetic auxin, NAA (Fig. 3e). GR24 treatment alone showed no effect on BFA-induced PIN intracellular accumulation (Supplementary Fig. 4a, b), but it clearly interfered with the NAA inhibition of this process, as shown by a substantial BFA-induced PIN1 and PIN2 intracellular accumulation when co-treated with GR24 (Fig. 3e, g, Supplementary Fig. 4c, d, f). In addition, the induction of endogenous SL biosynthesis in the *DEX>>MAX1* line showed the same antagonistic effect on auxin-mediated inhibition of PIN internalization (Supplementary Fig. 4g-i). Similarly, a

natural SL, (+)-5-deoxystrigol (5DS), interfered with the auxin effect on the BFA-induced PIN intracellular accumulation as well (Fig. 3i).

Note that some of our experiments required high concentrations of GR24. This is because wild type can be quite resistant to GR24, and 5 μM GR24 or higher is often required, particularly in roots[32,50-52]. High GR24 concentrations may impact on photoreceptor pathways[53] and the use of *rac*-GR24 may lead to non-SL responses due to stereoisomer specificity[54]. However, both issues can be readily resolved by comparing GR24 treatment responses with SL mutants, and with transgenic lines that stimulate endogenous SL production, such as *DEX>>MAXI*[26].

Next, we tested whether the effect of SLs in regulating PIN trafficking also depends on SL signaling components. In the absence of GR24, BFA-induced PIN1 and PIN2 internalization or NAA-mediated inhibition was similar in the *d14* SL-specific signaling mutant or the *max2* SL/KR signaling mutant (Fig. 3e-h, Supplementary Fig. 4d-f). However, these mutants showed insensitivity to GR24 in counteracting the NAA action on PIN endocytic trafficking (Fig. 3e-h, Supplementary Fig. 4d-f).

In summary, these data show that synthetic or endogenous SLs interfere with the auxin regulation of BFA-visualized PIN intracellular accumulation, acting through D14- and MAX2-dependent SL signaling.

2.5.2.5 SLs interfere non-transcriptionally with auxin feedback on clathrin-mediated endocytosis

PIN proteins are endocytosed by a clathrin-mediated mechanism[18] and this endocytic pathway is inhibited by auxin through a TIR1-independent mechanism[15]. Notably, in shoots, SL action has been linked to clathrin-mediated PIN internalization, independent of de novo protein synthesis[32]. To substantiate the mode of SL action in uncoupling auxin feed-back on PIN internalization and to get more insight into the targeted mechanism, we addressed whether SLs specifically interfere with the auxin effect on clathrin-mediated endocytosis in roots. Quantitative evaluation of the uptake of the fluorescent tracer of endocytosis FM4-64[55] revealed that, as for BFA-induced PIN internalization (Supplementary Fig. 4a, b), FM4-64 uptake itself was not influenced by GR24 treatment (Fig. 4c). In contrast, NAA-mediated inhibition of FM4-64 uptake was clearly diminished when combined with GR24 (Fig. 4a, c).

Auxin inhibition of endocytosis coincides with auxin depleting clathrin from the PM. As described, the clathrin light chain fused to GFP (CLC-GFP) is associated with intracellular endomembranes as well as with the PM[56], and NAA treatment leads to a decrease of

clathrinassociated fluorescence at the PM[15]. Treatment with GR24 showed no visible effect on CLC-GFP localization itself (Fig. 4d), but when co-incubated with NAA, GR24 counteracted the NAA-mediated depletion of the PM-localized CLC-GFP, resulting in a large recovery of a CLC-GFP distribution at the PM (Fig. 4b, d). These results show that while SLs do not have an obvious effect on PIN internalization, endocytosis or clathrin association with the PM, they specifically interfere with the auxin effect on these processes.

Notably, the GR24 effect on auxin-inhibited BFA-induced PIN internalization, FM4-64 uptake could also be observed in the presence of inhibitors of de novo protein synthesis (Fig. 4e, Supplementary Fig. 4j, k). This confirms that, as suggested previously for the SL effect on PIN internalization in shoots[32], SL regulation of auxin feed-back on PIN internalization occurs through a non-transcriptional mechanism in roots.

In summary, these observations reveal a non-transcriptional SL effect on the auxin regulation of PIN internalization by clathrin-mediated endocytosis.

2.5.3 Discussion

Our observations broaden the palette of developmental processes known to be regulated by SLs and provide novel insights into the cellular mechanism of SL action. We show that D14- and MAX2-dependent signaling negatively regulates vascularization of leaves, vasculature regeneration after wounding or de novo formation of vasculature from an artificial exogenous auxin source. All of these processes, along with the classical target of SL regulation, shoot branching, are thought to at least partly depend on the canalization of auxin flow through gradually narrower auxin-conducting channels that demarcate future vasculature. A key condition for canalization is the feed-back regulation of auxin transport directionality, as manifested at cellular level by the auxin effect on polar, subcellular localization of PIN auxin transporters[3,38]. Our results show that endogenous or exogenous SLs not only interfere with canalization-dependent developmental processes, but also specifically interfere with auxin feed-back on PIN polarity and related auxin feed-back on clathrinmediated endocytosis of PIN proteins. This SL action does not require regulation of transcription and occurs through the known D14- and MAX2-mediated signaling pathways. Thus, SLs may repress a mechanism that enables auxin to inhibit PIN internalization and polarization or SLs may inhibit auxin bioactivity in this cellular context. SLs have been proposed to inhibit auxin biosynthesis in the context of shoot gravitropism[28]. However, auxin biosynthesis and auxin levels can be repressed as a consequence of inhibition of auxin transport[57]. Moreover, in our tests, SLs also inhibit the

action of exogenously applied auxin, suggesting action downstream of biosynthesis. This might also explain why auxin applied to buds in intact wild type plants is not sufficient to stimulate their growth[36], presumably due to strong inhibition by endogenous SLs.

It was previously suggested that, in context of shoot branching, SLs destabilize PINs from the PM[26,32,58]. However, all of our cell biological analyses suggest that SLs do not affect endocytosis or PIN internalization in roots per se, but specifically uncouple the effect of auxin on endocytic processes. Alternatively, SLs could divert endocytic PIN trafficking into an auxin-insensitive pathway, thus making PIN retrieval from membranes more efficient and possibly auxin-insensitive. In any case, given that SLs also interfere with canalizationmediated processes in context of branching and vascular tissue formation and regeneration in shoots, it is likely that the above-mentioned PIN1-GFP-based observations in shoots[26,32,58] are in fact a result of the here identified SL effect on auxin feed-back on PIN internalization. Our findings identify a cellular mechanism downstream of MAX2-dependent SL signaling and provide a mechanistic framework for an important part of SL signalingmediated processes including vascularization and the regulation of root and shoot architecture. Further work will identify the precise molecular link between the SL pathway and auxin feedback on PIN polarity.

2.5.4 Material and Methods

Plant material

The following transgenic plants and mutants have been described previously: *DR5rev::GFP*[59] ; *PIN1::PIN1-GFP*[9]; *CLC::CLC-GFP*[56]; *max1-1*[60]; *DEX>>MAX1*, *max1*[26]; *max2-3*[61]; *max4-1*[62]; *d14-1*[63]; *d14-1htl-3*[40].

Growth conditions

Pisum sativum L. cv. Vladan (Pea) plants were grown in perlite soaked with Richter's nutrient solution under a 16-h light/8-h dark cycle at 20°C/18°C for 7 days. Intact or decapitated (10 mm above the upper bud) plants were used. *Arabidopsis thaliana* (L.) Heyhn. Columbia ecotype (Col-0), adult plants used for inflorescence stems wounding, were individually grown in pots with a soil and vermiculite mixture (1:1, v/v) under a 16-h light/8-h dark cycle at 20 °C for 7-8 weeks. *Arabidopsis* seedlings were grown vertically on half-strength Murashige and Skoog (MS) agar plates vertically under a 16-h light/8-h dark cycle at 21 °C for 4-5 days.

Drug applications and experimental conditions

Exogenous drugs were applied as following: GR24 (*rac*-GR24; 50 mM stock in acetone made freshly; Radboud University Nijmegen or Olchemim) (0.01/0.03/0.09/0.1/1/5/10/20/25/50 μM), (+)-5-deoxystrigol [5DS; 10 mM stock in dimethyl sulfoxide (DMSO); Olchemim] (50

μM), dexamethasone (Dex; 50 mM stock in DMSO; Sigma) (15/50 μM), indole-3-acetic acid (IAA; 10 mM stock in DMSO; Sigma) (0.16 μM), 1-naphthaleneacetic acid (NAA; 10mM stock in DMSO; Sigma) (10/30 μM), BFA (50 mM stock in DMSO; Invitrogen) (25 μM), or cycloheximide (CHX; 50 mM stock in DMSO; Sigma) (50 μM). Control treatments contained an equivalent amount of solvent.

For morphological analyses on vein patterning and development, *Arabidopsis* seedlings were grown on solid MS medium supplemented with GR24. Regarding Dex induction experiments, unless otherwise noted: seedlings were always germinated on medium containing 50 μM Dex. For vasculature regeneration detection, *DEX>>MAX1* plants were treated with 15 μM Dex for 5 h by applying Dex directly to the basal parts of inflorescence stems with a brush. For observations on NAA induced PIN1 relocation, *DEX>>MAX1* seedlings were treated with 50 μM Dex for 24 h. For testing NAA inhibition on BFA-induced internalization, if not mentioned otherwise: 90 min with 25 μM BFA; or 90 min with 10 μM NAA/BFA co-treatment after 50 min of NAA pretreatment; or 90 min with NAA/5 μM GR24/BFA co-treatment after 50 min of NAA/GR24 pretreatment. Only for experiments in Fig. 3h, i and Supplementary Fig 4c, conditions were slightly different: 60 min with 25 μM BFA; or 30 min pretreatment with 10 μM NAA, followed by 60 min co-treatment of NAA/BFA; or first a 30 min pretreatment with 25 or 50 μM GR24 or 50 μM 5DS, then another 30 min pretreatment with NAA/GR24 or NAA/5DS, followed by concomitant NAA/GR24/BFA or NAA/5DS/BFA treatment for 60 min. For the other BFA related visualization, seedlings were treated by 60 min with 25 μM BFA; or 60 min with 100 μM GR24/BFA co-treatment after 30 min of GR24 pretreatment. For evaluating NAA induced PIN relocation, seedlings were treated by 10 μM NAA for 4 h; or 50 μM GR24 for 4 h; or NAA/GR24 for 4 h following 1 h of GR24 pretreatment. For observation on FM4-64 uptake and CLC-GFP abundance at the PM, seedlings were treated by 10/30 μM NAA, 1/10 μM GR24, or NAA/GR24 for 80 min, respectively. For inhibition de novo protein synthesis, pretreatments of 30 min with 50 μM CHX were always applied beforehand. For all comparisons, independent experiments were done at least in duplicate and always showed similar significant results. Representative data are shown.

Auxin transport assay in Pea

For auxin transport assay on the axillary buds, the upper axillary buds were treated with water lanolin pastes or pastes with GR24 (0.03 μM). After 4 h, the treated and untreated plants were decapitated 10 mm above the upper bud. 0.5 μl of [5-^{3}H]-IAA (American Radiolabeled Chemicals, 925 Gbq mmol^{-1}, 6666 Bq μl^{-1}) diluted in a 50% ethanol was then applied to the

tip of the axillary buds after decapitation in 6 h. Following 1.5 h treatment, the stems at a distance of 0-4 and 4-8 mm below the upper axillary buds were cut into 4 mm segments, respectively. 10 plants were used for each treatment. All samples were incubated in a dioxanebased liquid scintillator cocktail overnight. The [^{3}H] activity was measured with a scintillation spectrophotometer Packard TRI/Carb 2000 (Packard).

Gene expression analysis

For gene expression of PsDRM1, GR24 (0.03 μM) in water lanolin paste was applied on the upper axillary bud of decapitated plants as a ring. PsDRM1 expression was then followed in the untreated lower and treated upper axillary buds. Total RNA for each sample was isolated from 30 buds using the RNeasy Plant Mini Kit (Qiagen) following the manufacturer's protocol. A DNase treatment with the RNase-free DNase Set (Qiagen) was carried out for 15 min at 25 °C. Total cDNA was synthesized from 0.5 μg of total RNA using the Superscript III cDNA kit (Invitrogen). Real-Time PCR (qPCR) was performed using LC 480 SYBR Green I Master Mix (Roche Diagnostics) with primers for PsDRM1 (primer sequences in 25). Cycling conditions for amplification were 95 °C for 10 min, 40 cycles of 95 °C for 15 s, 58 °C for 15 s, and 72 °C for 15 s. A gene expression normalization factor was calculated (Microsoft Excel geNorm, 2002) based on Psβ-tubulin, PsActin, and PsEF1-α (primer sequences in 54) expression levels. Two biological replicates were analyzed in duplicates.

Axillary bud length measurements

Measurements of axillary bud length under different hormonal treatments were done as described[38].

Vascular tissue formation analysis

Analyses of vasculature regeneration in wounded inflorescence stems of *Arabidopsis* were done as described[39].

In situ expression and localization analysis

In Arabidopsis, whole-mount immunolocalization was performed as described64,65. Antibodies were diluted as follows: 1:1000 for rabbit anti-PIN114; 1:1000 for rabbit anti-PIN2 (generously provided by C. Luschnig); and 1:600 for CY3-(Sigma) and Alexa488- (Invitrogen) conjugated anti-rabbit secondary antibodies. For each genotype or treatment, at least two independent experiments were performed, a minimum of 10 roots in total were analyzed, and representative images are presented. In pea, water lanolin pastes containing IAA (0.16 μM), or IAA/GR24 (0.16 μM/0.09 μM) were applied on the stem stump or on the stem 2 mm below lateral incision. Immunolocalization was performed on longitudinal pea stem segments with 40

replicates for each sample type, following the published protocol[66]. The *Arabidopsis* anti-PIN1 antibody also recognizes the homologous PIN protein in pea, which is presumed to be a PIN1 functional ortholog based on expression similarity and localization signal to *Arabidopsis*[3]. Antibodies were diluted as follows: 1:1000 for rabbit antiPIN1[14]; and 1:500 for CY3-(Sigma) conjugated anti-rabbit secondary antibody. All the fluorescence signals were evaluated on Zeiss LSM 700, Zeiss LSM 710, Zeiss Observer. Z1, Leica TCS SP2, Olympus Fluoview FV1000, or Olympus Fluoview 200 confocal scanning microscopes. The same microscope settings were always used for each independent experiment and pixel intensities were taken into account when comparing the images between control and mutants. Images were finally assembled in Adobe Photoshop 7.0 and Adobe Illustrator CS4.

2.5.5 Acknowledgements

We are grateful to David Nelson for providing published material and extremely helpful comments, and Elizabeth Dun and Christine Beveridge for helpful discussions. The research leading to these results has received funding from the European Research Council under the

European Union's Seventh Framework Program (FP7/2007-2013) / ERC grant agreement n° 28230. This work was also supported by CEITEC 2020 (LQ1601) project with financial contribution made by the Ministry of Education, Youth, and Sports of the Czech Republic within special support paid from the National Program of Sustainability II funds. (JB, VR, SP) and Australian Research Council grant FT180100081 (PBB).

2.5.6 Author contributions

J.F. designed and supervised the study. J.Z., E.M., J.B., P.K., Z.M., Y.L., T.P., M.V., V.R., S.P., R.H. and P.T. performed all the experiments. J.Z., P.B.B. and J.F. wrote the manuscript, which was discussed and approved by all authors.

2.5.7 Figures

Figure 1 - SL effects on PIN-dependent auxin canalization in pea

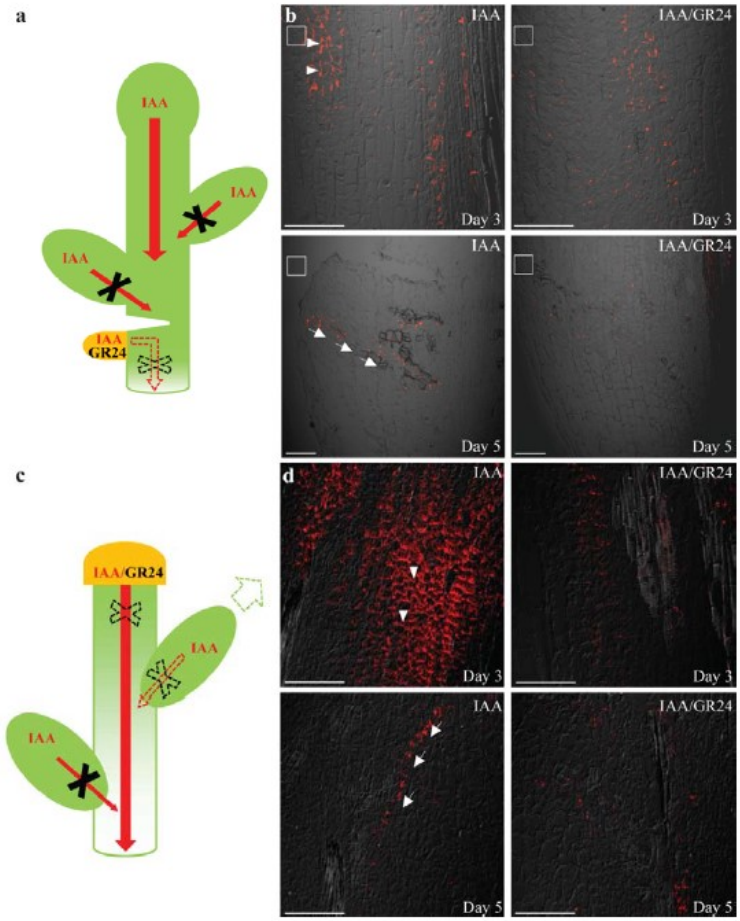

Figure 34 Section 2.5.7 - SL effects on PIN-dependent auxin canalization in pea

a Scheme representing plants wounded below the lower buds. Red arrows represent auxin (IAA) flow. Red arrows crossed with black X represent inhibited auxin flow. Lanolin pastes containing IAA or IAA/GR24 (marked in yellow) were applied to the side of the pea stem below the wound. Dashed red arrow crossed with dashed black X represents formation of a new auxin flow route from the auxin source that can be inhibited by GR24 application. **b** Immunolocalization of PIN1 in the primary stem. The concentrations of IAA and GR24 applied locally in lanolin pastes were 0.16 and 0.09 µM, respectively. In total, 10 plants were analyzed for each treatment. White rectangles indicate the places of IAA or IAA/GR24 application. Arrowheads indicate polarity of the PIN localization. Arrows indicate newly formed auxin channels. The fluorescence signals were evaluated on Olympus Fluoview 200 confocal scanning microscope with UPlanFI 20×/0.5 and/or UPlanApo 10×/0.40 objectives. PIN1 immunolocalization signals (red) are overlaid with the transmitted light images. Scale bar, 100 µm. **c** Scheme of decapitated plants treated with IAA or IAA/GR24 paste on the stump. Red arrows represent auxin (IAA) flow. Red arrow crossed with dashed black X represents formation of a new auxin flow route from the auxin application to the stump that is inhibited by GR24 application. Dashed red arrow crossed with dashed black X represents intermitted auxin flow after temporary bud activation. Dashed green arrow represents temporary bud outgrowth. Red arrows crossed with black X represent inhibited auxin flow. **d** Immunolocalization of PIN1 in the stem of decapitated plants. In total, 10 plants were analyzed for each treatment. Arrowheads indicate polarity of the PIN localization. Arrows indicate newly formed auxin channels. The fluorescence signals were evaluated on Olympus Fluoview 200 confocal scanning microscope with UPlanFI 20×/0.5 objective. PIN1 immunolocalization signals (red)

are overlaid with the transmitted light images. Scale bar, 100 µm. The above experiments were repeated three times with similar results. Images shown are representative of each treatment.

Figure 2 - SL regulation of vasculature regeneration after wounding in *Arabidopsis* stems

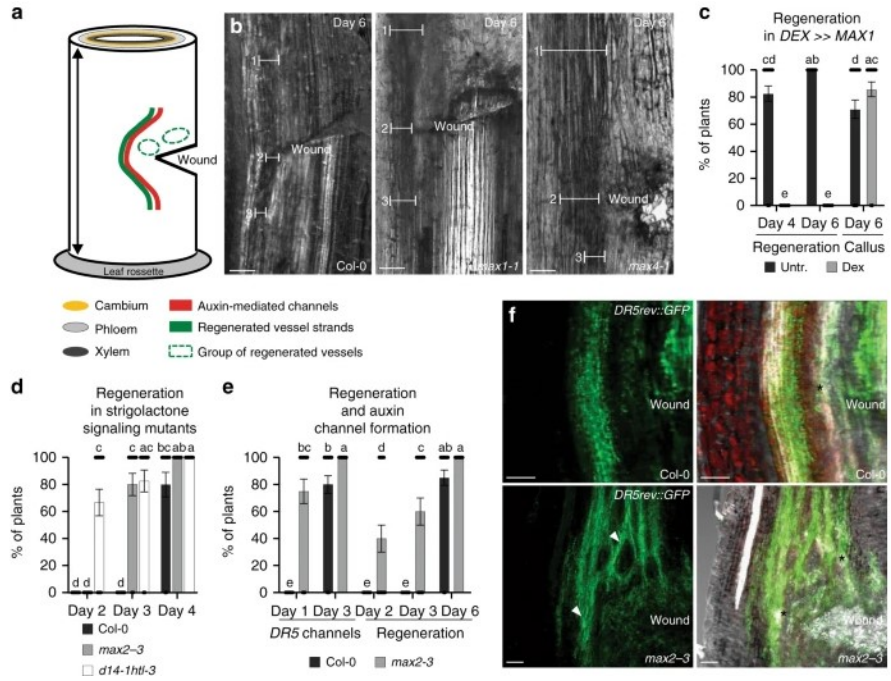

Figure 35 Section 2.5.7 - SL regulation of vasculature regeneration after wounding in Arabidopsis stems

a Scheme representing spatial changes around a wound during vascular tissue regeneration in incised stems of Arabidopsis. Wounding is made in the basal part of inflorescence stem just above the rosette leaves to disturb the longitudinal continuum of the vascular cambium. Green line represents development of regenerated vessel strands around a wound. Red line represents auxin-mediated channels formation. Green circles represent the groups of vessel-like cells developed from outer cortex or callus in the neighborhood of the wound. b Vascular tissue regeneration in SL biosynthesis defective mutants max1-1 and max4-1. Line segments indicate the thickness of regenerated vasculature; above the wound (1), close to the wound (2), below the wound (3). Scale bars: 100 µm. c Vascular tissue regeneration in wounded DEX≫MAX1 plants. Data are expressed as mean ± s.e.m. ($n \geq 22$ inflorescence stems). Means with different letters are significantly different at $P < 0.05$ (one-way ANOVA with Fisher LSD test). d Vascular tissue regeneration in SL/karrikin signaling-defective mutants max2-3 and d14-1 htl-3. Data are expressed as mean ± s.e.m. ($n \geq 15$ inflorescence stems). Means with different letters are significantly different at $P < 0.05$ (one-way ANOVA with Fisher LSD test). e, f The formation of auxin channels around a wound as inferred from DR5rev::GFP expression during vascular tissue regeneration. Data are expressed as mean ± s.e.m. ($n \geq 24$ inflorescence stems). Means with different letters are significantly different at $P < 0.05$ (one-way ANOVA with Fisher LSD test). Right panels in f are merged images of fluorescence and light transmitted signals. Arrowheads indicate abundant channels. Asterisks indicate regenerated vasculature. Scale bars: 100 µm. The above experiments were repeated twice with similar results. Images shown are representative of each treatment. Source data of c–e are provided in the Source data file.

Figure 3 - SL effect on auxin-regulated PIN subcellular dynamics

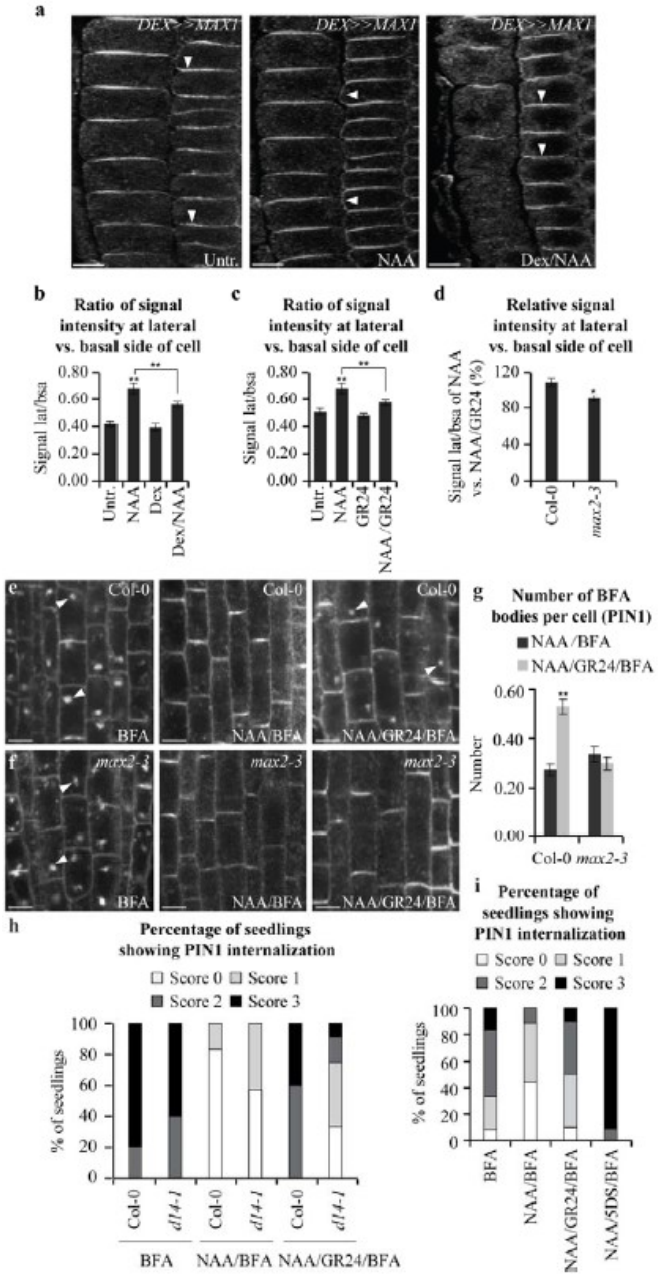

Figure 36 Section 2.5.7 - SL effect on auxin-regulated PIN subcellular dynamics

a, **b** Endogenous SL effect on auxin-mediated PIN2 polarity changes in young cortex cells. Immunolocalization of PIN2 is shown (**a**). Arrowheads indicate the polarity of PIN localization. Scale bars: 5 µm. Ratio between mean fluorescence intensity of the lateral and basal membrane in young cortex cells was scored (**b** $n \geq 34$ cells). **c** Exogenous SL effect on auxin-mediated PIN2 polarity changes in young cortex cells. Ratio between mean fluorescence intensity of the lateral and basal membrane in young cortex cells was scored (**c** $n \geq 70$ cells). Data are expressed as mean ± s.e.m. Means with different letters are significantly different at $P < 0.05$ (one-way ANOVA with Fisher LSD test) (**b**, **c**). **d** Less pronounced effect in *max2-3* SL/karrikin signaling mutant in terms of GR24 inhibition of NAA action on PIN2 lateralization (**d** $n \geq 30$ cells). Data are expressed as mean ± s.e.m. *P* value was calculated using Welch's two-tailed *t*-test. **e**, **f** GR24 effect on NAA inhibition of BFA-induced PIN1 internalization. Immunolocalization of PIN1 in root cells is shown (**e**). Arrowheads indicate PIN1 proteins internalized into BFA compartments. Scale bars: 5 µm. The number of BFA bodies per root

cell in NAA/BFA- or NAA/GR24/BFA-treated wild-type and *max2* seedlings was scored (**f** $n \geq 425$ cells). Data are expressed as mean ± s.e.m. Means with different letters are significantly different at $P < 0.05$ (one-way ANOVA with Fisher LSD test). **g**, **h** Quantification of PIN1 internalization in roots. Both synthetic SL GR24 (25 μM, **g**; 50 μM, **h**) and natural SL 5DS (50 μM, **h**) were applied. The same position of root tip was imaged with the same microscope settings for each independent experiment. The roots ($n \geq 5$) were then scored blind and the percentage of roots displaying almost undetectable (Score 0), weak (Score 1), stronger (Score 2), or very severe (Score 3) PIN1 internalization was determined. The above experiments were repeated three times with similar results. Images shown are representative of each treatment. Source data of **b**–**d** and **f**–**h** are provided in the Source data file.

Figure 4 - Regulation of auxin-mediated inhibition on endocytosis by SLs in *Arabidopsis*

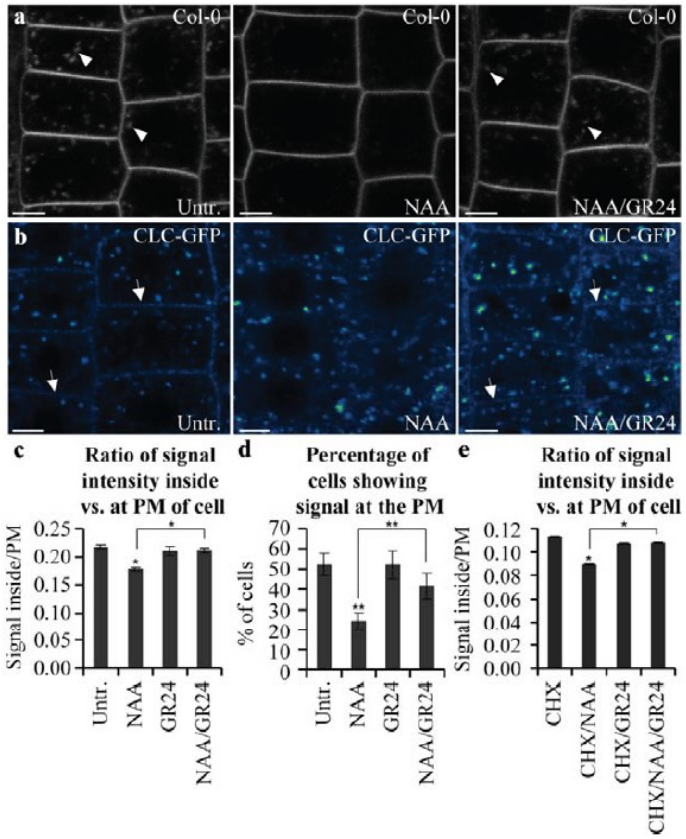

Figure 37 Section 2.5.7 - Regulation of auxin-mediated inhibition on endocytosis by SLs in Arabidopsis

a, **c**, **e** Effect of GR24 on NAA-inhibited FM4-64 uptake. GR24 (1 μM), which alone had no detectable effect on FM4-64 uptake, largely diminished the NAA (10 μM) action of inhibiting FM4-64 uptake (**a**, **c**). Quantitative evaluation of FM4-64 uptake: the quotient between mean fluorescence intensity of the intracellular and PM in the roots was scored (**c** $n \geq 150$ cells). GR24 treatment also effectively attenuated NAA-mediated inhibition of FM4-64 uptake, when protein synthesis was inhibited by 50 μM cycloheximide (CHX; **e** $n \geq 91$ cells). Arrowheads indicate endosomal compartments of FM4-64. Scale bars: 5 μm. Data are expressed as mean ± s.e.m. Means with different letters are significantly different at $P < 0.05$ (one-way ANOVA with Fisher LSD test). **b**, **d** Effect of GR24 on NAA-regulated clathrin localization. CLC-GFP distributed at the trans-Golgi network and the PM. NAA (30 μM) treatment induced a transient decrease of the CLC-GFP signal at the PM. GR24 (10 μM), which alone had no detectable effect on CLC-GFP signal, largely prevented NAA action on depletion of CLC-GFP signal from the PM. The percentage of root cells showing CLC-GFP labeling at the PM was scored (**d** $n \geq 7$ roots). Arrows indicate CLC-GFP distribution at the PM. Scale bars: 5 μm. Data are expressed as mean ± s.e.m. Means with different letters are significantly different at $P < 0.05$ (one-way ANOVA with Fisher LSD test). The above experiments were repeated three times with similar results. Images shown are representative of each treatment. Source data of **c**–**e** are provided in the Source data file.

2.5.8 Supplemental Figures

Figure S1 - SL effects on dormancy and auxin transport in pea

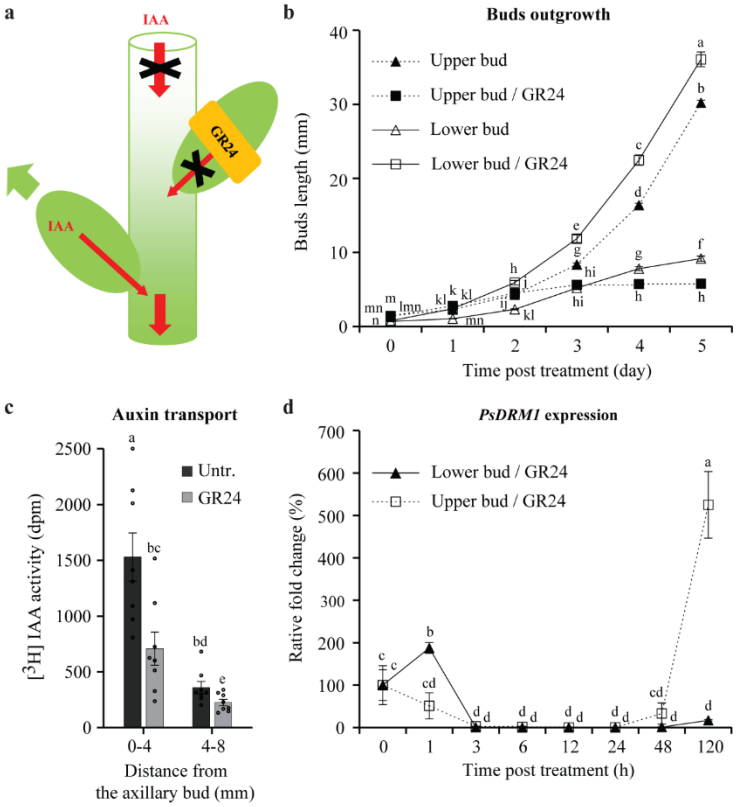

Figure 38 Section 2.5.8 - SL effects on dormancy and auxin transport in pea

a Scheme representing decapitated plants treated with the synthetic SL analog GR24 in a ring on the upper bud. Red arrows represent auxin (IAA) flow. Red arrows crossed with black X represent inhibited auxin flow. Green arrow represents bud outgrowth. Outgrowth of the upper bud, which is normally released from dormancy after decapitation, is inhibited by GR24 treatment, leading to the development of the lower bud instead. **b** Outgrowth of the axillary buds on the decapitated plant: untreated or upper buds treated with GR24 (0.03 µM). Untreated upper buds showed continuous outgrowth, whereas GR24 application allowed a short period of outgrowth for the treated buds but inhibits further outgrowth. The lower buds behaved oppositely to the upper buds, such that when the upper buds were growing, outgrowth of the lower buds were inhibited, and only after inhibition of outgrowth of the upper buds by GR24 application do the lower buds started to grow. Data are expressed as mean ± SE ($n \geq 26$ buds). Means with different letters are significantly different at $P < 0.05$ (One-way ANOVA with Fisher LSD test). **c** [^{3}H]-IAA transport applied on the upper axillary bud. Transport was measured in two segments of stem at a distance of 0-4 mm and 4-8 mm below the upper axillary bud. Application of GR24 (0.03 µM) decreased auxin transport from the bud. This contrasted with other results showing no effect of GR24 on [^{3}H]-IAA transport[1], but in that case outgrowing buds were examined. Data are expressed as mean ± s.e.m. ($n = 8$ plants). Means with different letters are significantly different at $P < 0.05$ (One-way ANOVA with Fisher LSD test). **d** Relative expression of *PsDRM1* in the pea axillary buds. The bud growth and transport observations were matched by bud activity status, as confirmed by the expression of the dormancy marker gene *DORMANCY-ASSOCIATED PROTEIN1* (*PsDRM1*). Gene expression was detected in the lower and upper axillary buds of decapitated plants treated with GR24-ring (0.03 µM) on the upper buds. Data are expressed as mean ± SE of two biological replicates. Means with different letters are significantly different at $P < 0.05$ (One-way ANOVA with Fisher LSD test).

Total RNA for each sample was isolated from 30 buds. Four technical replicates were analyzed in each independent experiment. The above experiments were repeated at least twice with similar results. Source data of b-d are provided in the Source Data file

Figure S2 - SL effect on vasculature regeneration after wounding in *Arabidopsis*

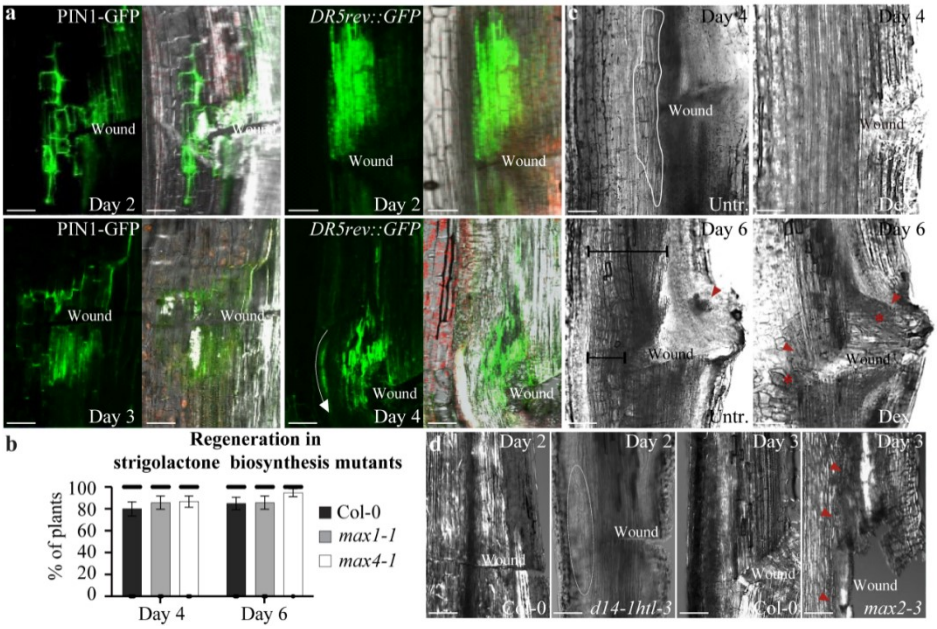

Figure 39 Section 2.5.8 - SL effect on vasculature regeneration after wounding in Arabidopsis

a Cellular events related to auxin canalization and vascular tissue development after wounding: initial broad and apolar PIN1 expression around the wound and auxin response accumulation (*DR5rev::GFP*) above the wound at 2 days after wounding; establishment of narrow and polarized PIN expressing at the day 3 and auxin-conducting channels circumventing the wound beginning from the day 4. Arrows indicate auxin channels. Right panels are merged images of fluorescence and light transmitted signals. Scale bars: 100 µm. **b** Vasculature regeneration in SL biosynthesis-defective mutants *max1-1* and *max4-1*. Temporal changes during vascular tissue reconstruction in *max1-1* and *max4-1* were comparable to that of the wild type. First vessels around a wound appeared at the day 4 and completely continued vessel strands developed at the day 6. However, the regenerated vasculature of *max1-1* and *max4-1* was more abundant as compared to wild-type control (see main Fig. 2b). Data are expressed as mean ± s.e.m. ($n \geq 35$ inflorescence stems). **c** Vasculature regeneration in *DEX>>MAX1* plants. In the untreated *DEX>>MAX1*, vascular tissue regenerated around a wound at the day 4 and the layer of regenerated vessels enlarged at the day 6. In contrast, there was no regenerated vasculature around the wound formed in Dex-induced *DEX>>MAX1* stems. Outline indicates developed vasculature. The line segments indicate thickness of regenerated vasculature above and around a wound. Arrowheads indicate the vessel-like cells differentiated from callus. Asterisks indicate extended callus. Scale bars: 100 µm. **d** Vascular tissue regeneration in SL/karrikin signaling-defective mutants *d14-1htl-3* and *max2-3*. Vasculature regeneration in wounded stems of *d14-1htl-3* and *max2-3* occurred faster than that in the wild type. The differentiated vessels initiated in *d14-1htl-3* and *max2-3* at the day 2 and the day 3 after wounding, respectively, whereas there was no regeneration in wild-type stems at these time points. Circle indicates a group of vessel-like cells differentiated around a wound. Arrowheads indicate differentiated vasculatures. Scale bars: 100 µm. The above experiments were repeated twice with similar results. Images shown are representative of each treatment. Source data of b are provided in the Source Data file

Figure S3 - SL effect on vein patterning in *Arabidopsis*

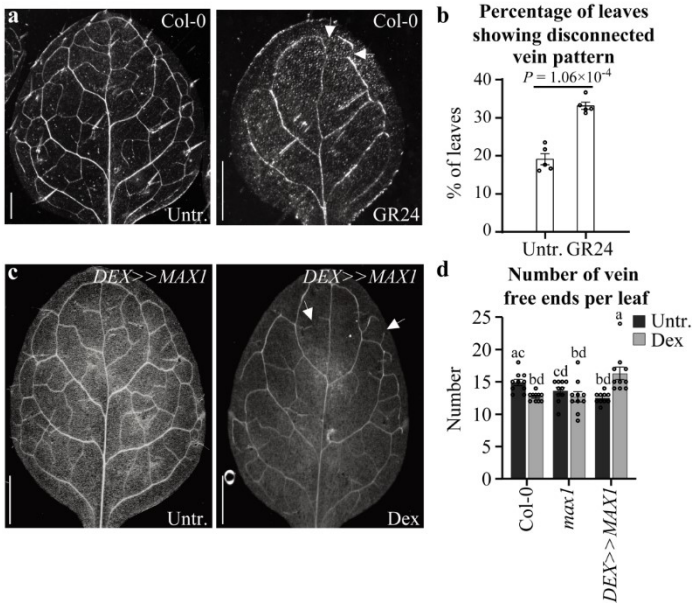

Figure 40 Section 2.5.8 - SL effect on vein patterning in Arabidopsis

a, **b** Effect of exogenous SLs on vein patterning in primary leaves. Wild-type leaves germinated on media supplemented with GR24 (20 µM) showed suppressed vascular network and disconnected vein pattern (**a**). Quantification of irregular vein pattern: GR24 treatment inhibited the formation of continuous veins (**b**; $n \geq 192$ leaves). Scale bars: 0.5 mm. Data are expressed as mean ± s.e.m. of five biological replicates. *P* value was calculated using Welch's two-tailed *t*-test. **c**, **d** Effect of endogenous SLs on vein patterning in primary leaves. *DEX>>MAX1* plants germinated on 50 µM Dex, inducing SL biosynthesis, developed more simplified vasculature with more free ends. Data are expressed as mean ± s.e.m. ($n = 10$ leaves). Means with different letters are significantly different at $P < 0.05$ (One-way ANOVA with Fisher LSD test). Scale bars: 0.5 mm. The above experiments were repeated at least three times with similar results. Images shown are representative of each treatment. Source data of b and d are provided in the Source Data file

Figure S4 - SL effect on PIN subcellular dynamics in *Arabidopsis*

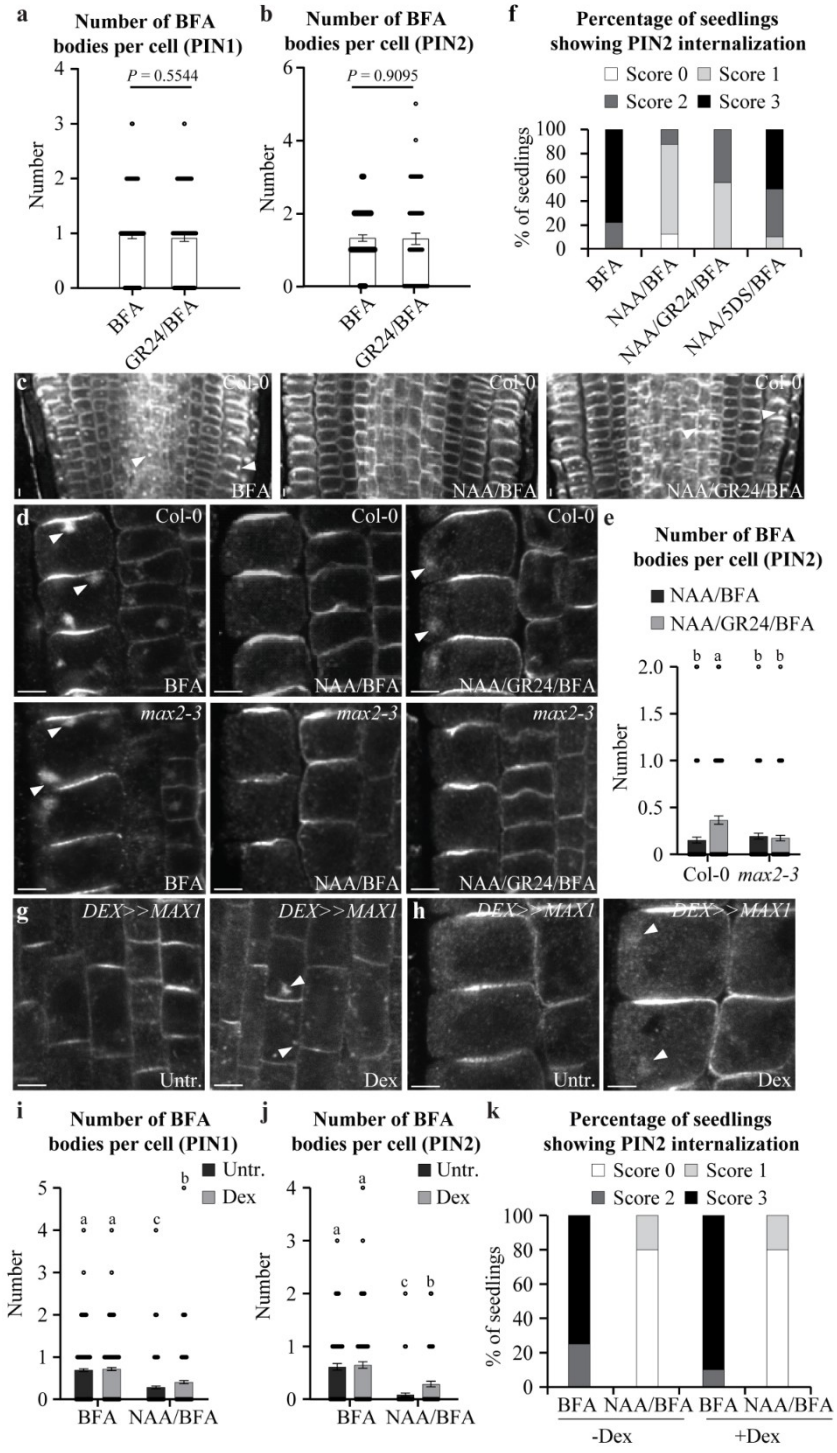

Figure 41 Section 2.5.8 - SL effect on PIN subcellular dynamics in Arabidopsis

a, **b** No effect of GR24 alone on BFA-visualized PIN internalization. BFA (25 µM)-induced PIN1 and PIN2 internalization was not influenced by 5 µM GR24, which was sufficient to attenuate the NAA effect in wild type. The number of BFA bodies in PIN1 (**a**) and PIN2 (**b**) per root cell was scored ($n \geq$ 67 cells). Data are expressed as mean ± s.e.m. *P* values were calculated using Welch's two-tailed *t*-tests. **c**-**e** Effect of GR24 on NAA-mediated inhibition of BFA-visualized PIN internalization. Immunolocalization of PIN1 (**c**) and PIN2 (**c**, **d**) in root cells: BFA-induced internalization of PIN1 and PIN2 was inhibited by NAA (10 µM) and this inhibitory effect of NAA was partially counteracted by GR24 at 50 µM (**c**) in wild-type roots. Lower dose of GR24 at 5 µM had the same effect (**d**) as in (**c**).

Overview pictures of PIN1 and PIN2 internalization are in **c** and close up pictures of PIN2 are in **d**. This competitive effect of GR24 (5 μM) on NAA action was reduced in the *max2-3* mutant (**d**). Arrowheads indicate PIN proteins internalized into BFA compartments. Scale bars: 5 μm. The number of PIN2-containing BFA bodies per root cell in NAA/BFA- or NAA/GR24/BFA-treated wild-type and *max2-3* mutant seedlings was scored (**e**; $n \geq 161$ cells). Data are expressed as mean ± s.e.m. Means with different letters are significantly different at $P < 0.05$ (One-way ANOVA with Fisher LSD test). **f** Interference with NAA effect on PIN2 internalization mediated by synthetic SL GR24 and natural SL 5DS. The roots ($n \geq 8$) were scored blind and the percentage of roots displaying almost undetectable (Score 0), weak (Score 1), stronger (Score 2), or very severe (Score 3) PIN2 internalization was determined. **g-k** Endogenous SLs-mediated interference with NAA-inhibited BFA-visualized PIN internalization. Immunolocalization of PIN1 and PIN2 in root cells: BFA-induced internalization of PIN1 (**g**) and PIN2 (**h**) was inhibited by NAA in root cells of non-induced control, but this effect was attenuated in 50 μM Dex induced *DEX>>MAX1* plants. Arrowheads indicate PIN proteins internalized into BFA compartments. Scale bars: 5 μm. The number of PIN1- and PIN2-containing BFA bodies per root cell was scored, respectively (**i, j**; $n \geq 111$ cells). Data are expressed as mean ± s.e.m. Means with different letters are significantly different at $P < 0.05$ (One-way ANOVA with Fisher LSD test). Dex-treated transgenic plants expressing the GVG system alone did not give significant phenotype in terms of auxin-mediated PIN2 trafficking, compared to the non-induced controls (**k**). The roots ($n \geq 8$) were scored blind and the percentage of roots displaying almost undetectable (Score 0), weak (Score 1), stronger (Score 2), or very severe (Score 3) PIN2 internalization was determined. The above experiments were repeated three times with similar results. Images shown are representative of each treatment. Source data of a, b, e, f, and i-k are provided in the Source Data file

Figure S5 - Non-transcriptional SL effect on PIN subcellular dynamics in *Arabidopsis*

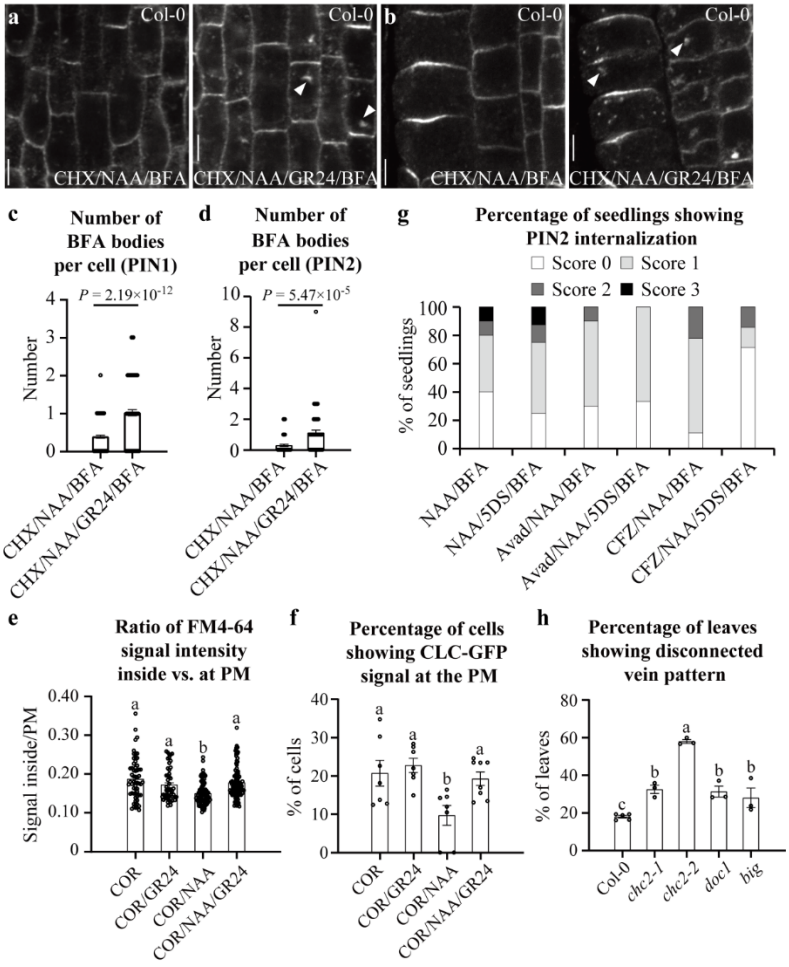

Figure 42 Section 2.5.8 - Non-transcriptional SL effect on PIN subcellular dynamics in Arabidopsis

a-**d** Non-transcriptional effect of GR24 on NAA inhibition of BFA-induced PIN internalization. GR24 treatment effectively attenuated NAA-mediated inhibition of PIN1 (**a**) and PIN2 (**b**) internalization when protein synthesis was inhibited by CHX (50 µM). Scale bars: 5 µm. The number of BFA bodies in PIN1 (**c**) and PIN2 (**d**) per root cell was scored ($n \geq 56$ cells). Data are expressed as mean ± s.e.m. *P* values were calculated using Welch's two-tailed *t*-tests. **e**, **f** Non-transcriptional effect of GR24 on NAA-mediated endocytosis and CLC abundance at the PM. GR24 treatment effectively attenuated NAA-mediated inhibition of FM4-64 uptake when transcription was inhibited by cordycepin (COR; 50 µM; **e**). The quotients between FM4-64 mean fluorescence intensity of the intracellular and PM in the roots were scored (**e**; $n \geq 50$ cells). GR24 treatment antagonized NAA-mediated depletion of CLC-GFP from the PM in presence of COR (**f**). The percentage of root cells showing CLC-GFP labelling at the PM was scored (**f**; $n \geq 7$ roots). Data are expressed as mean ± s.e.m. Means with different letters are significantly different at $P < 0.05$ (One-way ANOVA with Fisher LSD test). **g** Quantification of PIN2 internalization in roots. The inhibitory effect of NAA on BFA-induced PIN2 internalization was attenuated by 5DS (50 µM) in wild-type roots. Application of avadomide (Avad; 100 µM) or carfilzomib (CFZ; 100 µM) could prevent the 5DS effect. The roots ($n \geq 7$) were scored blind and the percentage of roots displaying almost undetectable (Score 0), weak (Score 1), stronger (Score 2), or very severe (Score 3) PIN2 internalization was determined. **h** Vasculature patterning in mutants interfering with CME (*chc2-1* and *chc2-2* alleles) and auxin effect on PIN trafficking (*doc1* and *big*). The overall frequency of irregular vein formation was markedly increased in these mutants as compared to that of wild type ($n \geq 57$ leaves). Data are expressed as mean ± s.e.m. Means with different letters are significantly different at $P < 0.05$ (One-way ANOVA with Fisher LSD test). The above experiments

were repeated at least twice with similar results. Images shown are representative of each treatment. Source data of c-h are provided in the Source Data file

Figure S6 - SL/karrikin signaling-mediated interference of auxin feedback at both tissue and cellular levels

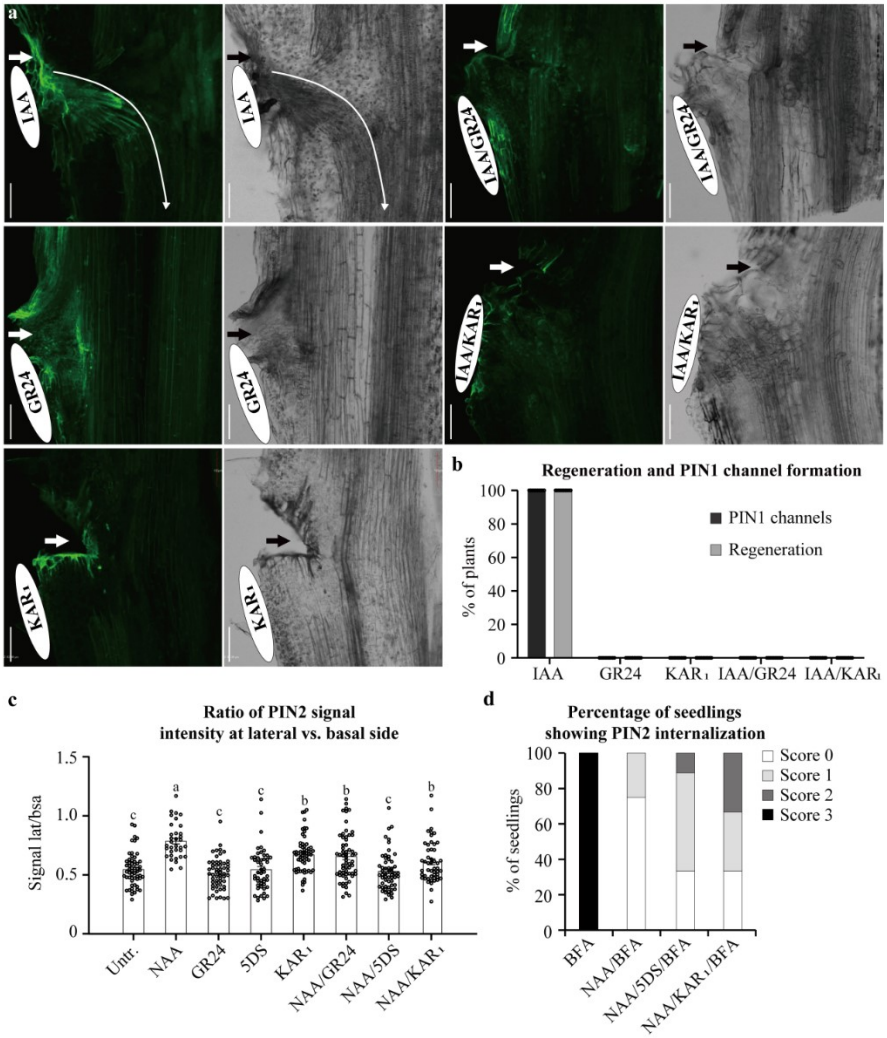

Figure 43 Section 2.5.8 - SL/karrikin signaling-mediated interference of auxin feedback at both tissue and cellular levels

a, **b** Auxin canalization and vascular strand formation in *Arabidopsis* stems. Chemicals were locally applied in droplets of lanolin pastes (indicated by white ovals) below the wounds (indicated by arrows). Both GR24 (10 µM) and KAR_1 (10 µM) treatments inhibited IAA (10 µM)-mediated vasculature regeneration and auxin channels formation (**a**). Both the fluorescence and light transmitted images are shown. Curved lines indicate formed PIN1 channels and regenerated vasculature. Scale bars: 100 µm. Vasculature regeneration and PIN1 channels formation were scored (n = 10 inflorescence stems) (**b**). **c** Quantification of auxin-mediated PIN2 lateralization in root cortex cells. Exogenously applied GR24 (50 µM), 5DS (50 µM), or KAR_1 (50 µM) attenuated NAA effect on PIN2 lateralization in wild-type roots. Ratio between mean fluorescence intensity of the lateral and basal membrane in young cortex cells were scored ($n \geq 34$ cells). Data are expressed as mean ± s.e.m. Means with different letters are significantly different at $P < 0.05$ (One-way ANOVA with Fisher LSD test). **d** Quantification of PIN2 internalization in roots. BFA-induced PIN2 internalization was inhibited by NAA. This inhibitory effect of NAA was partially counteracted by 5DS (50 µM) and KAR_1 (50 µM) in wild-type roots. The roots ($n \geq 8$) were scored blind and the percentage of roots displaying almost undetectable (Score 0), weak (Score 1), stronger (Score 2), or very severe (Score 3) PIN2 internalization was determined. The above

experiments were repeated at least twice with similar results. Images shown are representative of each treatment. Source data of b-d are provided in the Source Data file

2.5.9 References

1. Adamowski, M. & Friml, J. PIN-dependent auxin transport: action, regulation, and evolution. *Plant Cell* **27**, 20–32 (2015).
2. Sachs, T. The control of the patterned differentiation of vascular tissues. *Adv. Bot. Res.* **9**, 151–162 (1981).
3. Bennett, T. et al. Connective Auxin Transport in the Shoot Facilitates Communication between Shoot Apices. *PLoS Biol.* **14**, e1002446 (2016).
4. Sauer, M. et al. Canalization of auxin flow by Aux/IAA-ARF-dependent feedback regulation of PIN polarity. *Genes Dev.* **20**, 2902–2911 (2006).
5. Balla, J., Kalousek, P., Reinohl, V., Friml, J. & Prochazka, S. Competitive canalization of PIN dependent auxin flow from axillary buds controls pea bud outgrowth. *Plant J.* **65**, 571–577 (2011).
6. Scarpella, E., Marcos, D., Friml, J. & Berleth, T. Control of leaf vascular patterning by polar auxin transport. *Genes Dev.* **20**, 1015–1027 (2006).
7. Robert, H. S. et al. Local Auxin Sources Orient the Apical-Basal Axis in Arabidopsis Embryos. *Curr. Biol.* **23**, 2506–2512 (2013).
8. Robert, H. S. et al. Maternal auxin supply contributes to early embryo patterning in Arabidopsis. *Nat. Plants* **4**, 548-553(2018).
9. Benková, E. et al. Local, efflux-dependent auxin gradients as a common module for plant organ formation. *Cell* **115**, 591-602 (2003).
10. Heisler, M. G. et al. Patterns of auxin transport and gene expression during primordium development revealed by live imaging of the Arabidopsis inflorescence meristem. *Curr. Biol.* **15**, 1899-1911 (2005).
11. Bhatia, N. et al. Auxin Acts through MONOPTEROS to Regulate Plant Cell Polarity and Pattern Phyllotaxis. *Curr. Biol.* **26**, 3202-3208 (2016).
12. Rakusová, H. et al. Termination of Shoot Gravitropic Responses by Auxin Feedback on PIN3 Polarity. *Curr. Biol.* **26**, 3026-3032 (2016).
13. Wabnik, K. et al. Emergence of tissue polarization from synergy of intracellular and extracellular auxin signaling. *Mol. Syst. Biol.* **6**, 447 (2010).
14. Paciorek, T. et al. Auxin inhibits endocytosis and promotes its own efflux from cells. *Nature* **435**, 1251–1256 (2005).
15. Robert, S. et al. ABP1 mediates auxin inhibition of clathrin-dependent endocytosis in Arabidopsis. *Cell* **143**, 111-121 (2010).
16. Baster, P. et al. SCF(TIR1/AFB)-auxin signalling regulates PIN vacuolar trafficking and auxin fluxes during root gravitropism. *EMBO J.* **32**, 260-274 (2013).
17. Geldner, N., Friml, J., Stierhof,Y-D., Jürgens, G. & Palme, K. Auxin transport inhibitors block PIN1 cycling and vesicle trafficking. *Nature* **413**, 425–428 (2001).
18. Dhonukshe, P. et al. Clathrin-mediated constitutive endocytosis of PIN auxin efflux carriers in Arabidopsis. *Curr. Biol.* **17**, 520–527 (2007).
19. Kleine-Vehn, J. et al. ARF GEF-dependent transcytosis and polar delivery of PIN auxin carriers in Arabidopsis. *Curr. Biol.* **18**, 526–531 (2008).
20. Kleine-Vehn, J. et al. Cellular and molecular requirements for polar PIN targeting and transcytosis in plants. *Mol. Plant* **1**, 1056-1066 (2008).
21. Marhavý, P. et al. Cytokinin controls polarity of PIN1-dependent auxin transport during lateral root organogenesis. *Curr. Biol.* **24**, 1031-1037 (2014).
22. Willige, B. C., Isono, E., Richter, R., Zourelidou, M. & Schwechheimer, C. Gibberellin regulates PINFORMED abundance and is required for auxin transport-dependent growth and development in Arabidopsis thaliana. *Plant Cell* **23**, 2184-2195 (2011).
23. Löfke, C. et al. Asymmetric gibberellin signaling regulates vacuolar trafficking of PIN auxin transporters during root gravitropism. Proc Natl Acad Sci U S A **110**, 3627-3632 (2013).

24. Salanenka, Y. et al. Gibberellin DELLA signaling targets the retromer complex to redirect protein trafficking to the plasma membrane. *Proc. Natl. Acad. Sci. USA* **115**, 3716-3721 (2018).
25. Du, Y. et al. Salicylic acid interferes with clathrin-mediated endocytic protein trafficking. *Proc. Natl Acad. Sci. USA* **110**, 7946-7951 (2013).
26. Crawford, S. et al. Strigolactones enhance competition between shoot branches by dampening auxin transport. *Development* **137**, 2905–2913 (2010).
27. Waldie, T., McCulloch, H. & Leyser, O. Strigolactones and the control of plant development: lessons from shoot branching. Plant J. **79**, 607-622 (2014).
28. Sang, D. et al. Strigolactones regulate rice tiller angle by attenuating shoot gravitropism through inhibiting auxin biosynthesis. *Proc. Natl. Acad. Sci.* **111**, 11199–11204 (2014).
29. Agusti, J. et al. Strigolactone signaling is required for auxin-dependent stimulation of secondary growth in plants. *Proc. Natl. Acad. Sci.* **108**, 20242–20247 (2011).
30. Rasmussen, A. et al. Strigolactones suppress adventitious rooting in Arabidopsis and pea. *Plant Physiol.* **158**, 1976-1987 (2012).
31. Koltai, H. Cellular events of strigolactone signalling and their crosstalk with auxin in roots. *J. Exp. Bot.* **66**, 4855-4861 (2015).
32. Shinohara, N., Taylor,C. & Leyser, O. Strigolactone can promote or inhibit shoot branching by triggering rapid depletion of the auxin efflux protein PIN1 from the plasma membrane. *PLOS Biol.* **11**, e1001474 (2013).
33. Pandya-Kumar, N. et al. Strigolactone analog GR24 triggers changes in PIN2 polarity, vesicle trafficking and actin filament architecture. *New Phytol.* **202**, 1184-1196 (2014).
34. Kumar, M. et al. Arabidopsis response to low-phosphate conditions includes active changes in actin filaments and PIN2 polarization and is dependent on strigolactone signalling. *J. Exp. Bot.* **66**, 1499-1510 (2015).
35. Gomez-Roldan, V. et al. Strigolactone inhibition of shoot branching. *Nature* **455**, 189-194 (2008).
36. Brewer, P. B., Dun, E. A., Ferguson, B. J., Rameau, C. & Beveridge, C. A. Strigolactone acts downstream of auxin to regulate bud outgrowth in pea and Arabidopsis. *Plant Physiol.* 150, 482–493 (2009).
37. Brewer, P. B., Dun, E. A., Gui, R., Mason, M.G., & Beveridge, C. A. Strigolactone Inhibition of Branching Independent of Polar Auxin Transport. *Plant Physiol.* **168**, 1820-1829 (2015).
38. Balla, J. et al. Auxin flow-mediated competition between axillary buds to restore apical dominance. *Sci. Rep.* **6**, 35955 (2016).
39. Mazur, E., Benková, E. & Friml, J. Vascular cambium regeneration and vessel formation in wounded inflorescence stems of Arabidopsis. *Sci. Rep*. **6**, 33754 (2016).
40. Toh, S., Holbrook-Smith, D., Stokes, M. E., Tsuchiya, Y. & McCourt, P. Detection of parasitic plant suicide germination compounds using a high-throughput Arabidopsis HTL/KAI2 strigolactone perception system. *Chem. Biol.* **21**, 988–998 (2014).
41. Mattsson, J., Sung, Z. R., Berleth, T. Responses of plant vascular systems to auxin transport inhibition. *Development* **126,** 2979–2991 (1999).
42. Sieburth, L. E. Auxin is required for leaf vein pattern in Arabidopsis. *Plant Physiol.* **121**, 1179–1190 (1999).
43. Avsian-Kretchmer, O., Cheng , J-C., Chen, L., Moctezuma, E. & Sung, Z. R. Indole acetic acid distribution coincides with vascular differentiation pattern during Arabidopsis leaf ontogeny. *Plant Physiol.* **130**, 199–209 (2002).
44. Prát, T. et al. WRKY23 is a component of the transcriptional network mediating auxin feedback on PIN polarity. *PLoS Genet.* **14**, e1007177 (2018).
45. Sancho-Andrés, G. et al. Sorting Motifs Involved in the Trafficking and Localization of the PIN1 Auxin Efflux Carrier. *Plant Physiol.* **171**, 1965–1982 (2016).
46. Naramoto, S. et al. ADP-ribosylation factor machinery mediates endocytosis in plant cells. *Proc. Natl. Acad. Sci. USA* **107**, 21890–21895 (2010).
47. Kitakura, S. et al. Clathrin mediates endocytosis and polar distribution of PIN auxin transporters in Arabidopsis. *Plant Cell* **23**, 1920–1931 (2011).
48. Kleine-Vehn, J. et al. Recycling, clustering, and endocytosis jointly maintain PIN auxin carrier polarity at the plasma membrane. *Mol. Syst. Biol.* **7**, 540 (2011).

49. Tanaka, H. et al. Cell polarity and patterning by PIN trafficking through early endosomal compartments in Arabidopsis thaliana. *PLoS Genet.* **9**, e1003540 (2013).
50. Hu, Z. et al. Strigolactone and cytokinin act antagonistically in regulating rice mesocotyl elongation in darkness. *Plant Cell Physiol.* **55**, 30-41 (2014).
51. Bennett, T. et al. Strigolactone regulates shoot development through a core signalling pathway. *Biol. Open* **5**, 1806-1820. (2016).
52. Hu, Q. et al. DWARF14, A Receptor Covalently Linked with the Active Form of Strigolactones, Undergoes Strigolactone-Dependent Degradation in Rice. *Front Plant Sci.* 8, 1935 (2017).
53. Tsuchiya, Y. et al. A small-molecule screen identifies new functions for the plant hormone strigolactone. *Nat. Chem. Biol.* **6**, 741-749 (2010).
54. Scaffidi, A. et al. Strigolactone Hormones and Their Stereoisomers Signal through Two Related Receptor Proteins to Induce Different Physiological Responses in Arabidopsis. *Plant Physiol.* **165**, 1221-1232 (2014).
55. Jelínková, A. et al. Probing plant membranes with FM dyes: tracking, dragging or blocking? *Plant J.* 883–892 (2010).
56. Konopka, C. A., Backues, S. K. & Bednarek, S. Y. Dynamics of Arabidopsis dynamin-related protein 1C and a clathrin light chain at the plasma membrane. *Plant Cell* **20**, 1363–1380 (2008).
57. Ljung, K., Bhalerao, R. P. & Sandberg, G. Sites and homeostatic control of auxin biosynthesis in Arabidopsis during vegetative growth. *Plant J.* **28**, 465–474 (2001).
58. Soundappan, I. et al. SMAX1-LIKE/D53 Family Members Enable Distinct MAX2-Dependent Responses to Strigolactones and Karrikins in Arabidopsis. *Plant Cell* **27**, 3143–3159 (2015). Friml, J. *et al.* Effluxdependent auxin gradients establish the apical-basal axis of *Arabidopsis*. *Nature* **426**, 147-153 (2003).
59. Stirnberg, P., van De Sande, K. & Leyser, H. M. MAX1 and MAX2 control shoot lateral branching in Arabidopsis. *Development* **129**, 1131–1141 (2002).
60. Umehara, M. et al. Inhibition of shoot branching by new terpenoid plant hormones. *Nature* **455**, 195–200 (2008).
61. Sorefan, K. et al. *MAX4* and *RMS1* are orthologous dioxygenase-like genes that regulate shoot branching in *Arabidopsis* and pea. *Genes Dev.* **17**, 1469–1474 (2003).
62. Waters, M. T. et al. Specialisation within the DWARF14 protein family confers distinct responses to karrikins and strigolactones in Arabidopsis. *Development* **139**, 1285–1295 (2012).
63. Friml, J., Benková, E., Mayer, U., Palme, K. & Muster, G. Automated whole mount localisation techniques for plant seedlings. *Plant J.* **34**, 115–124 (2003).
64. Sauer, M., Paciorek, T., Benková, E. & Friml, J. Immunocytochemical techniques for whole mount *in situ* protein localization in plants. *Nat. Protocols* **1**, 98–103 (2006).
65. Paciorek, T., Sauer, M., Balla, J., Wiśniewska, J. & Friml, J. Immunocytochemical technique for protein localization in sections of plant tissues. *Nat. Protocols* **1**, 104–107 (2006).

2.6 SLs inhibit root growth by promoting mitochondrial retrograde signaling independently of MAX2

Adapted and modified from:

Gallei M, Lee CP, Baster P, Pěnčík A, Pottie R, Molnar G, et al. *SLs inhibit root growth by promoting mitochondrial retrograde signaling independently of MAX2*. (*Dev. Cell* 2022. Under revision)

In the recent years observations were accumulating on other SL physiological responses, which do not seem to require canonical signaling components such as MAX2. These include effect of high SL levels on hypocotyl elongation (Tsuchiya et al. 2010; Jia et al. 2014) and SL-induced inhibition of primary root elongation (Ruyter-Spira et al. 2011). Furthermore, transcriptional responses independent of the canonical signaling components were proposed (Carbonnel, Torabi, and Gutjahr 2021) but also non-transcriptional effects depending on MAX2 as described in Zhang et al 2020. This all suggests an existence of yet unknown non-canonical SL perception and signaling, whose identity and cellular destination remains mysterious.

In this study we identified a novel, MAX2-independent SL signaling mechanism, which initiates in mitochondria, signals to the nucleus and regulates root development. By a forward genetic approach, we identified the SL-insensitive *pig1* mutant, which altered the kinetic properties of the mitochondrial pyruvate dehydrogenase complex. SL has an unknown target in mitochondria, where it uncouples respiration. This leads to metabolic aberrations, mitochondria-to-nucleus retrograde signaling upregulating transcription of mitochondrial dysfunction genes and downregulating auxin-regulated genes. SL-triggered mitochondrial uncoupling is communicated to the nucleus via cleavage and translocation of the ER-localized transcription factor ANAC017. These observations establish a novel mechanism for SL signaling emanating from mitochondria and regulating development.

Contributions Michelle Gallei:

- Designing the experiments
- Phenotypic analysis of all mentioned mutant lines (Figure 1, Figure 2A-D, Figure 7C)
- Sequence alignment (Figure S2B)
- Confocal imaging for MitoTracker analysis of all mutant lines and treatments (Figure 3A-E, Figure 7D)

- Confocal imaging for DII-Venus Figure S6A)
- RNAseq sample preparation and data analysis of all RNAseq data (Figure 5, Figure 6, Figure S6B,C, Figure 7 A,B,G-I, Figure S7A)
- Confocal imaging for GFP-ANAC017 (Figure 7E,F)
- Writing and correcting the manuscript
- Construction of the figures

2.6.1 Introduction

A relatively recently discovered group of plant hormones are strigolactones (SLs) with a growing list of roles, both in development and in plant's interaction with the environment. SLs are carotenoid-derived compounds, found for the first time around 50 years ago as germination stimulants for the parasitic weed *Striga lutea* (Cook et al. 1966). Decades later it was found that SLs work as endogenous signals, promoting hyphal branching of arbuscular mycorrhizal fungi (Akiyama, Matsuzaki, and Hayashi 2005) and are involved in the repression of shoot branching (Gomez-Roldan et al. 2008). Recently it was shown that SLs influence an even broader range of plant traits ranging from shoot gravitropism (Sang et al. 2014), secondary growth (Agusti et al. 2011), adventitious root formation (Rasmussen et al. 2012), lateral rooting and hair elongation (Koltai 2015) as well as to vascular tissue formation and regeneration (Zhang et al. 2020).

In the model *Arabidopsis thaliana* SLs are perceived by the α/β hydrolase DWARF14 (D14), a dual-functional receptor that is responsible for both the perception and the hydrolysis of SLs in the nucleus (Yao et al. 2016). Following SL binding, D14 undergoes conformation change that leads to the interaction with the F-box protein MORE AXILLARY GROWTH2 (MAX2), a part of the SKP1-Cullin-F-box complex (SCF) ubiquitin ligase complex. This perception mechanism triggers ubiquitination and degradation of target proteins, including SUPPRESSOR OF MAX2 LIKE (SMXL) repressors (Yao et al. 2016; C. Wang et al. 2015). Degradation of SMXL proteins, alleviates transcriptional repression of downstream genes, which in turn leads to the activation of diverse SL-triggered responses. This described canonical signaling pathway, with its assigned transcriptional responses, has been a focus of SL research and most developmental responses were assigned to it. Nonetheless, some non-transcriptional and faster responses have also been proposed. SL action on shoot branching was assigned to rapid and non-transcriptional depletion of the auxin efflux carrier PIN1 from the cell surface (Shinohara et al. 2013). Furthermore, SL regulation of auxin canalization-mediated processes including

vascular tissue formation and regeneration has been shown to be MAX2-depedent but non-transcriptional (Zhang et al. 2020).

Meanwhile observations were accumulating on other SL physiological responses that do not seem to require canonical signaling components such as MAX2. These include the effect of high SL levels on hypocotyl elongation (Tsuchiya et al. 2010; Jia et al. 2014) and SL-induced inhibition of primary root growth (Ruyter-Spira et al. 2011). Furthermore, transcriptional responses independent of the canonical signaling components were proposed, responding also to lower levels of SL (Carbonnel, Torabi, and Gutjahr 2021). This all suggests an existence of yet unknown non-canonical SL perception and signaling, whose molecular identity and cellular destination remains mysterious.

In plant cells, most hormonal signaling pathways originate either at the cell surface, endomembranes or in the nucleus (Spartz and Gray 2008). Some observations indicate that the perturbation of mitochondrial function can also modulate hormonal signaling and that in turn, hormonal levels impact on mitochondrial function (Gleason et al. 2011; Kerchev et al. 2014; Berkowitz et al. 2016; Belt et al. 2017). In this view, mitochondria are more than the powerhouse of the cell producing ATP via oxidative phosphorylation, but are also providing essential metabolites for various cellular functions (Millar et al. 2011; Berkowitz et al. 2016). Thus, mitochondrial disturbance can have severe consequences on all aspects of plant development. As most of mitochondrial proteins are encoded in the nuclear genome, upon functional disturbance, mitochondria need to communicate to the nucleus (retrograde signaling) to alter gene expression, a process not fully understood yet. The versatile phytohormone auxin has been shown to inhibit this mitochondrial retrograde signaling as it inhibits the upregulation of genes (MDS - Mitochondrial Dysfunction Stimulon genes) that are targets of mitochondrial perturbation (Kerchev et al. 2014; Ivanova et al. 2014). Other hormones, such as salicylic acid (SA) and abscisic acid (ABA) also have a direct or indirect impact on mitochondrial functions (Norman et al. 2004; Liao et al. 2015; Li et al. 2014). Thus multiple lines of observations suggest an extensive crosstalk between hormones and mitochondria integrating cellular responses to facilitate growth, development and stress responses (Berkowitz et al. 2016). Nonetheless, the mechanistic links behind this crosstalk remain largely elusive.

Here we identified a novel signaling mechanism for the plant hormone strigolactone. This non-canonical pathway originates in mitochondria and via regulating their respiration activity, it

signals to the nucleus to regulate transcription of auxin-regulated genes, thus influencing root development.

2.6.2 Results

2.6.2.1 MAX2-independent effects of strigolactone on root growth and development

Inspired by the possibility that SL may have yet an uncharacterized signaling mechanism, we performed a thorough analysis of SL effects on root development and their dependence on MAX2, a key component of the canonical signaling pathway. We used the synthetic strigolactone analogue, natural stereoisomer $GR24^{5DS}$ (hereafter GR24).

We found that high concentrations of GR24 interfere with primary root growth, lateral root (LR) formation and root hair formation (Figure 1). Notably, *max2* mutant is still sensitive to high concentrations of SL in these processes. When grown on 25 µM GR24, *max2* primary root growth was inhibited to the same extent as wild type (Col-0) (Figure 1a). When observing LR formation the concentration-dependency of *max2* sensitivity becomes apparent. At lower concentrations, such as 2 and 5 µM GR24, the ability to form LRs in *max2* only drops by around 50%, whereas Col-0 shows almost complete inhibition. However, when the concentration is raised to 10 µM then this canonical signaling mutant becomes sensitive (Figure 1b). A similar pattern was observed for root hair formation. When using 10 µM GR24, *max2* shows the same ability to form root hairs as Col-0 (Figure 1c).

Together these results demonstrate that root development in *max2* shows normal sensitivity to higher concentrations of SL. The mutant is resistant to low SL concentrations, showing the involvement of the canonical signaling. However, at a concentration of 10 µM GR24 or higher the canonical signaling pathway is ousted by an enigmatic non-canonical mechanism.

2.6.2.2 Identification of *pig* (Plant Insensitive to GR24) mutants

In order to identify molecular components of this non-canonical signaling pathway, we performed a forward genetic screen for GR24-insensitive mutants. The screen was performed with an EMS-mutagenized population of *Arabidopsis thaliana pPIN::PIN1-GFP* seedlings (Tanaka et al. 2009). Seedlings were transferred 7 days after germination to medium supplemented with 50 µM GR24 (for the initial screening, *rac*-GR24 (racemic mix of + and - GR24) was used). Plants were gravistimulated and after 4 days seedlings showing GR24-resistant gravitropic root growth were selected. From about 4 000 M1 families (56 000 screened plants) we identified 14 plants insensitive to GR24 (*pig*) mutants showing recessive, heritable resistance to GR24. We further characterized the most GR24-insensitive candidate – *pig1*

(Figure 2a). Under normal growth conditions, *pig1* seedlings show only weak defects including slightly longer, skewed roots and shorter hypocotyls (data not shown). For GR24 sensitivity, we performed the same phenotype analysis with *pig1* as we did for *max2* (see Figure 1). In regard to primary root growth *pig1* shows significantly less inhibition at 25 µM GR24 than its background control (PIN1-GFP) or *max2* (Figure 2a,b and Figure 1a). *pig1* is resistant to SL-induced inhibition of lateral root formation at all GR24 concentration used. Even at 10 µM GR24 *pig1* still shows about 50% of LR formation (Figure 2c). We made a similar observation for root hair formation where *pig1* remains highly resistant to 10 µM GR24 (Figure 2d).

Thus, we identified *pig* mutants that are insensitive to higher levels of GR24 and better characterized *pig1*, which shows GR24 insensitivity in inhibition of root growth and lateral root formation as well as promotion of root hair formation.

2.6.2.3 *pig1* is defective in mitochondrial Pyruvate Dehydrogenase Complex E1-β subunit

To molecularly characterize the *pig1* mutation, we performed a map based cloning approach evaluating recombination events in approximately 900 chromosomes of the F2 progeny derived from the cross between *pig1* and *Landsberg erecta*. We found a substitution of a single nucleotide (G to A) in the coding region of At5g50850 (previously identified as *MAB1* (*MACCHI-BOU1*; (Ohbayashi et al. 2019)), which leads to arginine to lysine substitution in the protein. The identified gene encodes the E1-β subunit of the mitochondrial Pyruvate Dehydrogenase Complex (PDC) (Figure 2e). The mitochondrial PDC catalyzes the oxidative decarboxylation of pyruvate and esterification of an acetyl group to release acetyl-CoA. Acetyl-CoA is subsequently used as a carbon source in the tricarboxylic acid (TCA) cycle, releasing CO_2 and driving respiratory rate that is observed as O_2 consumption (Lernmark and Gardestrom 1994).

To confirm that the mutation in PDC E1-β subunit is responsible for the GR24-resistant phenotype, we transformed the *pig1* mutant with a genomic construct expressing the At5g50850 gene from its own 5' regulatory sequence, fused with a fluorescent tag at the C-terminus. We observed PIG1-GFP being localized to mitochondria, which is in line with previous findings (Ohbayashi et al. 2019; Figure 2f). Further, the expression of *pPIG1::PIG1-GFP* fully complemented the GR24-insensitive *pig1* phenotype (Supplemental Figure 1a). Thus, a mutation in the gene coding for the E1-β subunit of the PDC leads to GR24-resistant root growth. Although the mutation substituted arginine by another positively charged amino

acid, lysine, the observed functional effects are striking. This is probably due to the high rate of conservation of arginine at this site. The sequence alignment in Supplemental Figure 1b shows that this arginine residue is conserved between all analyzed species and kingdoms. To evaluate the direct effect of the mutation we purified mitochondria from *pig1* mutant and Col-0 and compared PDC catalytic function between them. The mutated PDC shows a significantly higher Km for pyruvate, and as a result less catalytic efficiency of the enzyme (K_{cat}/K_m) (Figure 2g), outlining again the importance of the mutated amino acid, and showing that the mechanism of *pig1* is directly on PDC function.

Together these results show the isolation of *pig1*, which is resistant to high GR24 concentration and is defective in the E1-β subunit of the mitochondrial PDC. This suggests that this mitochondrial protein might be involved in non-canonical SL signaling.

2.6.2.4 PIG1 role in MAX2-independent strigolactone effects on mitochondrial respiration

The observation that the nuclear-encoded *PIG1* codes for a mitochondrial protein, which when mutated confers SL resistance, together with the published observation that SL has an effect on mitochondria in arbuscular mycorrhizal fungi and in the fungal pathogens *Botrytis cinerea* (Besserer et al. 2008; Belmondo et al. 2017), made us consider that SL may directly affect mitochondrial function in plants.

To evaluate the effect of SL on mitochondria in Arabidopsis roots we treated seedlings with ascending GR24 concentrations and then used a fluorescent dye (MitoTracker Red CM-H2XRos) that stains only mitochondria with a membrane potential, which correlates with mitochondrial respiration rate or the degree of coupling of the respiration process. It becomes apparent that 5 µM GR24 lowers the mitochondrial membrane potential in Col-0. When treating with 25 or 50 µM GR24 almost no signal is retained, implying that mitochondrial membrane potential is severely reduced (Figure 3a). *pig1*, however, was strongly insensitive to the GR24 effect on mitochondrial membrane potential. Even at 50 µM GR24, the mitochondria in *pig1* were almost not affected and still retained its membrane potential (Figure 3b). In contrast, *max2* mitochondria showed normal sensitivity to this effect (Figure 3c). To ensure that the change in mitochondrial membrane potential is not an artefact due to the use of a synthetic SL analogue we employed a stable transgenic Arabidopsis line expressing *MAX1*, a SL biosynthesis gene under a dexamethasone (DEX) inducible promoter (Crawford et al. 2010) conditionally increasing endogenous SL levels *in planta* (Abe et al. 2014). After 6 h of DEX

treatment a reduction in MitoTracker fluorescence became apparent as well, whereas in a line expressing a neutral protein under the same promoter or in Col-0 no differences were observed (Figure 3d,e).

Changes in mitochondrial function can be stimulated by a magnitude of triggers, one of the most prominent are reactive oxygen species (ROS). In plants, chloroplasts can also be involved in the activation of mitochondrial signaling by the production of chloroplastic ROS upon a stress signal (Van Aken and Whelan 2012). Because of overlapping signaling events triggered by both chloroplastic and mitochondrial perturbations, we assessed the effect of SL treatment on chloroplasts. Therefore we measured the chlorophyll fluorescence parameter photosystem II (PSII) maximum efficiency (Fv'/Fm'). This was shown to be a stable and sensitive stress marker for chloroplasts (Kerchev et al. 2014). The measurement revealed that there is no change in the Fv'/Fm' ratio even after 6h of GR24 treatment (Supplemental Figure 2f).

These results show that PIG1-dependent but MAX2-independent SL signaling specifically targets mitochondrial membrane potential.

2.6.2.5 Direct strigolactone effect on mitochondrial respiration

To assess quantitatively the direct capability of SL to alter mitochondrial respiration and lower membrane potential, we performed *in vitro* measurements on purified mitochondria. We measured Respiratory Control Ratio (RCR), where high RCR indicates good function with a coupling of respiration to membrane potential whereas low RCR indicates uncoupling of mitochondrial respiration from membrane potential (Brand and Nicholls 2011). GR24 treatment of isolated mitochondria decreased RCR in a concentration-dependent manner for both, malate + pyruvate and malate respiration alone (Figure 3f). This is consistent with the *in planta* results using MitoTracker (see Figure 3a). To evaluate which state of respiration is targeted, we had a closer look on state III (+ADP) and state IV (-ADP) respiration. A high concentration (50 µM) of GR24 lowers the rate of malate+pyruvate oxidation (State III, Supplemental Figure 2a). At the same time, this GR24 concentration results in a higher proton leak, referred to as uncoupling, which will lower mitochondrial membrane potential, as indicated by an increased rate of State IV respiration (Supplemental Figure 2a). GR24 does not affect malate oxidation alone, however, uncoupling at higher GR24 concentrations persists even in the absence of added pyruvate (Supplemental Figure 2b). This shows SL perception in mitochondria, which then respond by a combination of uncoupling and decreased respiration rate.

When analyzing the *pig1* mutant it becomes evident that respiration is already in a more uncoupled state compared to Col-0 (Figure 3g) and it does not perceive an additional effect anymore of increasing concentrations of GR24. Similar to GR24 treatment, the State III respiration rate is not affected in *pig1* whereas state IV increases, showing uncoupling (Supplemental Figure 2c,d). So *pig1* mitochondria are presumably less sensitive to GR24, because they already resemble GR24 treatment and are thus resistant to additional GR24-induced uncoupling.

We have identified specific and direct SL effects on mitochondrial respiration by acting as an uncoupling agent similar to *pig1* mutation. These results suggest that mitochondria can directly perceive and respond to SL.

2.6.2.6 Strigolactone effect on metabolites in primary metabolism

Mitochondrial respiration and membrane potential can be disrupted by higher activity of the plant alternative oxidase (AOX) pathway. AOX consumes oxygen without contributing to membrane potential or energy production in the cell (Vanlerberghe 2013). Since *pig1* roots showed higher MitoTracker signal after GR24 treatment than Col-0 *in vivo* (Figure 3a,b) suggesting higher membrane potential, but lower RCR in isolated mitochondria, changes in the level of AOX activity were investigated (Jayawardhane et al. 2020). To dissect if altered AOX activity might contribute to the lower RCR in *pig1*, we assessed AOX activity directly in isolated mitochondria. *pig1* has severely increased AOX activity in comparison to Col-0, which did not further change in response to GR24 (Figure 4a). The increased AOX activity can lower the ATP production rate by respiration leading to imbalances in primary metabolism and the TCA cycle in *pig1*. To explain the changes in MitoTracker signal *in vivo*, we evaluated the state of primary metabolism and TCA cycle metabolites in *pig1* using targeted MS-MRM-based (Mass Spectrometry-Multiple Reaction Monitoring) metabolite analysis. *pig1* plants clearly showed increased abundance in TCA cycle-related metabolites and respiratory substrates (sugars) (Figure 4b and Supplemental Figure 3a). This suggests that the mutation in the PDC, increased AOX activity, but also impacts strongly on primary metabolism and mitochondrial substrate availability. This can explain the higher MitoTracker signal *in vivo* in *pig1* but the lower RCR in isolated mitochondria.

2.6.2.7 Strigolactone effects on transcription of mitochondrial dysfunction genes

Mitochondrial function disturbances are linked to a wide variety of downstream effects, including specific changes in the transcriptome. To evaluate the genome-wide downstream

effects of SL-induced mitochondrial dysfunction, we performed an RNAseq analysis. Genes were considered to be significantly differentially regulated if $P_{adj} < 0.05$ with a log fold change of > 1.5x. In Col-0, 6h treatment with 25 µM GR24 induced 1934 differentially expressed genes (DEGs), whereas 1008 transcripts were downregulated and 926 were upregulated. To verify the observed transcriptional changes after GR24 treatment we correlated our dataset with transcriptomics data from a recently published study (Wang et al. 2020), where transcriptional changes were analyzed using 5 µM of the synthetic SL analogue 4DO after 2 and 4h. In total they identified 401 DEGs of which 131 were also identified in the GR24 regulon from our study which corresponds to an over enrichment of 4.31-fold (hypergeometric p-value: $3.15x10^{-49}$) (Figure 5a). This shows that the two different SL analogues are inducing overlapping responses even though concentration and timeframes were different.

As GR24 uncouples the respiratory chain in mitochondria (see Figure 3) we evaluated if there is an effect on the transcription of genes known to respond to mitochondrial dysfunction. In a gene ontology (GO) analysis we found the mitochondria-nucleus signaling pathway being enriched 8-fold. Further we correlated the GR24 regulon to the core mitochondrial dysfunction responsive genes as identified previously (Van Aken et al. 2016). From a total of 98 mitochondrial dysfunction responsive genes, 42 were differentially regulated by GR24 which corresponds to a 7.4-fold overrepresentation (hypergeometric p-value: $8.65x10^{-23}$) (Figure 5b). From the 42 DEGs, 34 were significantly upregulated and only 8 genes were downregulated (Figure 5d) which is clearly indicating that GR24, next to decreasing mitochondrial respiration, is also inducing the upregulation of core dysfunction genes. To further confirm the SL potential to alter the transcription of mitochondrial dysfunction genes we overlaid the 4DO regulon (Wang et al. 2020) to the same 98 mitochondrial dysfunction responsive genes and found an overlap of 6 DEGs which corresponds to a 3.8-fold overrepresentation (hypergeometric p-value: 0.0046) (Figure 5c).

To test whether the mitochondrial dysfunction responsive genes can also be regulated by endogenous SL we used the *DEX::MAX1* line, which induces SL biosynthesis. A q-RT-PCR analysis confirmed a significant overexpression of *AOX1a*, a marker gene for mitochondrial dysfunction (Supplemental Figure 4a).

In summary, SL treatment leads to transcriptional reprogramming including a prominent upregulation of mitochondrial dysfunction genes. This is very similar to what is observed with other described uncouplers of mitochondrial respiration (De Clercq et al. 2013; Van Aken and

Whelan 2012; Schwarzländer et al. 2012) thus further confirming this SL effect on mitochondria.

2.6.2.8 Transcriptional regulation in *pig1*

In *pig1* without any treatment, 101 genes were identified to be differentially regulated in comparison to control. From those, 18 transcripts were downregulated and 83 upregulated. Groups of genes represented in the GO terms are related amongst others to anthocyanin production, systemic resistance, immune and defense responses. When comparing the DEGs in untreated *pig1* to the core mitochondrial dysfunction responsive genes identified previously (Van Aken et al. 2016), there is an overlap of 2 genes (hypergeometric p-value: 0.06), which are upregulated (Supplemental Figure 4b). Those 2 genes, AT5G08030 and AT5G42800, are also significantly upregulated upon GR24 treatment in Col-0. From the 8 GR24-induced downregulated mitochondrial dysfunction responsive genes in Col-0 (Figure 5d), 7 of them (amongst others AT5G08030 and AT5G42800) are upregulated in untreated *pig1* compared to Col-0 (Figure 5e).

Overall *pig1* reacts to GR24 with 2615 DEGs, corresponding to an increase of number of DEGs by 35% when compared to Col-0. However the GR24-induced upregulation of mitochondrial dysfunction genes in *pig1* is of a much smaller magnitude than in Col-0, with less of those genes being significantly differentially regulated (Figure 5e). Overall, *pig1* exhibits a weaker transcriptional response to GR24, which is consistent with the reduction in sensitivity of *pig1* root growth to GR24 (see Figure 2).

Thus, mitochondrial respiration defects, whether induced by GR24 or by *pig1* mutation are also reflected in the transcriptome changes. GR24 is inducing mitochondrial retrograde signaling leading to strong upregulation of mitochondrial dysfunction genes. Even though those also get upregulated in *pig1*, the response is strongly attenuated in comparison to Col-0.

2.6.2.9 Strigolactone effect on transcription of auxin-regulated genes

Previously it was shown that SLs transcriptionally repress auxin-inducible genes (Mashiguchi et al. 2009) and further that mitochondrial perturbation negatively affects the auxin signaling machinery, thus downregulating auxin-regulated genes (Kerchev et al. 2014). This suggests that SL downregulates auxin-regulated genes via its effect on mitochondria. To substantiate this notion, we evaluated the transcript levels of auxin-regulated genes in the GR24 regulon. We screened the GR24 regulon for auxin-regulated genes involved in its signaling and transport (ARFs, IAAs, LAX, PINs, SAURs) and found that most of these genes are downregulated

(Figure 6a). Thus, similar to other mitochondrial uncoupling agents like Antimycin-A (AA) (Kerchev et al. 2014), GR24 alters mitochondrial respiration, leading to the upregulation of mitochondrial dysfunction genes and the downregulation of auxin-regulated genes.

On the other hand, the *pig1* mutant shows less GR24-induced upregulation of mitochondrial dysfunction genes (see Figure 5e), and, accordingly, auxin-regulated genes are also less severely downregulated in response to GR24 (on average log-fold change of 0.4 less with a p-value of < 0.05), even though more genes are differentially regulated (Figure 6b).

Taken together, GR24 acts similar to other mitochondrial uncouplers, by not only upregulating transcription of mitochondrial dysfunction genes but also by downregulating auxin-inducible genes.

2.6.2.10 Strigolactone targets WRKY and ANAC017 mediators of mitochondrial retrograde signaling

Several transcription factor (TF) families have been identified to mediate mitochondrial retrograde signaling, induced either by chemical or genetic disturbance of mitochondrial respiration, prominent among them, the WRKY, NAC and the AP2/ERF families (Van Aken et al. 2013; Vanderauwera et al. 2012; Ivanova et al. 2014; Ng et al. 2013; De Clercq et al. 2013).

To identify the components of the regulatory mechanism of SL-induced retrograde signaling, we screened the GR24 regulon for over-enriched TF families and found the WRKY family being enriched 2.3-fold (hypergeometric p-value: 0.005) with 12 out of 68 TFs being differentially regulated by GR24 (Figure 7a). In addition, several TFs from the NAC family were found to be upregulated by GR24, amongst others ANAC013 and ANAC053. NAC transcription factors are very prominent mediators of mitochondrial retrograde signaling. The main regulator of genes containing the Mitochondrial Dysfunction Motif (MDM) is ANAC017. The N-terminus of the ER-localized ANAC017 can translocate to the nucleus and bind to the MDM cis-Regulatory Elements, which are commonly found in promotors of many mitochondrial dysfunction genes and are necessary and sufficient for their transcriptional activation (De Clercq et al. 2013). We overlaid the GR24 regulon with ANAC017-dependent retrograde signaling genes (ANAC017 regulon from Kacprzak et al. 2020) and found that out of 104 ANAC017-regulated genes 53 transcripts were also differentially regulated by GR24 (Figure 7b). This corresponds to a 6.3-fold enrichment (hypergeometric p-value of 7.4×10^{-32}). Similar to that 4DO also significantly induces ANAC017-regulated genes (5.5-fold

enrichment, hypergeometric p-value: $3.96x10^{-5}$) with 9 genes being differentially regulated (Figure 7c).

In brief, this result shows that NAC and WRKY TFs are involved in the SL-induced retrograde signaling from mitochondria to nucleus to regulate transcription.

2.6.2.11 Strigolactone-induced transcriptional regulation mediated by ANAC017

Next, we tested the SL-induced regulation over NAC TFs on a global level by performing an RNAseq analysis in the GR24 treated *anac017* mutant. Following GR24 treatment in *anac017*, 217 DEGs were identified. From those, 158 transcripts were downregulated and 59 upregulated. In comparison to GR24 treated Col-0, in *anac017* DEGs are reduced by 61%. This shows that overall transcriptional SL regulation highly depends on ANAC017.

To evaluate the specific effect of GR24 on ANAC017 dependent genes we analyzed the previously identified ANAC017 regulon (Kacprzak et al. 2020) and revisited the SL effect on auxin-regulated genes in the *anac017* mutant. In Col-0, after GR24 treatment, a significant subset of ANAC017 regulon genes gets upregulated (Figure 7d). In *anac017*, the expression of ANAC017-regulated genes is decreased relative to Col-0, under control conditions. (Figure 7e). Upon GR24 treatment, a different set of genes are significantly upregulated compared to Col-0 and only a few genes connected to mitochondrial dysfunction exhibited significant increase in expression in anac017, showing that the mutant reacts only moderately to GR24 in terms of gene transcription. In contrast, following GR24 treatment, auxin-regulated genes were downregulated in *anac017* in a similar fashion as in Col-0 (Supplemental Figure 5a,b).

In summary this shows that ANAC017 is involved in overall transcriptional regulation by SL, necessary for the transcription of mitochondrial dysfunction genes but dispensable for auxin-related gene regulation.

2.6.2.12 Strigolactone-triggered translocation of ANAC017 to the nucleus

ANAC017 is crucial for optimal plant growth under conditions of disrupted organelle function (van Aken et al. 2016b).

To confirm the role of ANAC017 in GR24-induced inhibition of mitochondrial respiration, we tested primary root growth of the *anac017* mutant and found it hypersensitive to GR24 (Supplemental Figure 5c). Also the mitochondria of *anac017* show increased sensitivity to GR24-induced inhibition of membrane potential as indicated by a strong reduction in MitoTracker signal (Supplemental Figure 5d). A crucial part of ANAC017 regulation is that

the N-terminus of the ER-localized TF is cleaved and moves to the nucleus (Ng et al. 2013). After treating an *ANAC017::GFP-ANAC017* expressing line with GR24, the GFP signal is no longer confined to the ER but can as well be observed strongly in the cytoplasm and the nucleus (Figure 7f,g), confirming that GR24 induces the re-localization of ANAC017.

Ultimately this shows that ANAC017 is required for optimal plant growth after SL treatment and further that SL can induce the cleavage of the N-terminus of ANAC017 and its subsequent translocation.

2.6.3 Discussion

In this study we identified a novel mechanism for signaling by strigolactones, a relatively recently identified class of plant hormones. We show that SL signal perception occurs in mitochondria independently of the canonical SL signaling pathway. This leads to mitochondria-to-nucleus retrograde signaling, mediated by a cleavage and nuclear translocation of the ANAC017 transcription factor. This ultimately leads to transcriptional reprograming and root architecture modulation.

2.6.3.1 Novel, MAX2-independent strigolactone signaling for root growth regulation

Our analysis of SL (exemplified by the synthetic analogue GR24) effects on root growth and development supports the growing body of evidence for the existence of SL responses independent of the key canonical signaling component MAX2 (Carbonnel, Torabi, and Gutjahr 2021; Tsuchiya et al. 2010; Jia et al. 2014; Ruyter-Spira et al. 2011; Vismans et al. 2016). Effects of lower SL concentrations on primary root growth, lateral roots and root hair formation depends to some extent on MAX2, whereas at GR24 concentrations above 5 µM, *max2* mutant show Col-0-like sensitivity. A genetic screen identified a *pig1* mutant showing insensitivity to low as well as to higher GR24 levels suggesting PIG1 as a potential component of this non-canonical SL signaling. *PIG1* codes for the E1β-subunit component of the Pyruvate Dehydrogenase Complex (PDC), a key metabolic enzyme in mitochondria.

Mitochondrial PDC has been brought into connection to hormonal responses and signaling before. *PIG1* was previously identified as *MAB1* in a forward genetic screen for factors involved in auxin-regulated organ development (Ohbayashi et al. 2019). Moreover the E1α-subunit of the PDC, IAR4 (IAA-ALANINE RESISTANT4), was identified multiple times in screens for mutants with reduced sensitivity to IAA-amino acid conjugates, enhancers of *tir1* auxin perception mutant or suppressors of swollen root phenotypes (Leclere et al. 2004; Quint et al. 2009; Steinwand et al. 2014). The observed phenotypes of *iar4* were mainly explained

by altered auxin homeostasis and reduced auxin signaling. In support of this, we found metabolic aberrations in *pig1*, showing that PDC activity is crucial for mitochondria-based metabolism. This would explain the disturbed auxin metabolism in *iar4* (Leclere et al. 2004; Quint et al. 2009; Steinwand et al. 2014).

Notably, a strong SL insensitivity of mitochondrial *pig1* mutant also in root growth processes independent of MAX2 highlights a possible role of mitochondria in non-canonical SL signaling.

2.6.3.2 Strigolactone targets mitochondrial respiration directly

Strigolactone targets mitochondrial respiration as observed both, *in planta* and in isolated mitochondria. The latter shows that GR24 has a target directly in mitochondria, where it uncouples the respiration chain. The mitochondria of the *pig1* mutant are already in an uncoupled state resembling the SL-treated situation and are hence not reacting to SL treatment anymore.

Studies in tomato suggested a similar phenomenon for the hormone salicylic acid, which decreases the activity of the tricarboxylic acid cycle enzyme 2-oxoglutarate dehydrogenase leading to mitochondrial uncoupling (Liao et al. 2015). Studies in Arabidopsis show that salicylic acid alters the rate of ROS production from the succinate dehydrogenase complex leading to retrograde signaling to the nucleus (Gleason et al. 2011; Belt et al. 2017).

The specific molecular target of SL in mitochondria awaits identification. SL may directly bind to mitochondrial proteins in the respiration chain to induce uncoupling or it may directly modulate the mitochondrial membrane permeability, thus creating a proton leak resulting in uncoupling of the respiration chain (Jastroch et al. 2010). Regardless what the exact SL target in mitochondria is, the MAX2-independent SL effect on both, mitochondrial respiration and root growth together with a resistance of *pig1* mutant to both these effects implies that SL initiates a signaling in mitochondria ultimately leading to root growth regulation.

2.6.3.3 Strigolactone triggers ANAC017-mediated retrograde signaling for transcriptional reprogramming

Chemical and genetic perturbation of mitochondria leads to the consistent and reproducible induction of organelle-to-nuclear retrograde signaling, which is characterized by the upregulation of, among others, mitochondrial dysfunction genes (Van Aken and Whelan 2012; Van Aken et al. 2007; De Clercq et al. 2013). The transcription factor ANAC017 is one of the main regulators of those MDS genes. Similarly, SL, by uncoupling mitochondria, induces

strong upregulation of a common subset of MDS genes, among them many that are under ANAC017 control. Furthermore, SL is unable to regulate these genes in *anac017* mutant. This demonstrates that ANAC017 is required for SL-induced transcriptional regulation. However not all SL-regulated genes are under the control of ANAC017. Even though the downregulation of auxin-inducible genes is a common characteristic of mitochondrial uncoupling (Kerchev et al. 2014), our global transcription profiling shows that this particular regulation is independent of ANAC017. Presumably, it is a secondary consequence of uncoupling of the respiration chain and is not a direct target of this branch of SL signaling.

The exact mechanism, by which the mitochondrial status is read and induces retrograde signaling is unclear but it involves cleavage of ANAC017 N-terminus in the ER and its translocation to the nucleus (De Clercq et al. 2013; Ng et al. 2013). Indeed, consistently with SL-induced transcriptional regulation of ANAC017-targeted genes, SL triggers ANAC017 N-terminus translocation to the nucleus. Thus, SL signaling from mitochondria triggers ANAC017-mediated retrograde signaling to regulate transcription and root development.

2.6.4 Conclusions

In conclusion, our forward genetic and transcriptomic studies identified a new mechanism of SL signaling that is emanating from mitochondria. After SL perception in the mitochondria, a signal of yet unknown nature transmits to the nucleus, largely via the cleavage and nuclear translocation of the ER-localized ANAC017 transcription factor. In the nucleus, among others, mitochondrial dysfunction genes are induced. Secondary consequences of this signaling are on the one hand the downregulation of auxin-inducible genes and on the other hand metabolic aberrations caused by mitochondrial uncoupling (Figure 8).

The mitochondria-originating branch of SL signaling may be the more ancestral one, integrating presumably the most basic SL responses such as quorum sensing, rhizoid promotion, growth regulation and others, which are observed also in systems lacking canonical signaling components, including non-seed plants, bacteria, fungi and human cancer cells (Akiyama et al. 2005; Proust et al. 2011; Belmondo et al. 2017; Hasan et al. 2018; Mozes and Meijler 2020). This opens the question when and how canonical signaling came into the picture and at which responses the two signaling mechanisms converge.

2.6.5 Material and Methods

Gene codes

The Arabidopsis thaliana genes studied and their corresponding accession numbers are listed: AT5G50850 – *PIG1*, AT2G42620 - *MAX2*, AT1G34190 - *ANAC017*, AT2G26170 – *MAX1*.

Plant Material

All the plant material is from the model organism Arabidopsis thaliana. The marker lines used are: pPIN1::PIN1-GFP (Benkova et al. 2003); DEX::MAX1, *max1* (Crawford et al. 2010); PIG1::PIG1-GFP, *pig1* (this study). ANAC017::GFP-ANAC017 (generously contributed by James Whelan); DEX::12-5 (Arabidopsis was transformed with pTA7002 vector to express the empty Dex-inducible GVG cassette (Aoyama and Chua 1997)). Mutants: pig1 (this study), max2 (SALK_092836), anac017 (SALK_022174).

Primer and genotyping

For PIG1 CDS:

Fw: GGGGACAAGTTTGTACAAAAAAGCAGGCTTCttgcttgtatcagctcagtaac

Rev: ACCACTTTGTACAAGAAAGCTGGGTGtttcgatctgtaacaagctctct

For PIG1 Promoter:

Fw: GGGGACAACTTTGTATAGAAAAGTTGTCttgcttgtatcagctcagtaac

Rev: GGGGACTGCTTTTTTGTACAAACTTGGtctctctgattaacaaacaaa

Genotyping *pig1*:

Fw: TCTTTCTTTGACTTGATTATGC

Rev: GCTTGTGGCCTTGTAACTGTAT

The primers amplify a 500bp genomic DNA fragment of the coding region for PIG1 which harbors the mutated base pair creating a unique cutting site for DraI. Digest with DraI, cuts the 500bp amplicon in 2 fragments with different size.

q-RT-PCR from Kerchev et al. 2014:

AOX1a_Fw: TGGTTGTTCGTGCTGACG

AOX1a_Rev: CACGACCTTGGTAGTGAATATCAG

Plant growth and treatment conditions

For root growth assays: Seeds were surface sterilized by chlorine gas and sown on ½ MS 0.8% agar (w/v) medium supplemented with 1% (w/v) sucrose. After stratification for 2 days in the dark at 4°C, the seedlings were grown at 21°C in a 16 h/8 h day/night cycle for up to 7 days. For mitochondrial metabolite measurements: Plants were grown on compost supplemented with Perlite and Vermiculite (3:1:1) under long photoperiod. For the isolation of mitochondria: surface-sterilized seeds were grown in ½MS medium supplemented with 1% (w/v) sucrose and 0.1% (w/v) agar for 14-16 days with gentle agitation (40-60 rpm) under long day conditions. For root growth analysis (primary root growth) 7 day-old seedlings were transferred to ½ MS plates containing the indicated GR24 ($GR24^{5DS}$, GR24+, Strigolab) concentration or for LR root and root hair analysis seeds were directly germinated on ½ MS plates containing the indicated GR24 concentration. For localization studies of GFP-ANAC017 5-day-old seedlings were treated for 6h in ½ MS liquid medium containing 25 µM GR24. For Chlorophyll fluorescence imaging: seeds were surface-sterilized with chlorine gas, stratified at 4ºC for 3d, germinated on ½ MS medium containing 1% (w/v) sucrose and 0.7% (w/v) agar. 7-day-old seedlings were treated for 1,3 and 6h in ½ MS liquid medium containing 25 µM GR24 in a 12-well VWR tissue culture plate (Avantor™).

EMS Mutagenesis, Mutant Forward Genetic Screen and Map Based Cloning

The forward genetic screen was performed using a 3% EMS mutagenized population of *pPIN1::PIN1-GFP Arabidopsis thaliana* seeds. 7-day-old seedlings were transferred to the ½ MS medium supplemented with 50 µM GR24. Plants were gravistimulated twice, by consecutive, 90° clockwise and counterclockwise rotation of the plates, with 48h incubation after each rotation. Following, the plates were scored for seedlings exhibiting root growth resistant to GR24 and proper gravitropic response. 188 pools were screened in the primary screen (of the 294 pools in total – approximately 64 % of the EMS mutagenized population). Each pool consisted of M2 seeds being progeny of 20 pooled M1 plants. For each pool approximately 300 seedlings were screened (in total approximately - 3760 M1 plants; 56400 M2 plants). In the primary screen 401 candidates of the M2 generation were identified, in which upon treatment with 50 µM GR24 root growth followed the gravity vector. From 401 primary candidates, the gravitropic growth, resistant to 50 µM GR24, was confirmed in 9 candidates in the next generation. The mutation responsible for GR24 resistance was mapped in one candidate by the use of insertion/deletion (InDel) markers which are based on simple sequence length polymorphisms (SSLP) which were analyzed by PCR amplification and subsequent agarose gel electrophoresis.

Mitotracker

5-day-old seedlings were treated for 3 hours with the indicated control or GR24 concentration in ½ MS liquid medium. After 2.5 hours of treatment, 500 nM MitoTracker™ Red CMXRos (Invitrogen, M7512) was added for 30 minutes. Before imaging seedlings were washed once in ½ MS liquid medium.

Isolation of mitochondria

Mitochondria were isolated from two-week-old Arabidopsis seedlings as described previously (Sweetlove et al. 2007). Single or dual substrate-dependent O_2 consumption by purified mitochondria was measured at pH 7.2 in a computer-controlled Clark-type O_2 electrode unit according to and using substrate and cofactor concentrations outlined in Lee et al. 2010. GR24 was added to isolated mitochondria prior to the addition of respiratory substrates and cofactors. In vitro activities of PDC in isolated mitochondria were measured as described by Huang et al. 2015, supplemented with ascending GR24 as indicated.

Metabolite analysis by liquid chromatography-mass spectrometry (LC-MS)

Metabolite extraction and analyses by selective reaction monitoring (SRM) LC-MS were carried out exactly as previously described (Le et al. 2021).

Chlorophyll fluorescence imaging

Chlorophyll fluorescence measurements were performed using an Imaging-PAM M-Series chlorophyll fluorometer (Heinz Walz, Germany) and ImagingWin software application (Walz) on light-adapted plants. In the absence of actinic illumination, the minimal fluorescence level of light-adapted plants (F'o) was determined. For assessment

of the maximum fluorescence yield of light-adapted plants (F'm), a saturation pulse of blue light (450 nm) with an intensity of ~2800 µmol m–2s–1 was applied for 1 s. Both fluorescence parameters were used to calculate the PSII maximum efficiency (F'v/F'm= (F'm– F'o)/F'm) (Baker 2008).

RNASeq and q-RT-PCRs

7 day-old seedlings were treated for 6h in ½ MS liquid medium with 25 µM GR24. Total RNA was extracted with on-column DNase treatment (Quiagen RNeasy Mini Kit, 74104 for RNAseq and Monarch total RNA Miniprep Kit, T2010S for q-RT-PCR). cDNA was obtained (iScript™ cDNA Synthesis Kit, 1708890) and subjected to q-RT-PCRs (Luna® Universal qPCR Master Mix, M3003S) using a Roche Lightcycler 480. The RNAseq experiments were performed by the Next Generation Sequencing Facility at Vienna BioCenter Core Facilities (VBCF), member of the Vienna BioCenter (VBC), Austria.

Microscopy

All MitoTracker and GFP-ANAC017 localization images were acquired using a Zeiss LSM800 confocal microscope, with a Plan-Apochromat 40x, NA 1.2 water objective. MitoTracker excitation 561nm and emission detection 600-700nm, GFP excitation 488nm and emission detection 500-600nm. Images were processed after imaging in Fiji ImageJ.

Bioinformatic analysis

Statistical analysis of significance was performed either in Microsoft Excel or in Graphpad Prism. Reads from RNAseq were analyzed using DESeq2 and aligned to the *Arabidopsis thaliana* TAIR10 genome. GO-terms were assigned using the PANTHER classification system. Significance of gene list overlaps was calculated in R Studio using phyper.

2.6.6 Author contribution

MG, GM and JF conceived the idea. PB performed the forward genetic screen. PV performed physical mapping. MG, CPL, RP, AP performed experiments. FVB, ON, AHM, PB supported the study with discussions, ideas and supervision. MG wrote the paper. JF supervised the work.

2.6.7 Acknowledgements

The authors thank Prof. James Whelan (Latrobe University) for providing the *ANAC017::GFP-ANAC017* line and for valuable discussion. The authors thank the Next Generation Sequencing Facility at Vienna BioCenter Core Facilities (VBCF), member of the Vienna BioCenter (VBC), Austria for performing the RNASeq experiments. This project has received funding from the European Research Council (ERC) under the European Union's Horizon 2020 research and innovation program (grant agreement No 742985). GM was supported by FWF Stand-alone Project P29988 to JF. AHM was supported by, Australian Research Council (CE140100008, FL200100057) to AHM.

2.6.8 Conflict of Interest

The authors declare no conflict of interest.

2.6.9 Figures

Figure 1 - Strigolactone effects in max2 mutant in Arabidopsis roots

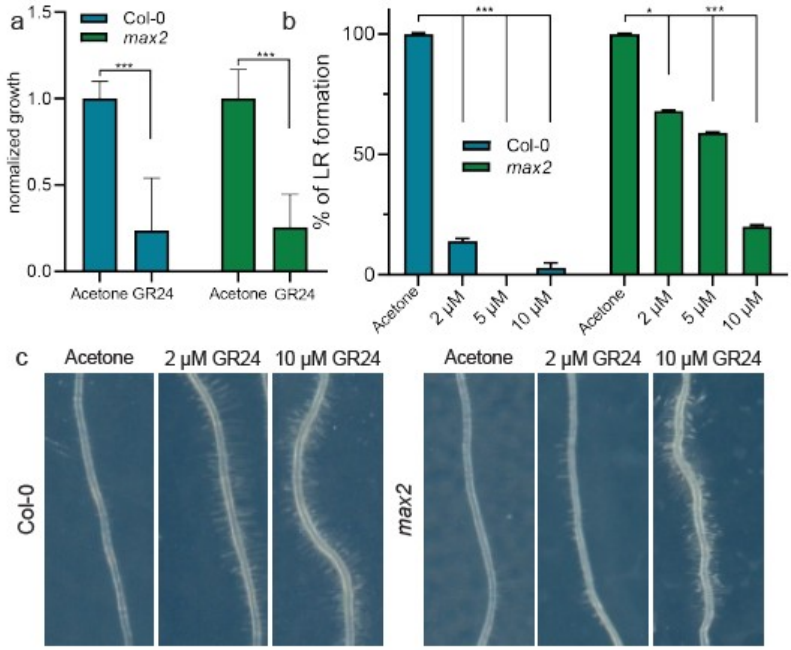

Figure 44 Section 2.6.9 - Strigolactone effects in max2 mutant in Arabidopsis roots

a. Primary root growth. 7 day old seedlings were transferred to plates containing 25 µM GR24 or Acetone. *max2* shows the same sensitivity to 25 µM GR24 as Col-0. Root growth was evaluated 48h after transfer and normalized to growth on the control condition acetone. t-test with ***P < 0.01
b. LR formation. After 14 days of growth on plates with the indicated GR24 concentration *max2* mutants show to become sensitive at 10 µM GR24 whereas Col-0 is already sensitive at 2 µM GR24. Data was normalized to LR formation on the control condition acetone. t-test with *P < 0.05; ***P < 0.01
c. Root hair formation. At a concentration of 10 µM GR24 *max2* gets sensitive and form root hairs to the same extend as Col-0. Root hair formation was evaluated 9 days after growth on with indicated GR24 concentration.

Figure 2 - *pig1* is resistant to Strigolactone in responses *max2* is sensitive

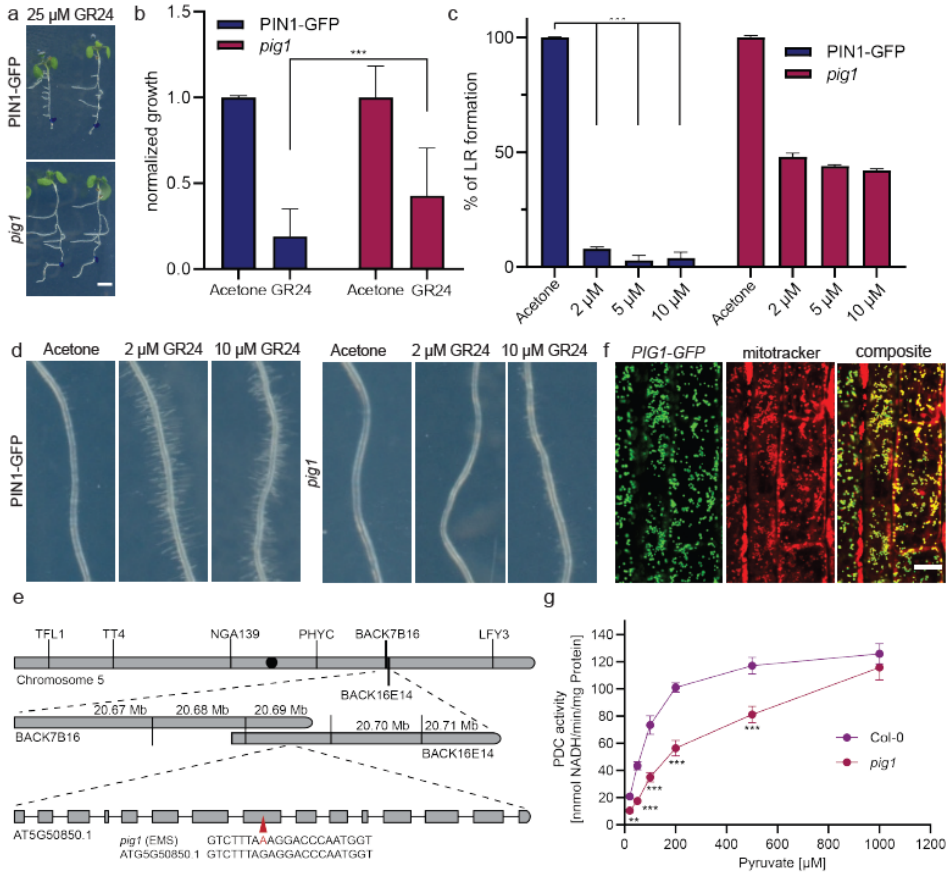

Figure 45 Section 2.6.9 - pig1 *is resistant to Strigolactone in responses* max2 *is sensitive*

a,b. Primary root growth. 7-day old seedlings were transferred to plates containing 25 µM GR24 or Acetone. *pig1* shows to maintain primary root growth when compared to the control PIN1-GFP. Root growth was evaluated 48h after transfer and normalized to growth on the control condition acetone. Scale bar: 0.1 cm, t-test with ***P < 0.01.

c. LR formation. After 14 days of growth on plates with the indicated GR24 concentration, *pig1* mutants show the same level of resistance to all GR24 concentrations whereas PIN1-GFP already becomes highly sensitive at 2 µM GR24. Data was normalized to LR formation on the control condition acetone. t-test with ***P < 0.01.

d. Root hair formation. Even at a concentration of 10 µM GR24, *pig1* still stays resistant to GR24-induced root hair formation. Root hair formation was evaluated 9 days after growth on plates with the indicated GR24 concentration.

e. Mapping of *pig1*. By a map-based cloning approach, the EMS induced mutation was identified to be localized on chromosome 5 at around 20.69 Mb in the gene AT5G50850. A single nucleotide is substituted in the *pig1* mutant.

f. Localization of PIG1-GFP. PIG1-GFP was found to be localized to the mitochondria. To confirm the localization, mitochondria were stained with MitroTracker Red. The composite image shows co-localization of the signals. Scale bar 10 µM.

g. PDC activity in isolated mitochondria. PDC in *pig1* mitochondria, which harbors a single amino acid substitution, shows significantly less activity than the one in Col-0 mitochondria at almost all pyruvate concentrations as indicated. Values are means ± standard error. **P < 0.05; ***P < 0.01.

Figure 3 - SL reduces mitochondrial activity in Col-0 but not in *pig1*

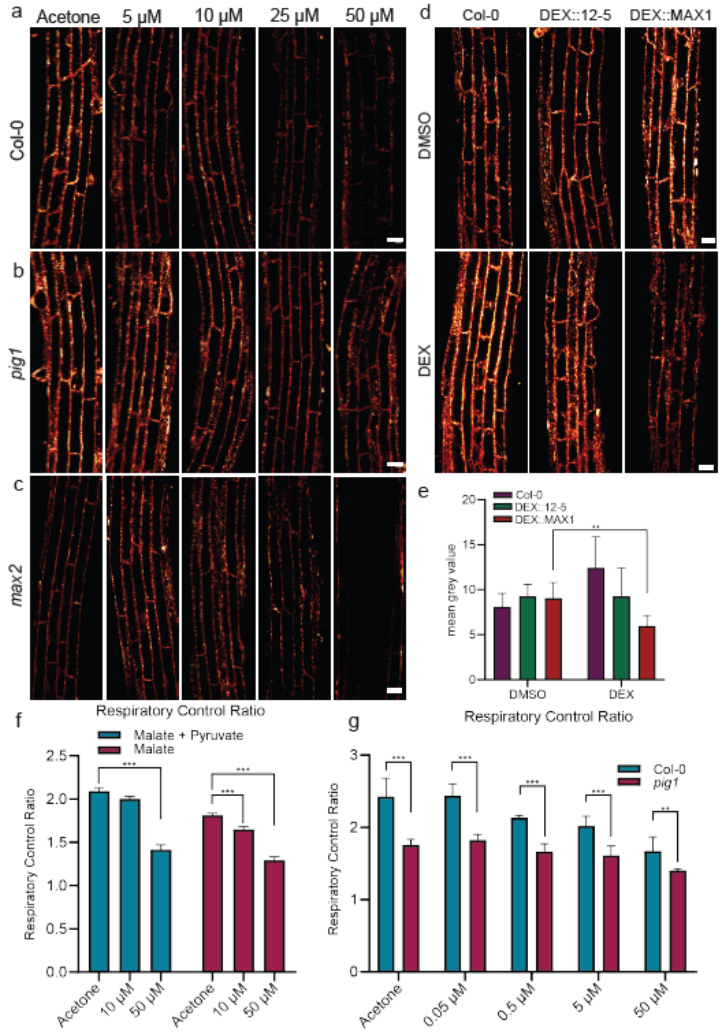

Figure 46 Section 2.6.9 - SL reduces mitochondrial activity in Col-0 but not in pig1

a-c. MitoTracker fluorescence in different mutants. 5-day-old mutant and control seedlings were treated with the indicated GR24 concentration or Acetone and stained for 30 min with 500 nM MitoTracker Red CM-H2XRos. Mitochondria in Col-0 and max2 show dramatic reduction of fluorescence with ascending GR24 concentrations whereas mitochondria in *pig1* seem to be resistant. Scale bar 20 µM.
d,e. Mitotracker fluorescence with endogenous SL. 5-day-old *DEX::MAX1*, *DEX::12-5* and Col-0 seedlings were treated with 30 µM dexamethasone for 6h to induce production of the SL biosynthesis gene *MAX1* in the line DEX::MAX1 and were then stained for 30 min with 500 nM MitoTracker. Only the dexamethasone treated line expressing MAX1 showed a reduction in fluorescence which is quantified in e. Dexamethasone treatment alone does not interfere with mitochondrial membrane potential. Scale bar 20 µM.
f. *In vitro* respiration in Col-0. The Respiratory Control Ratio of purified Col-0 mitochondria with Acetone, ascending GR24 concentrations and different substrates was measured. With both Malate + Pyruvate and Malate alone, the RCR reduced significantly upon GR24 treatment. Values are means ± standard error. **P < 0.05; ***P < 0.01.
g. *In vitro* respiration in *pig1*. The Respiratory Control Ratio of purified *pig1* mitochondria was measured with Acetone and ascending GR24 concentrations. *pig1* mitochondria show significantly reduced RCR already on the control condition Acetone and GR24 does not impose an additional effect. Values are means ± standard error. **P < 0.05; ***P < 0.01.

Figure 4 - AOX activity and metabolic aberrations in *pig1*

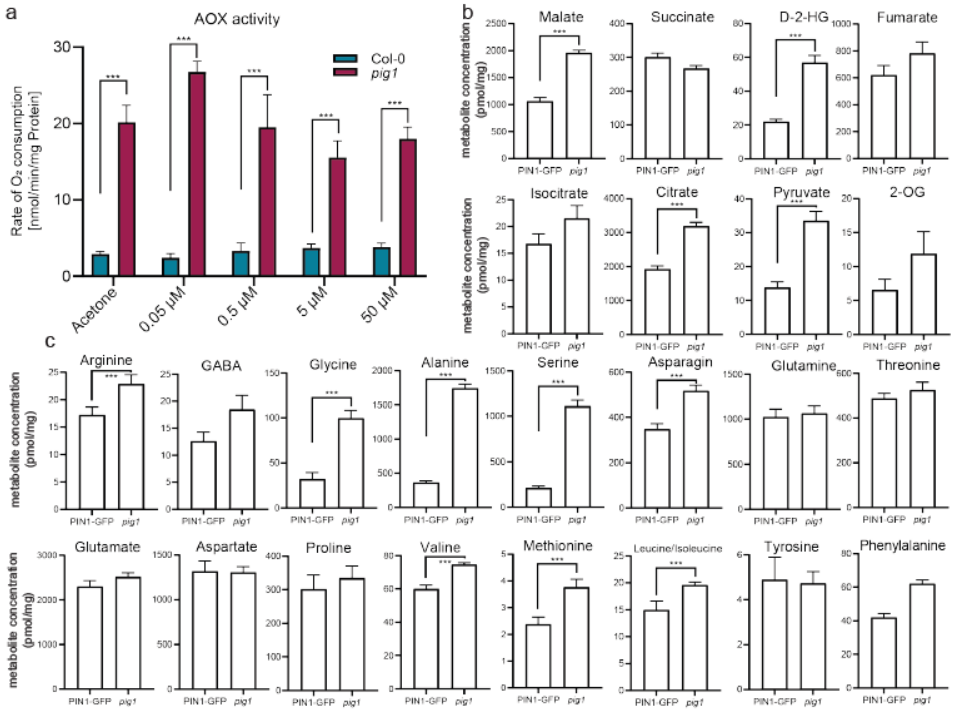

Figure 47 Section 2.6.9 - AOX activity and metabolic aberrations in pig1

a. AOX activity. The activity of alternative oxidase in *pig1* and Col-0 was measured after inhibiting the respiration chain by potassium cyanide and dithiothreitol, with acetone control and ascending GR24 concentration. GR24 alone had no significant affect AOX activity. *pig1* shows a significantly higher AOX activity in control conditions and GR24 does not impose an additional effect.
b. Mitochondrial metabolism. Levels of TCA cycle related metabolites and potential respiratory substrates were measured *in vivo* in *pig1*. The mutant shows an upwards trend in the abundance of almost all metabolites but only the increase for Malate, D-2-HG (D-2-Hydroxyglutarate), Pyruvate, Arginine, Glycine, Alanine, Serine, Asparagine, Valine, Methionine, Leucine and the sugars (see Supplemental Figure 3) is significant. Values are pmol/mg FW means ± standard error. **P < 0.05; ***P < 0.01.

Figure 5 - Transcriptomic effects of strigolactone on mitochondria dysfunction genes

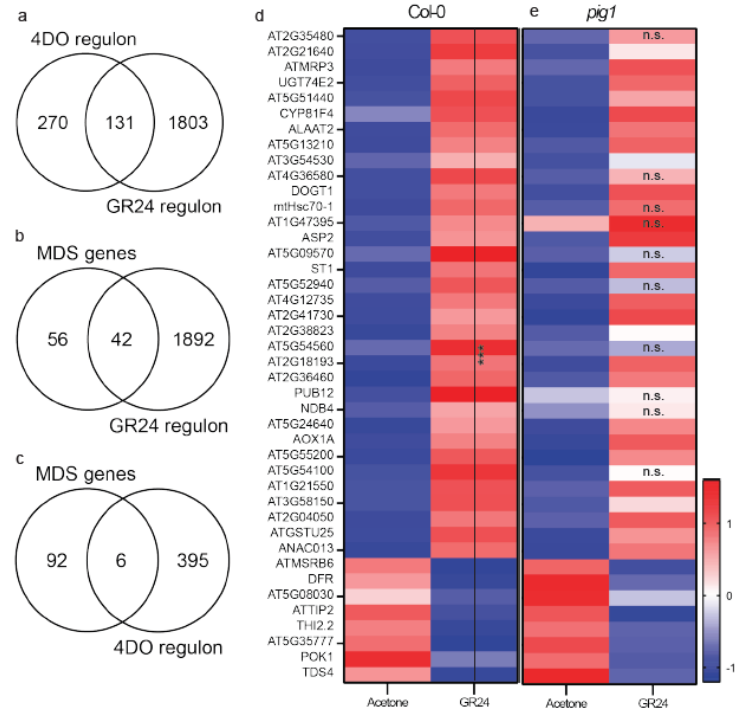

Figure 48 Section 2.6.9 - Transcriptomic effects of strigolactone on mitochondria dysfunction genes

a-c. Venn diagrams showing gene list overlaps. a. overlap between GR24 induced DEGs (first replicate from this study) with 4DO regulated genes. b. overlap between MDS genes with GR24 regulon from this study. C. overlap between MDS genes and 4DO regulon.
d,e. Heatmaps of MDS genes after GR24 treatment. d. Significantly differentially expressed MDS genes in Col-0, whereas 8 genes are downregulated and 34 are upregulated. e. Heatmap of *pig1* GR24 treated representing MDS genes which were significantly differentially regulated in Col-0 (d). 10 out of the 42 genes do not get differentially regulated in pig1 anymore. The color bar applies for d and e. In d horizontal line indicates all genes being significantly differentially regulated compared to control treatment. n.s. – not significant. Heatmaps show vst-normalized expression (variance stabilizing transformation).

Figure 6 - Strigolactone effect on transcription of auxin-regulated genes

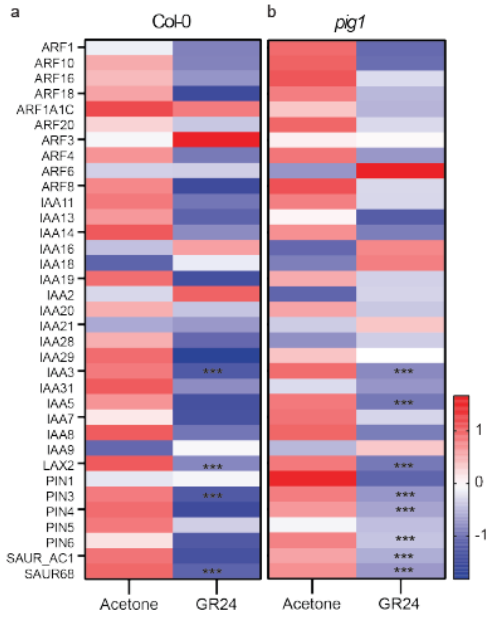

Figure 49 Section 2.6.9 - Strigolactone effect on transcription of auxin-regulated genes

a.b. Heatmaps for auxin-inducible genes inCol-0 and *pig1* after GR24 treatment. a. Differentially expressed auxin-inducible genes in Col-0. The trend goes towards downregulation after GR24 treatment with some of the analyzed genes being significantly downregulated. b. Differentially expressed auxin-inducible genes in *pig1*. In terms of magnitude, auxin-inducible genes get less severely downregulated, even though more genes are reaching significant differential regulation.

Figure 7 - Strigolactone targets WRKY and ANAC17-mediated mechanisms

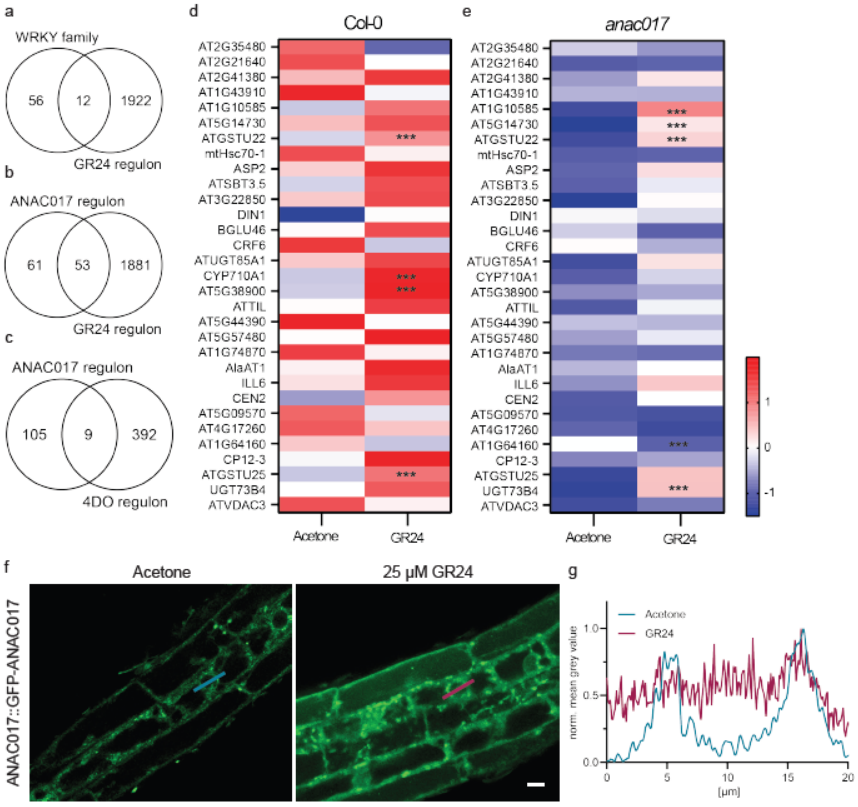

Figure 50 Section 2.6.9 - Strigolactone targets WRKY and ANAC17-mediated mechanisms

a-c. Venn diagrams showing gene list overlaps. a. Overlap between GR24 regulon from this study with WRKY family TFs. b. Overlap between GR24 regulon from this study with ANAC017 regulon. C. Overlap of 4DO regulon with ANAC017 regulon.
d,e. Heatmaps of the ANAC017 regulon after GR24 treatment. d. Differentially expressed ANAC017 regulon genes in Col-0. The trend goes towards an upregulation of this subset of genes after GR24 treatment. e. Differentially expressed ANAC017 regulon genes in *anac017* mutant. Baseline level expression is in the negative range, GR24 treatment only slightly elevates the expression, whereas most genes still remain in the negative range.
f. GR24 treatment of ANAC017::GFP-ANAC017. The N-terminal proportion of ANAC017 is no longer confined to the ER but can also be observed very strongly in the cytoplasm and the nucleus after 6h of 25 µM GR24 treatment. Scale bar 10 µM.
g. Linescans of ANAC017::GFP-ANAC017. Linescans, which are indicated in blue (acetone treatment) and magenta (GR24 treatment), were drawn through nuclei from images in e. For acetone treatment two peaks which are representing the nuclear membrane are clearly discernible whereas after GR24 no boarders are discernible anymore showing that GFP fluorescence is also observable in the nucleus.

Figure 8 - Model of non-canonical strigolactone signal perception and integration

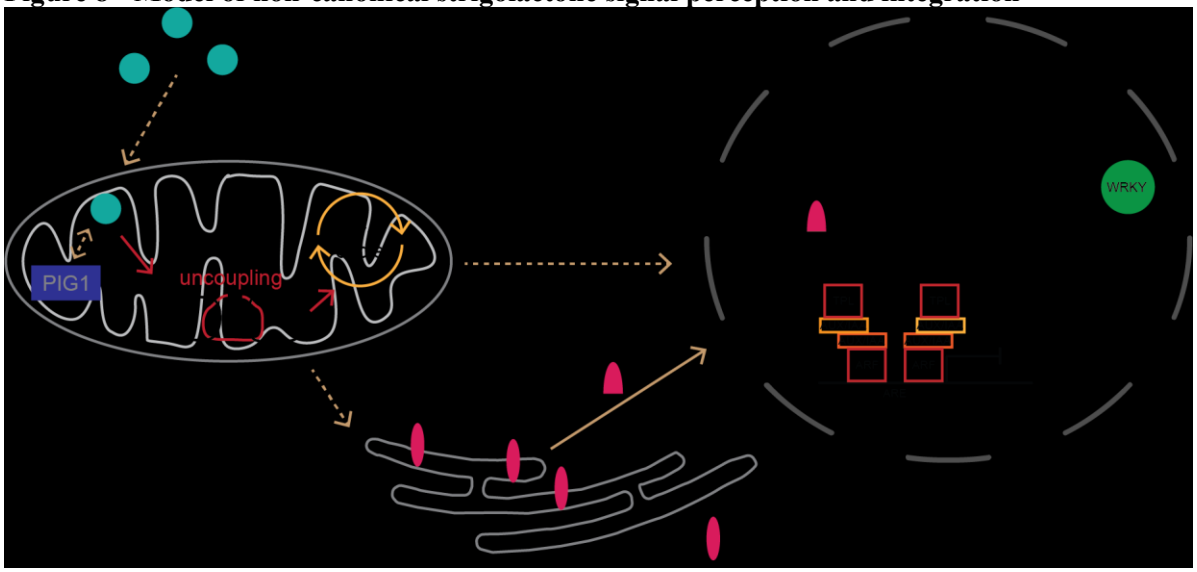

Figure 51 Section 2.6.9 - Model of non-canonical strigolactone signal perception and integration

(1) Strigolactone is perceived by the mitochondria. (2) This leads to interference with mitochondrial respiration and metabolism. (3) At the same time, mitochondria transfer information to the nucleus via the ER-localized TF ANAC017 and via other yet-to-be characterized mechanisms. (4) In the nucleus, the N-terminal fraction of ANAC017 binds to promoter regions of mitochondrial dysfunction genes and upregulates their expression. (5) Auxin-inducible genes are downregulated. The involvement of WRKY TFs remains to be elusive. Red arrows indicate interferences. Dashed lines indicate not fully explained events. Figure elements adapted and modified from Gallei et al. 2020.

2.6.10 Supplemental Figures

Supplemental Figure 1 – complementation and sequence conservation

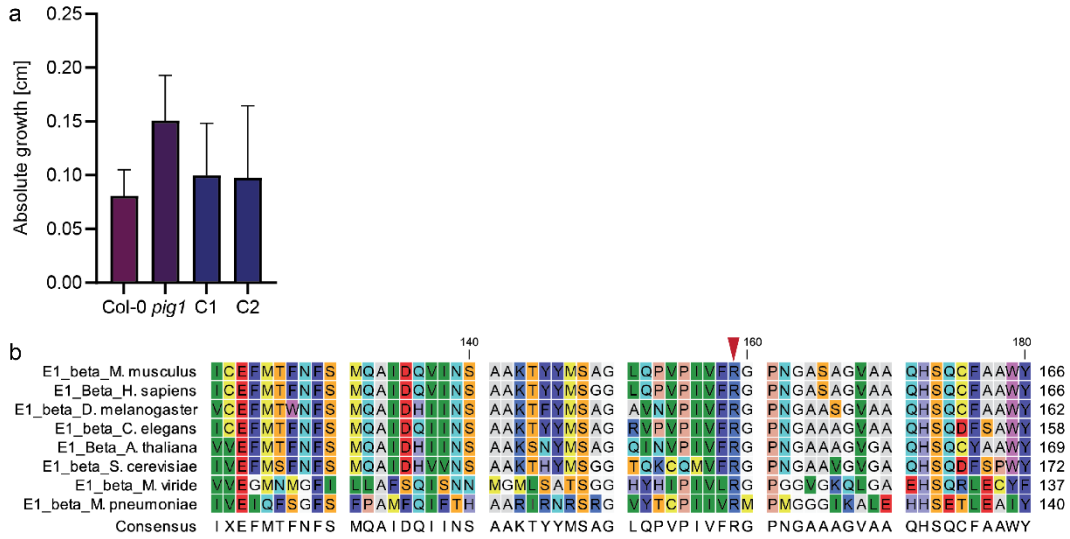

Figure 52 Section 2.6.10 - complementation and sequence conservation

a. Complementation of *pig1* phenotype. The complementation lines C1 and C2 (*pPIG1::PIG1-GFP* in *pig1*) are reverting GR24 sensitivity to WT levels.
b. PDC sequence alignment. The protein sequence of the PDC E1β-subunit from different organisms (M. musculus, H. sapiens, D. melanogaster, C. elegans, A. thaliana, S. cerevisiae, M. viride, M. pneunomiae) was aligned. The red arrowhead indicates the amino acid which is substituted in *pig1* to Lysine (K). The side is conserved in all analyzed sequences.

Supplemental Figure 2 – mitochondrial respiration

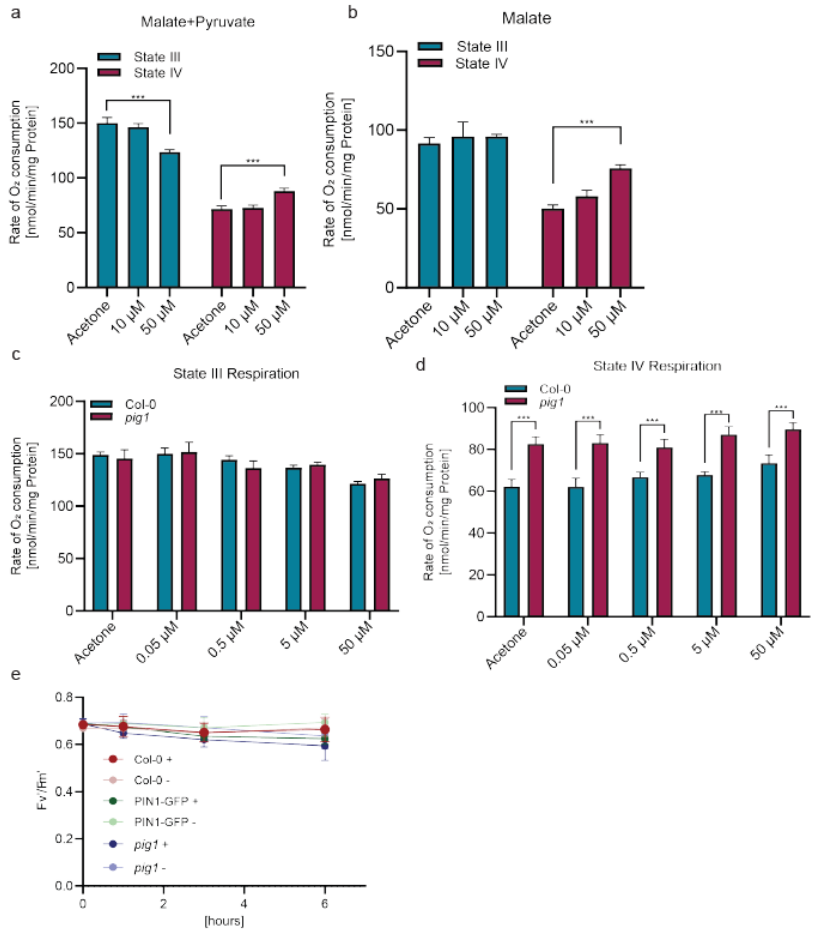

Figure 53 Section 2.6.10 - mitochondrial respiration

a. *in vitro* respiration in Col-0 with Malate + Pyruvate as substrate. State III and state IV respiration in purified Col-0 mitochondria with Acetone and ascending GR24 concentrations was measured. With the substrate Malate + Pyruvate both states of respiration are significantly affected with 50 µM GR24.
b. *in vitro* respiration in Col-0 with Malate. State III and state IV respiration in purified Col-0 mitochondria with Acetone and ascending GR24 concentrations was measured. With the substrate Malate alone only state IV respiration is significantly affected with 50 µM GR24.
c. *in vitro* state III respiration in *pig1*. State III respiration in purified *pig1* mitochondria was measured with Acetone and ascending GR24 concentrations and no significant differences were observed.
d. *in vitro* state IV respiration in *pig1*. State IV respiration in purified *pig1* mitochondria was measured with Acetone and ascending GR24 concentrations. *pig1* already shows an increase in state IV respiration in the control condition and GR24 does not impose an additional effect.
e. GR24 effect on chloroplasts. The effect of 25 µM GR24 on chloroplasts was read out by the chlorophyll fluorescence parameter photosystem II maximum efficiency (Fv'/Fm') for *pig1* and WT over 6h. There was no difference in the ratio of Fv'/Fm' with GR24 treatment in the mutant or in WT, thus chloroplasts are unlikely to be grossly affected.

Supplemental Figure 3 – sugars in *pig1*

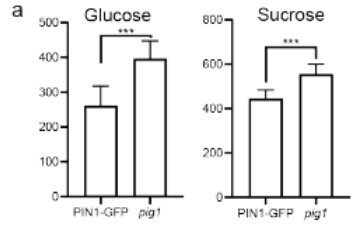

Figure 54 Section 2.6.10 – suagrs in pig1

a. Abundance of sugars in *pig1*. Glucose and sucrose abundance is increased in *pig1*. Values are pmol/mg FW means ± standard error. ***P < 0.01.

Supplemental Figure 4 – MDS genes in *pig1*

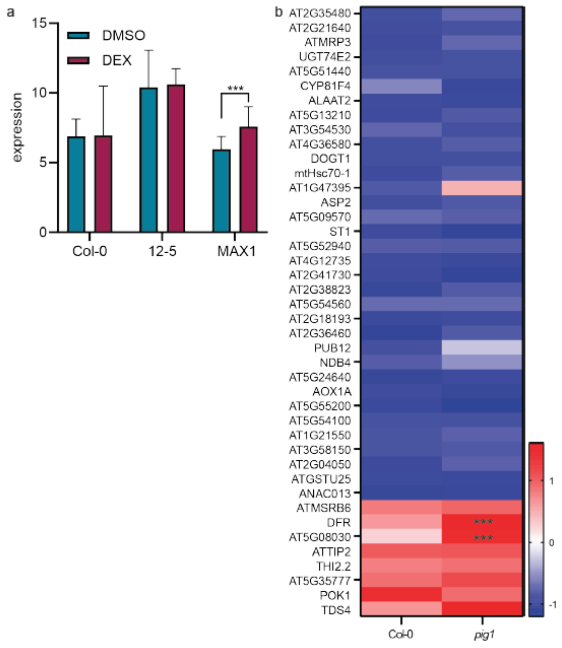

Figure 55 Section 2.6.10 – MDS genes in pig1

a. q-RT-PCR to evaluate the effect of endogenous SL on mitochondria dysfunction gene regulation. *DEX::MAX1*, *DEX::12-5* and Col-0 seedlings were treated with 30 µM dexamethasone for 6h to induce production of the SL biosynthesis gene *MAX1* in the line *DEX::MAX1*. Endogenously produced SL in the line *DEX::MAX1* lead to the significant overexpression of *AOX1a* whereas the control lines shows now response to dexamethasone treatment.
b. Heatmaps of MDS genes in untreated *pig1*. The heatmap is representing MDS genes which were significantly differentially regulated in Col-0 (Figure 5d). From the mentioned 8 GR24-induced downregulated mitochondrial dysfunction responsive genes in Col-0, 7 of them are upregulated in untreated *pig1*.

Supplemental Figure 5 – *anac017* after GR24 treatment

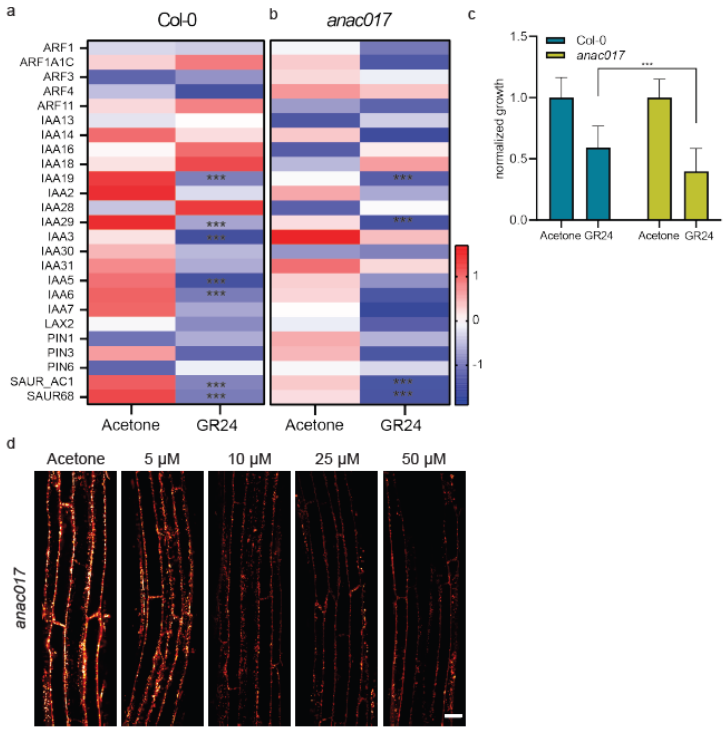

Figure 56 Section 2.6.10 - anac017 *after GR24 treatment*

a.b Heatmaps for auxin-inducible genes after GR24 treatment. a. Differentially expressed auxin-inducible genes in Col-0 (second replicate of this study). The trend goes towards downregulation after GR24 treatment with many of the analyzed genes being significantly downregulated. b. Differentially expressed auxin-inducible genes in *anac017*. The downregulation of the genes after GR24 treatment in the mutant still happens, even though with a slightly reduced magnitude compared to Col-0.
c. Primary root growth. 7 day old seedlings were transferred to plates containing 25 µM GR24 or Acetone. *anac017* shows significantly more sensitivity to 25 µM GR24 as Col-0. Root growth was evaluated 48h after transfer and normalized to growth on the control condition acetone. , t-test with ***P < 0.01.
d. MitoTracker florescence in different mutants. 5-day-old *anac017* seedlings were treated with the indicated GR24 concentration or Acetone and stained for 30 min with 500 nM MitoTracker Red CM-H2XRos. Mitochondria in *anac017* show dramatic reduction of fluorescence with ascending GR24 concentrations. The reduction in fluorescence is comparable to what was observed for Col-0 (Figure 3a). Scale bar 10 µM.

2.6.11 References

1. Abe, Satoko, Aika Sado, Kai Tanaka, Takaya Kisugi, Kei Asami, Saeko Ota, Hyun Il Kim, et al. 2014. "Carlactone Is Converted to Carlactonoic Acid by MAX1 in Arabidopsis and Its Methyl Ester Can Directly Interact with AtD14 in Vitro." *Proceedings of the National Academy of Sciences of the United States of America* 111 (50): 18084–89. https://doi.org/10.1073/pnas.1410801111.
2. Agusti, Javier, Silvia Herold, Martina Schwarz, Pablo Sanchez, Karin Ljung, Elizabeth A. Dun, Philip B. Brewer, et al. 2011. "Strigolactone Signaling Is Required for Auxin-Dependent Stimulation of Secondary Growth in Plants." *Proceedings of the National Academy of Sciences of the United States of America* 108 (50): 20242–47. https://doi.org/10.1073/pnas.1111902108.
3. Aken, Olivier van, Inge de Clercq, Aneta Ivanova, Simon R. Law, Frank van Breusegem, A. Harvey Millar, and James Whelan. 2016. "Mitochondrial and Chloroplast Stress Responses Are Modulated in Distinct Touch and Chemical Inhibition Phases." *Plant Physiology* 171 (3): 2150–65. https://doi.org/10.1104/pp.16.00273.
4. Aken, Olivier Van, Ethan Ford, Ryan Lister, Shaobai Huang, and A. Harvey Millar. 2016. "Retrograde Signalling Caused by Heritable Mitochondrial Dysfunction Is Partially Mediated by ANAC017 and Improves Plant Performance." *Plant Journal* 88 (4): 542–58. https://doi.org/10.1111/tpj.13276.
5. Aken, Olivier Van, Tamara Pečenková, Brigitte Van De Cotte, Riet De Rycke, Dominique Eeckhout, Hillel Fromm, Geert De Jaeger, et al. 2007. "Mitochondrial Type-I Prohibitins of Arabidopsis Thaliana Are Required for Supporting Proficient Meristem Development." *Plant Journal* 52 (5): 850–64. https://doi.org/10.1111/j.1365-313X.2007.03276.x.
6. Aken, Olivier Van, and James Whelan. 2012. "Comparison of Transcriptional Changes to Chloroplast and Mitochondrial Perturbations Reveals Common and Specific Responses in Arabidopsi." *Frontiers in Plant Science* 3 (DEC): 1–18. https://doi.org/10.3389/fpls.2012.00281.
7. Aken, Olivier Van, Botao Zhang, Simon Law, Reena Narsai, and James Whelan. 2013. "AtWRKY40 and AtWRKY63 Modulate the Expression of Stress-Responsive Nuclear Genes Encoding Mitochondrial and Chloroplast Proteins." *Plant Physiology* 162 (1): 254–71. https://doi.org/10.1104/pp.113.215996.
8. Akiyama, Kohki, Ken Ichi Matsuzaki, and Hideo Hayashi. 2005. "Plant Sesquiterpenes Induce Hyphal Branching in Arbuscular Mycorrhizal Fungi." *Nature* 435 (7043): 824–27. https://doi.org/10.1038/nature03608.
9. Belmondo, S., R. Marschall, P. Tudzynski, J. A. López Ráez, E. Artuso, C. Prandi, and L. Lanfranco. 2017. "Identification of Genes Involved in Fungal Responses to Strigolactones Using Mutants from Fungal Pathogens." *Current Genetics* 63 (2): 201–13. https://doi.org/10.1007/s00294-016-0626-y.
10. Belt, Katharina, Shaobai Huang, Louise F. Thatcher, Hayley Casarotto, Karam B. Singh, Olivier Van Aken, and A. Harvey Millar. 2017. "Salicylic Acid-Dependent Plant Stress Signaling via Mitochondrial Succinate Dehydrogenase." *Plant Physiology* 173 (4): 2029–40. https://doi.org/10.1104/pp.16.00060.
11. Berkowitz, Oliver, Inge De Clercq, Frank Van Breusegem, and James Whelan. 2016. "Interaction between Hormonal and Mitochondrial Signalling during Growth, Development and in Plant Defence Responses." *Plant Cell and Environment* 39 (5): 1127–39. https://doi.org/10.1111/pce.12712.
12. Besserer, Arnaud, Guillaume Bécard, Alain Jauneau, Christophe Roux, and Nathalie Séjalon-Delmas. 2008. "GR24, a Synthetic Analog of Strigolactones, Stimulates the Mitosis and Growth of the Arbuscular Mycorrhizal Fungus Gigaspora Rosea by Boosting Its Energy Metabolism." *Plant Physiology* 148 (1): 402–13. https://doi.org/10.1104/pp.108.121400.
13. Brand, Martin D., and David G. Nicholls. 2011. "Assessing Mitochondrial Dysfunction in Cells." *Biochemical Journal* 435 (2): 297–312. https://doi.org/10.1042/BJ20110162.
14. Carbonnel, Samy, Salar Torabi, and Caroline Gutjahr. 2021. "MAX2-Independent Transcriptional Responses to Rac-GR24 in Lotus Japonicus Roots." *Plant Signaling and Behavior* 16 (1). https://doi.org/10.1080/15592324.2020.1840852.

15. Clercq, Inge De, Vanessa Vermeirssen, Olivier Van Aken, Klaas Vandepoele, Monika W. Murcha, Simon R. Law, Annelies Inzé, et al. 2013. “The Membrane-Bound NAC Transcription Factor ANAC013 Functions in Mitochondrial Retrograde Regulation of the Oxidative Stress Response in Arabidopsis.” *Plant Cell* 25 (9): 3472–90. https://doi.org/10.1105/tpc.113.117168.
16. Cook, C. E., Leona P. Whichard, Beverly Turner, and Monroe E. Wall. 1966. “Germination of Witchweed (Striga Lutea Lour .): Isolation and Properties of a Potent Stimulant Author (s): C . E . Cook , Leona P . Whichard , Beverly Turner , Monroe E . Wall and Grant H . Egley Published by : American Association for the Advancement.” *Science* 154 (3753): 1189–90.
17. Crawford, Scott, Naoki Shinohara, Tobias Sieberer, Lisa Williamson, Gilu George, Jo Hepworth, Dörte Müller, Malgorzata A. Domagalska, and Ottoline Leyser. 2010. “Strigolactones Enhance Competition between Shoot Branches by Dampening Auxin Transport.” *Development* 137 (17): 2905–13. https://doi.org/10.1242/dev.051987.
18. Gleason, Cynthia, Shaobai Huang, Louise F. Thatcher, Rhonda C. Foley, Carol R. Anderson, Adam J. Carroll, A. Harvey Millar, and Karam B. Singh. 2011. “Mitochondrial Complex II Has a Key Role in Mitochondrial-Derived Reactive Oxygen Species Influence on Plant Stress Gene Regulation and Defense.” *Proceedings of the National Academy of Sciences of the United States of America* 108 (26): 10768–73. https://doi.org/10.1073/pnas.1016060108.
19. Gomez-Roldan, Victoria, Soraya Fermas, Philip B. Brewer, Virginie Puech-Pagès, Elizabeth A. Dun, Jean Paul Pillot, Fabien Letisse, et al. 2008. “Strigolactone Inhibition of Shoot Branching.” *Nature* 455 (7210): 189–94. https://doi.org/10.1038/nature07271.
20. Hasan, Mohammed Nihal, Hani Choudhry, Syed Shoeb Razvi, Said Salama Moselhy, Taha Abduallah Kumosani, Mazin A. Zamzami, Ziad Omran, et al. 2018. “Synthetic Strigolactone Analogues Reveal Anti-Cancer Activities on Hepatocellular Carcinoma Cells.” *Bioorganic and Medicinal Chemistry Letters* 28 (6): 1077–83. https://doi.org/10.1016/j.bmcl.2018.02.016.
21. Ivanova, Aneta, Simon R. Law, Reena Narsai, Owen Duncan, Jae Hoon Lee, Botao Zhang, Olivier Van Aken, et al. 2014. “A Functional Antagonistic Relationship between Auxin and Mitochondrial Retrograde Signaling Regulates Alternative Oxidase1a Expression in Arabidopsis.” *Plant Physiology* 165 (3): 1233–54. https://doi.org/10.1104/pp.114.237495.
22. Jayawardhane, Jayamini, Devin W. Cochrane, Poorva Vyas, Natalia V. Bykova, Greg C. Vanlerberghe, and Abir U. Igamberdiev. 2020. “Roles for Plant Mitochondrial Alternative Oxidase Under Normoxia, Hypoxia, and Reoxygenation Conditions.” *Frontiers in Plant Science* 11 (May). https://doi.org/10.3389/fpls.2020.00566.
23. Jia, Kun Peng, Qian Luo, Sheng Bo He, Xue Dan Lu, and Hong Quan Yang. 2014. “Strigolactone-Regulated Hypocotyl Elongation Is Dependent on Cryptochrome and Phytochrome Signaling Pathways in Arabidopsis.” *Molecular Plant* 7 (3): 528–40. https://doi.org/10.1093/mp/sst093.
24. Kacprzak, Sylwia M., Anton Dahlqvist, and Olivier Van Aken. 2020. “The Transcription Factor ANAC017 Is a Key Regulator of Mitochondrial Proteotoxic Stress Responses in Plants.” *Philosophical Transactions of the Royal Society B: Biological Sciences* 375 (1801). https://doi.org/10.1098/rstb.2019.0411.
25. Kerchev, Pavel Ivanov, Inge De Clercq, Jordi Denecker, Per Mühlenbock, Robert Kumpf, Long Nguyen, Dominique Audenaert, Wim Dejonghe, and Frank Van Breusegem. 2014. “Mitochondrial Perturbation Negatively Affects Auxin Signaling.” *Molecular Plant* 7 (7): 1138–50. https://doi.org/10.1093/mp/ssu071.
26. Koltai, Hinanit. 2015. “Cellular Events of Strigolactone Signalling and Their Crosstalk with Auxin in Roots.” *Journal of Experimental Botany* 66 (16): 4855–61. https://doi.org/10.1093/jxb/erv178.
27. Leclere, Sherry, Rebekah A Rampey, and Bonnie Bartel. 2004. “IAR4 , a Gene Required for Auxin Conjugate Sensitivity in Arabidopsis , Encodes a Pyruvate Dehydrogenase” 135 (June): 989–99. https://doi.org/10.1104/pp.104.040519.1.
28. Lernmark, Ulrika, and Per Gardestrom. 1994. “Distribution of Pyruvate Dehydrogenase Complex Activities between Chloroplasts and Mitochondria from Leaves of Different Species Author (s): Ulrika Lernmark and Per Gardeström Stable URL : Https://Www.Jstor.Org/Stable/4276242 Linked References Are Avail” 106 (4): 1633–38.

29. Li, Chun Long, Mei Wang, Xiao Yan Ma, and Wei Zhang. 2014. “NRGA1, a Putative Mitochondrial Pyruvate Carrier, Mediates ABA Regulation of Guard Cell Ion Channels and Drought Stress Responses in Arabidopsis.” *Molecular Plant* 7 (10): 1508–21. https://doi.org/10.1093/mp/ssu061.
30. Liao, Yangwenke, Miaoying Tian, Huan Zhang, Xin Li, Yu Wang, Xiaojian Xia, Jie Zhou, et al. 2015. “Salicylic Acid Binding of Mitochondrial Alpha-Ketoglutarate Dehydrogenase E2 Affects Mitochondrial Oxidative Phosphorylation and Electron Transport Chain Components and Plays a Role in Basal Defense against Tobacco Mosaic Virus in Tomato.” *New Phytologist* 205 (3): 1296–1307. https://doi.org/10.1111/nph.13137.
31. Martin Jastroch, Ajit S. Divakaruni, Shona Mookerjee, Jason R. Treberg, and Martin D. Brand, Jason R Treberg, and D Martin. 2010. “Mitochondrial Proton and Electron Leaks Oxygen Consumption and PH Data.” *Essays Biochem* ., 53–67. https://doi.org/10.1042/bse0470053.Mitochondrial.
32. Mashiguchi, Kiyoshi, Eriko Sasaki, Yukihisa Shimada, Miyu Nagae, Kotomi Ueno, Takeshi Nakano, Koichi Yoneyama, Yoshihito Suzuki, and Tadao Asami. 2009. “Feedback-Regulation of Strigolactone Biosynthetic Genes and Strigolactone-Regulated Genes in Arabidopsis.” *Bioscience, Biotechnology and Biochemistry* 73 (11): 2460–65. https://doi.org/10.1271/bbb.90443.
33. Millar, A. Harvey, James Whelan, Kathleen L. Soole, and David A. Day. 2011. “Organization and Regulation of Mitochondrial Respiration in Plants.” *Annual Review of Plant Biology* 62: 79–104. https://doi.org/10.1146/annurev-arplant-042110-103857.
34. Mozes, Chen, and Michael M. Meijler. 2020. “Modulation of Bacterial Quorum Sensing by Strigolactones.” *ACS Chemical Biology* 15 (8): 2055–59. https://doi.org/10.1021/acschembio.0c00509.
35. Ng, Sophia, Aneta Ivanova, Owen Duncan, Simon R. Law, Olivier Van Aken, Inge De Clercq, Yan Wang, et al. 2013. “A Membrane-Bound NAC Transcription Factor, ANAC017, Mediates Mitochondrial Retrograde Signaling in Arabidopsis.” *Plant Cell* 25 (9): 3450–71. https://doi.org/10.1105/tpc.113.113985.
36. Norman, Christel, Katharine A. Howell, A. Harvey Millar, James M. Whelan, and David A. Day. 2004. “Salicylic Acid Is an Uncoupler and Inhibitor of Mitochondrial Electron Transport.” *Plant Physiology* 134 (1): 492–501. https://doi.org/10.1104/pp.103.031039.
37. Ohbayashi, Iwai, Shaobai Huang, Hidehiro Fukaki, Xiaomin Song, Song Sun, Miyo Terao Morita, Masao Tasaka, A. Harvey Millar, and Masahiko Furutani. 2019. “Mitochondrial Pyruvate Dehydrogenase Contributes to Auxin-Regulated Organ Development.” *Plant Physiology* 180 (2): 896–909. https://doi.org/10.1104/pp.18.01460.
38. Proust, Hélène, Beate Hoffmann, Xiaonan Xie, Kaori Yoneyama, Didier G. Schaefer, Koichi Yoneyama, Fabien Nogué, and Catherine Rameau. 2011. “Strigolactones Regulate Protonema Branching and Act as a Quorum Sensing-like Signal in the Moss Physcomitrella Patens.” *Development* 138 (8): 1531–39. https://doi.org/10.1242/dev.058495.
39. Quint, Marcel, Lana S Barkawi, Kai-ting Fan, Jerry D Cohen, and William M Gray. 2009. “Arabidopsis IAR4 Modulates Auxin Response By” 150 (June): 748–58. https://doi.org/10.1104/pp.109.136671.
40. Rasmussen, Amanda, Michael Glenn Mason, Carolien de Cuyper, Philip B. Brewer, Silvia Herold, Javier Agusti, Danny Geelen, et al. 2012. “Strigolactones Suppress Adventitious Rooting in Arabidopsis and Pea.” *Plant Physiology* 158 (4): 1976–87. https://doi.org/10.1104/pp.111.187104.
41. Ruyter-Spira, Carolien, Wouter Kohlen, Tatsiana Charnikhova, Arjan van Zeijl, Laura van Bezouwen, Norbert de Ruijter, Catarina Cardoso, et al. 2011. “Physiological Effects of the Synthetic Strigolactone Analog GR24 on Root System Architecture in Arabidopsis: Another Belowground Role for Strigolactones?” *Plant Physiology* 155 (2): 721–34. https://doi.org/10.1104/pp.110.166645.
42. Sang, Dajun, Dongqin Chen, Guifu Liu, Yan Liang, Linzhou Huang, Xiangbing Meng, Jinfang Chu, et al. 2014. “Strigolactones Regulate Rice Tiller Angle by Attenuating Shoot Gravitropism through Inhibiting Auxin Biosynthesis.” *Proceedings of the National Academy of Sciences of the United States of America* 111 (30): 11199–204. https://doi.org/10.1073/pnas.1411859111.

43. Schwarzländer, Markus, Ann Christine König, Lee J. Sweetlove, and Iris Finkemeier. 2012. "The Impact of Impaired Mitochondrial Function on Retrograde Signalling: A Meta-Analysis of Transcriptomic Responses." *Journal of Experimental Botany* 63 (4): 1735–50. https://doi.org/10.1093/jxb/err374.
44. Shinohara, Naoki, Catherine Taylor, and Ottoline Leyser. 2013. "Strigolactone Can Promote or Inhibit Shoot Branching by Triggering Rapid Depletion of the Auxin Efflux Protein PIN1 from the Plasma Membrane." *PLoS Biology* 11 (1). https://doi.org/10.1371/journal.pbio.1001474.
45. Spartz, Angela K., and William M. Gray. 2008. "Plant Hormone Receptors: New Perceptions." *Genes and Development* 22 (16): 2139–48. https://doi.org/10.1101/gad.1693208.
46. Steinwand, Blaire J, Shouling Xu, Joanna K Polko, Stephanie M Doctor, Mike Westafer, and Joseph J Kieber. 2014. "Alterations in Auxin Homeostasis Suppress Defects in Cell Wall Function" 9 (5). https://doi.org/10.1371/journal.pone.0098193.
47. Tanaka, Hirokazu, Saeko Kitakura, Riet De Rycke, Ruth De Groodt, and Jiří Friml. 2009. "Fluorescence Imaging-Based Screen Identifies ARF GEF Component of Early Endosomal Trafficking." *Current Biology* 19 (5): 391–97. https://doi.org/10.1016/j.cub.2009.01.057.
48. Tsuchiya, Yuichiro, Danielle Vidaurre, Shigeo Toh, Atsushi Hanada, Eiji Nambara, Yuji Kamiya, Shinjiro Yamaguchi, and Peter McCourt. 2010. "A Small-Molecule Screen Identifies New Functions for the Plant Hormone Strigolactone." *Nature Chemical Biology* 6 (10): 741–49. https://doi.org/10.1038/nchembio.435.
49. Vanderauwera, Sandy, Korneel Vandenbroucke, Annelies Inzé, Brigitte Van De Cotte, Per Mühlenbock, Riet De Rycke, Naïra Naouar, Tim Van Gaever, Marc C.E. Van Montagu, and Frank Van Breusegem. 2012. "AtWRKY15 Perturbation Abolishes the Mitochondrial Stress Response That Steers Osmotic Stress Tolerance in Arabidopsis." *Proceedings of the National Academy of Sciences of the United States of America* 109 (49): 20113–18. https://doi.org/10.1073/pnas.1217516109.
50. Vanlerberghe, Greg C. 2013. "Alternative Oxidase: A Mitochondrial Respiratory Pathway to Maintain Metabolic and Signaling Homeostasis during Abiotic and Biotic Stress in Plants." *International Journal of Molecular Sciences* 14 (4): 6805–47. https://doi.org/10.3390/ijms14046805.
51. Vismans, Gilles, Tom van der Meer, Olivier Langevoort, Marielle Schreuder, Harro Bouwmeester, Helga Peisker, Peter Dörman, Tijs Ketelaar, and Alexander van der Krol. 2016. "Low-Phosphate Induction of Plastidal Stromules Is Dependent on Strigolactones but Not on the Canonical Strigolactone Signaling Component MAX2." *Plant Physiology* 172 (4): 2235–44. https://doi.org/10.1104/pp.16.01146.
52. Waldie, Tanya, Hayley McCulloch, and Ottoline Leyser. 2014. "Strigolactones and the Control of Plant Development: Lessons from Shoot Branching." *Plant Journal* 79 (4): 607–22. https://doi.org/10.1111/tpj.12488.
53. Wang, Chunyang, Yang Liu, Si-shen Li, and Guan-zhu Han. 2015. "Insights into the Origin and Evolution of the Plant Hormone Signaling Machinery 1" 167 (March): 872–86. https://doi.org/10.1104/pp.114.247403.
54. Wang, Lei, Bing Wang, Hong Yu, Hongyan Guo, Tao Lin, Liquan Kou, Anqi Wang, et al. 2020. "Transcriptional Regulation of Strigolactone Signalling in Arabidopsis." *Nature* 583 (7815): 277–81. https://doi.org/10.1038/s41586-020-2382-x.
55. Yao, Ruifeng, Zhenhua Ming, Liming Yan, Suhua Li, Fei Wang, Sui Ma, Caiting Yu, et al. 2016. "DWARF14 Is a Non-Canonical Hormone Receptor for Strigolactone." *Nature* 536 (7617): 469–73. https://doi.org/10.1038/nature19073.
56. Zhang, Jing, Ewa Mazur, Jozef Balla, Michelle Gallei, Petr Kalousek, Zuzana Medveďová, Yang Li, et al. 2020. "Strigolactones Inhibit Auxin Feedback on PIN-Dependent Auxin Transport Canalization." *Nature Communications* 11 (1). https://doi.org/10.1038/s41467-020-17252-y

3. Conclusions

This study provides a comprehensive overview over auxin non-canonical signalling in the form of two reviews presenting most recent discoveries in the field with state-of-the-art methods used to decipher the signalling. However as mentioned in Li et al. 2021 (see Apendix) some outstanding questions still remain about non-canonical auxin signalling. To name a few it still remains enigmatic how exactly the molecular mechanism of auxin-triggered H+ influx for root growth inhibition works, how the non-transcriptional AFBs/TIR1 signaling branch looks like, if cytosolic and nuclear fractions of TIR1/AFBs mediate distinct functions or how the TMK pathway perceives auxin. In terms of the last question the work of Friml et al. 2022, also presented in this thesis, sheds light into the TMK-mediated auxin signalling, support a role of ABP1-TMK1 in cell surface auxin perception mediating global auxin phospho-response and regenerative development. Nevertheless the exact mechniasm of how TMKs can perceive the auxin signal still awaits further detailed characterization.

Another work presented in this thesis, Narasimhan et al. 2021, identified auxin effect on rapid endocytosis of PIN2 protein. Long-term, auxin-mediated PIN2 degradation depends on the TIR1/AFB mediated signalling but faster responses seem to be independent of the canonical signaling. As mentioned in the introduction in Gallei et al. 2020 it has been shown that TIR1/AFB components, mediate also a non-transcriptional rapid regulation of root growth. Thus it might be possible that rapid PIN2 endocytosis and degradation are also mediated by the TIR1/AFB mechanism, however in a non-canonical way. Figuring out the involvement of the canonical components in a rapid response like the one of PIN2 endocytosis could answer the outstanding question if cytosolic and nuclear TIR1/AFBs mediate distinct functions or work in the same pathways.

Lastly this thesis shows identification of non-canonical strigolactone signalling and its crosstalk with auxin signalling and canalization. As presented in Zhang et al. 2020 strigolactones inhibit essentially all processes of auxin canalization. This could be explained by the downregulation of auxin-mediated genes by strigolactone presented in Gallei et al. 2022. Downregulating auxin-regulated genes over long-term could lead to the block of auxin canalization processes. This implicates that the newly identified non-canonical SL signalling interferes or crosstalks with canonical MAX2 and D14 dependent canonical SL signalling at least to some extend as it was shown that SL-mediated interference with canalization happends downstreams of those components. Furhter work should identify the overlap of canonical and non-canonical SL signalling.

4. Additional References

References used in the introduction and result and discussion sections.

1. Adamowski, Maciek, and Jiří Friml. 2015. "PIN-Dependent Auxin Transport: Action, Regulation, and Evolution." The Plant Cell Online 27 (1): 20–32. https://doi.org/10.1105/tpc.114.134874.
2. Agusti, Javier, Silvia Herold, Martina Schwarz, Pablo Sanchez, Karin Ljung, Elizabeth A. Dun, Philip B. Brewer, et al. 2011. "Strigolactone Signaling Is Required for Auxin-Dependent Stimulation of Secondary Growth in Plants." Proceedings of the National Academy of Sciences of the United States of America 108 (50): 20242–47. https://doi.org/10.1073/pnas.1111902108.
3. Akiyama, Kohki, Ken Ichi Matsuzaki, and Hideo Hayashi. 2005. "Plant Sesquiterpenes Induce Hyphal Branching in Arbuscular Mycorrhizal Fungi." Nature 435 (7043): 824–27. https://doi.org/10.1038/nature03608.
4. Badescu, George O., and Richard M. Napier. 2006. "Receptors for Auxin: Will It All End in TIRs?" Trends in Plant Science 11 (5): 217–23. https://doi.org/10.1016/j.tplants.2006.03.001.
5. Balla, Jozef, Petr Kalousek, Vilém Reinöhl, Jiåí Friml, and Stanislav Procházka. 2011. "Competitive Canalization of PIN-Dependent Auxin Flow from Axillary Buds Controls Pea Bud Outgrowth." Plant Journal 65 (4): 571–77. https://doi.org/10.1111/j.1365-313X.2010.04443.x.
6. Benkova, Eva, Marta Michniewicz, Michael Sauer, Thomas Teichmann, and Molekularbiologie Der Pflanzen. 2003. "Local , Efflux-Dependent Auxin Gradients as a Common Module for Plant Organ Formation" 115: 591–602.
7. Bohn-Courseau, Isabelle. 2010. "Auxin: A Major Regulator of Organogenesis." Comptes Rendus - Biologies 333 (4): 290–96. https://doi.org/10.1016/j.crvi.2010.01.004.
8. Carbonnel, Samy, Salar Torabi, and Caroline Gutjahr. 2021. "MAX2-Independent Transcriptional Responses to Rac-GR24 in Lotus Japonicus Roots." Plant Signaling and Behavior 16 (1). https://doi.org/10.1080/15592324.2020.1840852.
9. Cook, C. E., Leona P. Whichard, Beverly Turner, and Monroe E. Wall. 1966. "Germination of Witchweed (Striga Lutea Lour .): Isolation and Properties of a Potent Stimulant Author (s): C . E . Cook , Leona P . Whichard , Beverly Turner , Monroe E . Wall and Grant H . Egley Published by : American Association for the Advancement." Science 154 (3753): 1189–90.
10. Crawford, Scott, Naoki Shinohara, Tobias Sieberer, Lisa Williamson, Gilu George, Jo Hepworth, Dörte Müller, Malgorzata A. Domagalska, and Ottoline Leyser. 2010. "Strigolactones Enhance Competition between Shoot Branches by Dampening Auxin Transport." Development 137 (17): 2905–13. https://doi.org/10.1242/dev.051987.
11. Dai, Ning, Wuyi Wang, Sara E Patterson, and Anthony B Bleecker. 2013. "The TMK Subfamily of Receptor-Like Kinases in Arabidopsis Display an Essential Role in Growth and a Reduced Sensitivity to Auxin" 8 (4): 1–12. https://doi.org/10.1371/journal.pone.0060990.
12. Darwin C., The power of movement in plants, 1880, London John Murray Publishers
13. Dhonukshe, Pankaj, Fernando Aniento, Inhwan Hwang, David G. Robinson, Jozef Mravec, York Dieter Stierhof, and Jiří Friml. 2007. "Clathrin-Mediated Constitutive Endocytosis of PIN Auxin Efflux Carriers in Arabidopsis." Current Biology 17 (6): 520–27. https://doi.org/10.1016/j.cub.2007.01.052.
14. Dhonukshe, Pankaj, Fernando Aniento, Inhwan Hwang, David G Robinson, and Jozef Mravec. 2007. "Report Clathrin-Mediated Constitutive Endocytosis of PIN Auxin Efflux Carriers in Arabidopsis," 1–8. https://doi.org/10.1016/j.cub.2007.01.052.
15. Du, Yunlong, Ricardo Tejos, Martina Beck, Ellie Himschoot, Hongjiang Li, Silke Robatzek, Steffen Vanneste, and Jiří Friml. 2013. "Salicylic Acid Interferes with Clathrin-Mediated Endocytic Protein Trafficking." Proceedings of the National Academy of Sciences of the United States of America 110 (19): 7946–51. https://doi.org/10.1073/pnas.1220205110.
16. Firn, R D, and J Digby. 1980. "The Establishment of Tropic Curvatures in Plants." Annu. Rev. Plant Physiol. 31: 131–48.

17. Gallei, Michelle, Christian Luschnig, and Jiří Friml. 2020. “Auxin Signalling in Growth: Schrödinger’s Cat out of the Bag.” Current Opinion in Plant Biology 53: 43–49. https://doi.org/10.1016/j.pbi.2019.10.003.
18. Gao, Yangbin, Yi Zhang, Da Zhang, Xinhua Dai, Mark Estelle, and Yunde Zhao. 2015. “Auxin Binding Protein 1 (ABP1) Is Not Required for Either Auxin Signaling or Arabidopsis Development” 1. https://doi.org/10.1073/pnas.1500365112.
19. Geldner, Niko, Jiří Friml, York Dieter Stierhof, Gerd Jürgens, and Klaus Palme. 2001. “Auxin Transport Inhibitors Block PIN1 Cycling and Vesicle Trafficking.” Nature 413 (6854): 425–28. https://doi.org/10.1038/35096571.
20. Gelová, Zuzana, Michelle Gallei, Marketa Pernisov, Geraldine Brunoud, Xixi Zhang, Matouš Glanc, Lanxin Li, et al. 2020. “Developmental Roles of Auxin Binding Protein 1 in Arabidopsis Thaliana.” Plant Science. https://doi.org/https://doi.org/10.1016/j.plantsci.2020.110750.
21. Gomez-Roldan, Victoria, Soraya Fermas, Philip B. Brewer, Virginie Puech-Pagès, Elizabeth A. Dun, Jean Paul Pillot, Fabien Letisse, et al. 2008. “Strigolactone Inhibition of Shoot Branching.” Nature 455 (7210): 189–94. https://doi.org/10.1038/nature07271.
22. Gray, W. M. 2004. “Hormonal Regulation of Plant Growth and Development.” PLoS Biology 2 (9). https://doi.org/10.1371/journal.pbio.0020311.
23. Grones, Peter, Xu Chen, Sibu Simon, Walter A. Kaufmann, Riet De Rycke, Tomasz Nodzyński, Eva Zažímalová, and Jiří Friml. 2015a. “Auxin-Binding Pocket of ABP1 Is Crucial for Its Gain-of-Function Cellular and Developmental Roles.” Journal of Experimental Botany 66 (16): 5055–65. https://doi.org/10.1093/jxb/erv177.
24. Grones, Peter, and Jiří Friml. 2015. “Auxin Transporters and Binding Proteins at a Glance.” Journal of Cell Science 128 (1): 1–7. https://doi.org/10.1242/jcs.159418.
25. Hajný, Jakub, Shutang Tan, and Jiří Friml. 2022a. “Auxin Canalization: From Speculative Models toward Molecular Players.” Current Opinion in Plant Biology 65. https://doi.org/10.1016/j.pbi.2022.102174.
26. Jasik, Jan, and Elmon Schmelzer. 2016. “Effects of Auxins on PIN-FORMED2 (PIN2) Dynamics Are Not Mediated by Inhibiting PIN2 Endocytosis 1” 172 (October): 1019–31. https://doi.org/10.1104/pp.16.00563.
27. Jia, Kun Peng, Qian Luo, Sheng Bo He, Xue Dan Lu, and Hong Quan Yang. 2014. “Strigolactone-Regulated Hypocotyl Elongation Is Dependent on Cryptochrome and Phytochrome Signaling Pathways in Arabidopsis.” Molecular Plant 7 (3): 528–40. https://doi.org/10.1093/mp/sst093.
28. Kleine-Vehn, Jürgen, Pankaj Dhonukshe, Michael Sauer, Philip B Brewer, Justyna Wiśniewska, Tomasz Paciorek, Eva Benkova, and Jiří Friml. 2008. “ARF GEF-Dependent Transcytosis and Polar Delivery of PIN Auxin Carriers in Arabidopsis,” 526–31. https://doi.org/10.1016/j.cub.2008.03.021.
29. Kleine-Vehn, Jürgen, Johannes Leitner, Marta Zwiewka, Michael Sauer, Lindy Abas, Christian Luschnig, and Jiří Friml. 2008. “Differential Degradation of PIN2 Auxin Efflux Carrier by Retromer-Dependent Vacuolar Targeting.” Proceedings of the National Academy of Sciences of the United States of America 105 (46): 17812–17. https://doi.org/10.1073/pnas.0808073105.
30. Koltai, Hinanit. 2015. “Cellular Events of Strigolactone Signalling and Their Crosstalk with Auxin in Roots.” Journal of Experimental Botany 66 (16): 4855–61. https://doi.org/10.1093/jxb/erv178.
31. Kögl F, Erxleben H, Haagen-Smit AJ. Über die Isolierung der Auxine a und b aus pflanzlichen Materialien. 9. Mitteilung über pflanzliche Wachstumsstoffe. Hoppe-Seyler's Zeitschrift fur Physiologische Chemie. 1934a;225:215–229.
32. Liu, Cm. 1993. “Auxin Polar Transport Is Essential for the Establishment of Bilateral Symmetry during Early Plant Embryogenesis.” The Plant Cell Online 5 (6): 621–30. https://doi.org/10.1105/tpc.5.6.621.
33. Marhavý, Peter, Jérôme Duclercq, Benjamin Weller, Elena Feraru, Agnieszka Bielach, Remko Offringa, Jiří Friml, Claus Schwechheimer, Angus Murphy, and Eva Benková. 2014. “Cytokinin Controls Polarity of PIN1-Dependent Auxin Transport during Lateral Root Organogenesis.” Current Biology 24 (9): 1031–37. https://doi.org/10.1016/j.cub.2014.04.002.

34. Marzec, Marek. 2016. “Perception and Signaling of Strigolactones.” Frontiers in Plant Science 7 (AUG2016): 1–6. https://doi.org/10.3389/fpls.2016.01260.
35. Mazur, Ewa, Michelle Gallei, Maciek Adamowski, Huibin Han, Hélène S. Robert, and Jiří Friml. 2020. “Clathrin-Mediated Trafficking and PIN Trafficking Are Required for Auxin Canalization and Vascular Tissue Formation in Arabidopsis.” Plant Science 293 (November 2019). https://doi.org/10.1016/j.plantsci.2020.110414.
36. Michalko, Jaroslav, Marta Dravecká, Tobias Bollenbach, and Jiří Friml. 2015. “Embryo-Lethal Phenotypes in Early Abp1 Mutants Are Due to Disruption of the Neighboring BSM Gene [Version 1; Referees: 3 Approved].” F1000Research 4. https://doi.org/10.12688/f1000research.7143.1.
37. Narasimhan, Madhumitha, Michelle Gallei, Shutang Tan, Alexander Johnson, Inge Verstraeten, Lanxin Li, Lesia Rodriguez, et al. 2021. “Systematic Analysis of Specific and Nonspecific Auxin Effects on Endocytosis and Trafficking.” Plant Physiology 186 (2): 1122–42. https://doi.org/10.1093/PLPHYS/KIAB134.
38. Oochi, Akihiro, Jakub Hajny, Kosuke Fukui, Yukio Nakao, Michelle Gallei, Mussa Quareshy, Koji Takahashi, et al. 2019. “Pinstatic Acid Promotes Auxin Transport by Inhibiting Pin Internalization.” Plant Physiology 180 (2): 1152–65. https://doi.org/10.1104/pp.19.00201.
39. Overvoorde, Paul, Hidehiro Fukaki, and Tom Beeckman. 2010. “Auxin Control of Root Development.” Cold Spring Harbor Perspectives in Biology 2 (6): 1–16. https://doi.org/10.1101/cshperspect.a001537.
40. Paciorek, Tomasz, Eva Zažímalová, Nadia Ruthardt, Jan Petrášek, York Dieter Stierhof, Jürgen Kleine-Vehn, David A. Morris, et al. 2005. “Auxin Inhibits Endocytosis and Promotes Its Own Efflux from Cells.” Nature 435 (7046): 1251–56. https://doi.org/10.1038/nature03633.
41. Paponov, Ivan A., Julian Dindas, Elżbieta Król, Tatyana Friz, Vadym Budnyk, William Teale, Martina Paponov, Rainer Hedrich, and Klaus Palme. 2019. “Auxin-Induced Plasma Membrane Depolarization Is Regulated by Auxin Transport and Not by AUXIN BINDING PROTEIN1.” Frontiers in Plant Science 9 (January). https://doi.org/10.3389/FPLS.2018.01953.
42. Paponov, Ivan, and Klaus Palme. 2019. “Natural Auxin Does Not Inhibit Brefeldin A Induced PIN1 and PIN2 Internalization in Root Cells” 10 (May): 1–7. https://doi.org/10.3389/fpls.2019.00574.
43. Prát, Tomáš, Jakub Hajný, Wim Grunewald, Mina Vasileva, Gergely Molnár, Ricardo Tejos, Markus Schmid, Michael Sauer, and Jiří Friml. 2018. “WRKY23 Is a Component of the Transcriptional Network Mediating Auxin Feedback on PIN Polarity.” PLoS Genetics 14 (1): 1–18. https://doi.org/10.1371/journal.pgen.1007177.
44. Rasmussen, Amanda, Michael Glenn Mason, Carolien de Cuyper, Philip B. Brewer, Silvia Herold, Javier Agusti, Danny Geelen, et al. 2012. “Strigolactones Suppress Adventitious Rooting in Arabidopsis and Pea.” Plant Physiology 158 (4): 1976–87. https://doi.org/10.1104/pp.111.187104.
45. Retzer, Katarzyna, Maria Akhmanova, Nataliia Konstantinova, Kateřina Malínská, Johannes Leitner, Jan Petrášek, and Christian Luschnig. 2019. “Brassinosteroid Signaling Delimits Root Gravitropism via Sorting of the Arabidopsis PIN2 Auxin Transporter.” Nature Communications 10 (1). https://doi.org/10.1038/s41467-019-13543-1.
46. Robert, Stéphanie, Jürgen Kleine-vehn, Elke Barbez, Michael Sauer, Tomasz Paciorek, Pawel Baster, Steffen Vanneste, et al. 2010. “NIH Public Access” 143 (1): 111–21. https://doi.org/10.1016/j.cell.2010.09.027.ABP1.
47. Ruyter-Spira, Carolien, Wouter Kohlen, Tatsiana Charnikhova, Arjan van Zeijl, Laura van Bezouwen, Norbert de Ruijter, Catarina Cardoso, et al. 2011. “Physiological Effects of the Synthetic Strigolactone Analog GR24 on Root System Architecture in Arabidopsis: Another Belowground Role for Strigolactones?” Plant Physiology 155 (2): 721–34. https://doi.org/10.1104/pp.110.166645.
48. Sachs, T. 1991. “Cell Polarity and Tissue Patterning in Plants.” Development 112 (SUPPL. 1): 83–93.
49. Sachs, Tsvi. 1975. “The Induction of Transport Channels by Auxin.” Planta 127 (3): 201–6. https://doi.org/10.1007/BF00380716.

50. Sang, Dajun, Dongqin Chen, Guifu Liu, Yan Liang, Linzhou Huang, Xiangbing Meng, Jinfang Chu, et al. 2014. “Strigolactones Regulate Rice Tiller Angle by Attenuating Shoot Gravitropism through Inhibiting Auxin Biosynthesis.” Proceedings of the National Academy of Sciences of the United States of America 111 (30): 11199–204. https://doi.org/10.1073/pnas.1411859111.
51. Sauer, Michael, Jozef Balla, Christian Luschnig, Justyna Wis, Vilém Reinöhl, and Eva Benková. 2006. “Canalization of Auxin Flow by Aux / IAA-ARF-Dependent Feedback Regulation of PIN Polarity,” 2902–11. https://doi.org/10.1101/gad.390806.integrated.
52. Shinohara, Naoki, Catherine Taylor, and Ottoline Leyser. 2013. “Strigolactone Can Promote or Inhibit Shoot Branching by Triggering Rapid Depletion of the Auxin Efflux Protein PIN1 from the Plasma Membrane.” PLoS Biology 11 (1). https://doi.org/10.1371/journal.pbio.1001474.
53. Steeves T.A, Sussex I.M., Patterns in plant development, Cambridge University Press; Cambridge, UK, 1989
54. Tian, H., D. Klambt, and A. M. Jones. 1995. “Auxin-Binding Protein 1 Does Not Bind Auxin within the Endoplasmic Reticulum despite This Being the Predominant Subcellular Location for This Hormone Receptor.” Journal of Biological Chemistry 270 (45): 26962–69. https://doi.org/10.1074/jbc.270.45.26962.
55. Tsuchiya, Yuichiro, Danielle Vidaurre, Shigeo Toh, Atsushi Hanada, Eiji Nambara, Yuji Kamiya, Shinjiro Yamaguchi, and Peter McCourt. 2010. “A Small-Molecule Screen Identifies New Functions for the Plant Hormone Strigolactone.” Nature Chemical Biology 6 (10): 741–49. https://doi.org/10.1038/nchembio.435.
56. Verna, Carla, Sree Janani Ravichandran, Megan G. Sawchuk, Nguyen Manh Linh, and Enrico Scarpella. 2019. “Coordination of Tissue Cell Polarity by Auxin Transport and Signaling.” ELife 8: 1–30. https://doi.org/10.7554/eLife.51061.
57. Vernoux, Teva, Fabrice Besnard, and Jan Traas. 2010. “Auxin at the Shoot Apical Meristem.” Cold Spring Harbor Perspectives in Biology 2 (4): 1–14. https://doi.org/10.1101/cshperspect.a001487.
58. Wisniewska, Justyna, Jian Xu, Daniela Seifartova, Philip B. Brewer, Kamil R????i??ka, Lkram Blilou, David Rouqui, Eva Benkova, Ben Scheres, and Jiri Friml. 2006. “Polar PIN Localization Directs Auxin Flow in Plants.” Science 312 (5775): 883. https://doi.org/10.1126/science.1121356.
59. Woo, Eui Jeon, Jacqueline Marshall, James Bauly, Jin Gui Chen, Michael Venis, Richard M. Napier, and Richard W. Pickersgill. 2002. “Crystal Structure of Auxin-Binding Protein 1 in Complex with Auxin.” EMBO Journal 21 (12): 2877–85. https://doi.org/10.1093/emboj/cdf291.
60. Xu, T, N Dai, J Chen, S Nagawa, M Cao, H Li, Z Zhou, et al. 2014. “Cell Surface ABP1-TMK Auxin-Sensing Complex Activates ROP GTPase Signaling.” Science 343 (6174): 1025–28. https://doi.org/10.1126/science.1245125.

5. Appenidx

The following research articles are included in the appendix (on ISTA Rex):

1. Li L, **Gallei M**, Friml J. Bending to auxin: fast acid growth for tropisms. Trends Plant Sci. 2021:1-10. doi:10.1016/j.tplants.2021.11.006
2. Oochi A, Hajny J, Fukui K, Nakao Y, **Gallei M**, et al. Pinstatic acid promotes auxin transport by inhibiting pin internalization. Plant Physiol. 2019;180(2):1152-1165. doi:10.1104/pp.19.00201
3. Gelová Z, **Gallei M**, Pernisová M, et al. Developmental roles of Auxin Binding Protein 1 in Arabidopsis thaliana. Plant Sci. 2021;303. doi:10.1016/j.plantsci.2020.110750